

New Electron-Deficient Polycyclic Aromatic
Dicarboximides by Palladium-Catalyzed C–C Coupling
and Core Halogenation–Cyanation

Dissertation zur Erlangung des
naturwissenschaftlichen Doktorgrades
der Julius-Maximilians-Universität Würzburg

vorgelegt von
Sabine Seifert
aus Marktredwitz

Würzburg 2017

Eingereicht bei der Fakultät für Chemie und Pharmazie am:

18.10.2017

Gutachter der schriftlichen Arbeit:

1. Gutachter: Prof. Dr. Frank Würthner
2. Gutachter: Prof. Dr. Anke Krüger

Prüfer des öffentlichen Promotionskolloquiums:

1. Prüfer: Prof. Dr. Frank Würthner
2. Prüfer: Prof. Dr. Anke Krüger
3. Prüfer: Prof. Dr. Ingo Fischer

Datum des öffentlichen Promotionskolloquiums:

15.12.2017

Doktorurkunde ausgehändigt am:

Abbreviations

abs	absorbance/absorption
Ac	acetyl
Ar	aryl
ap	applied
a.u.	arbitrary unit
(I)CT	(intramolecular) charge transfer
CV	cyclic voltammetry
dba	dibenzylideneacetone
DBN	1,5-diazabicyclo[4.3.0]non-5-ene
DBU	1,8-diazabicyclo[5.4.0]undec-7-ene
DCM	dichloromethane
DDQ	2,3-dichloro-5,6-dicyano-1,4-benzoquinone
(TD-)DFT	(time-dependent) density functional theory
DIPEA	diisopropylethylamine
DMAP	4-dimethylaminopyridine
DMF	dimethylformamide
DMSO	dimethyl sulfoxide
dppf	1,1'-bis(diphenylphosphino)ferrocene
em	emission
ESI	electrospray ionization
ex	excitation
Fc ⁺ /Fc	ferrocenium/ferrocene redox couple
fl	fluorescence
ⁱ Pr	<i>iso</i> -propyl
HOMO	highest occupied molecular orbital
HPLC	high performance liquid chromatography
HR	high-resolution
<i>I</i>	intensity
L	ligand
LUMO	lowest unoccupied molecular orbital
PADI	polycyclic aromatic dicarboximide
PAH	polycyclic aromatic hydrocarbon

PBI	perylene bisimide
Ph	phenyl
PIFA	phenyliodine bis(trifluoroacetate)
pin	pinacolato
(T)M	(transition) metal
MALDI	matrix-assisted laser desorption/ionization
Me	methyl
MO	molecular orbital
MS	mass spectrometry
<i>m/z</i>	mass-to-charge ratio
NBI	naphthalene bisimide
NBS	<i>N</i> -bromosuccinimide
<i>n</i> -Bu	<i>n</i> -butyl
NI	naphthalene imide
NIR	near infra-red
NMR	nuclear magnetic resonance
OFET	organic field effect transistor
OLED	organic light emitting diode
OTf	triflate
ox	oxidation/oxidant
QBI	quaterylene bisimide
red	reduction/reductant
rt	room temperature
SEC	spectroelectrochemistry
SPhos	2-dicyclohexylphosphino-2',6'-dimethoxybiphenyl
SWV	square wave voltammetry
TBAF	tetrabutylammonium fluoride
TBAHFP	tetrabutylammonium hexafluorophosphate
TBI	terrylene bisimide
<i>t</i> Bu	<i>tert</i> -butyl
THF	tetrahydrofuran
TIPS	triisopropylsilyl
TMS	trimethylsilyl or tetramethylsilane
Tol	tolyl

Ts	tosyl
UV	ultra violet
V	potential
Vis	visible
vt	virtual

Table of Contents

Chapter 1 Aim of the Thesis	1
Chapter 2 Literature Survey	6
2.1 C–C Coupling Reactions for the Construction of Polycyclic Aromatic Hydrocarbons .	6
2.1.1 Introduction	6
2.1.2 Mechanistic Aspects	7
2.1.3 Application of C–C Coupling Reactions for the Construction of PAHs	13
2.2 Polycyclic Aromatic Dicarboximides	22
2.2.1 Introduction	22
2.2.2 Polycyclic Aromatics containing Six-Membered Dicarboximides	23
2.2.3 Polycyclic Aromatics containing Five-Membered Dicarboximides	45
Chapter 3 Results and Discussion	49
3.1 Palladium-Catalyzed Suzuki-Miyaura Cross-Coupling of Naphthalene Dicarboximides with Pyrene	49
3.1.1 Introduction	49
3.1.2 Synthesis of Mono-, Di- and Tetra-Naphthalimide-Substituted Pyrenes	50
3.1.3 Optical Properties	52
3.1.4 Electrochemical Properties	57
3.1.5 Conclusion	59
3.2 Palladium-Catalyzed C–C Coupling Cascade Reactions: An Efficient Route to Electron-Poor Polycyclic Aromatic Dicarboximides on the Nanoscale	60
3.2.1 Introduction	60
3.2.2 Synthesis and Mechanistic Rationale	61
3.2.3 Structural Elucidation	66
3.2.4 Optical and Electrochemical Properties	68
3.2.4 Conclusion	73
3.3 Base-Selective Six- versus Five-Membered Ring Annulation in Palladium-Catalyzed C–C Coupling Cascade Reactions: Synthesis of New Polycyclic Aromatic Dicarboximides and Mechanistic Rationale	74
3.3.1 Introduction	74
3.3.2 Synthesis and Mechanistic Rationale	75

3.3.3 Structural Elucidation	80
3.3.4 Optical and Electrochemical Properties	83
3.3.5 Conclusion	88
3.4 An Ambient Stable Core-Substituted Perylene Bisimide Dianion	89
3.4.1 Introduction	89
3.4.2 Synthesis	90
3.4.3 Structural Elucidation	91
3.4.4 Electrochemical Studies	96
3.4.5 Conclusion	100
Chapter 4 Summary	101
Chapter 5 Zusammenfassung	108
Chapter 6 Experimental Part	115
6.1 Materials and Methods	115
6.2 Synthesis and Characterization	119
6.2.1 Synthesis of Aryl Boronic Acid Pinacol Esters	119
6.2.2 Synthesis of Naphthalimide-Substituted Pyrenes	123
6.2.3 Synthesis of Six-Membered Ring Annulated Systems by C–C Coupling Cascade Reactions	127
6.2.4 Synthesis of Five-Membered Ring Annulated Systems by C–C Coupling Cascade Reactions	133
6.2.5 Synthesis of Core-Functionalized Perylene Bisimides	139
6.3 Single Crystal Data	142
Appendix	146
Literature	147

Chapter 1

Aim of the Thesis

Nanoscience is an emergent field of interdisciplinary science combining research fields of chemistry, physics, materials science and biology and will probably evolve to one of the key-technologies of the 21st century. This area of research is concerned with the exploration of materials on the scale of few nanometers up to 100 nm and has great influence on nearly all economic sectors such as optics, electronics, information technology, mechanical engineering, health and environmental science.^[1] Materials of this size are either comparatively large single molecules or defined assemblies of small molecules like they exist in nature since the origin of life. Examples are the DNA, viruses, subcellular organelles and the natural photosystems which can be described as supramolecular or multicomponent structures possessing a specific function due to particular interactions between individual moieties.^[2] Nowadays, scientists aim to mimic such complex architectures by construction of artificial systems and functional molecular machines.^[3] Continuing development of new materials on the nanoscale and the investigation of their structure-property-relationships will be crucial for advanced applications in energy conversion/storage devices, medicine and computing.^[4]

In this regard chemistry plays a particularly important role by creating discrete new structures through the connection of atoms or molecules by covalent bonds or weak intermolecular interactions. For the preparation of single molecules having the size of few nanometers, organic chemistry made huge progress towards functional materials based on extended π -conjugated molecules, which was recently highlighted by Klaus Müllen in *ACS Nano*.^[5] One reason for the huge activity in this area of research was the isolation of graphene in 2004.^[6] Graphene is a single two-dimensional sheet composed of sp^2 -hybridized carbon atoms that are connected in a hexagonal fashion like an isolated layer of graphite. Geim and Novoselov isolated such a single graphite layer for the first time by mechanical exfoliation (repeated peeling) and studied its ambipolar electric field effect with mobilities of about $10000 \text{ cm}^2\text{V}^{-1}\text{s}^{-1}$, which was honored with the Nobel Prize in Physics in 2010.^[7] By virtue of the exceptional properties of graphene like ultra-light weight, mechanical robustness, high

flexibility, transparency, high conductivity and mobility,^[8] many scientists devoted their efforts to this area of research and initiatives like the Graphene Flagship^[9] funded by the European Union have been established. As the physical properties of graphene are mainly influenced by its edge-structure, various nanometer-sized molecules, so called nanographenes (size of 1–100 nm), were developed by bottom-up synthetic approaches and serve as model systems to deduce important structure-property relationships.^[10] As depicted in Figure 1 the number of published articles on the topics nanoscience and nanographene continuously increased over the last twenty years demonstrating the importance of these research areas.

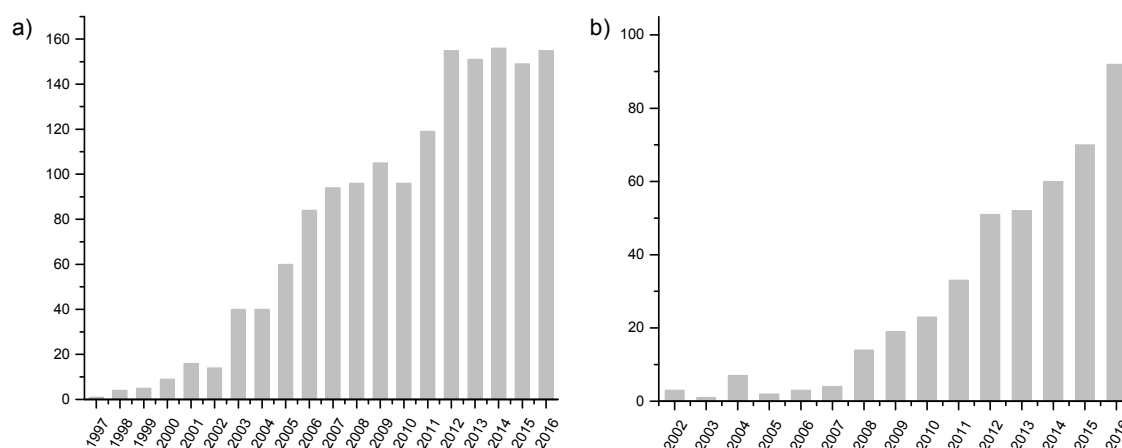
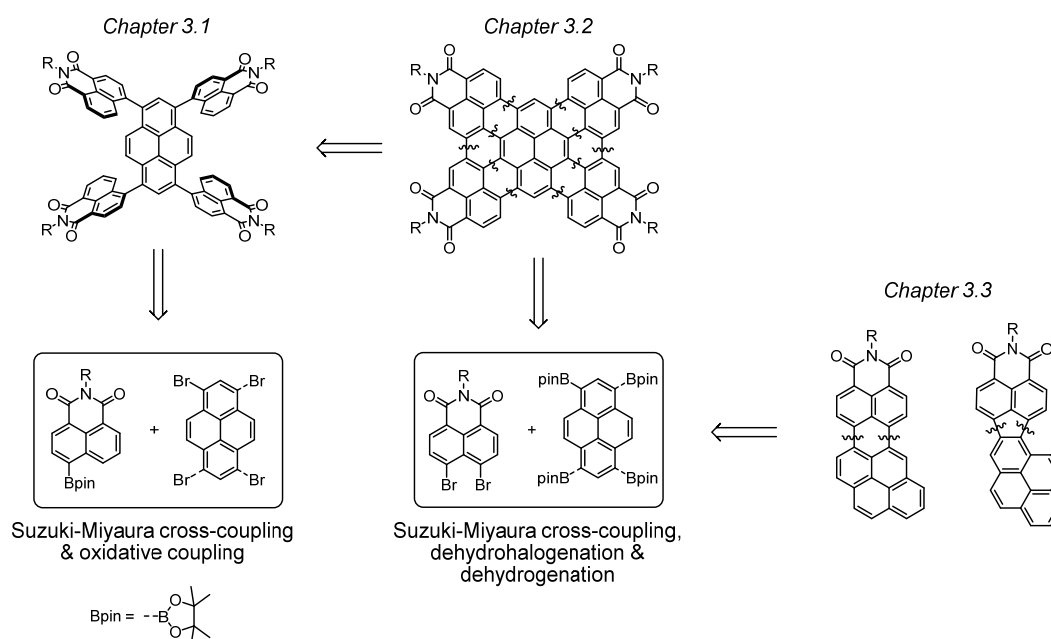


Figure 1 Number of published articles on the topics nanoscience (a) and nanographene (b) registered by the web of science.^[11]

Regarding different synthetic methodologies for the construction of nanometer-sized molecules based on extended two dimensional sp^2 -hybridized carbon frameworks the combination of different C–C coupling reactions in either sequential procedures or cascade reactions using readily accessible precursors are the most convenient strategies. Such methods are well established for the synthesis of two dimensional unfunctionalized polycyclic aromatic hydrocarbons (PAHs), that are electron-rich π -conjugated systems.^[12] In contrast, synthetic strategies towards similarly sized electron-poor and planar π -scaffolds are rather scarce. One of the most frequently applied strategies is concerned with the introduction of electron-withdrawing dicarboximides to polycyclic aromatic hydrocarbons to generate electron-poor counterparts to the parent PAHs with energetically low lying frontier molecular orbitals. In this regard, rylene bisimides are one of the most elaborated class of π -conjugated chromophores that possess an electron-poor character due to two six-membered cyclic imide groups attached at the terminal positions making them suitable as n-type semiconducting materials for the fabrication of organic electronic devices.^[13] One approach for the synthesis of polycyclic aromatic systems containing multiple dicarboximide groups in the scale of few

nanometers is based on the core-expansion of rylene imides. The most prevalent strategy is concerned with the connection of multiple perylene bisimides (PBIs) either by direct fusion^[14] or by introduction of conjugated spacer units.^[15] However, these methodologies lead to distorted π -scaffolds in most cases due to the steric congestion between the individual PBI moieties. On the other hand, electron deficient polycyclic aromatic systems containing multiple naphthalimide subunits can be prepared by connecting the latter to a π -conjugated core *via* five membered rings.^[16] Such structures exhibit similarly distorted non-planar π -scaffolds preventing desirable long range π - π -interactions in most cases.

Therefore, the major aim of this thesis is the development of new synthetic strategies for the preparation of planar nanometer-sized multi-dicarboximides (see Scheme 1) as electron-poor counterparts to hitherto extensively studied unfunctionalized electron-rich nanographenes.



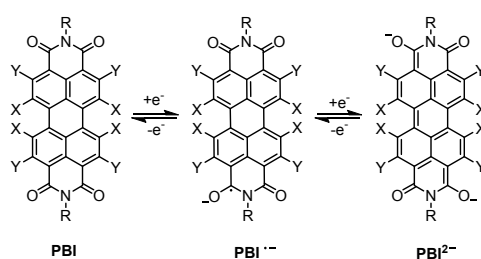
Scheme 1 Synthetic concepts for the development of multichromophoric systems and electron-poor two dimensional π -scaffolds based on (multi-)dicarboximides (R = 2,6-diisopropylphenyl).

In this regard, the development of multichromophoric systems based on a polycyclic aromatic core and multiple aromatic imides as suitable precursors for subsequent planarizing cyclization reactions was to be studied. Due to the promising properties of several arylated pyrene derivatives making them suitable for applications in organic electronics,^[17] a central pyrene core and naphthalimide groups were chosen for this purpose. These chromophore moieties should directly be connected by covalent bonds *via* C–C cross-coupling reactions and the obtained multichromophoric systems should be investigated with regard to their optical and electrochemical properties. Alternatively, a cascade synthetic concept combining different C–C coupling strategies in one single chemical transformation and its mechanistic details should be elaborated. Therefore, the coupling of *peri*-dibromonaphthalimide to

different aromatic polycyclic systems was to be investigated to elucidate the scope of the substrates suitable for such C–C coupling annulation reactions. Thus, different mono-, di- and tetra-boronate esters were chosen as coupling components. Furthermore, a variety of mono-substituted aryl boronic esters should be investigated, which differ by the position of their functional group and the electronic character. Since the second C–C bond formation can occur at different positions of the aromatic substrate, the annulation mode (six- versus five-membered ring annulation) should be controlled by variation of the reaction conditions. Furthermore, structure-property relationships should be deduced for the new polycyclic aromatic dicarboximides by UV/Vis absorption and fluorescence spectroscopy, electrochemical analyses and X-ray diffraction experiments.

Due to the importance of reduced species in several technologies like energy storage and conversion in organic electronics, the isolation and characterization of ambient stable reduced species of polycyclic aromatic dicarboximides (see Scheme 2) was another aim of this thesis. Perylene bisimides were chosen for this purpose as they can easily be functionalized and their molecular properties are well-investigated. Highly electron-withdrawing groups attached to the perylene core should facilitate the (electro)chemical reduction and protect the reduced scaffold against reoxidation under ambient conditions. The reduced species should further be investigated with regard to their solid state structures as well as their stabilities in solution and in the bulk solid material.

Chapter 3.4



Scheme 2 Representation of the reduction process of PBIs (X, Y = electron-withdrawing groups, R = CH₂C₃F₇).

Chapter 2 provides a brief overview on C–C coupling techniques that can be applied for the construction of polycyclic aromatic hydrocarbons and summarizes most fundamental mechanistic aspects. Furthermore, the latest developments in the synthesis of new polycyclic aromatic dicarboximides (PADIs) as electron-deficient counterparts to the large variety of polycyclic aromatic hydrocarbons (PAHs) are summarized. The synthetic procedures that will be discussed include synthetic approaches towards nanometer-sized molecules containing multiple electron-withdrawing dicarboximide groups.

In *Chapter 3* the results regarding the synthesis of new polycyclic aromatic dicarboximides and their molecular properties will be presented. This Chapter is divided into four parts. *Subchapter 3.1* provides an overview on the synthesis and the optical and electrochemical properties of naphthalimide-functionalized pyrenes, which depend on the position of the linkage between the individual chromophore moieties. In *Subchapter 3.2* the application of such multichromophoric systems in the synthesis of planar nanometer-sized multidicarboximides by oxidative cyclodehydrogenation is discussed. The development of an alternative synthetic strategy including the combination of multiple C–C bond forming reactions will be introduced, followed by a detailed analysis of the molecular properties of the newly synthesized compounds. *Subchapter 3.3* delivers deeper insights into the scope of the substrates and the mechanism of the developed C–C coupling cascade reactions and summarizes the structural, electrochemical and optical properties of the prepared polycyclic aromatic dicarboximides. In the last *Subchapter 3.4* the development and characterization of ambient stable reduced species based on core-functionalized perylene bisimides will be elucidated, that are one of the most attractive and elaborated class of polycyclic aromatic dicarboximides.

Chapters 4 and *5* summarize the results of this thesis in English and German.

Chapter 6 describes the experimental details including materials and methods that were applied as well as detailed synthetic procedures and the characterization of all new compounds.

Chapter 2

Literature Survey

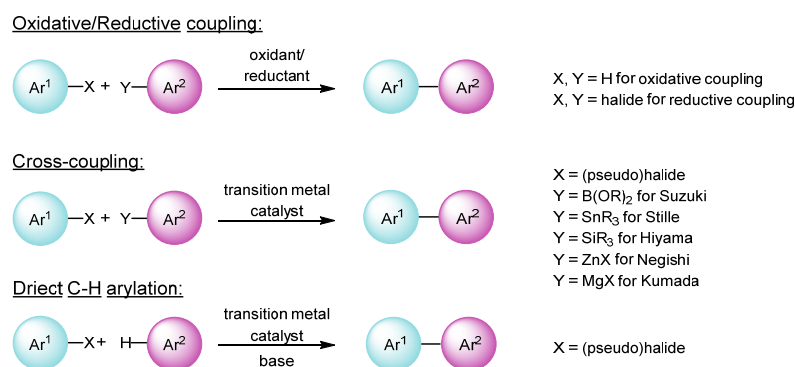
The first part of this literature survey provides a brief overview on different C–C bond formation strategies for the preparation of biaryls and their mechanistic aspects, which are prerequisite for the interpretation of the synthetic results discussed in *Chapter 3*. In the following, some examples for the application of these synthetic methods in the construction of polycyclic aromatic hydrocarbons are illustrated. The second part of this chapter summarizes synthetic strategies including the former C–C coupling methods for the construction of polycyclic aromatic dicarboximides based on core-expanded rylene imides and other aromatic structures with six-membered imide group. Finally, some examples for the construction of polycyclic aromatics with five-membered imide groups will be provided.

2.1 C–C Coupling Reactions for the Construction of Polycyclic Aromatic Hydrocarbons

2.1.1 Introduction

One of the key reactions in organic synthesis is the construction of C–C bonds since organic materials based on carbon-rich compounds cover a broad variety of valuable classes of compounds including natural products, biomolecules, pharmaceuticals, polymers and organic (opto)electronic materials based on π -conjugated small molecules. However, a major challenge for organic chemists is the construction of C–C bonds between two aromatic molecules (overview of basic methods is given in Scheme 3). One of the first discovered coupling reactions between two aromatic moieties is the copper-catalyzed reductive coupling of aryl-halides, known as the Ullmann-reaction.^[18] Another early methodology is the oxidative coupling of two aromatic components, including the intermediate formation of free radicals.^[19] This initial development was followed by the discovery of the Scholl reaction, where oxidative dehydrogenation is accomplished by the initial formation of a σ -complex between the Lewis acid and the respective arene providing access to a crucial arenium cation

intermediate.^[20] During the last decades transition-metal-catalyzed C–C coupling reactions (in particular palladium-catalyzed ones) between two aromatic moieties have been developed, which now predominate the field of C–C bond formation to prepare biaryls. These transition-metal-catalyzed C–C coupling methods can further be divided into cross-coupling reactions of two activated aromatic molecules initially developed by Stille,^[21] Suzuki,^[22] Negishi,^[23] Hiyama^[24] and Kumada^[25] and the direct arylation of C–H bonds by C–H activation.^[26]



Scheme 3 Overview of principal methods for C–C bond formation between two aromatic molecules.

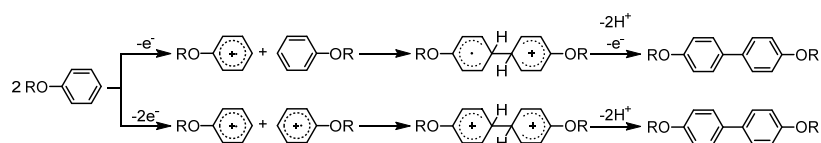
Another common strategy for the generation of C–C bonds resulting in aromatic compounds is the cyclotrimerization of acetylene derivatives, which has been developed in 1867^[27] with the synthesis of benzene starting from acetylene and was later optimized by Reppe in nickel-catalyzed cyclization reactions.^[28] Related are [4+2] or [2+2+2] cycloadditions of sp^2 -hybridized systems followed by oxidative rearomatization, which play an important role not only for the construction but also for the core-expansion of aromatic compounds.^[29] In the following subchapters an overview on mechanistic aspects and the utilization of C–C coupling reactions will be provided, that are important for the construction of polycyclic aromatic hydrocarbons.

2.1.2 Mechanistic Aspects

Oxidative Coupling

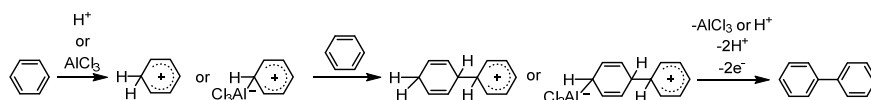
The oxidative coupling between two unactivated aromatic moieties can proceed *via* several different mechanisms. However, the general result is a biaryl generated by the formation of a new C–C bond that is associated with the release of two protons and two electrons, and therefore with the oxidation of carbon atoms from the oxidation state -1 (in the initial C–H-bonds) to carbon atoms of the oxidation state 0 (in the final C–C-bonds).

Radical cation mechanism: An oxidative coupling involving the formation of free radicals is associated with electron-rich aromatics such as phenols, ethers or related molecules.^[19b] The first reports regarding this strategy are concerned with the oxidative coupling of gallic acid to ellagic acid^[19c] and of 2-naphthol to 1,1'-bi-2-naphthol.^[30] The common mechanism (see Scheme 4) includes the formation of a radical cation by abstraction of a single electron that is consumed by a sacrificial oxidant. This reactive intermediate can subsequently interact with the neutral arene or a second radical cation forming a distonic biaryl radical cation or dication. Additionally, the release of two protons, often trapped by quinoidal oxidants, is prerequisite to obtain the neutral biaryl product.^[20b, 31]



Scheme 4 Exemplary reaction mechanism for an oxidative coupling of arenes involving free radicals.

Arenium ion mechanism (Scholl reaction): The Scholl reaction has originally been developed for the oxidative coupling of aromatic compounds in the presence of Lewis acids like AlCl_3 .^[20a] Mechanistic considerations (Scheme 5) include the formation of an arenium ion by protonation of an aromatic molecule or by preceding formation of a σ -complex between the arene and a Lewis acid such as AlCl_3 .^[32] The arenium cation is then attacked by a neutral arene, eventually forming the new C–C bond. After elimination of the Lewis or protic acid, rearomatization by proton-coupled oxidation can be accomplished by relatively mild oxidants like oxygen (air) to yield the final biaryl.

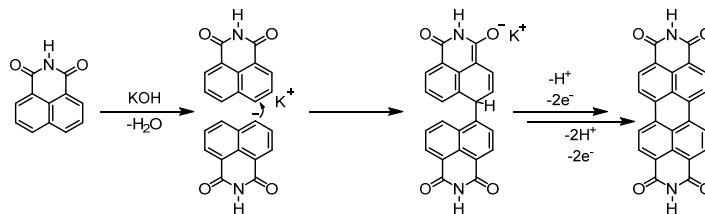


Scheme 5 Reaction mechanism for an oxidative coupling involving the formation of arenium ions.

However, several reports object this simplistic mechanistic picture, due to the fact that some of the Lewis acids, which recently became popular for Scholl-type reactions, including FeCl_3 , MoCl_5 , CuCl_2 or hypervalent iodine in PIFA/ BF_3 , exhibit oxidation strengths that are strong enough to even generate radical cations. Additionally, the coexistence of both intermediates – radical cation and arenium ion – cannot be distinguished in some cases and therefore neither the mechanistic pictures.^[20b, 33]

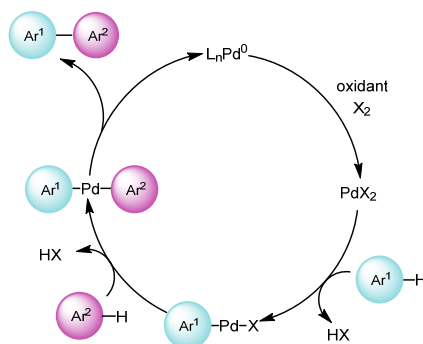
Base-induced oxidative coupling: Oxidative coupling reactions induced by Brønsted-bases are known for aromatic molecules with C–H acidic bonds like for example naphthalimides (Scheme 6). This procedure was the initial synthetic access to perylene bisimides and

bisanhydrides and was originally accomplished in molten KOH.^[34] The C–C coupling proceeds *via* (□) deprotonation, (□) nucleophilic attack of the aromatic anion at the aromatic coupling partner and (□) release of a second proton and two electrons, initiated by a sacrificial oxidant (in most cases air).^[35]



Scheme 6 Reaction mechanism for a base-induced oxidative coupling.

Catalytic oxidative cross-coupling: Oxidative coupling of two arenes utilizing catalytically active transition-metal complexes (see Scheme 7) has two major advantages: (□) This methodology can be applied to unactivated arenes and (□) cross-coupling of two different arenes can be achieved, which is usually not the case for other oxidative coupling reactions. The key step of the catalytic cycle is the activation of the C–H bond by a Pd[□] species which is generated by an auxiliary oxidant. This C–H activation step is discussed to proceed either *via* an electrophilic aromatic metalation or by a concerted proton-transfer metalation pathway. Independently, one of the major challenges is, that the catalyst should selectively activate only one arene in the first step of the catalytic cycle and invert its selectivity in the next step towards the second arene to avoid homo-coupling. It is generally accepted that the electronic nature of the substrates affect the selectivity, due to a faster activation of more electron-rich arenes.^[36]

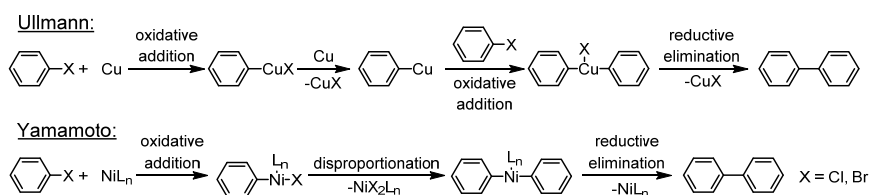


Scheme 7 Catalytic cycle for a Pd-catalyzed oxidative coupling.

Reductive Coupling

Reductive coupling of aromatic compounds is related to halogenated arenes with C–X bonds (C[□]-oxidation state), which are converted into biaryls with C–C bonds (C⁰-oxidation state) by reduction with a (transition) metal, acting as electron- and halogen-acceptor (Scheme 8). In this regard, one of the first methods for C–C coupling between two aromatic compounds is

the Ullmann reaction, discovered in 1901.^[18b] Typically, this strategy is used for the homo-coupling of halogenated (most commonly chlorinated) aromatic compounds by Cu^0 , which has initially been used in stoichiometric amounts. Mechanistically, the reaction follows typical steps of transition-metal-catalyzed reaction sequences, where the initial step is the oxidative addition of the aryl-halide to Cu^0 . Subsequently, this intermediate is reduced to the active Cu^{\square} species by a second equivalent of copper, which then undergoes oxidative addition to an aryl halide, forming a three-coordinate Cu-intermediate which reductively eliminates the final product under formation of CuX .

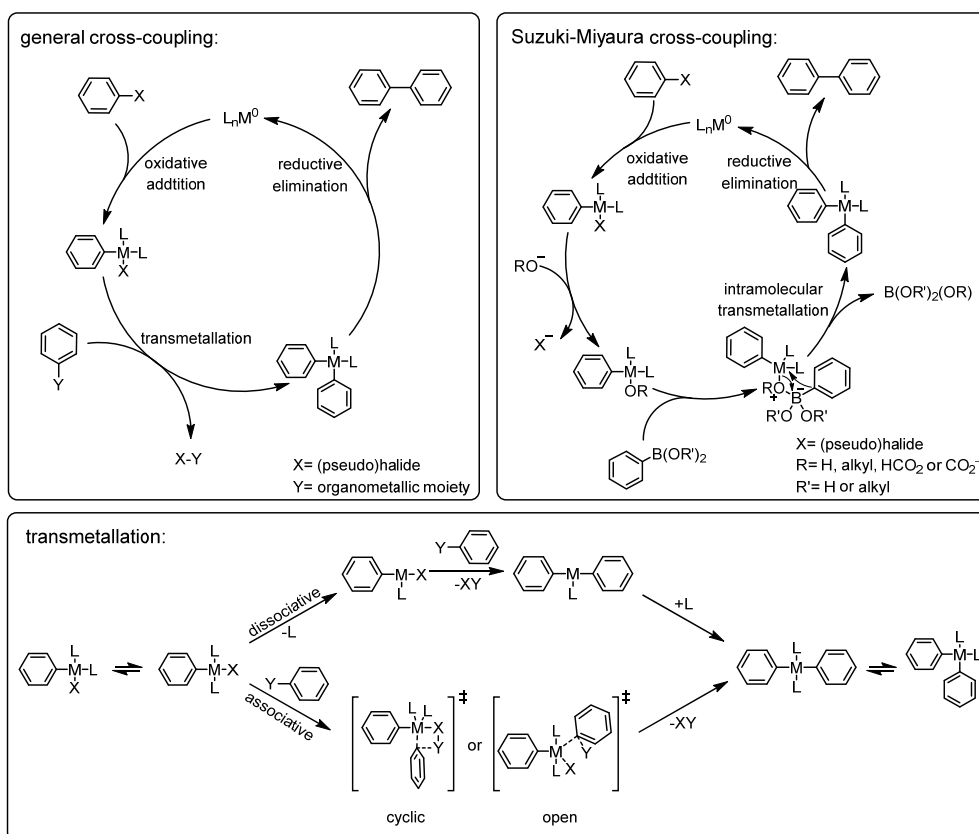


Scheme 8 Reaction mechanism of the reductive coupling of halogenated aromatics.

Likewise, nickel can be used as catalyst for the Yamamoto coupling of mainly brominated derivatives^[37] which has initially been reported by Semmelhack.^[38] Usually $[\text{Ni}(\text{cod})_2]$ is used as Ni^0 -species and the intermediate Ni-complex formed by oxidative addition of the aryl-halide undergoes disproportionation and reductive elimination for the formation of the corresponding biaryl.

Cross-Coupling Reactions

Cross-coupling is a general term for a variety of reactions in which organometallic compounds react with organic halides under formation of a new C–C bond in the presence of catalytically active transition metals. All transition-metal-catalyzed cross-coupling reactions are characterized by three fundamental catalytic steps (see Scheme 9, top), that are (□) oxidative addition of an aryl halide or pseudo-halide (e.g. OTf) to a M^0 species. (□) Transmetalation, placing both coupling components on the same metal center under elimination of the functional groups followed by (□) reductive elimination of the biaryl product, while regenerating the catalytically active M^0 -species.^[39] In most cases the oxidative addition of the $\text{C}(\text{sp}^2)\text{-X}$ bond proceeds *via* a concerted mechanism in which the active M^0 -intermediate inserts into the C–X-bond through a three-center transition-state forming a *cis*- $[\text{M}(\text{ArXL}_2)]$. Depending on the nature of the ligands, isomerization to the *trans*-isomer can occur. Other mechanistic pathways for oxidative addition include radical mechanisms or nucleophilic substitution, that are dependent on the nature of the transition metal and the substrate.



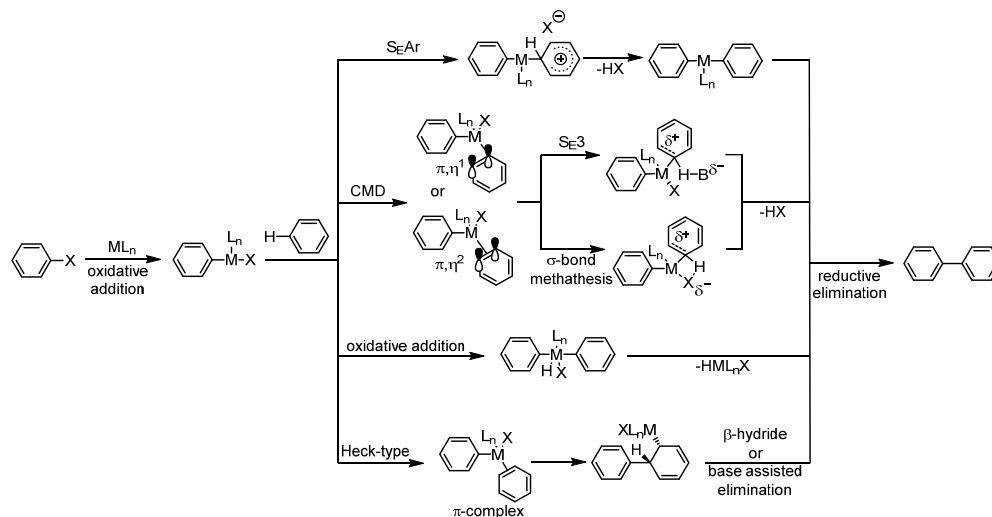
Scheme 9 Catalytic cycles for general or Suzuki-Miyaura cross-coupling reactions and different pathways for the transmetallation step.

Moreover, the oxidative addition is often the rate determining step of the catalytic cycle.^[40] The second step of the catalytic cycle is the transmetalation, which is different for the individual types of cross-coupling reactions. In general, this step can proceed *via* a dissociative or an associative mechanism (Scheme 9, bottom). The former includes the dissociation of one ligand from the metal center to generate a coordinatively unsaturated metal species prior to the exchange of the (pseudo)halide by the second aryl group. Such a mechanistic pathway probably takes place with sterically demanding ligands such as $P(o-Tol)_3$.^[41] An associative mechanism can either proceed *via* a cyclic or an open transition state. For associative mechanisms, it is assumed that the transmetalation occurs at the *trans*- $[MArXL_2]$ intermediate which is formed after oxidative addition and isomerization of *cis*- $[MArXL_2]$.^[42] The transmetalation in Suzuki-Miyaura coupling differs from others due to the low nucleophilicity of the organoborane reagents and therefore requires the addition of an auxiliary base. This auxiliary base diversely effects the catalytic process, however, it has a major influence on the transmetalation step. Thus, the reaction of the base, typically a RO^- species, with the boronic acid derivative generates a more reactive negatively charged quaternary borate which reacts with the $[MArXL_2]$ intermediate. Furthermore, base induced halide exchange at the metal center might occur prior to the transmetalation step, resulting in

a [M₂ArORL₂] intermediate suitable for an intramolecular process (as shown in Scheme 9).^[43] Similarly, organosilanes which are used in Hiyama cross-coupling are usually activated by addition of a fluoride source.^[39] The final reductive elimination is similar for all types of cross-coupling reactions, although the rate of this step is dependent on the nature of ligands.

C–H Arylation

C–H arylation is the functionalization of unactivated aromatic compounds by transition-metal-catalyzed coupling with halogenated arenes to create biaryls. The basic mechanism is similar to that of other traditional cross-coupling reactions, with exception of the transmetalation step that is replaced by a C–H bond activation. Mechanistically, this key C–H bond activation step can proceed *via* several different pathways (see Scheme 10) and depends on the substrate, the active catalyst, the solvent and the base. The most frequently discussed mechanisms in the literature are the electrophilic aromatic substitution, the oxidative addition or a Heck-type carbopalladation followed by β-hydride elimination.^[26a, b] However, these C–H activation pathways could be excluded for several examples, and new metalation mechanism such as the concerted metalation deprotonation (CMD) were proposed which include either a concerted S_E3 process or a σ-bond metathesis and the assistance of an internal or external base.^[44]



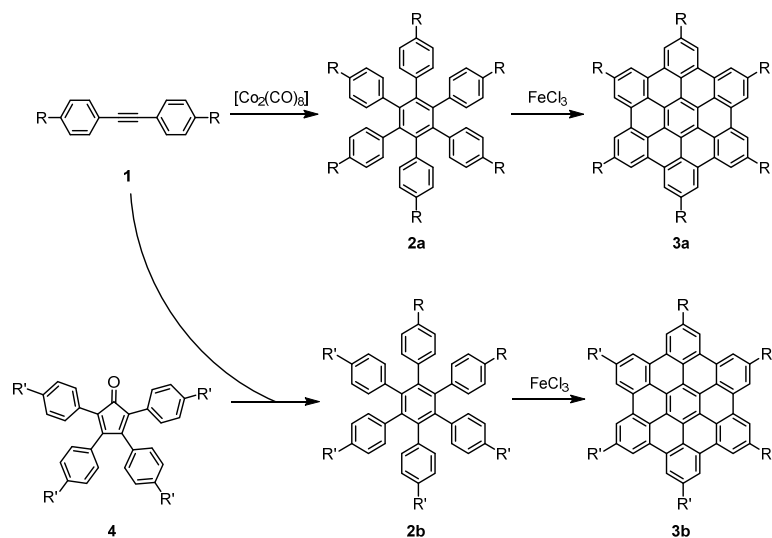
Scheme 10 Overview of mechanistic pathways for C–H arylation.

A major challenge in direct C–H arylation reactions, is the precise control of regioselectivity as chemically different C–H-bonds in one single substrate usually still exhibit similar reactivities. However, it has been shown that the regioselectivity can be manipulated by changing the reaction conditions like solvent polarity,^[45] introduction of directing groups^[46] and/or variation of ligand systems.^[47]

2.1.3 Application of C–C Coupling Reactions for the Construction of PAHs

Oxidative coupling

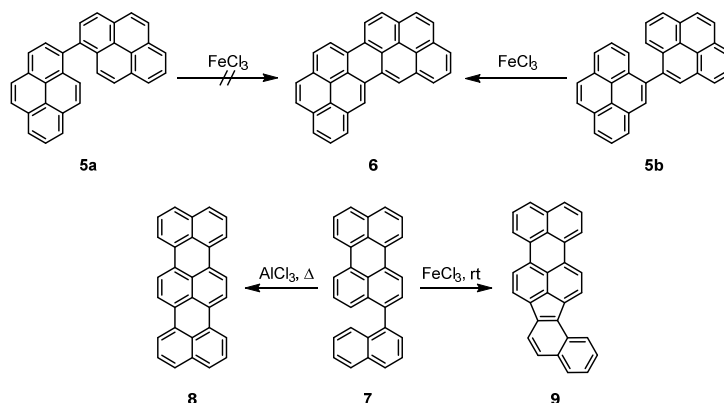
Oxidative coupling between aromatic moieties was extensively applied to oligophenylenes, providing access to all-benzenoid PAHs such as **3a** and **3b** (Scheme 11). Particularly the group of Müllen exploited this synthetic methodology for the construction of several nanographenes, nanotube-cutouts or nanoribbons.^[10b, 48] In some examples other small-sized PAHs were already attached to the oligophenylene starting material providing access to graphene-type molecules with different edge structures and non-all-benzenoid characters.^[49] The key step for cyclization is an oxidative dehydrogenation, that is usually accomplished with Lewis acids/oxidants like FeCl₃ under mild reaction conditions. The large variety of oligophenylene precursors suitable for oxidative coupling reactions can be prepared by transition-metal-catalyzed cyclotrimerization reactions of suitable diarylacetylenes (e.g. **1**) or by Diels-Alder reactions of such acetylene derivatives with tetraarylcyclopentadienones (e.g. **4**).^[50] However, the oxidative coupling reaction^[50] is generally limited to the size of the product structure, since no quantitative dehydrogenation could be achieved for a C474 oligophenylene (ca. 4.8 nm) dendrimer.^[12b]



Scheme 11 Synthetic methods for the creation of oligophenylenes and their oxidative coupling to PAHs (R and R' = alkyl or aryl).

Such methods were further applied for the synthesis of graphene nanoribbons with defined edge structures, which are responsible for their physical properties.^[49b, 51] However, when such oxidative coupling conditions are applied to larger polycyclic aromatic systems, the radical cations are differently stabilized due to an inhomogeneous spin density distribution. Therefore, only the most reactive sites undergo oxidative coupling as it has exemplarily been shown for the intramolecular coupling of 1,1'-bipyrene and 4,4'-bipyrene (**5a** and **5b**,

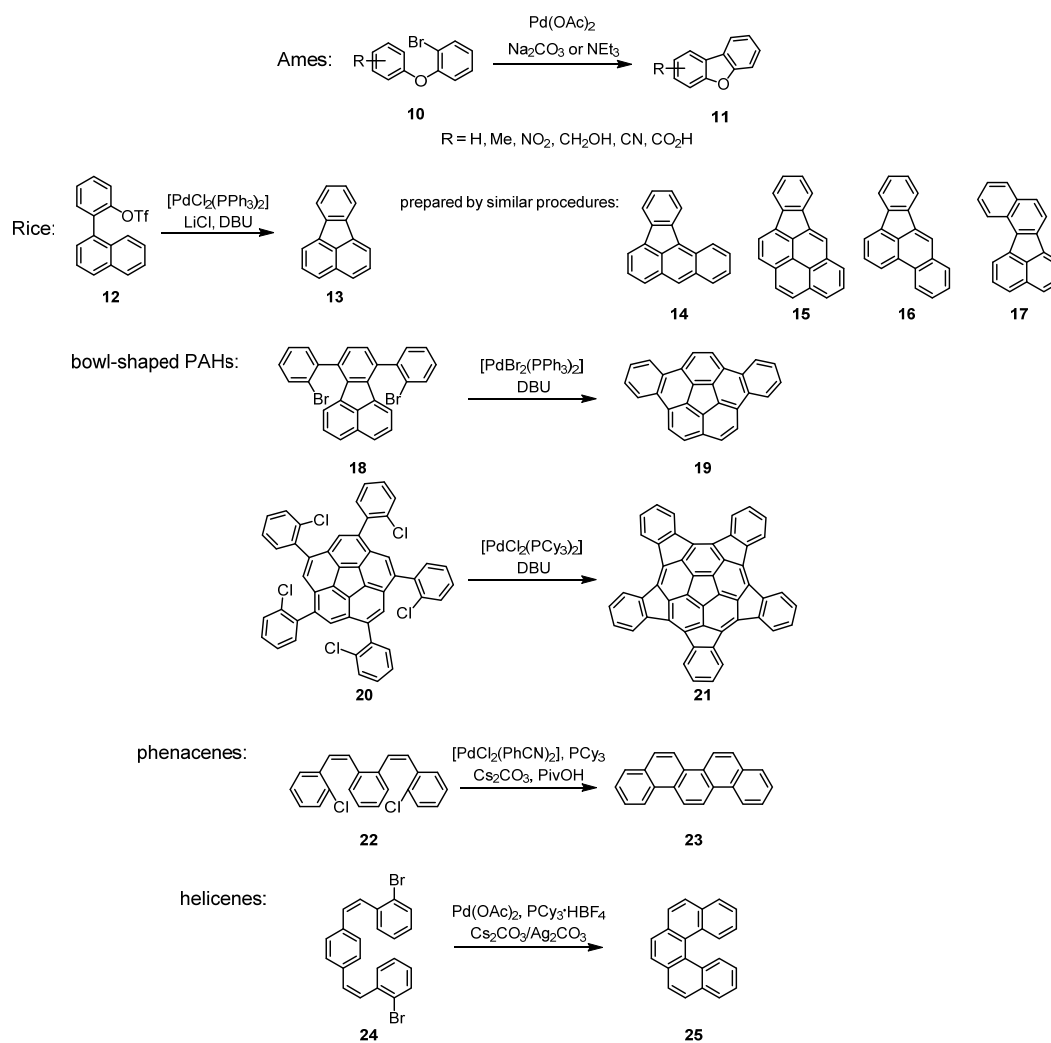
Scheme 12).^[52] Moreover, the position where C–C bond formation occurs can be influenced by the choice of Lewis acid/oxidant presumably due to different mechanisms for the oxidative coupling. For example, the intramolecular C–C coupling of 3-(1-naphthyl)perylene (**7**) in the presence of AlCl_3 at elevated temperatures leads to the six-membered terrylene **8**, whereas FeCl_3 at room temperature provides the five-membered benzo-[4,5]-indeno-[1,2,3-*cd*]-perylene **9**.^[53]



Scheme 12 Oxidative coupling of small sized PAHs.

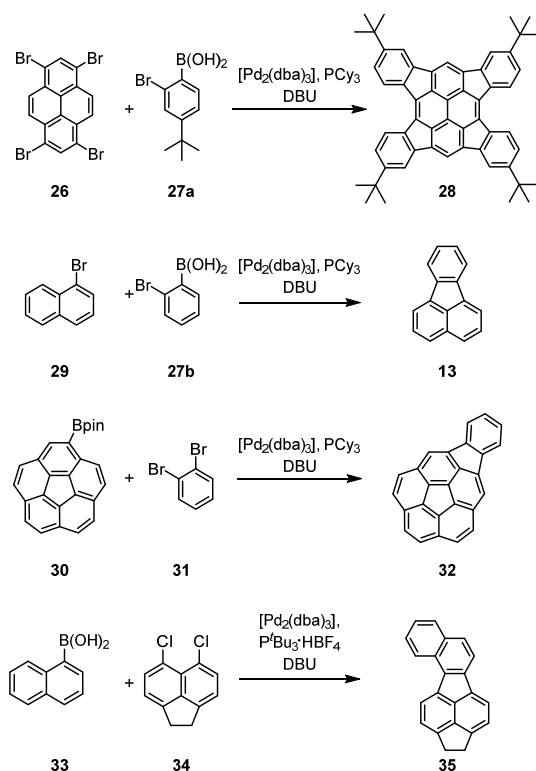
Intramolecular C–H arylation

One of the first examples for intramolecular C–H arylation by palladium-catalyzed dehydrohalogenation was reported by Ames and coworkers, who synthesized dibenzofurans (e.g. **11**) by dehydrohalogenation of 2-bromophenyl phenyl ethers and other diaryl-derivatives.^[54] The groups of Fagnou^[44, 55] and Echavarren^[56] spent much effort in the optimization and mechanistic elucidation of reactions yielding biaryls that are connected with different linkers. One of the first broad applications of intramolecular C–H arylation towards fully conjugated aromatic polycycles (**13–17**) was reported by Rice and coworkers in the early 90s.^[57] Since that time, this synthetic methodology has frequently been applied by different groups even for the construction of larger PAHs including fullerene fragments and other bowl-shaped PAHs (e.g. **19**, **21**) as well as phenacene- and helicene-type structures (e.g. **23**, **25**, see Scheme 13).^[56c, 58] Typically, Pd^{\square} complexes were used as the catalysts, sometimes in combination with additional phosphine ligands. Although the auxiliary base required for HX-elimination can be varied in many cases, carbonate bases and 1,8-diazabicyclo(5.4.0)undec-7-ene (DBU) seem to be most frequently used.



Scheme 13 Overview of some PAHs synthesized by intramolecular C–H arylation.

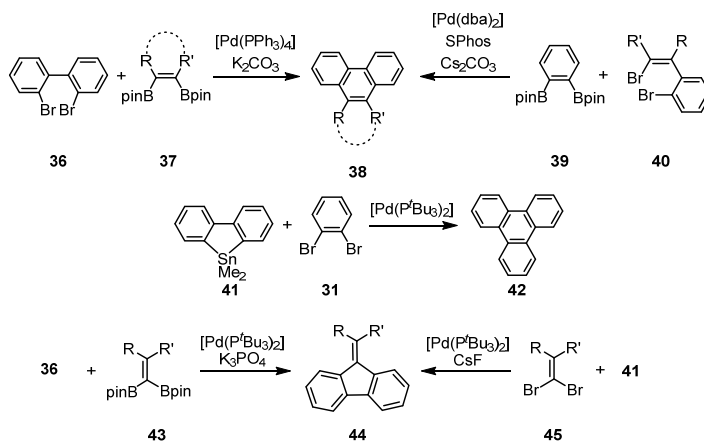
Moreover, this strategy has been combined with Suzuki-Miyaura cross-coupling to intermolecularly couple two aromatic units, followed by intramolecular cyclization *via* C–H arylation in a cascade reaction (Scheme 14). In such cases, Pd⁰ complexes with DBU as auxiliary base are usually applied to obtain the best results. Following this approach, tetraindenopyrene **28**, indenocorannulene **32** and fluoranthene-derivatives (**13**, **35**) could be prepared in one pot procedures.^[59] If this cascade reaction is utilized for the annulation of larger arenes than benzene, different isomers can principally be obtained, although only pentannulation was observed for the coupling of naphthalene-1-boronic acid **33** with 5,6-dichloro-1,2-dihydroacenaphthylene **34**.^[60]



Scheme 14 Synthesis of PAHs by cascade reactions including Suzuki-Miyaura cross-coupling and intramolecular C–H arylation.

Double cross-coupling

Regarding classical cross-coupling reactions for the fabrication of polycyclic aromatics, difunctionalized aromatic compounds (like **31**, **36** and **39**) are more valuable precursors for the construction of new extended π -conjugated polycyclic systems through double cross-coupling (Scheme 15). This coupling methodology includes Suzuki-Miyaura cross-coupling reactions with 1,2-diborylalkenes (e.g. **37**) and -arenes (e.g. **39**) to yield phenanthrene-type PAHs (e.g. **38**) as well as Stille or Negishi coupling reaction between cyclic stannanes, like 9-stannafluorenes (**41**), or organozinc compounds, with *ortho*-dihalogenated arenes (e.g. **31**).^[61]

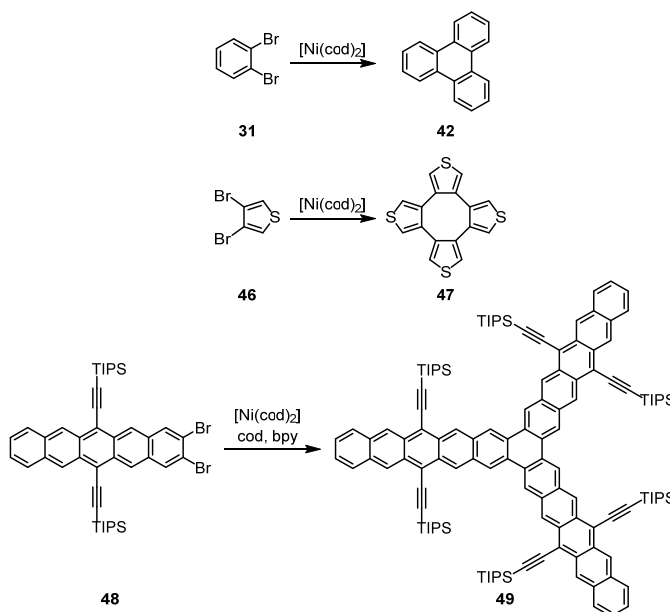


Scheme 15 Synthesis of PAHs by double cross-coupling reactions (R and R' = aryl).

Moreover, 1,1-diboryl- or 1,1-dibromoalkenes (e.g. **43** and **45**) can be coupled with cyclic stannanes or 2,2'-dibromobiaryls (e.g. **36**) to provide dibenzofulvenes (e.g. **44**).^[61]

Reductive coupling

Closely related to double cross-coupling reactions is the Ni-catalyzed Yamamoto-type coupling of *ortho*-dihaloarenes (e.g. **31**, **46**), which led to polycyclic aromatics like triphenylenes (**42**) and cyclic tetrathiophenes (**47**) (Scheme 16).^[62]

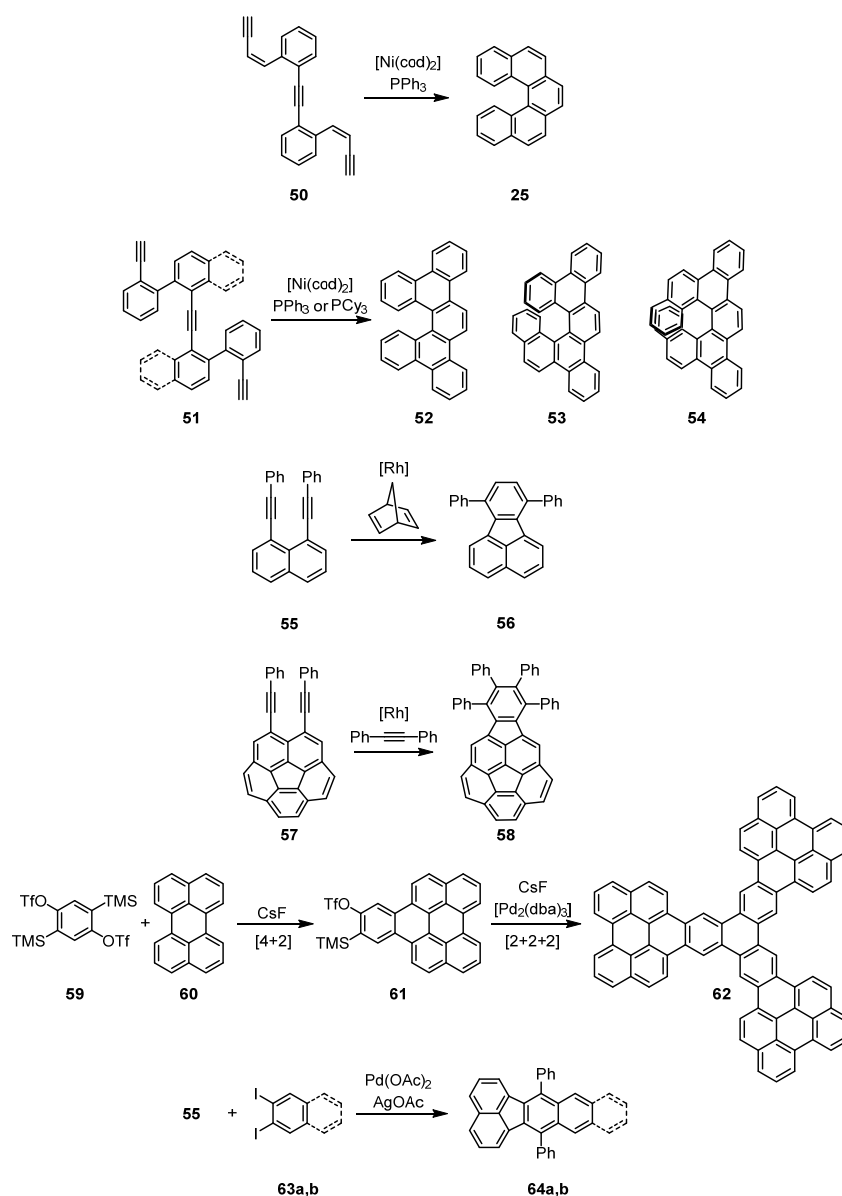


Scheme 16 Reductive Yamamoto-type coupling of *ortho*-dihaloarenes.

In 2014 the group of Bunz utilized this strategy and reported on unprecedented large starphenes (**49**) prepared by cyclotrimerization of *ortho*-dibromoacenes (**48**) under Yamamoto-type coupling conditions.^[63]

[4+2], [2+2+2] cycloadditions including arynes

Transition-metal-catalyzed [2+2+2] cycloadditions of acetylenes were developed around 1950 and became a useful synthetic tool for the fabrication of a broad variety of polycyclic aromatics (Scheme 17). Nickel-catalyzed cycloadditions of *cis,cis*-dienetriynes (e.g. **53** and **54**) provided access to helicenes (e.g. **25** and **52-54**) in excellent yields.^[64] The utilization of *peri*-diynes (e.g. **55** and **57**) as precursors for [2+2+2] cycloadditions was reported by Siegel and coworkers to synthesize different fluoranthene-derivatives (e.g. **56** and **58**).^[65] Moreover, arynes are valuable reactants for the synthesis of novel PAHs by [4+2] or [2+2+2] cycloadditions.^[66] They are typically generated in situ by fluoride induced elimination of TMS- and triflate-groups placed in *ortho*-position to each other (like **59**).

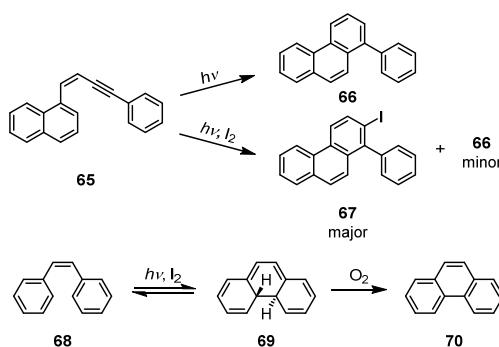


Scheme 17 Synthesis of PAHs by transition-metal-catalyzed cycloadditions.

Arynes can be coupled with acetylenes, dienes, aryl halides and other arynes, and therefore provide access to a wide range of different polycyclic structures. One example in which these different coupling types were combined in a stepwise [4+2] and [2+2+2] cycloaddition-procedure was reported only recently and is concerned with the synthesis of a C_3 -symmetrical extended triphenylene with three perylene subunits and 22 conjugated aromatic rings (**62**).^[67] However, also iodoarenes and *ortho*-diiodoarenes (e.g. **63**) are appropriate aryne precursors in the presence of palladium/silver catalysts. Applying such iodoarenes and *peri*-diynes like **55** in palladium-catalyzed cycloadditions, a series of benzo[*k*]fluoranthene-based linear acenes (e.g. **64**) was reported in 2010.^[68]

Photocyclization

Another strategy for the cyclization of alkynes is a photoinduced process. One of the first examples in which photocyclizations have been used to produce aromatic compounds is the photocyclization of hexadienyne to benzene and fulvene.^[69] Subsequently, Laroooven and coworkers reported on the photocyclization of 1,4-diarylbutenyne (e.g. **65**)^[70] and they could already demonstrate that the purely photochemical reaction cannot be trapped by the addition of radical or triplet scavengers, whereas the iodine mediated photocyclization leads to the halogenated derivative **67** with only minor amounts of the unhalogenated phenanthrene derivative (**66**) (Scheme 18). Therefore, the iodine mediated reaction most likely includes the formation of iodo-radicals that subsequently react with the acetylene subunit following a radical mechanism, whereas the purely photoinitiated reaction is proposed to proceed *via* a 1,5 H-shift after changing the acetylene configuration in the first excited state.^[71] Likewise, stilbene-like substrates (e.g. **68**) are appropriate precursors for various PAHs synthesized by Mallory-type photocyclizations where iodine acts as the catalyst.^[72]

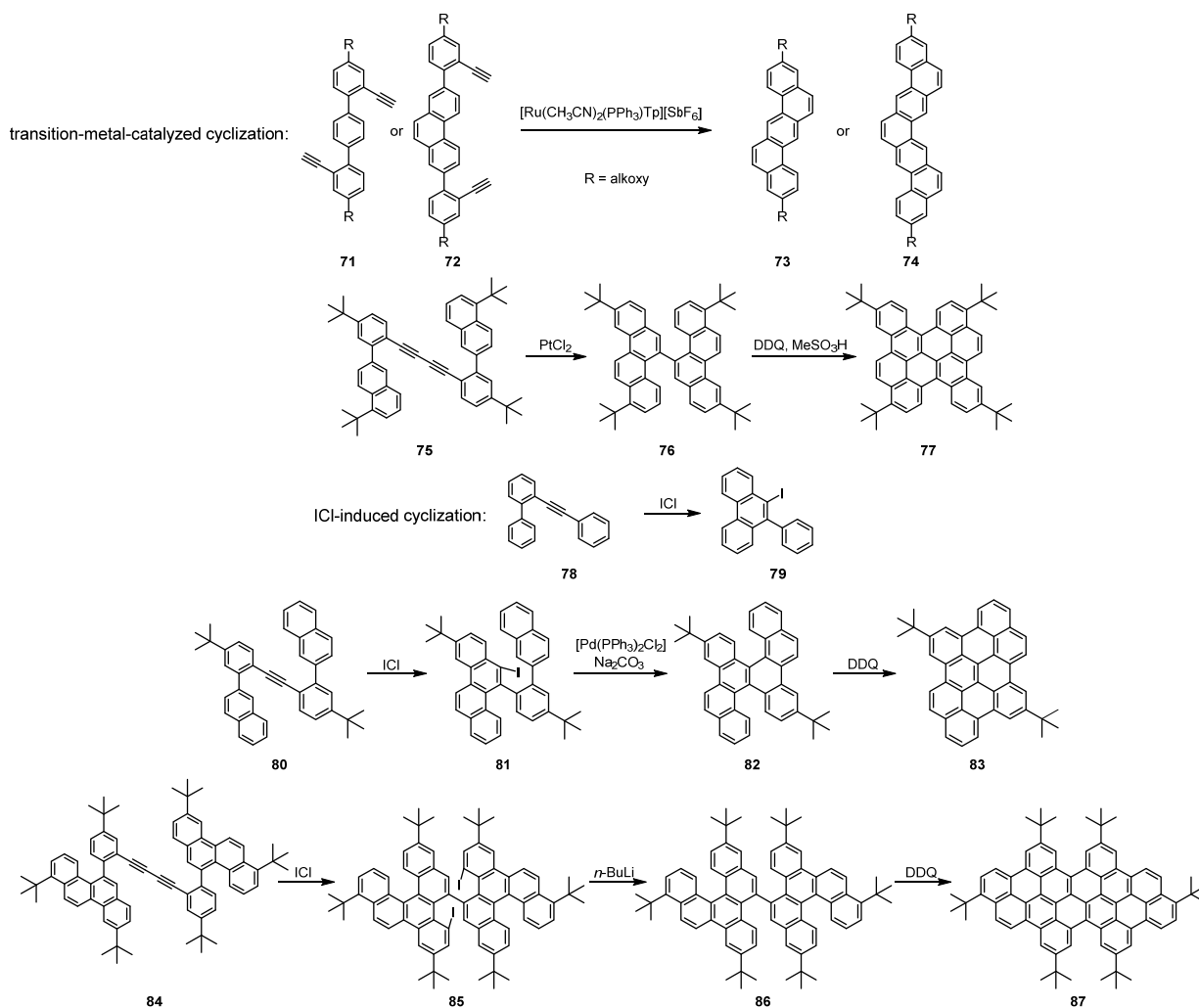


Scheme 18 Formation of PAHs by photocyclization.

Transition-metal-catalyzed electrophilic cycloaromatization of ortho-alkynylated biaryls & ICl induced cyclization

Besides the above mentioned synthetic methods, cyclization of *ortho*-alkynylated biaryl compounds (e.g. **71**, **72**, **78**) can either be achieved *via* transition-metal-catalyzed processes or by initiation with ICl leading to unfunctionalized (**73**, **74**) or iodinated PAHs (**79**) (Scheme 19). In case of transition-metal-catalyzed cyclizations, the C–C triple bond becomes activated in form of cationic intermediates by π -coordination of electron-deficient alkynes, which then act as electrophiles for the subsequent electrophilic aromatic substitution. Therefore, ruthenium- or palladium-catalyzed cyclization reactions are valuable methods for the construction of larger PAHs, which are easily accessible starting from diacetylene linked aromatic precursors (e.g. **75**). After transition-metal-catalyzed cycloaromatization (giving **76**) oxidative coupling has to take place to generate the completely π -conjugated system **77**.^[73]

Similarly, utilization of ICl induces the formation of electrophilic alkynes by iodonium ion formation and the subsequent electrophilic aromatic substitution provides access to iodinated arenes (e.g. **79**, **81**, **85**) which are themselves valuable precursors for further transformations.^[74] Therefore, such substrates can be used for intramolecular C–H arylation reactions followed by oxidative cyclization (like for **83**) or they can be dehalogenated using *n*-BuLi and oxidatively coupled to yield large PAHs (e.g. **87**).^[75]

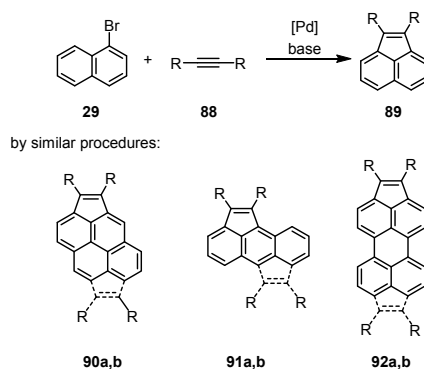


Scheme 19 Construction of PAHs by transition-metal-catalyzed or ICl-induced cyclization of *ortho*-alkynylated biaryls.

Intermolecular pentannulation by C–H/alkyne coupling & cascade alkyne annulation

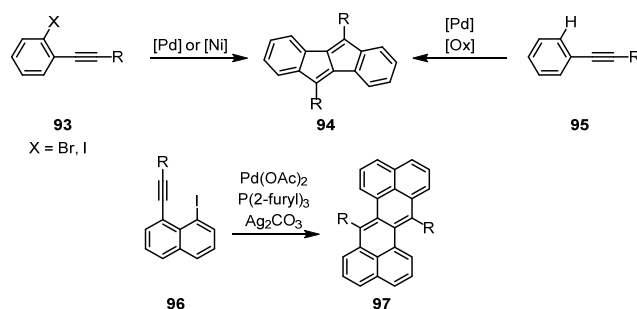
Transition-metal-catalyzed coupling reactions of halogenated aromatics (e.g. **29**) with alkynes (**88**) are another tool for the construction of new PAHs including systems bearing external five-membered cycles (e.g. **89**) which constitute fragments of fullerene and thus exhibit high electron affinities (Scheme 20). Such reactions have been developed by Grigg and coworkers in the 1990s^[76] and include Heck-type carbopalladation of the alkyne by insertion of the Pd-alkene bond into an aromatic double bond followed by β -hydride elimination.^[77] Likewise, the group of Müllen applied this reaction sequence to a variety of

mono- and dihalogenated pyrenes, perylenes and anthracenes and isolated the corresponding mono- and di-cyclopentannulated products (**90-92**).^[78] Despite the structural similarity of these systems, they have proposed an alternative mechanism for the second step of the catalytic cycle that is an intramolecular electrophilic attack of the arene by the alkenylpalladium intermediate followed by reductive elimination.



Scheme 20 Synthesis of PAHs by intermolecular pentannulation reactions (R = (hetero)aryl or alkyl).

Moreover, such alkyne arylations have been used in nickel- and palladium-catalyzed homocoupling cascade reactions of *ortho*-halogenated arylacetylenes (e.g. **93**) to produce a variety of dibenzopentalene derivatives such as **94** (Scheme 21).^[79] Similarly, zethrenes like **97** can be prepared starting from 1-ethynyl-8-iodonaphthalenes (**96**)^[80] and even unactivated arylacetylenes (e.g. **95**) can be converted into dibenzopentalenes using PdCl₂ as the catalyst, AgOTf as an additive and *o*-chloranil as the oxidant.^[81] Furthermore, unsymmetrical substituted derivatives could be prepared following similar procedures.^[82]



Scheme 21 Synthesis of PAHs by Pd- or Ni-catalyzed cascade alkyne annulations (R = H or aryl).

2.2 Polycyclic Aromatic Dicarboximides

2.2.1 Introduction

In this thesis polycyclic aromatic dicarboximides (PADIs) are defined as polycyclic aromatic hydrocarbons bearing cyclic dicarboximide structural motives. Dependent on the position of the two carbonyl groups with respect to each other different types of polycyclic aromatic dicarboximides can be distinguished. The arrangement of the two carbonyl functions in *ortho*-position to each other leads to cyclic five-membered imides whereas the attachment of two carbonyl groups in *peri*-position on a naphthalene core gives six-membered dicarboximides. Therefore, the smallest polycyclic aromatic dicarboximides are naphthalene dicarboximides (shortened naphthalimides). The molecular structures of the three different isomers, each showing distinct molecular properties, are shown in Chart 1.

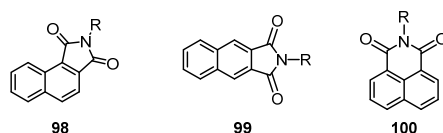


Chart 1 Molecular structures of naphthalimides (R = H, alkyl or aryl).

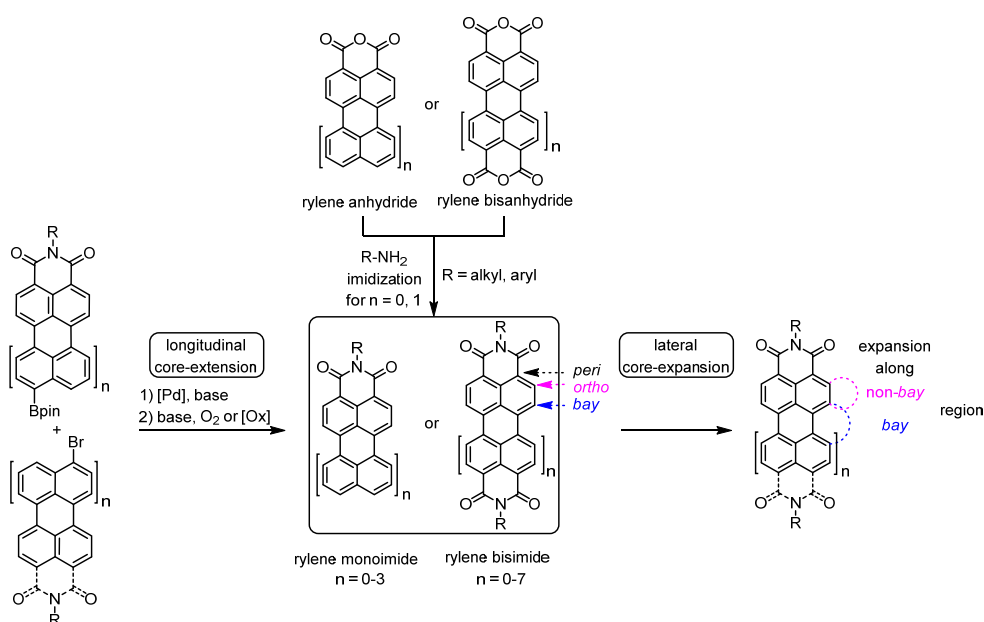
In general, the attachment of electron-withdrawing dicarboximide groups to aromatic polycycles leads to an extension of the π -scaffold and lowers the frontier molecular orbital energies. As a consequence, most polycyclic aromatic dicarboximides exhibit bathochromically shifted absorption and emission maxima compared with the parent PAHs and their electron-poor character leads to their application as n-type semiconductors in some cases.^[13, 83] Moreover, aromatic imides exhibit high thermal and chemical resistance and are stable towards photo-oxidative degradation. Whereas the cyclic five-membered imides attracted less attention, the six-membered aromatic imides are explored in great detail. This is probably due to the industrial production of 1,8:4,5-naphthalene tetracarboxylic acid bisanhydride and 3,4:9,10-perylene tetracarboxylic acid bisanhydride,^[84] which are universal precursors for the construction of naphthalene and perylene bisimides (NBIs, PBIs). These chromophores are by far the most extensively studied class of aromatic imides and can easily be obtained by condensation with numerous aryl- and alkylamines.^[13b, 83a, 85] While the imide-substituents have a major influence on the solubility and the aggregation/packing behaviour, the introduction of electron-donating or -withdrawing substituents at the aromatic core enables a fine-tuning of the electronic and optical properties.^[13b, 85-86]

This chapter will summarize recent progress in the synthesis of dicarboximide-functionalized PAHs focusing on synthetic methods that involve C–C coupling reactions.

2.2.2 Polycyclic Aromatics containing Six-Membered Dicarboximides

2.2.2.1 The Class of Rylene Imides

Rylene mono- and bisimides consist of fused naphthalene subunits that are linked *via* the *peri*-positions and bear terminal dicarboximide groups, which exert an electron-withdrawing effect on the aromatic core.^[13b, 86-87] Rylene bisimides are among the most intensively studied classes of π -conjugated dyes since more than one century due to their extraordinary properties such as intense and tuneable absorption and emission (ranging from the ultra-violet to near-infrared spectral region), adjustable frontier molecular orbital energies, reversible reduction processes as well as high thermal and photochemical stability, which enable their application as electron-acceptor materials in (opto)electronic devices.^[13, 83, 88] The parent rylene dyes like naphthalene^[13d, 83a] and perylene mono- and bisimides^[13b] can easily be synthesized by imidization of the corresponding anhydrides, a procedure that is known since their discovery as industrial pigments around 1913.^[89] In contrast, higher rylene imides are typically synthesized by cross-coupling of naphthalene and/or perylene moieties followed by intramolecular oxidative coupling under basic conditions or with the help of Lewis acids/oxidants like FeCl_3 (see Scheme 22).^[87]



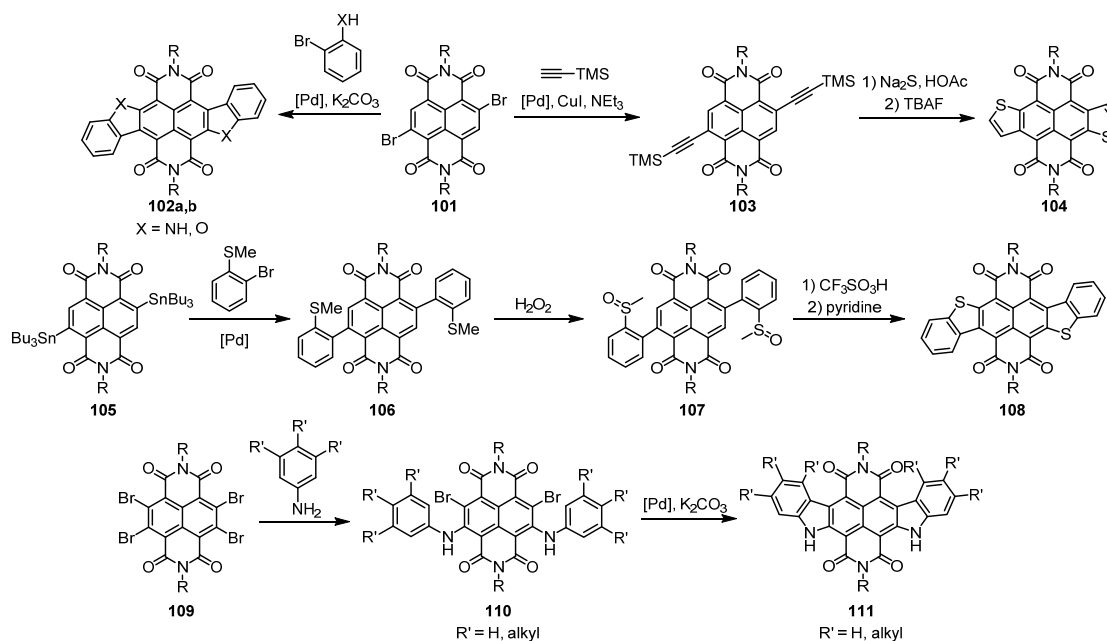
Scheme 22 Concepts for core-enlargement of rylene imides in longitudinal or lateral direction.

On the following pages the synthetic concepts for core-expansion of rylene mono- and bisimides will be discussed focusing on the expansion of the parent rylene-core along lateral direction.

Synthetic Concepts towards Core-Expanded Rylene Imides

Naphthalene imides

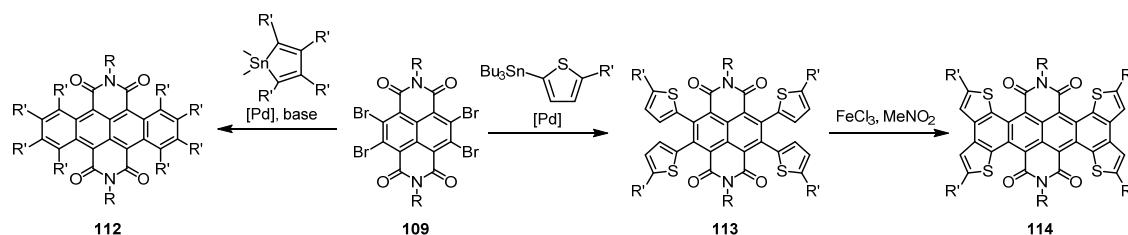
The expansion of the smallest representative of this class of dyes gained substantial attention after the development of direct halogenation procedures of naphthalene bisimides, that are extremely valuable precursors (like **101** and **109**) for a large variety of C–C coupling methods. Therefore, synthetic approaches towards laterally expanded NBIs became available only during the last 20 years.^[83a] Frequently applied strategies include transition-metal-catalyzed cross-coupling reactions in combination with various cyclization techniques (Scheme 23). For instance, the Sonogashira coupling of 2,6-dibromonaphthalene bisimide **101** with trimethylsilylacetylene leads to a bisacetylene-functionalized NBI (**103**), which can be cyclized by the use of highly nucleophilic Na₂S followed by oxidative rearomatization yielding the thieno-functionalized NBI **104**.^[90] Another approach towards thio-functionalized heteroaromatic derivatives was described by the group of Wang who introduced thioanisole substituents *via* Stille coupling into the NBI core (to **106**) followed by oxidation (**107**) and subsequent intramolecular ring closure in the presence of trifluoromethanesulfonic acid and phosphorous pentoxide and final demethylation (**108**).^[91] The heteroaromatic nitrogen- and oxygen-analogues **102a,b** were realized by nucleophilic substitution of 2,6-dibromonaphthalene bisimide **101** with 2-bromoaniline or 2-bromophenol followed by intramolecular C–H arylation in a one-pot procedure.^[92] The 2,7-isomeric diindole-annulated NBI (**111**) could be obtained by sequential nucleophilic substitution of tetrabromo-NBI **109** followed by palladium-catalyzed C–H arylation.^[92b]



Scheme 23 Synthetic concepts for heteroatom containing core-expanded NBIs (R = alkyl or aryl).

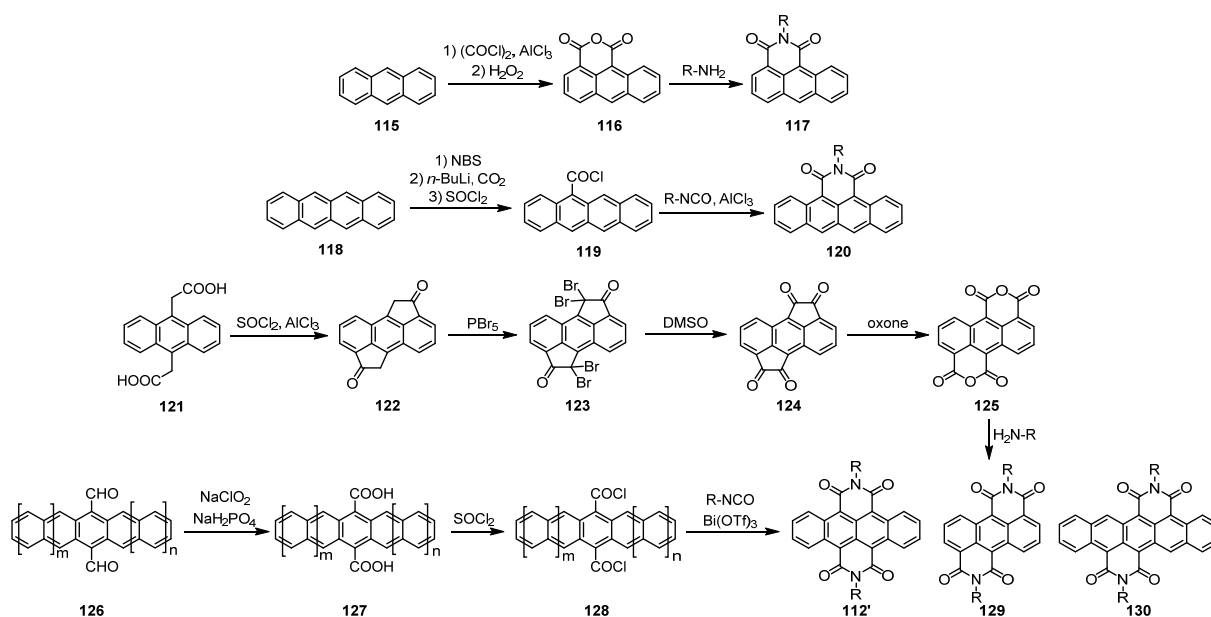
All these heteroatom containing core expanded NBIs exhibit good performance in electronic devices as n- or p-type semiconducting materials due to the expansion of the π -surface and the concomitant tuning of the frontier molecular orbitals.

Core-expanded NBIs with acene-type core structures were prepared by Stille cross-coupling of tetrabromonaphthalene bisimide **109** with different organostannanes as illustrated in Scheme 24. Cyclization can either be achieved by oxidative coupling in the presence of Fe^{\square} (to **114**) or by utilization of cyclic organotin compounds (to **112**).^[93] Such tetracene bisimides exhibit comparatively low band gaps giving rise to absorption in the near-infrared spectral region and ambipolar charge transport.



Scheme 24 Synthetic access to acene-type bisimides by C–C coupling reactions (R = alkyl, R' = alkyl or aryl).

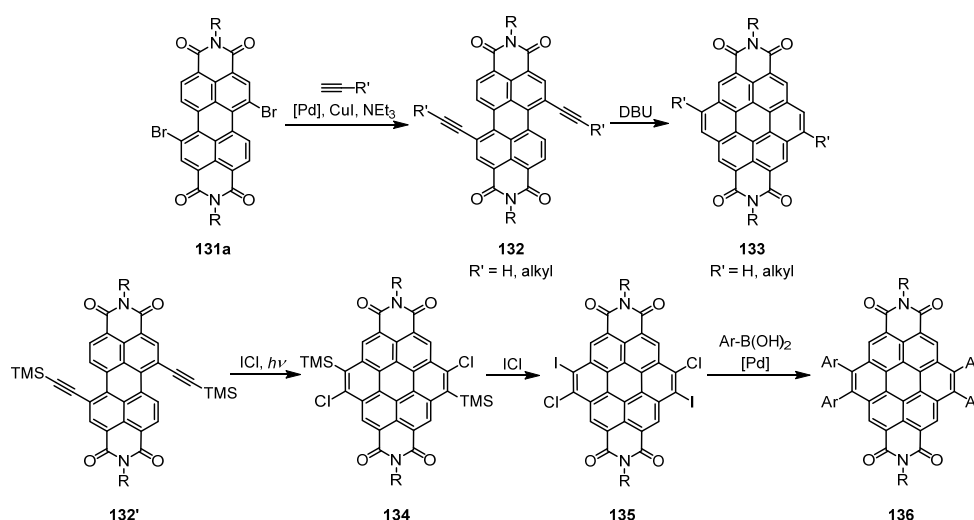
Another strategy to obtain aromatic imides with acene-type core structures is the chemical modification of the parent unfunctionalized hydrocarbons (e.g. **115**, **118**; see Scheme 25). The synthesis of acene monoimides **117** and **120** was realized by carboxylation of anthracene or tetracene followed by oxidation (e.g. **116**) and imidization (e.g. **117**) or by formation of an acyl chloride (e.g. **119**) and Lewis-acid mediated cyclization with an isocyanate (e.g. **120**).^[94] Similar approaches were reported for various acene bisimides (e.g. **112'**, **129** and **130**) which can be applied as n-type semiconducting materials in OFETs.^[95]



Scheme 25 Synthetic access to acene-type imides and bisimides (R = H or alkyl).

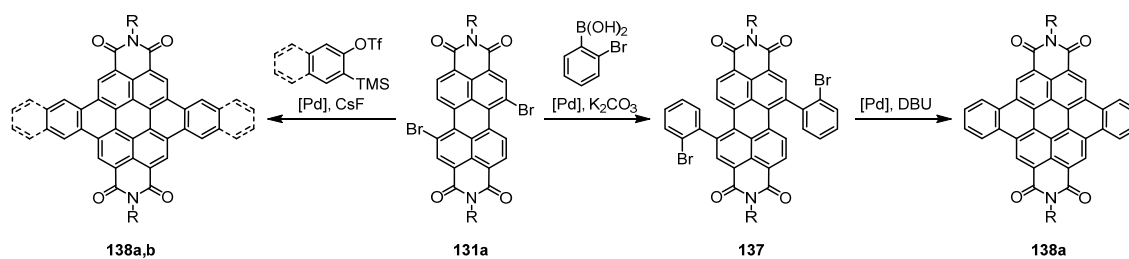
Perylene imides

Similar to the core-expansion of naphthalene imides, the key building blocks for the lateral core-expansion of perylene imides along the *bay*-area are halogenated derivatives like 1,7-dibromoperylene bisimides (**131a**), which can be obtained by bromination of the perylene bisanhydride under acidic conditions followed by imidization.^[96] One of the first attempts of core-expansion was reported by the group of Müllen, who developed coronene imides (e.g. **133**) as a new class of dyes by Sonogashira coupling of brominated perylene imides with alkynes and subsequent cyclization using the strong nonnucleophilic base DBU (Scheme 26).^[96a, 97] Later on the group of Zhao reported on another cyclization methodology for alkynylated PBIs (**132'**) where ICl is used as initiator for the cyclization reaction. The main advantage of this strategy is the simultaneous introduction of halogen atoms (e.g. **134**, **135**) that can be further functionalized by the introduction of aromatic substituents (e.g. **136**)^[98] or electron-withdrawing chloro and cyano groups as desired for the application as n-type semiconductors.^[99]



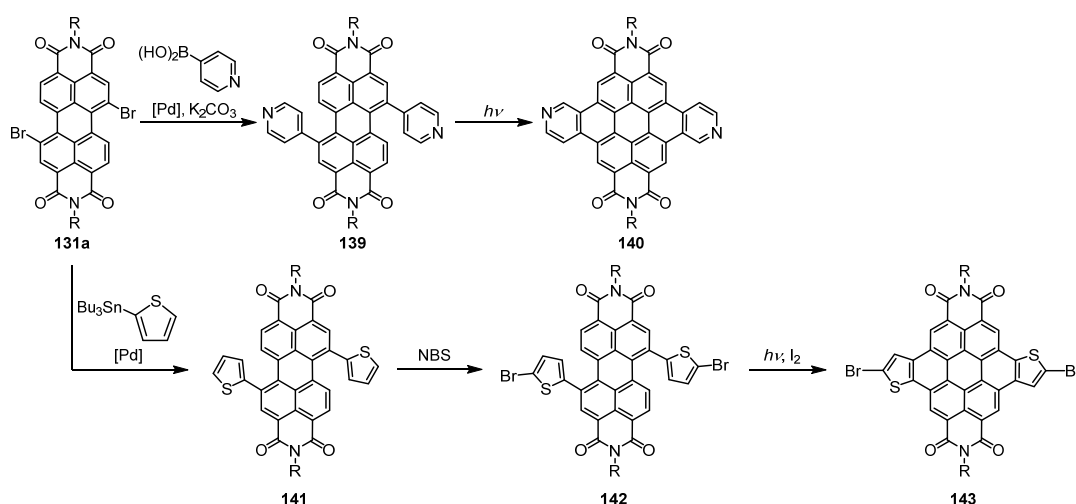
Scheme 26 Synthetic procedures for the construction of coronene bisimides (R = alkyl or aryl).

Another approach towards core-expanded PBIs involves Suzuki-Miyaura cross-coupling between 1,7-dibromoperylene bisimide (**131a**) and 2-bromophenylboronic acid followed by Pd-catalyzed dehydrohalogenation in the presence of DBU (see Scheme 27).^[100] The same dibenzocoronene bisimide **138a** can be obtained by palladium-catalyzed benzannulation of 1,7-dibromoperylene bisimide with 2-(trimethylsilyl)phenyl trifluoromethanesulfonate that is a valuable precursor for in situ generated benzyne.^[100b] This synthetic method benefits from a one-pot reaction procedure, which results in increased yields and a reduced amount of side products. Moreover, this strategy has been proven to be applicable for the annulation of naphthalene moieties to the *bay*-region of PBIs (**138b**).^[101]



Scheme 27 Core extension along the *bay*-region of PBIs (R = alkyl or aryl).

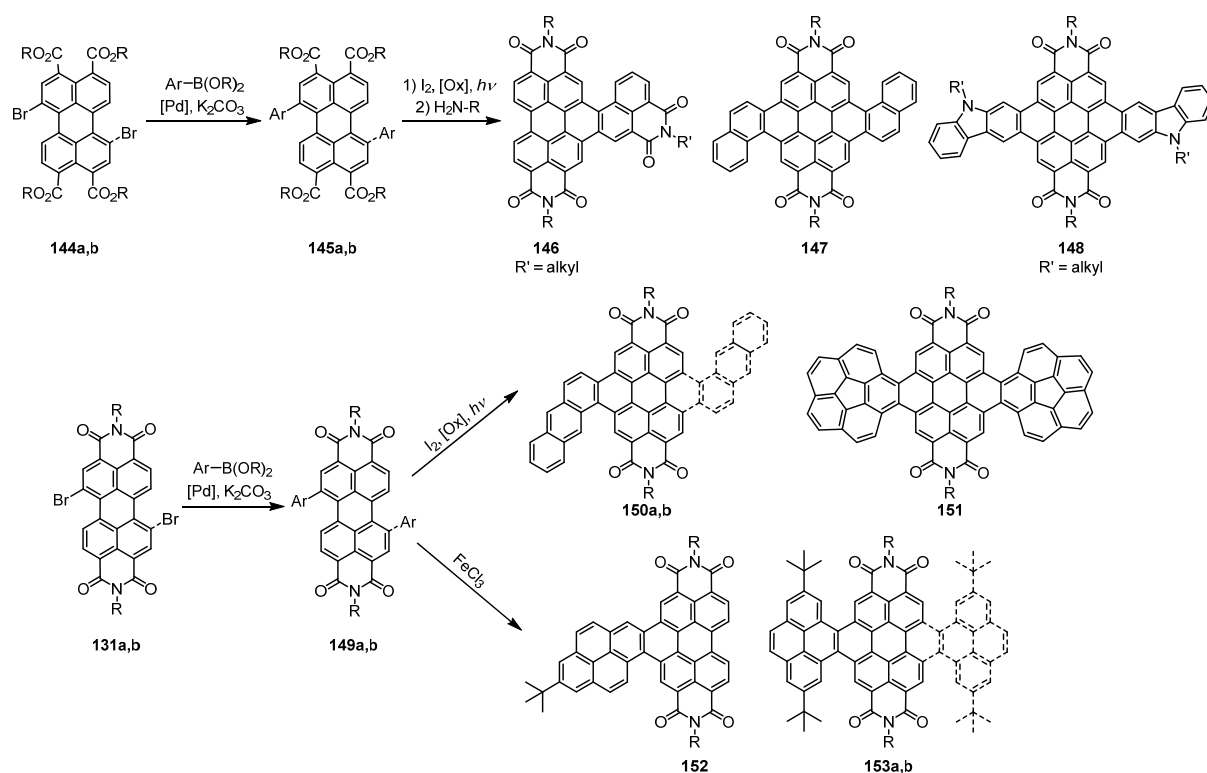
Furthermore, Wang and Facchetti reported on the cyclization of pyridine and thiophene functionalized PBIs providing access to heteroaromatic dipyrindylcoronene bisimides (e.g. **140**)^[102] and dithienocoronene bisimides (e.g. **143**).^[103] After introduction of thiophene or pyridine substituents at the PBI core by Suzuki-Miyaura or Stille cross-coupling, cyclization can be achieved in a photoinduced reaction (see Scheme 28). Introduction of bromine-substituents on the thiophene moieties prior to ring annulation facilitates further functionalization by cross-coupling reactions giving rise to a variety of donor-acceptor copolymers that were successfully implemented as organic semiconducting materials in thin film transistor and solar cell devices.^[103-104]



Scheme 28 Synthetic strategies for the preparation of dipyrindyl- and dithienocoronene bisimides (R = alkyl or aryl).

Similarly, several core-expanded PBIs were synthesized by palladium-catalyzed cross-coupling reactions followed by photoinduced oxidative cyclization (Scheme 29). For the preparation of some of these materials, the less electron-poor perylene tetraester derivatives (**144a,b**) were used as coupling components facilitating rearomatization under oxidative conditions.^[105] Therefore, this strategy can be applied for a broad variety of substrates including electron-rich and electron-poor precursors. Besides photocyclization, FeCl₃ could be used for the oxidative core-annulation of pyrenyl-substituted PBIs (e.g. **152**, **153a,b**).^[106] By introducing long alkyl chains at the imide positions of distorted and core-expanded

perylene bisimides liquid crystalline phases could be obtained for compound **146** that can be applied in organic electronic devices.^[105a] The annulation of PBIs to electron-rich aromatic subunits like carbazoles (**148**) provides access to new chromophores with intramolecular charge transfer properties giving rise to enhanced nonlinear optical properties.^[105c] In general, the enlargement of the PBI core along the *bay*-area leads to molecules with enhanced π - π interactions, high electron-accepting abilities and small HOMO-LUMO gaps, making them promising electron-acceptor materials for organic electronics.^[107]



Scheme 29 Synthesis of core-extended PBIs by combining Suzuki-Miyaura cross-coupling with photoinduced or oxidative cyclization (a = 1,7-disubstituted derivative, b = 1-monosubstituted derivative, R = alkyl or aryl).

Moreover, this synthetic strategy has been applied for the introduction of *ortho*-phenylenediamine (e.g. **154**) and pyrazine derivatives (e.g. **156**), which can further be transformed into pyrazine-type (e.g. **155**) and pyrazino[2,3-*b*]pyrazine structural motives (e.g. **157**) leading to new heteroaromatic systems (Chart 2).^[108] Interestingly, compound **157** contains 13 linearly fused aromatic six-membered rings, constituting the largest stable heteroacene synthesized so far.^[108b]

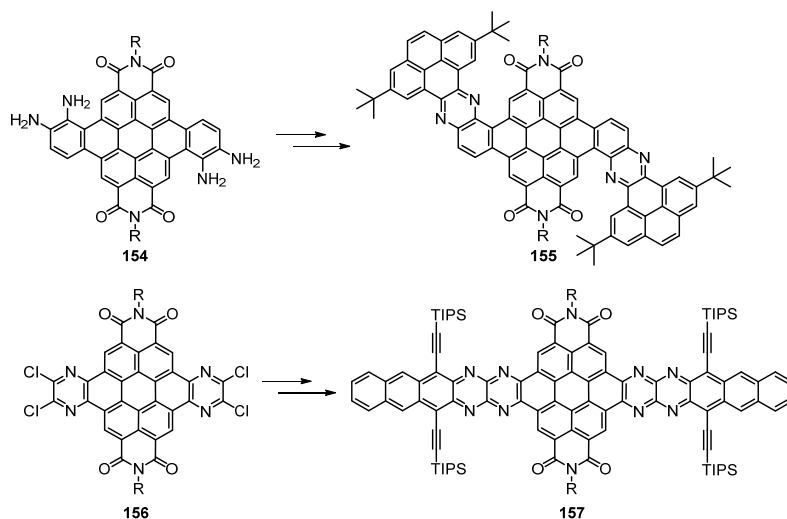


Chart 2 Pyrazine- and pyrazino[2,3-*b*]pyrazine annulated PBIs (R = alkyl or aryl).

The coupling of monobrominated PBIs (e.g. **131b**) with di- or trifunctionalized aromatic hydrocarbons leads to a large diversity of extended π -conjugated systems containing multiple dicarboximide groups, which are desirable in the field of organic semiconductors and organic photovoltaics.^[15a, c, 105c, 109] While plenty of such PBI dimers or trimers (see Chart 3) were synthesized by the preciously described sequential cross-coupling – photocyclization process, compound **158** has been prepared by a multiple-step procedure that includes Sonogashira-coupling of a diethynylterphenylene derivative with two monobrominated PBIs followed by ICl-mediated intramolecular cyclization of the linker-moiety and subsequent dehalogenation and photocyclization.^[109] Wasielewski and Marks demonstrated that the introduction of π -conjugated spacer units between two PBIs can improve the performance of organic solar cells due to an increased electron mobility. However, planar PBI-dimers (e.g. **159a**) exhibit a reduced efficiency due to the formation of crystalline films and excimers in contrast to core-twisted systems (e.g. **159b**), which remain amorphous in thin films.^[15c] The group of Nuckolls reported on the synthesis of helicene derivatives composed of two PBIs linked by acene spacer units (**160** and **161**) and investigated their electronic delocalization. While the naphthalene fused helicene is resistant to racemization and characterized by a strong through space electronic communication due to overlapping π -orbitals, the anthracene fused derivative exhibits larger π - π -distance between the PBI-cores resulting in a reduced electronic interaction.^[15a] Another recent study is concerned with the synthesis and the electronic properties of propeller like PBI-trimers (**162**), which were likewise obtained by cross-coupling of brominated PBI precursors to a trifunctionalized benzene unit, followed by photocyclization. Due to their high molar absorptivities, high electron mobilities and good thin film morphology, these materials exhibit high PCEs of up to 8.3 % in solar cells with

PDBT-T1 (a wide band-gap copolymer) as donor material, which are among the highest values reported so far for solar cells based on PBI-acceptors.^[15d] Another PBI-trimer (**163**) fused by a central truxene-moiety was reported by the group of Qu.^[110] In contrast to **162**, this star shaped multichromophoric system exhibits a nearly planar structure with a high photostability and interesting two-photon absorption properties.

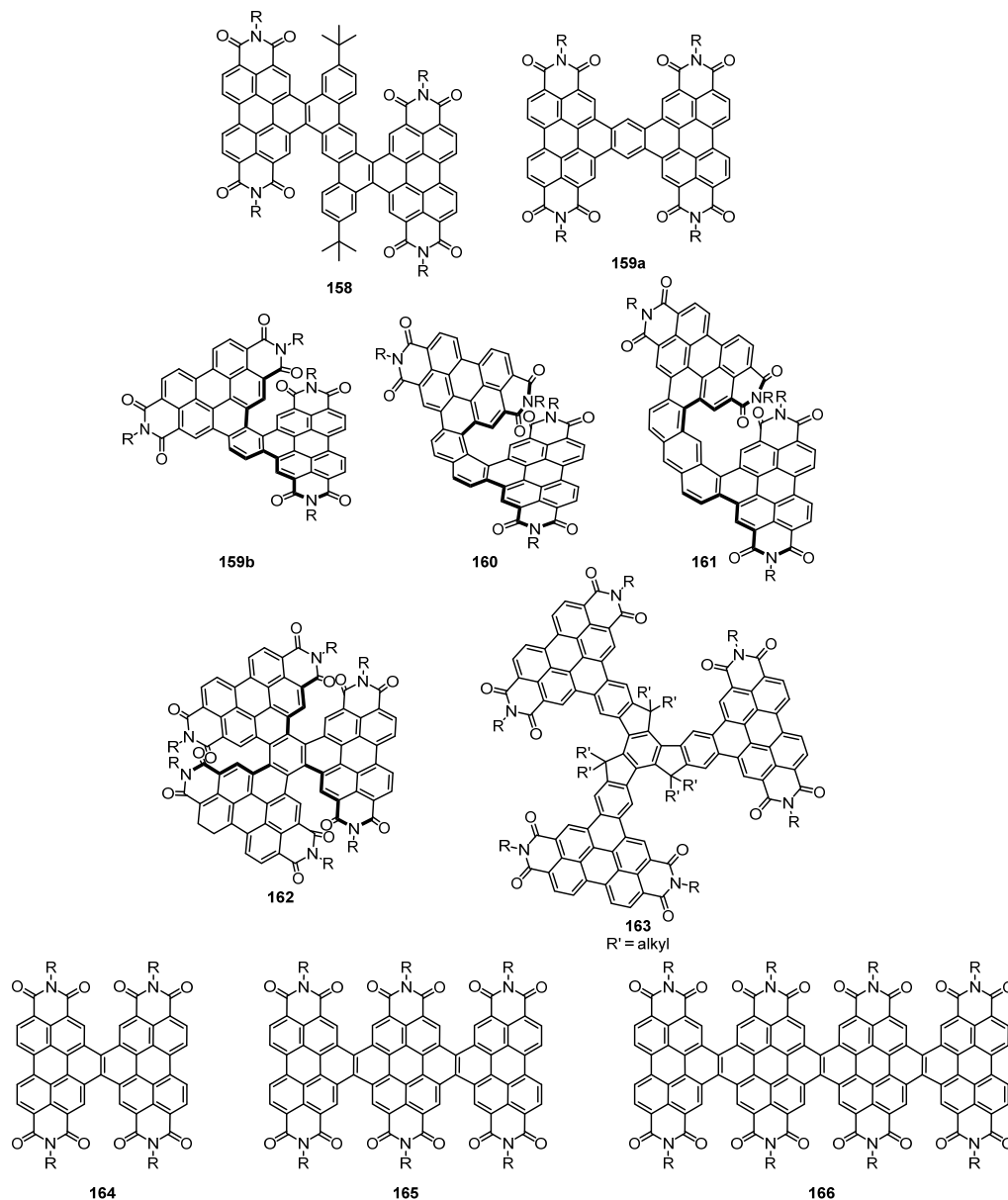
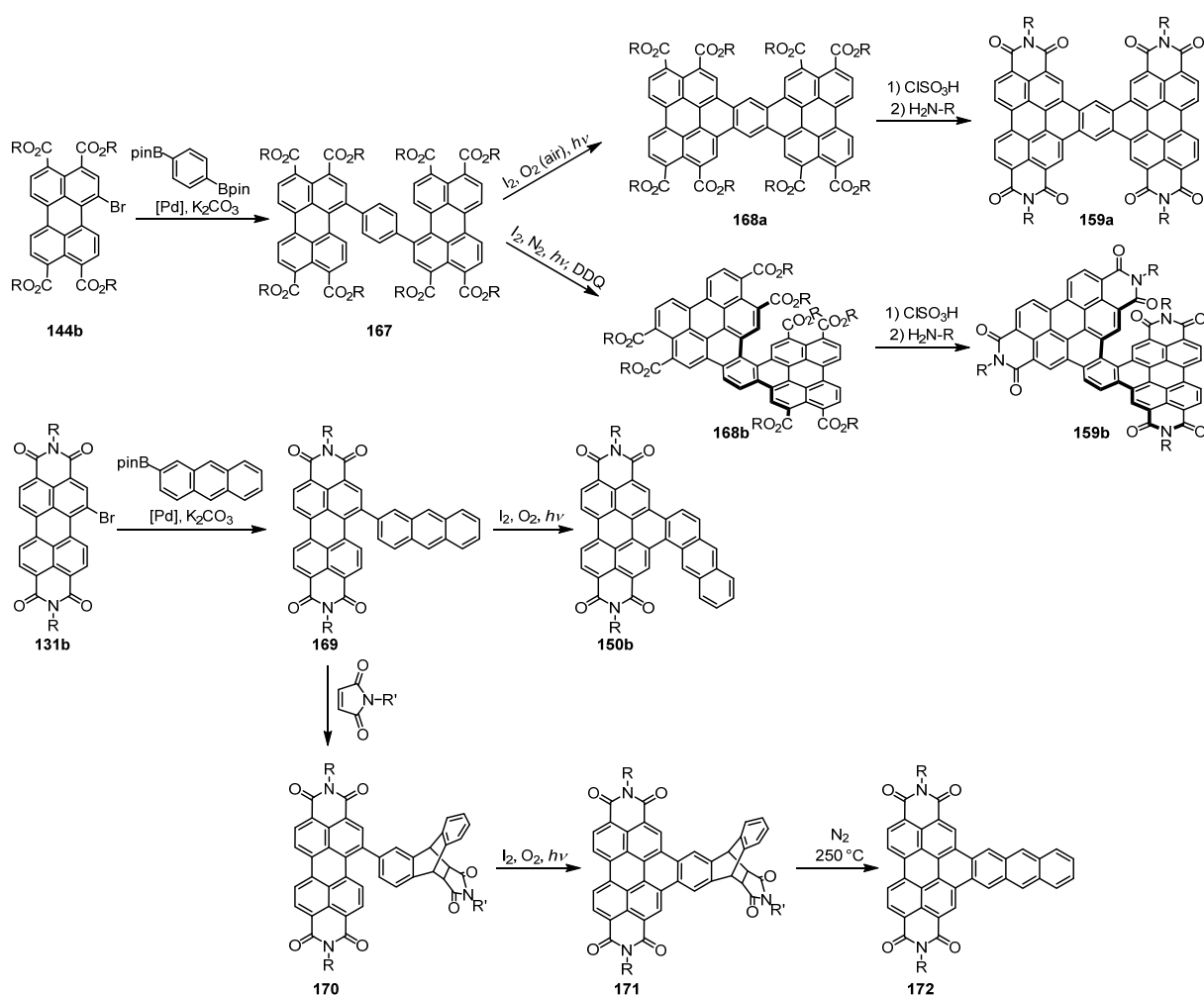


Chart 3 PAHs containing multiple dicarboximide groups synthesized by linking PBIs (R = alkyl or aryl) to different π -conjugated bridges.

PBI dimers fused by simple vinylene bridges (e.g. **164**) were already reported in 2012 by the group of Wang and are characterized by distorted π -scaffolds due to spatial proximity of neighbouring imide groups.^[111] Whereas the original synthetic procedure included ICl induced cyclization of a ethynylene bridged PBI dimer followed by Heck-type intramolecular cyclization, the corresponding PBI trimer and tetramer (**165**, **166**) containing the same

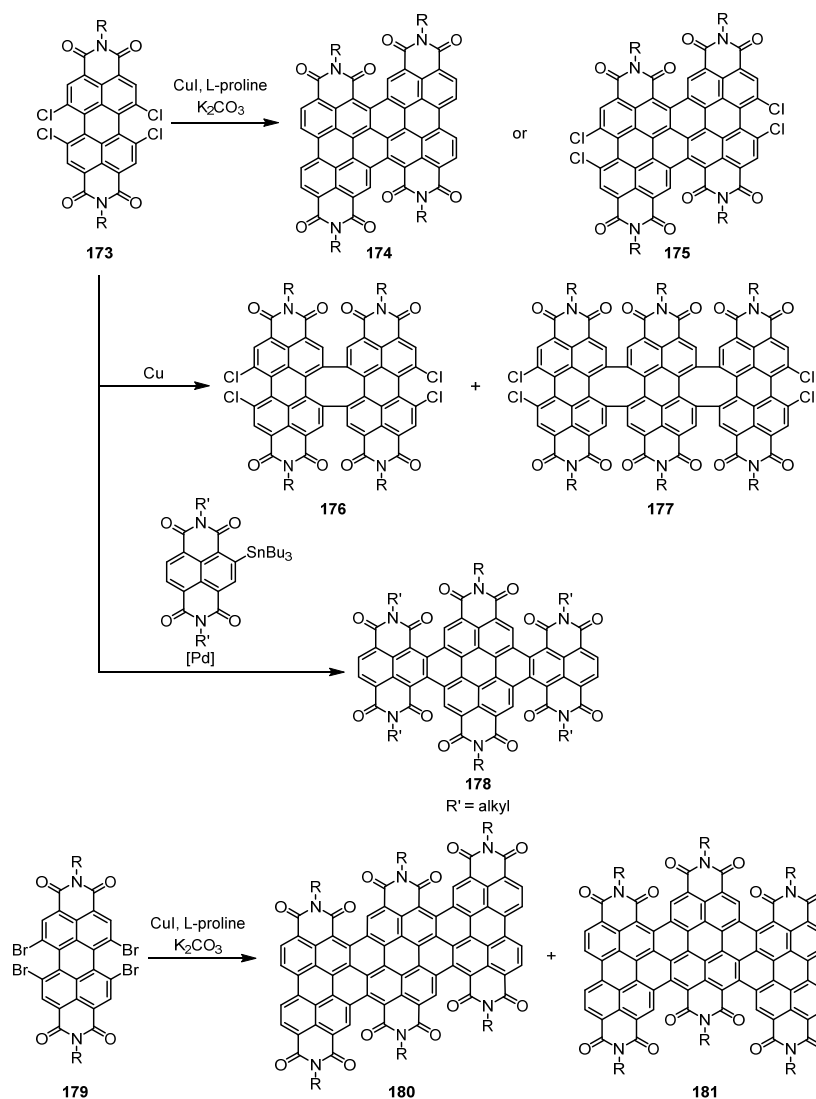
structural motives were prepared to years later by the group of Nuckolls by photocyclization of ethenylene bridged precursors.^[15b, 112] Due to the distortion of the individual PBI subunits and the good semiconducting properties this class of compounds exhibits high efficiencies in organic photovoltaics.

Most interestingly, for some photoinduced cyclization reactions a high regioselectivity could be achieved, that can be controlled by variation of the reaction conditions or the introduction of protecting groups (Scheme 30). For instance, the photocyclization and subsequent imidization of compound **167** in the presence of oxygen leads to a linear planar structure (**159a** and **168a**), whereas the same reaction under an atmosphere of nitrogen in the presence of DDQ as oxidant leads to an angularly distorted structure (**159b** and **168b**).^[15c] Likewise, by introducing the bulky maleimide protecting group into the anthracene substituent of **169** by Diels-Alder reaction (**170**), the linearly annulated derivative **172** could be obtained by photocyclization and retro-Diels-Alder reaction, whereas direct photocyclization leads to the angularly annulated isomer **150b**.^[107b]



Scheme 30 Synthetic strategies for regioselective photocyclization towards core-expanded PBIs (R = alkyl or aryl).

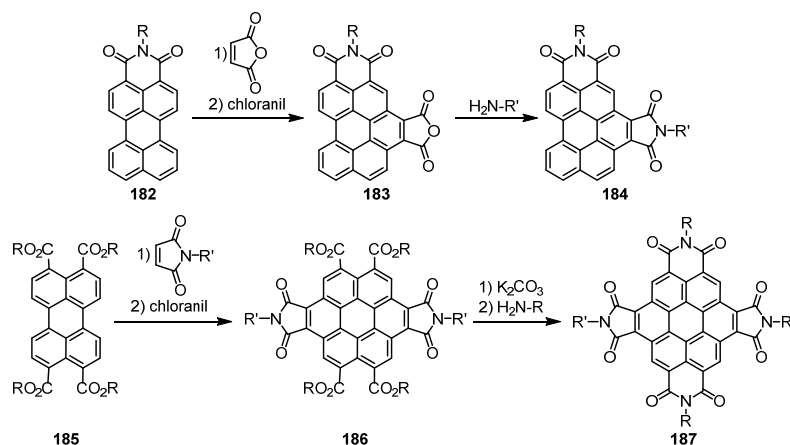
Another interesting class of large-sized polycyclic aromatic hydrocarbons containing multiple dicarboximide groups are rylene bisimide oligomers directly fused *via* the *bay*- and *ortho*-positions that were developed in the group of Wang (Scheme 31). Dependent on the applied temperature, homo-coupling of tetrachloro-substituted PBI (**173**) in the presence of CuI, L-proline and K_2CO_3 affords tetrachloro-substituted PBI-dimer **174** or the respective dehalogenated dimer **175**.^[14b] By replacing the chloro by more reactive bromo substituents (**179**), perylene bisimide trimers (**180** and **181**) can be prepared following the same synthetic strategy. Since the annulation of the second PBI can take place at different positions of the PBI-core, two structural isomers are formed that can be separated by HPLC. Due to steric congestions between the carbonyl oxygen atoms and the adjacent hydrogen atoms, the PBI subunits of trimers **180** and **181** are torsionally twisted against each other giving rise to a helical and non-helical conformer.^[14a]



Scheme 31 Direct annulation of rylene bisimides reported by the group of Wang (R = alkyl or aryl).

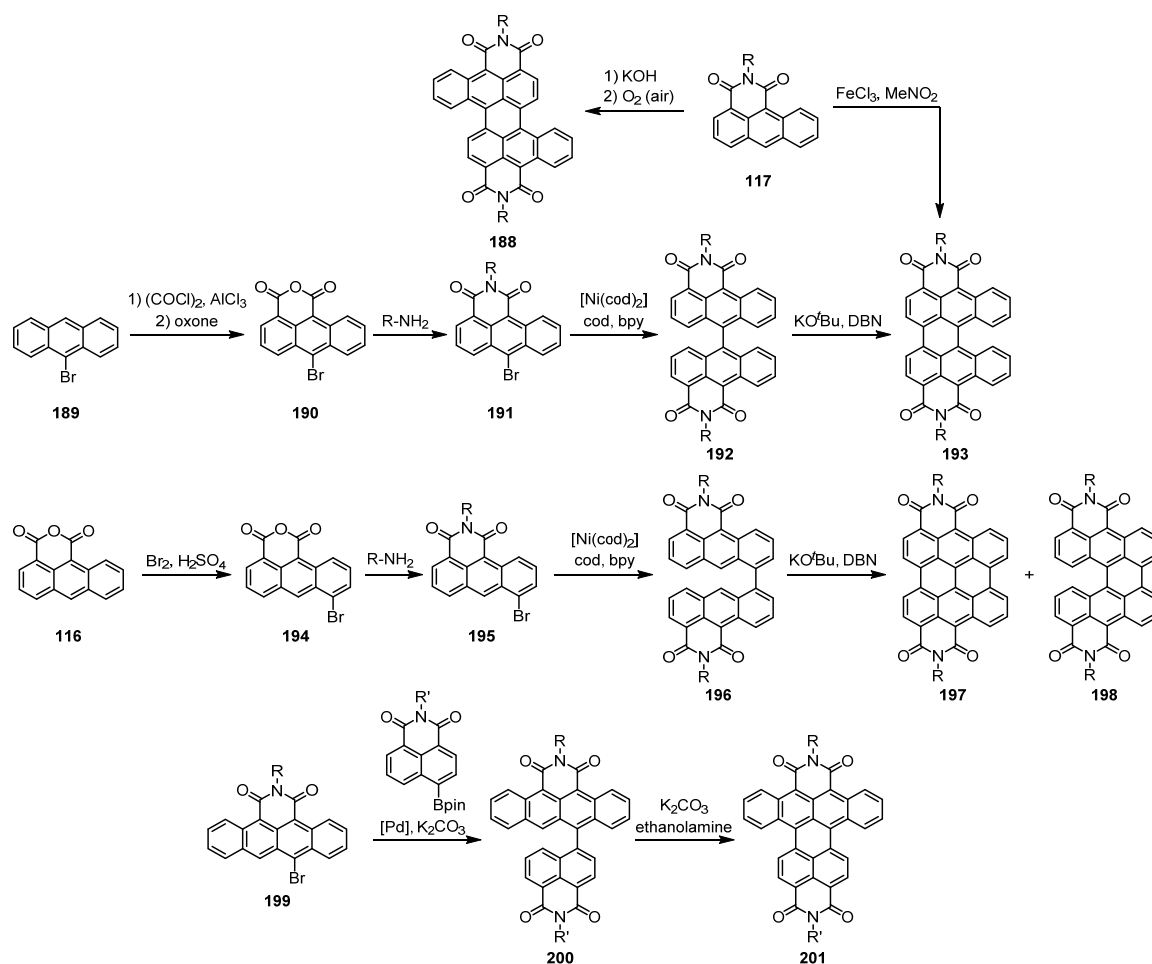
Most interestingly, by using copper powder the same tetrachloro-substituted PBI precursors can be annulated solely at the *bay*-positions resulting in PBI dimers and trimers with considerably distorted π -scaffolds (**176** and **177**) and high energy barriers for the interconversion of the different enantiomers.^[113] Furthermore, different rylene bisimides can be annulated by Stille-coupling and C–H arylation as it has been demonstrated for a NBI and tetrachloro-substituted PBI derivatives leading to hybrid rylene bisimide arrays (e.g. **178**) with high electron mobilities.^[14c]

Another approach combining both, core-expansion and the introduction of additional imide-functionalities to perylene mono- or bisimides is the Diels-Alder reaction of perylene monoimides (e.g. **182**) or perylene tetraesters (e.g. **185**) with maleimide or maleic anhydride, followed by oxidative rearomatization (Scheme 32).^[114] Following this strategy, angular bisimides (**184**) and coronene tetraimides (**187**) were synthesized that are interesting materials combining the properties of n-type semiconductors and columnar liquid crystals.



Scheme 32 Synthesis of core-expanded perylene imides by Diels-Alder reactions (R = alkyl, R' = alkyl or aryl).

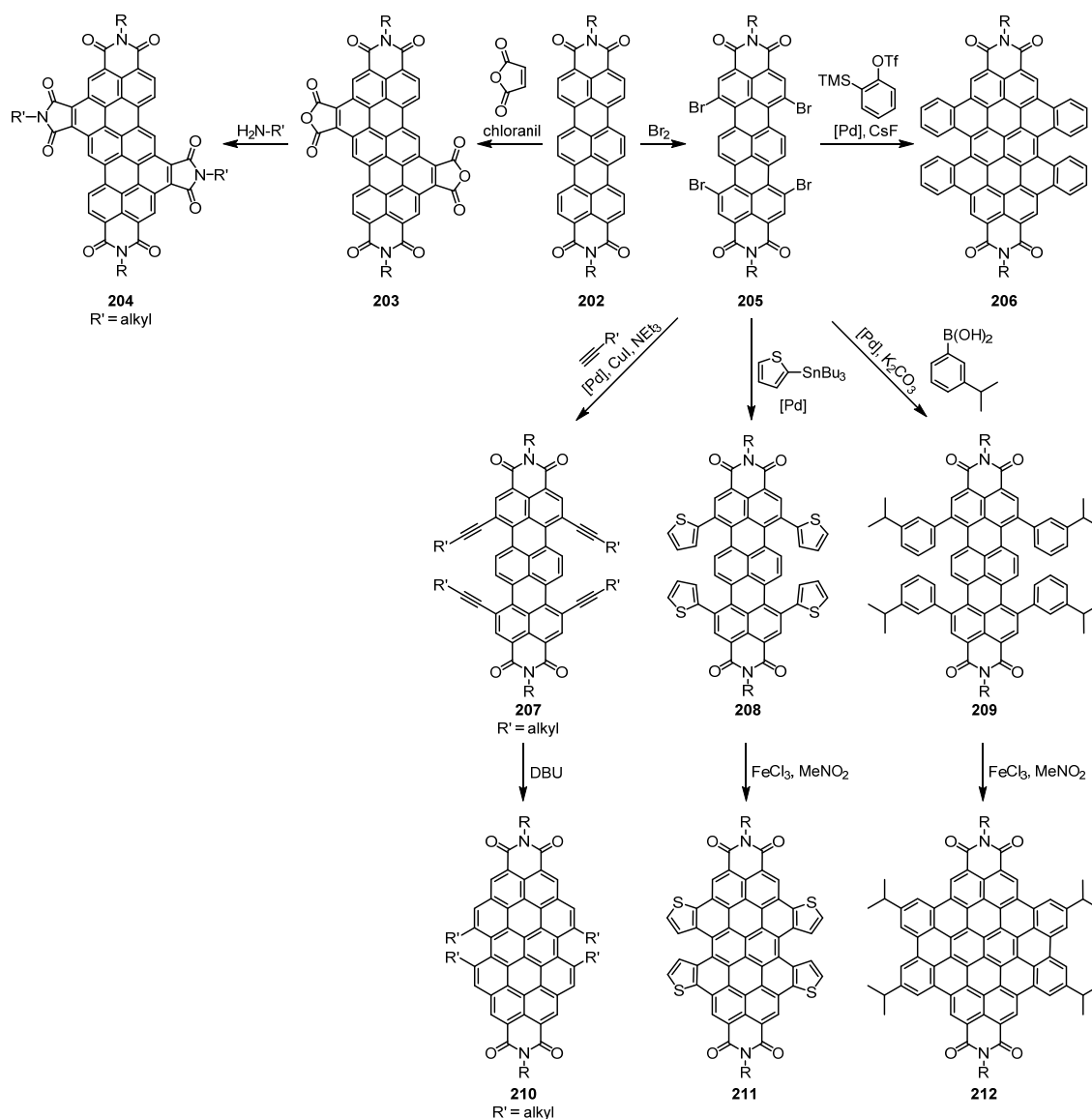
Whereas various examples of core-expanded PBIs annulated *via* the *bay*-positions have been reported in the last few years, examples for core-expanded perylene bisimides annulated *via* the non-*bay*-region are rather scarce, because no analogous direct annulation procedure has been developed for these positions so far. However, by coupling reactions of previously described acene monoimides, different core-expanded perylene bisimides (e.g. **188**, **193**, **197** and **201**) could be obtained by variation of the coupling conditions and the position of the activating bromine substituents (e.g. **191**, **195**, **199**) or by oxidative coupling of non-activated acene imides (e.g. **117**, Scheme 33).^[94a, 115] Moreover, cross-coupling of two differently sized acene imides followed by oxidative cyclization under basic conditions leads to compound **201** with core-twisted π -scaffold and remarkably NIR absorption spectral features.^[116]



Scheme 33 Synthesis of core-extended PBIs along the non-*bay*-region (R = alkyl or aryl, R' = alkyl).

Higher rylene imides

Longitudinally extended rylene imides like terrylene, quarterrylene, pentarylene, hexarylene and octarylene imides^[87] can be prepared by cross-coupling of perylene and/or naphthalene precursors followed by oxidative annulation. The lateral expansion of these molecules is likewise possible by cross-coupling of appropriately halogenated precursors followed by subsequent cyclization or by Diels-Alder reactions (see Scheme 34). The bromination of the parent terrylene bisimide (TBI, **202**) leads to tetrabromo-TBI (**205**), which is a valuable precursor for Sonogashira, Stille and Suzuki-Miyaura cross-coupling reactions. Thus, the core-substituted derivatives **207**, **208** and **209** could be prepared, which can further be converted into the core-expanded TBIs **210**, **211** and **212** by oxidative coupling or base induced cyclization.^[117] The lateral expansion of the π -scaffold can also be achieved by palladium-catalyzed benzannulation of tetrabromo-TBI with *o*-trimethylsilyl-phenyltriflate giving **206**.^[118] Due to the steric congestion between the neighbouring benzene rings two atropo-enantiomers with high racemization barriers could be separated being of interest for chiral molecular switches.

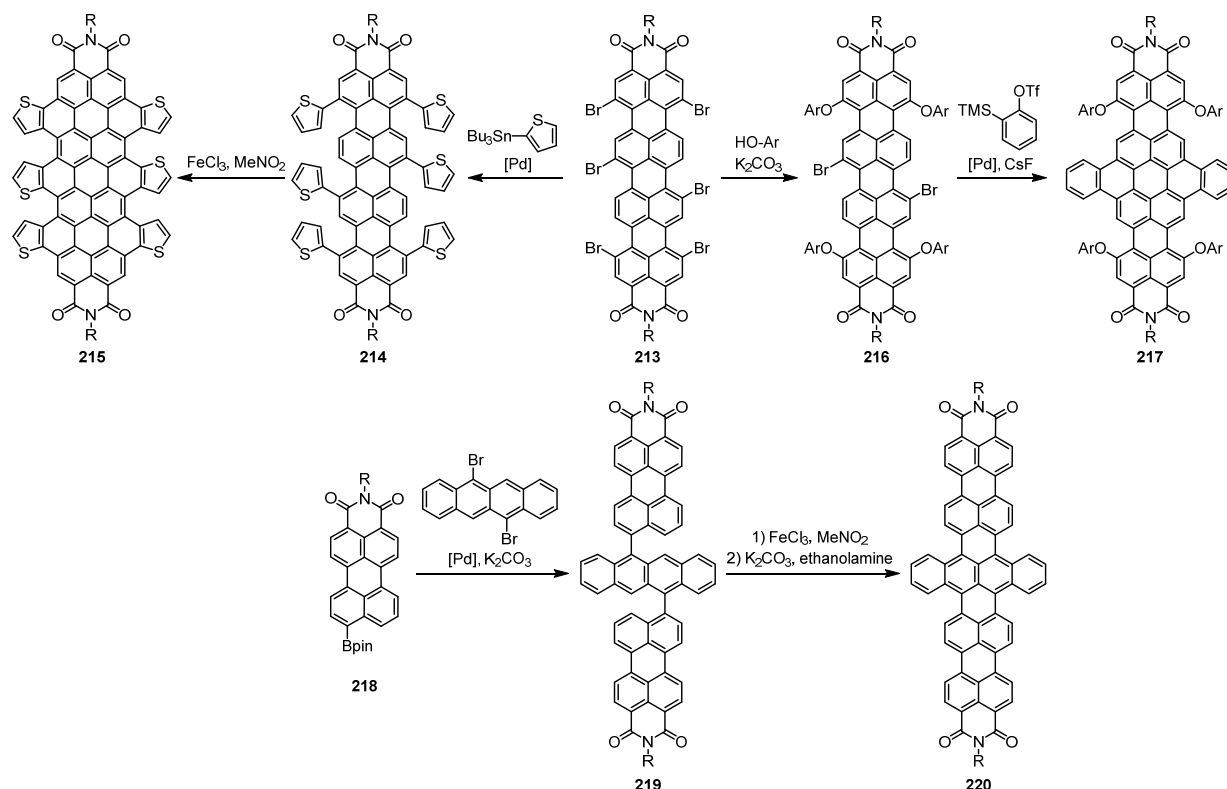


Scheme 34 Core extension of terrylene bisimides along the bay-areas (R = alkyl or aryl).

Similar to some examples of core expanded PBI derivatives additional imide-functionalities can be introduced by Diels-Alder cycloaddition of maleic anhydride to the unfunctionalized TBI core (**202**) followed by imidization (**204**).^[119]

The same synthetic approaches are known for quarterrylene bisimides (QBIs, Scheme 35). Bromination of the parent QBI leads to hexabromo-QBI **213**, which can subsequently be converted to core-extended QBIs **215** and **217**. Sequential introduction of solubilizing aryloxy-substituents (to **216**) and palladium catalyzed benzannulation gives dinaphthoquaterrylene bisimide (**217**) that is characterized by intense absorption and emission in the NIR region with high photostability making this core-expanded rylene bisimide derivative a promising dye for biolabelling applications.^[100b] The introduction of six thiophene substituents by Stille coupling (to intermediate **214**) and the oxidative cyclization to yield **215** was reported by the group of Wang.^[117b] While direct bromination, followed by

C–C cross-coupling and cyclization reactions provides access to core-expanded rylene bisimides along the *bay*-regions, the lateral expansion along the non-*bay*-area towards higher rylene bisimides could be accomplished by introduction of a tetracene subunit in between two perylene monoimides leading to core-expanded pentarylene bisimides (**220**).^[120] This synthetic approach includes Suzuki-Miyaura cross-coupling of dibromotetracene with boronate esters of perylene monoimide (**218**) and subsequent oxidative cyclization under Scholl-type and basic reaction conditions. This laterally expanded rylene dye exhibits intense absorption between 1000 and 1100 nm with low absorptivity in the visible spectral range making it useful for laser-induced applications.



Scheme 35 Synthesis of core-expanded quarterylene and pentarylene bisimides (R = alkyl or aryl).

Molecular Properties of Core-Expanded Rylene Imides

The longitudinal core-extension of rylene mono- and bisimides leads to a bathochromic shift of the absorption and emission maxima of about 100 nm per naphthalene subunit which is accompanied by an increase of the extinction coefficients (see Figure 2). In contrast, the fluorescence quantum yield reaches a maximum for perylene imides and decreases with increasing size of the π -scaffold.^[87-88, 121] The gradual red-shift of the absorption maxima is associated with decreasing HOMO-LUMO gaps, which is also consistent with the electrochemical properties of differently sized rylene bisimides. While the first reduction potentials (these are related to the energies of the LUMOs) are only marginally influenced

($\Delta E \sim 0.05$ eV) by the core-extension, the second reduction becomes more easily accessible for the extended systems due to decreased Coulombic repulsion. Therefore, only one two electron transfer process is observed for the reduction of rylene bisimides with $n \geq 2$.^[122] The introduction of additional naphthalene moieties into the core of rylene bisimides leads to a decrease of the electrochemical potential for the oxidation process that are related to the HOMO energy levels. Therefore, the HOMOs become stabilized until $n \geq 5$.^[123] From thereon, the HOMO and LUMO energies do not change considerably.

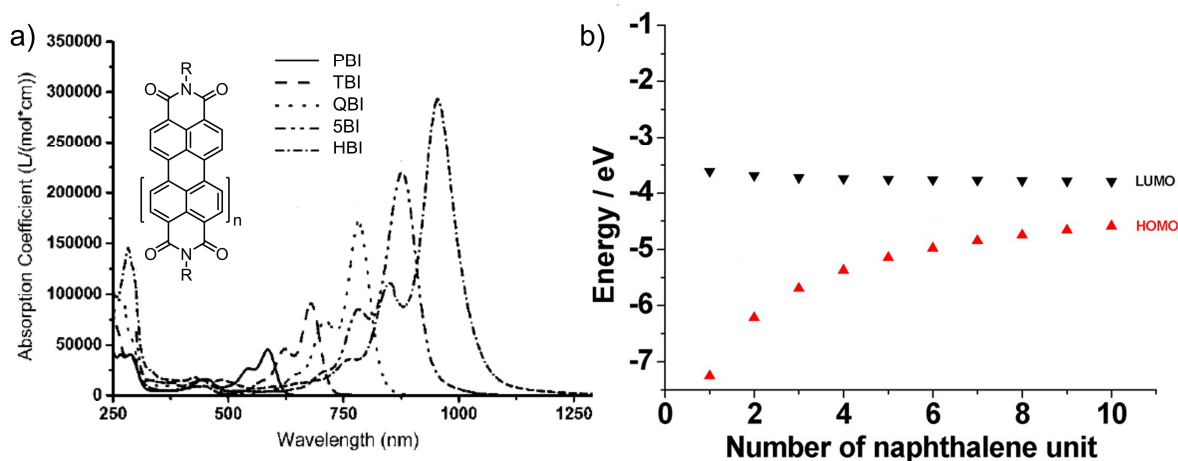


Figure 2 a) UV/Vis/NIR absorption spectra of rylene bisimides (with four aryloxy-substituents at the bay positions) and b) calculated HOMO and LUMO levels of rylene bisimides. Reproduced and adapted with permission of ref. [121] and [123b], copyright 2010, Wiley-VCH and 2016, ACS.

For laterally core-expanded rylene imides, two groups with distinct molecular properties can be distinguished. The first one includes rylene bisimides that are expanded along the *bay*-regions whereas the second one includes structures that are core-expanded along the non-*bay*-regions, like acene bisimides and *peri*-acene-like bisimides. The molecular properties of rylene bisimides expanded at the *bay*-region considerably differ from those of the parent compounds due to the mixing of orbitals of the polycyclic aromatic core and the parent rylene bisimide scaffold.^[121, 124] Therefore, both the optical and the electrochemical properties are influenced considerably. For coronene bisimides like **133** the lowest energy transition that can typically be ascribed to the HOMO-LUMO transition is therefore a transition from a coronene-like HOMO to a PBI-like LUMO and in consequence appearing at higher energies than the S_0 - S_1 transition of the PBI, due to an enlarged energetic gap (see Figure 3). Further expansion towards dibenzocoronene (**138a**) or dinaphthocoronene (**138b**) bisimides similarly influences the optical properties due to stabilization of the HOMO-level that reproduce or diminish the HOMO-LUMO gaps of parent PBIs and therefore shift the absorption maxima to higher wavelength compared to coronene bisimides.^[100b, 101] For such

systems the electronic transitions to higher excited states are generally more pronounced compared to core-unsubstituted PBIs due to a change of molecular geometry that is accompanied by an increased number of symmetry allowed transitions. Similar trends are observed for higher rylene bisimides that are likewise extended along the *bay*-regions.^[100b, 117a, 118-119]

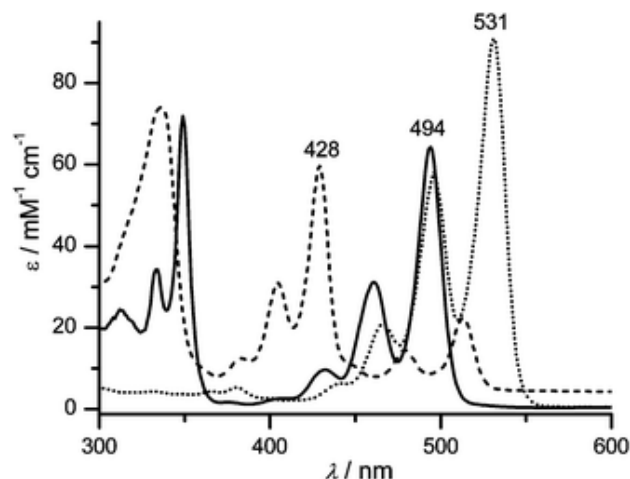


Figure 3 UV/Vis/NIR absorption spectra of coronene bisimide (dashed line), dibenzocoronene bisimide (solid line) and the parent PBI (dotted line). Reproduced with permission of ref. [121], copyright 2010, Wiley-VCH.

For bis- and oligo-PBIs such as **164**, **165** and **166** annulated at the *bay*-positions via π -conjugated bridges, the group of Nuckolls has demonstrated that the frontier molecular orbitals become energetically reduced with an increasing number of PBI monomers with a larger influence on the LUMO level, resulting in decreased band gaps and bathochromically shifted absorption maxima. Moreover, additional electronic transitions become allowed which include contributions from the orbitals of the conjugated bridging units.^[15b] By replacing the bridging units by aromatic moieties inducing a helical arrangement (e.g. **160**, **161**), a hypsochromic shift of the absorption maxima is observed, that can be rationalized by intramolecular through-space excitonic coupling.^[15a] Depending on the electron-donating ability of the linker moiety and its electronic delocalization, additional intramolecular charge-transfer bands and a destabilization of the first reduction potential (compared to the parent PBI) can be observed. Very similar trends were reported by Marks, Wasielewski and Zhao for phenylene- (**159a,b**), thiophene-, thienothiophene- and phenacene-bridged bis-PBIs.^[15c, 109] Likewise, propeller-like or star-shaped tris-PBIs like those reported by Wang (**162**) and Qu (**163**) preserve this structure-dependent molecular features.^[15d, 110] The direct fusion of PBIs at the *bay*-positions with eight-membered rings (e.g. **176**, **177**) has a different effect on the molecular properties. The linkage through an eight-membered ring results in a drastic distortion of the PBI-units against each other and therefore reduced efficient π -conjugation.

Therefore, the absorption and emission spectra are very similar to the parent PBI-monomers, while the MO-levels are slightly decreased.^[113]

Core-expansion along the non-*bay*-regions (e.g. **188**, **193**, **197**, **201**) leads to bathochromically shifted absorption maxima, due to the acene-like HOMO, which decreases the band gap.^[94a, 95, 115] Moreover, the introduction of additional benzene units at opposite positions of the molecule leads to distortion of the core caused by steric congestions between adjacent hydrogen atoms.^[116, 120] Direct fusion of PBIs along the *bay*- and non-*bay*-regions *via* six-membered rings gives rise to distorted nanoribbons (e.g. **174**, **180**, **181**) with red-shifted absorption maxima and electronic transitions to several excited states. Moreover, the reduction potentials and LUMO energies are significantly decreased compared to the parent PBI, making them much stronger electron-acceptors.^[14a, b]

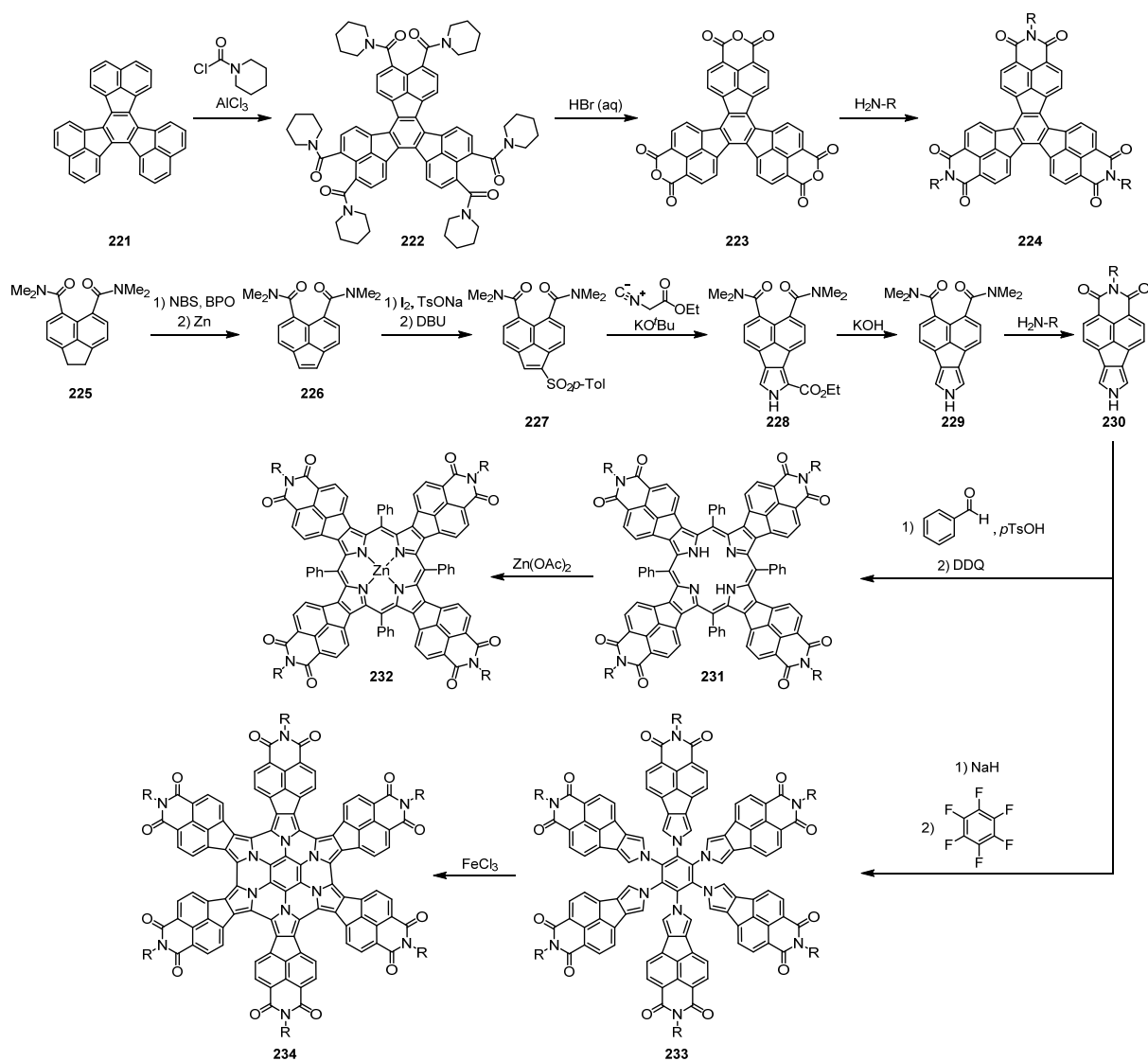
2.2.2.2 Other Polycyclic Aromatic Systems containing Six-Membered Dicarboximides

As already discussed previously, aromatic imides with a six-membered imide ring generally contain 1,8-naphthalimide substructures. In contrast to the core-expanded rylene imides presented in the preceding chapter, the structures that will be discussed in this section are not composed of rylene-type polycyclic aromatic hydrocarbons that are connected to additional naphthalene-moieties *via* the *peri*-positions or constructed from acene-type imides such as anthracene, tetracene or pentacene imides. However, the six-membered aromatic dicarboximides presented herein contain (multiple) naphthalimide subunits that are incorporated into larger aromatic scaffolds different from those discussed before.

Synthetic Concepts

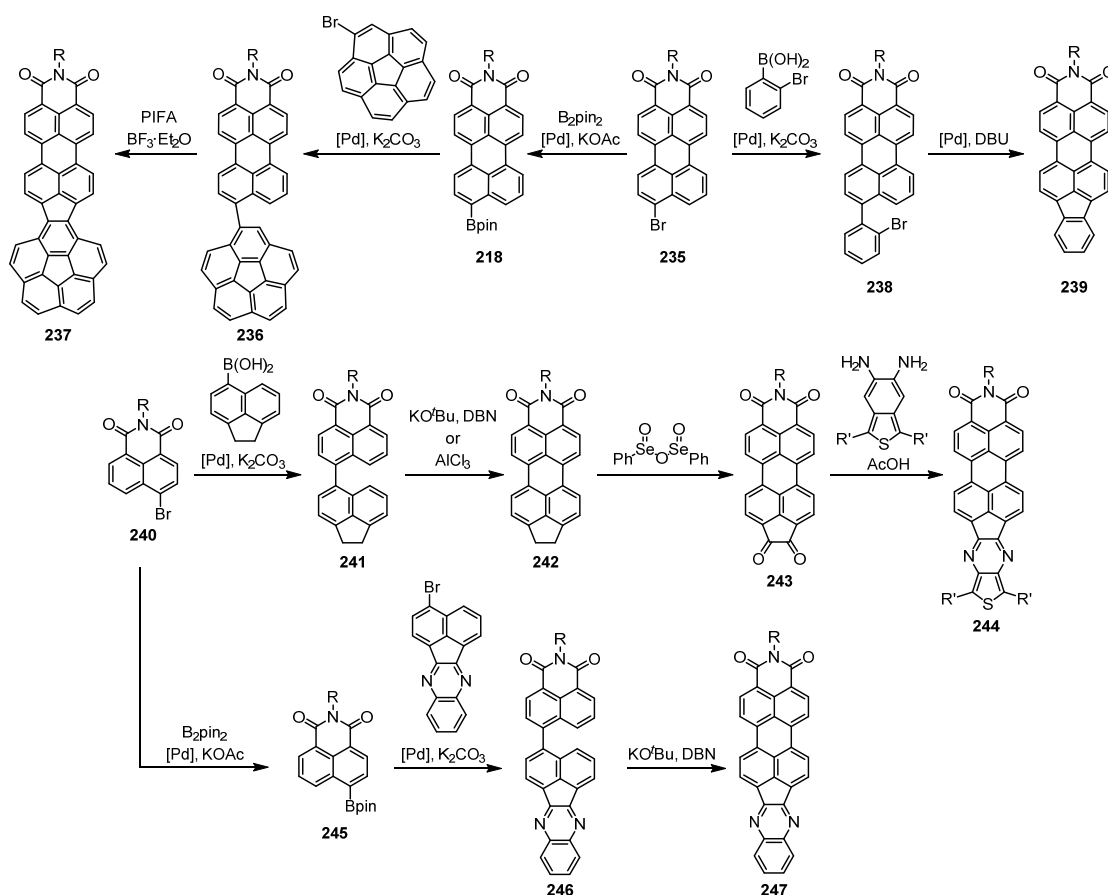
One potential synthetic methodology is concerned with the construction of appropriate polycyclic aromatic anhydrides that can ultimately be converted into the aromatic imides by imidization. The group of Wudl reported on a three step reaction procedure (see Scheme 36) that includes Friedel-Crafts carbamylation of decacylene (**221**), followed by hydrolyzation to the trianhydride (**223**) and subsequent imidization to the triimide (**224**).^[16b] Due to the introduction of branched alkyl-chains at the imide-positions, this triimide self-assembles into hexagonal pillars or long fibers and can be used as electron-acceptor material in organic solar cells.^[16b, 125] Only recently the group of Stępień published another highly interesting aromatic imide, which has been proven to be a valuable precursor for the construction of large π -conjugated systems containing multiple naphthalimide subunits.^[16c, 126] The key structure is a pyrrole-fused naphthalimide (**230**), that could be prepared by a multiple step procedure

starting from 1,2-dihydroacenaphthylene-5,6-dicarboxamide (**225**). The reaction sequence includes its oxidation to the acenaphthylene derivative (**226**) and introduction of a tosylate substituent (**227**) that served as the precursor for the pyrrole formation step followed by decarboxylation and imidization. Due to the reactivity of the pyrrole subunit, this imide can easily be converted into porphyrins (**231** and **232**) by condensation with benzaldehyde and aromatization with DDQ.^[126] Likewise, it can be used for the preparation of azacoronene derivatives (**234**) by six fold substitution of hexafluorobenzene and oxidative cyclization with FeCl_3 .^[16c] Due to the four and six naphthalimide subunits, respectively, both molecules can take up multiple electrons. This unique property and the desirable optical features make **231**, **232** and **234** interesting materials for applications in organic (opto)electronic devices.



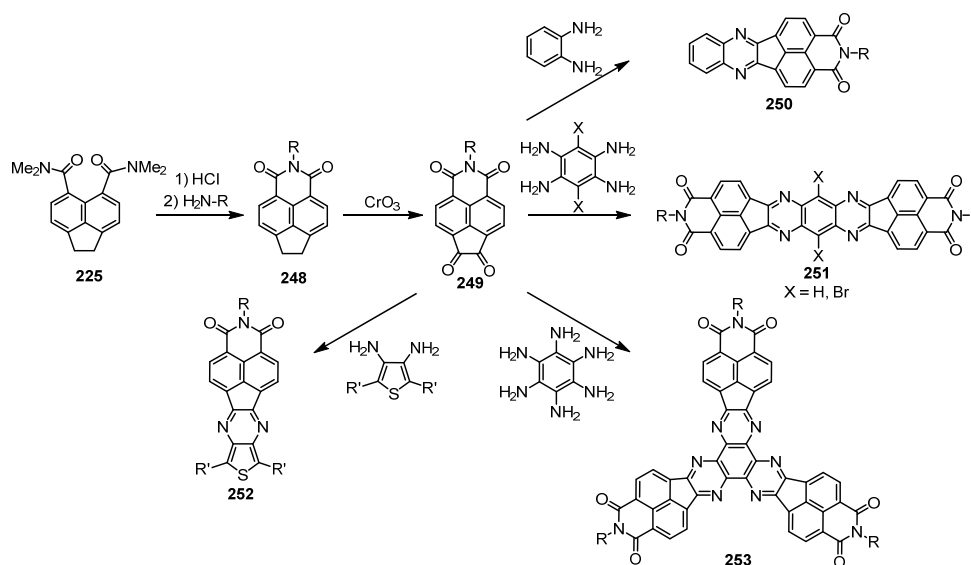
Scheme 36 Synthesis of PADIs containing multiple naphthalimide subunits (R = alkyl or aryl).

Another synthetic concept towards PADIs is the coupling of rylene monoimide precursors to different aromatic subunits followed by intramolecular cyclization (Scheme 37) like it has previously been described for the lateral core-expansion of rylene imides. Starting from *peri*-halogenated or borylated derivatives (like **218**, **235**), five-membered ring annulated perylene monoimides (**237**, **239**) become accessible by Suzuki-Miyaura cross-coupling followed by cyclization either through Pd-catalyzed C–H arylation or oxidative dehydrogenation.^[100a, 107a] Similarly, Suzuki-Miyaura cross-coupling and oxidative cyclization of *peri*-functionalized naphthalene derivatives lead to heteroaromatic imides **244** and **247**.^[127]



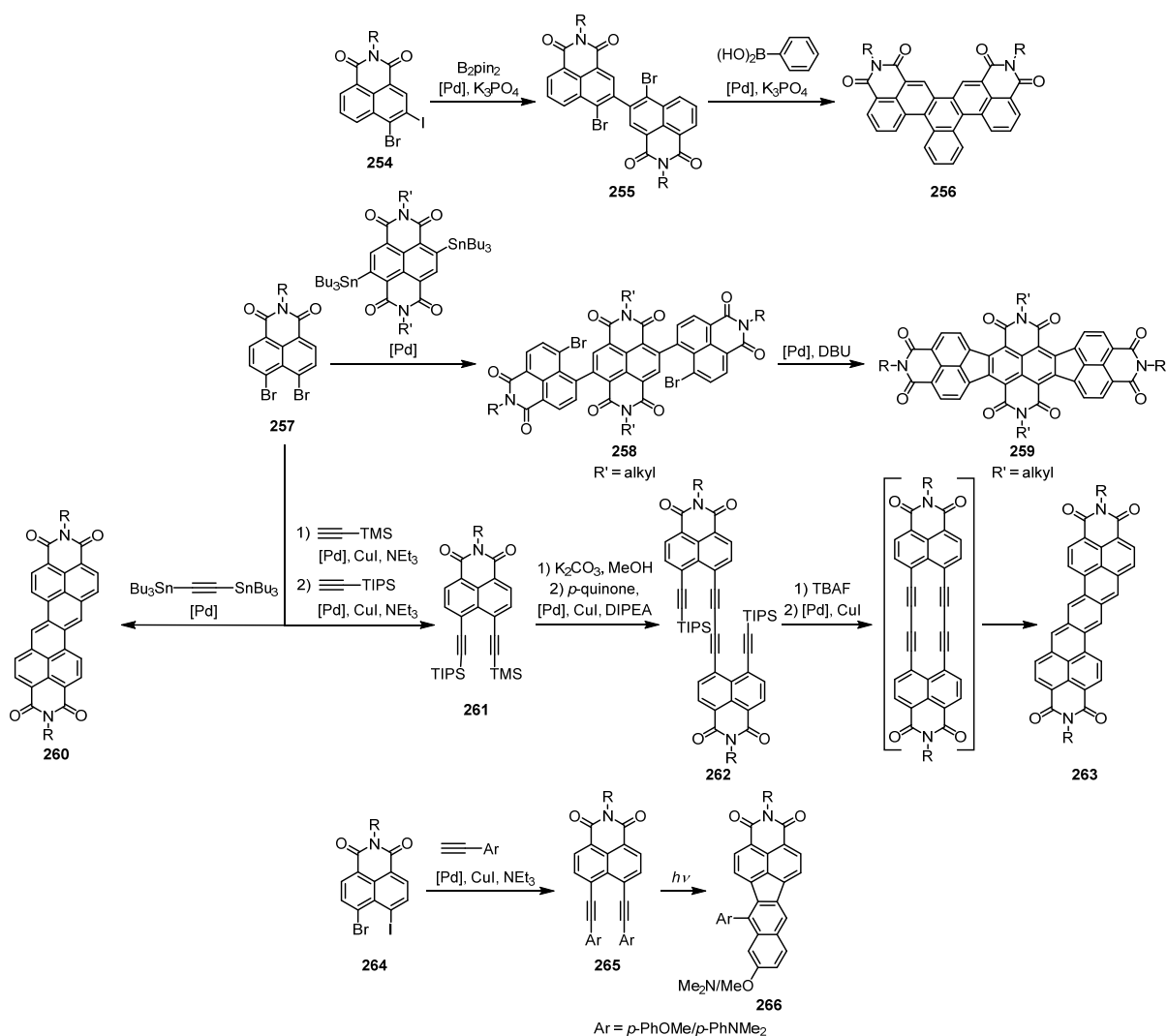
Scheme 37 Synthesis of PADIs by functionalization of the *peri*-position of rylene monoimides (R = alkyl or aryl).

Similar structures with only one naphthalene subunit, however, were already reported in 2013 (Scheme 38). The key-intermediate of this reaction sequence is the diketone **249** which can easily be converted into pyrazine derivatives (**250**, **251**, **253**) with various di-, tetra- or hexaamines. The attachment of thiophene moieties to the naphthalimide diketone leads to **252**, which can be applied as ambipolar charge transport material.^[128] By using tetra- or hexaamines as linking units, new linear and star-shaped di- and triimides (**251**, **253**) could be prepared that are interesting candidates as n-type semiconductors due to enhanced π - π -stacking interactions and readily accessible LUMO energy levels.^[129]



Scheme 38 Synthesis of PADIs by functionalization of an acenaphthene monoimide (R = alkyl or aryl).

3,4- or 4,5-dihalogenated naphthalimides (**254**, **257**, **264**) provide access to a variety of core-extended compounds (Scheme 39) by combining of Suzuki-Miyaura or Stille cross-coupling with Pd-catalyzed C–H arylation. Applying these procedures provides access to benzopicene bisimide (**256**)^[130] and a orthogonal tetraimide **259**.^[16a] By introduction of acetylene moieties to these halogenated precursors by Sonogashira cross-coupling techniques, a subsequent photoinduced cyclization of the diethynylene-substituted derivative **265** gave access to **266**.^[131] The group of Wu performed transannular cyclizations of ethynylene-moieties in **261** and **262** instead of photoinitiated reactions leading to zethrene (**260**) and heptazethrene bisimides (**263**), which exhibit higher stability compared to unsubstituted zethrenes resulting in isolable biradicaloid structures.^[132]



Scheme 39 Synthesis of PADIs by functionalization of 3,4- or 4,5-dihalo-naphthalene monoimides (R = alkyl or aryl).

Molecular Properties

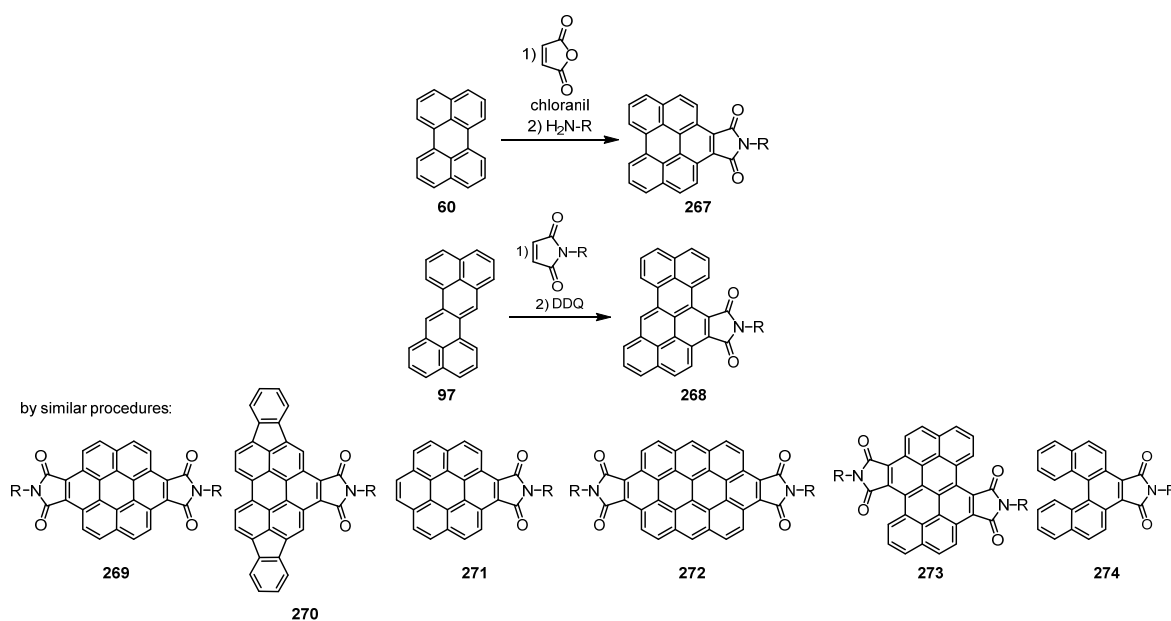
Polycyclic aromatic dicarboximides composed of naphthalene imide or perylene imide moieties extended *via* five-membered rings in the *peri*-positions typically maintain similar molecular properties as their parent polycyclic aromatic core structures without imide groups. Moreover, compounds with multiple naphthalimide moieties, like those reported by Stępień (**231**, **232**, **234**) and Wudl (**224**) can exhibit incomplete delocalization of electrons over the whole π -system and degenerated molecular orbitals, which make the lowest energy transition symmetry forbidden.^[16b, c, 126] Compared to naphthalene or perylene monoimides, the absorption and emission of *peri*-annulated systems containing five-membered rings are bathochromically shifted and the FMO energies are decreased with major influence on the unoccupied orbitals.^[100a, 107a, 129, 131] Furthermore, lateral five-membered ring annulation of naphthalene bisimides (like for **259**) leads to a decreased oscillator strength of the S_0 - S_1 -transition and a stabilization of the LUMO-level compared to the parent naphthalene

bisimide.^[16a] The benzopicene (**256**), zethrene (**260**) and heptazethrene (**263**) bisimides are characterized by optical transitions that are similar to those of the respective unfunctionalized PAHs but with red-shifted absorption and emission maxima and reduced HOMO-LUMO gaps, which can be explained by the electron-withdrawing character of the imide-groups.^[130, 132a, b]

2.2.3 Polycyclic Aromatics containing Five-Membered Dicarboximides

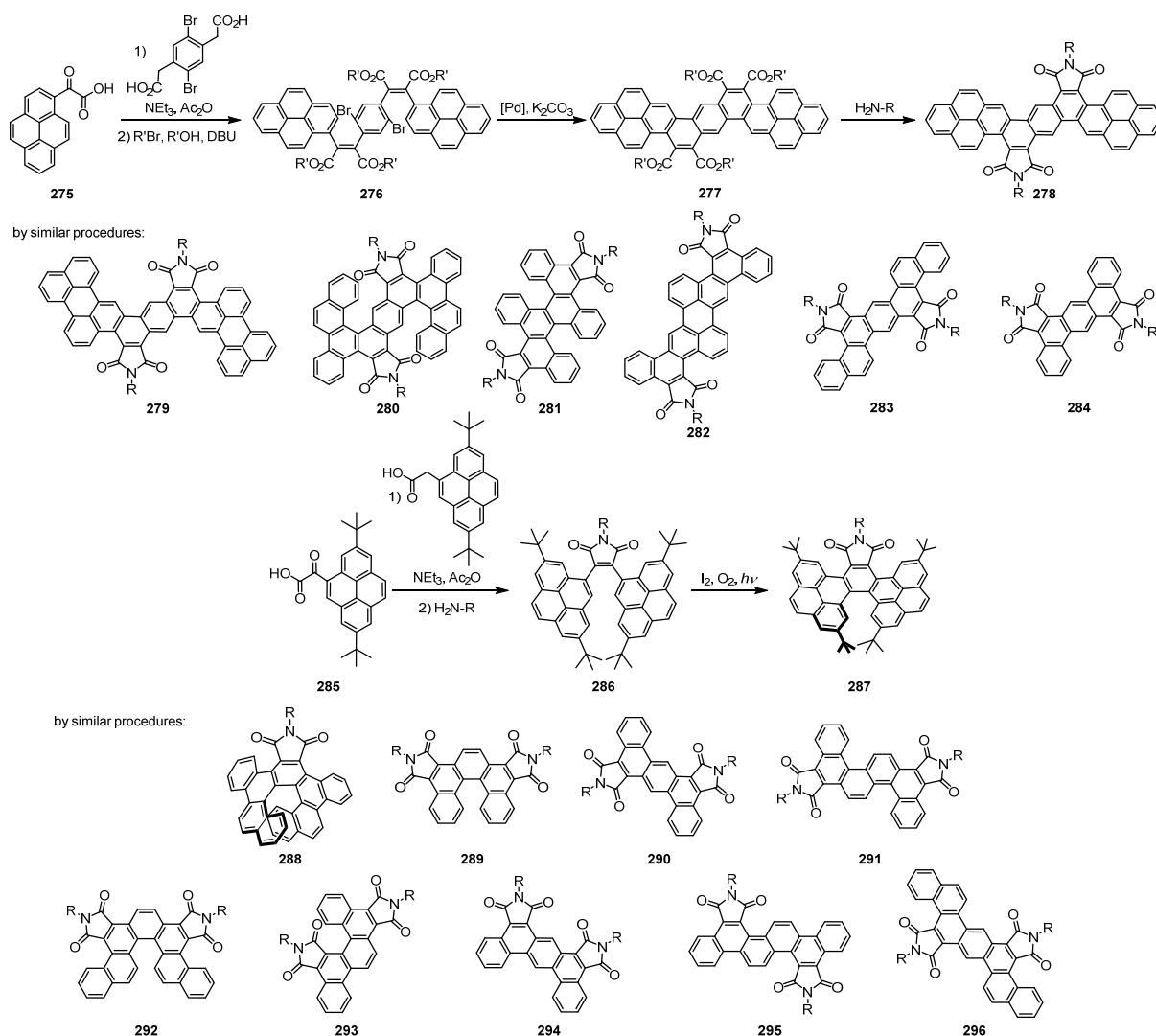
Synthetic Concepts

Less synthetic strategies are known for the introduction of five-membered dicarboximides into polycyclic aromatic scaffolds. The most common one is the Diels-Alder [4+2]-cycloaddition of maleic anhydride or maleimide to an appropriately polycyclic aromatic system followed by oxidative rearomatization and subsequent imidization (Scheme 40). While the reactivity of maleic anhydride towards common dienes is already known for several decades, the first attempts to attach this dienophile to polycyclic aromatic hydrocarbons were reported by Clar in the 1960s.^[133] By Diels-Alder reactions of maleic anhydride with different PAHs and subsequent decarboxylation a series of new polycyclic aromatic structures could be developed. The combination of [4+2]-cycloaddition with imidization for the development of highly soluble and thermostable fluorescent dyes was described by Langhals around 30 years later.^[134] Following this approach, compounds **267**, **270** and **271** could be obtained starting from perylene, diindenoperylene and benzo[*ghi*]perylene. This strategy has frequently been applied during the last decade to synthesize larger bisimides like coronene bisimides **269**,^[114a] ovalene bisimides **272**^[135] and benzo[*pqr*]-naphtho[8,1,2-*bcd*]perylene bisimides **273**.^[136] Similarly, first attempts to prepare an imide containing pentahelicene were concerned with the Diels-Alder reaction of 3,3',4,4'-tetrahydro-1,1'-binaphthalene with maleimide. Unfortunately, the yields for the final oxidation to produce the aromatic compound **274** are low.^[137]



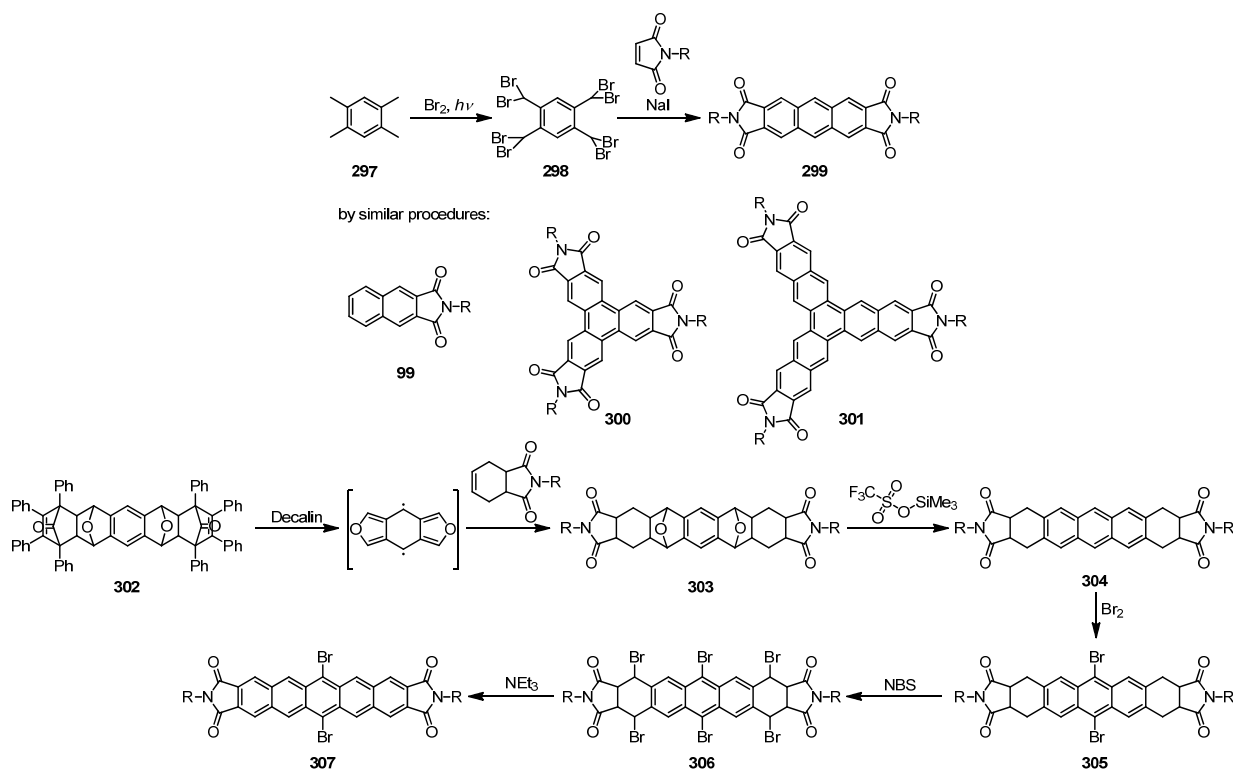
Scheme 40 Synthesis of imide containing PAHs by Diels-Alder reaction of unfunctionalized PAHs with maleic anhydrides or maleimides (R = alkyl or aryl).

Recently, **274** could also be synthesized in better yield by the initial construction of a pentahelicene containing two carboxylic ester groups followed by anhydride formation and final imidization.^[138] The development of related helicene- and phenacene-type structures containing one or two five-membered imide rings was extensively studied by the groups of Bock, Durola, Pei and Zhao (Scheme 41).^[139] By condensation of arylglyoxylic acids (like **275** and **285**) with arylacetic acids the corresponding aryl-substituted maleic acid derivatives can be obtained that can further be converted into carboxylic esters or anhydrides prior to imidization. The annulation of both aromatic subunits connected by the maleic acid derivative can either be achieved by photoinduced oxidative cyclization or Heck-type C–H arylation.



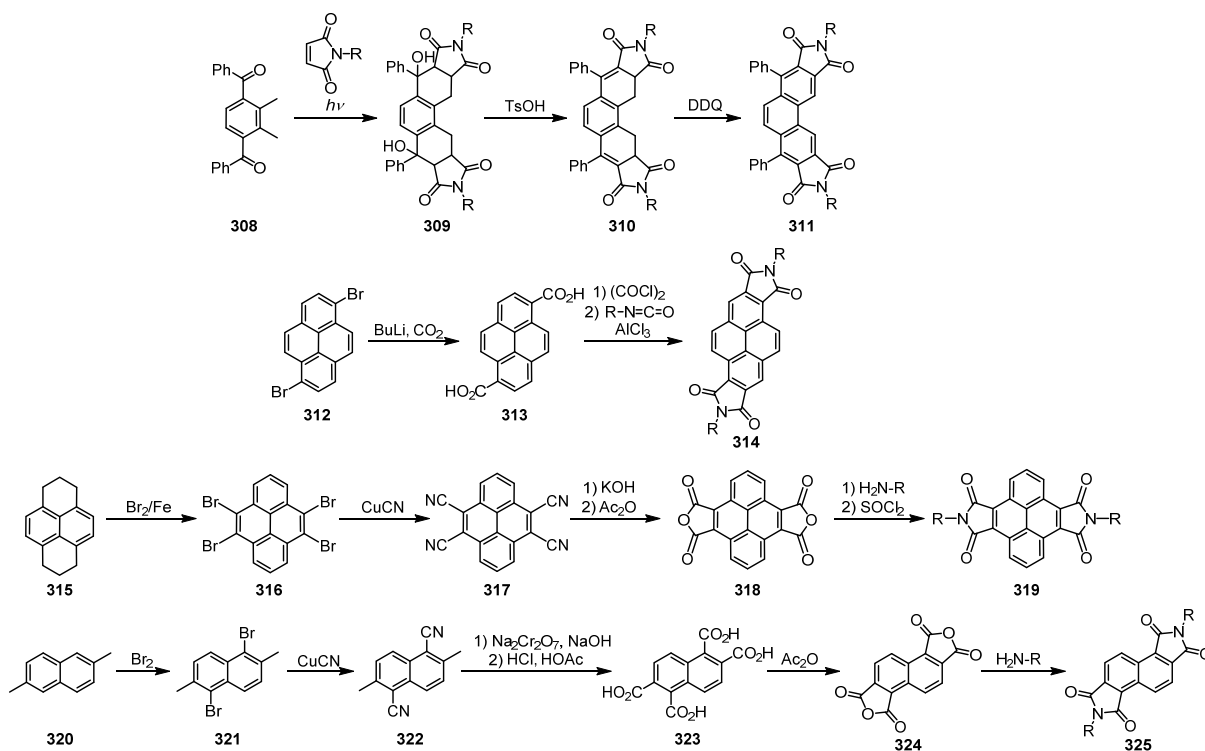
Scheme 41 Synthesis of polycyclic aromatics containing five-membered imide groups (R and R' = alkyl).

Acene-type imides with linearly linked five-membered dicarboximide groups were reported by Facchetti and Marks and showed good n-type semiconducting properties.^[140] The synthesis was accomplished by Diels-Alder cycloaddition of tetrakis(dibromomethyl)benzene **298** with different maleimides followed by aromatization (Scheme 42). The same synthetic strategy has been applied to produce naphthalene monoimide **99** and star-shaped triimides **300** and **301** which have good electron-accepting properties and pack into desirable long range columnar stacks.^[141] Likewise, a linear pentacene bisimide **307** was reported in 2011, which was synthesized by multiple steps including Diels-Alder cycloaddition, bromination and HBr-elimination.^[142]



Scheme 42 Synthesis of acene-type imides with five-membered imide groups (R = alkyl).

Moreover, other linear- and angular-shaped bisimides containing five-membered imide rings (Scheme 43) were prepared by Diels-Alder trapping of photogenerated xylylenols to yield **309**, which can subsequently be dehydrated and oxidatively rearomatized (like for **311**).^[143] Alternatively, they can sequentially be prepared by preparation of carboxylic acid derivatives for imidization (e.g. **318/319**, **324/325**)^[144] or Friedel-Crafts type carbamylation (e.g. **313/314**).^[145]



Scheme 43 Synthesis of five-membered aromatic imides (R = alkyl).

Molecular Properties

Like it has already been discussed for the cyclic six-membered dicarboximides, the introduction of cyclic five-membered imide functionalities induces a decrease of the frontier molecular orbital energy levels due to the highly electron-withdrawing character of the cyclic imide. Moreover, a bathochromic shift of the absorption and emission is observed due to the extension of the π -system by the imide subunit.^[114a, 135-136, 145] While the planar structures such as **273** and **299** exhibit good performances in organic electronics,^[136, 140] the helicene-like compounds such as **274**, **287** and **288** are valuable luminescent materials that can exhibit circularly polarized luminescence.^[138, 139b]

Chapter 3

Results and Discussion

3.1 Palladium-Catalyzed Suzuki-Miyaura Cross-Coupling of Naphthalene Dicarboximides with Pyrene

3.1.1 Introduction

Pyrene is one of the most intensively studied planar polycyclic aromatic hydrocarbons (PAHs) with desirable optical and electronic properties. Due to the long lived fluorescence of pyrene and its tendency to form emissive excimers in solution it became one of the most attractive molecules for photophysicists.^[146] Moreover, these desirable properties in combination with an electron-rich character allowed its application as semiconducting material in organic electronic devices such as field effect transistors (FETs) and light emitting diodes (LEDs).^[17] While for the application in FETs a tight π - π -stacking is favorable to optimize charge carrier mobility, it is an apparent disadvantage for application in LEDs because of self-quenching of luminescence. To prevent these interactions, the introduction of bulky aryl substituents to the pyrene scaffold was elucidated extensively. The majority of aryl-functionalized pyrene derivatives known to date are mono-substituted at position 1 or tetra-substituted at positions 1, 3, 6 and 8 due to commercial accessibility of the respective precursors 1-bromopyrene and 1,3,6,8-tetrabromopyrene. These halogenated pyrene derivatives are valuable starting materials for the synthesis of arylated pyrene derivatives by different transition-metal-catalyzed cross-coupling reactions. By this approach many mono- and tetraaryl-substituted pyrenes were prepared that show promising properties for application in OLEDs.^[147] Selective disubstitution in 1,6- or 1,8-positions, in contrast, is still challenging due to the difficult separation of 1,6- and 1,8-dibromopyrene that are formed by direct bromination of pyrene. Similar to above described mono- and tetra-substituted derivatives linear or angular shaped aryl- or ethynyl-substituted derivatives were prepared by transition-metal-catalyzed coupling reactions.^[148] The angular functionalized 1,3-dibromopyrene is accessible by incorporation of a sterically protecting *tert*-butyl group in 2-

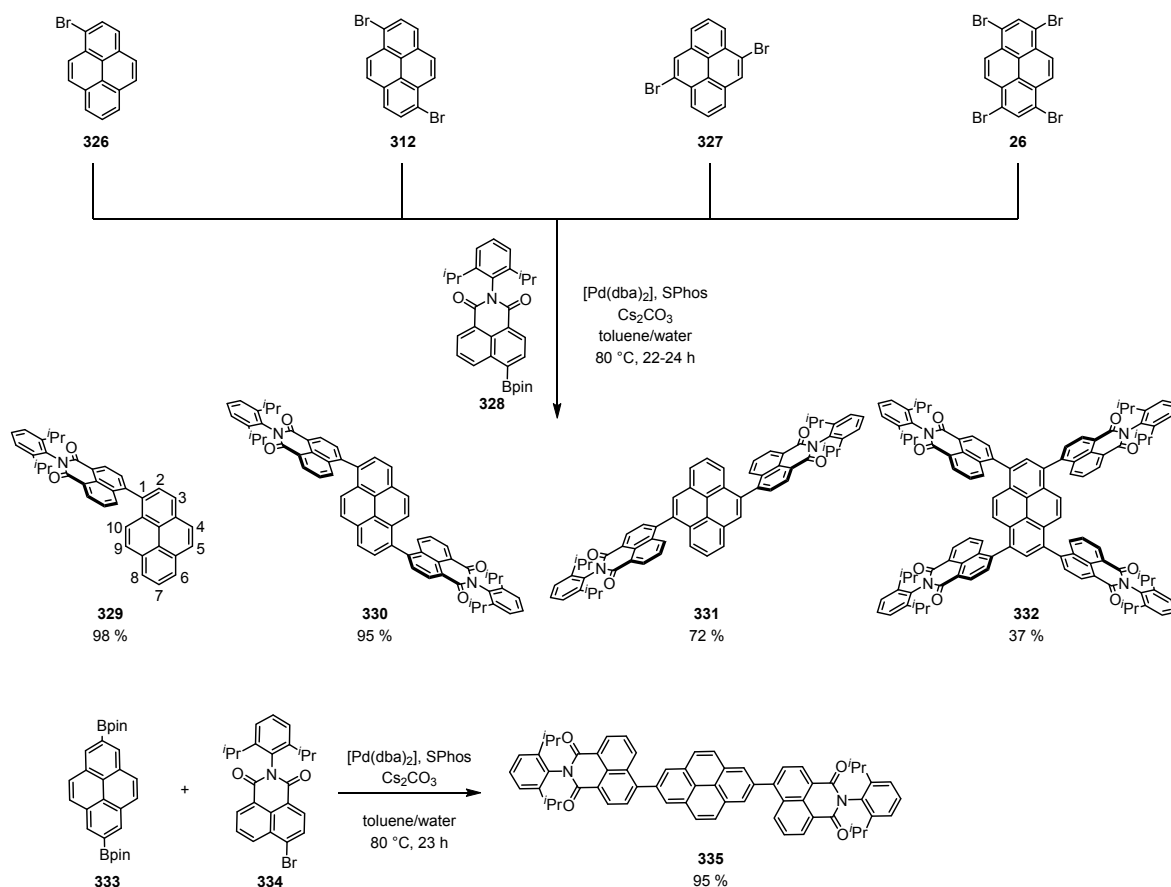
position prior to its bromination, leading to 1,3-dibromo-7-*tert*-butylpyrene.^[149] This precursor was used for different coupling reactions to obtain polypyrenes and macrocyclic structures.^[150] The substitution at 2,7-positions is similarly challenging, since they are only accessible by indirect methods due to nodes at these particular positions in the frontier molecular orbitals and hence not accessible by electrophilic substitution. A key step towards the functionalization of these positions was made by the groups of Marder and Perutz. They have developed the selective direct borylation of pyrene in 2,7-positions by iridium-catalyzed C–H activation.^[151] Various transformations to alkylated, arylated or heteroatom-substituted derivatives were reported.^[152] Another possibility to introduce functional groups selectively in positions 2 and 7 is the bromination of 4,5,9,10-tetrahydropyrene followed by oxidative rearomatization.^[153] Similarly, the inner 4,5,9,10-positions of the pyrene core are accessible through functionalization of 1,2,3,6,7,8-hexahydropyrene followed by oxidative aromatization.^[144b, 154] By the latter approach mono-, di- and tetra-brominated pyrenes are accessible that can be converted into arylated or π -extended derivatives.^[154b, c, 155] Another possibility for the functionalization of these particular positions is the oxidation of pyrene to di- or tetra-ketones^[156] or the introduction of sterically protecting *tert*-butyl groups in 2,7-positions prior to bromination.^[157]

Although many syntheses have been developed for the functionalization of pyrene apparently pyrene derivatives containing naphthalene dicarboximide (shortened naphthalimide) substituents are not known to date. Therefore, we have made efforts to develop a synthetic route for naphthalimide decorated pyrene by palladium-catalyzed Suzuki-Miyaura cross-coupling reactions. The design of these structures aimed at developing multichromophoric systems as precursors for the synthesis of planar multidicarboximide-functionalized PAHs by oxidative cyclodehydrogenation as presented in *Chapter 3.2*. The synthesis of newly designed naphthalimide-substituted pyrenes and the influence of substitution pattern on their optical and electrochemical properties are discussed in the following.

3.1.2 Synthesis of Mono-, Di- and Tetra-Naphthalimide-Substituted Pyrenes

The synthesis of compounds **329-332** was accomplished by palladium-catalyzed Suzuki-Miyaura cross-coupling reaction of the respective brominated pyrene derivatives **26**, **312**, **326** and **327** with naphthalimideboronic acid pinacol ester **328**, while for compound **335** bromo-naphthalimide **334** and pyrene boronate ester **333** were used as coupling components (Scheme 44). The starting compounds 1,6-dibromopyrene (**312**),^[158] 4,9-dibromopyrene (**327**)^[154b] and pyrene-2,7-diboronic acid pinacol ester (**333**)^[151] were synthesized according

to literature known procedures. The halogenated or borylated naphthalimide derivatives **328** and **334** were synthesized by imidization of commercially available 4-bromo-1,8-naphthalic anhydride with 2,6-diisopropylaniline and subsequent palladium-catalyzed Miyaura borylation.^[159] The cross-coupling of 1-bromopyrene (**326**) with naphthalimide boronate ester **328** in the presence of 15 mol% of [Pd(dba)₂] and 30 mol% of SPhos as catalytic system afforded the mono-arylated pyrene derivative **329** in 98 % yield (Scheme 44). The same C–C coupling procedure was applied to 1,6-dibromopyrene (**312**), 4,9-dibromopyrene (**327**) and 1,3,6,8-tetrabromopyrene (**26**) with two or four equivalents of compound **328** affording the corresponding di- and tetra-naphthalimide-substituted products **330**, **331** and **332** in 95, 72 and 37 % yield, respectively. The moderate yield of 37 % for the tetra-substituted derivative **332** might be explained by steric hindrance between the neighboring naphthalimide units.



Scheme 44 Synthesis of naphthalimide-substituted pyrenes **329-332**^{*} and **335** by Suzuki-Miyaura cross-coupling (dba: dibenzylideneacetone, SPhos: 2-dicyclohexylphosphino-2',6'-dimethoxybiphenyl).

^{*} Compound **332** was synthesized by Dr. Kazutaka Shoyama.

The synthesis of **332** was published in [160] S. Seifert, K. Shoyama, D. Schmidt, F. Würthner, *Angew. Chem. Int. Ed.* **2016**, *55*, 6390. Reproduced and adopted with permission. Copyright 2016 Wiley-VCH Verlag GmbH & Co. KGaA, Weinheim.

The 2,7-disubstituted derivative **335** was synthesized in high yield of 95 % by applying identical conditions for the coupling reaction of pyrene-2,7-diboronic acid pinacol ester **333** with 4-bromo-1,8-naphthalimide **334**.

3.1.3 Optical Properties

The polycyclic aromatic hydrocarbon (PAH) pyrene itself shows multiple electronic transitions in the UV spectral region that can be assigned to S_0 - S_1 (weak transition around 372 nm), S_0 - S_2 (334 nm), S_0 - S_3 (272 nm) and S_0 - S_4 (243 nm) transitions, all with vibrational modes (Figure 4).^[152a] Marder and coworkers^[152a, 161] have shown that the substitution pattern on the pyrene core influences these transitions to a different extent due to changes in the symmetry of the molecule and hence the oscillator strength and allowance of electronic transitions. Substitution in 2 and 7 positions leads to transitions that are similar to the parent pyrene, only influencing the S_0 - S_1 transition depending on the electronic character of the substituents but not the S_0 - S_2 transition (attributed to HOMO-LUMO transition) due to nodes in the frontier molecular orbitals at these positions. However, the substitution in 1, 3, 6 and 8 positions influences both S_0 - S_1 and S_0 - S_2 transitions, while the substitution in positions 4, 5, 9 and 10 has only weak influence on these transitions.^[154b, 162] The first electronic transition of *N*-(2,6-diisopropylphenyl)-naphthalene-1,8-dicarboxylic acid imide (in the following denoted as naphthalimide or abbreviated as NI) itself appears also in the UV range at around 350 nm showing a broad absorption with less prominent vibronic features than pyrene.^[163] The individual spectra of pyrene and naphthalimide and a superposition of both spectra in dichloromethane is shown in Figure 4.

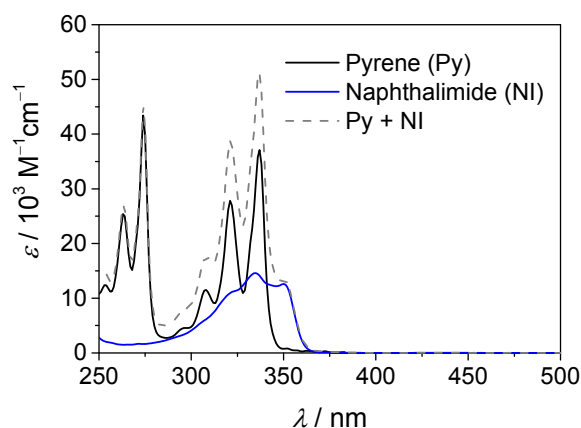


Figure 4 UV/Vis absorption spectra of pyrene ($c = 4 \cdot 10^{-5}$ M), naphthalimide ($c = 6 \cdot 10^{-5}$ M) and the superposition of both (dashed line) measured in dichloromethane at room temperature.

The absorption spectra of the synthesized naphthalimide-functionalized pyrenes **329-332** and **335** are compared with the superposition of the pyrene and naphthalimide spectra in appropriate ratios (Figure 5). All the newly synthesized pyrene derivatives clearly show spectral features similar to the superposition of the respective moieties, indicating that the optical properties of both chromophores that are connected by a covalent bond are maintained. For derivatives **329**, **330** and **332** containing naphthalimide moieties at 1, 1,6- or 1,3,6,8-positions of the pyrene core the absorption band at around 350 nm can be attributed to the S_0 - S_2 transition of pyrene with the underlying absorption of the naphthalimide moieties, which leads to a bathochromic shift compared to unsubstituted pyrene due to the electron-withdrawing effect of the naphthalimide and the underlying spectral band shape of the latter. Similarly, the band around 280 nm can be assigned to the S_0 - S_3 transition of the pyrene moiety which is again bathochromically shifted compared to that of parent pyrene due to the introduction of naphthalimide substituents. Interestingly, a new intense broad band in the range of 375-475 nm appears which can be attributed to a charge transfer transition with pronounced intramolecular interaction between the donor (Py) and acceptor (NI) moieties leading to a loss of vibronic features and the broadening of the band.

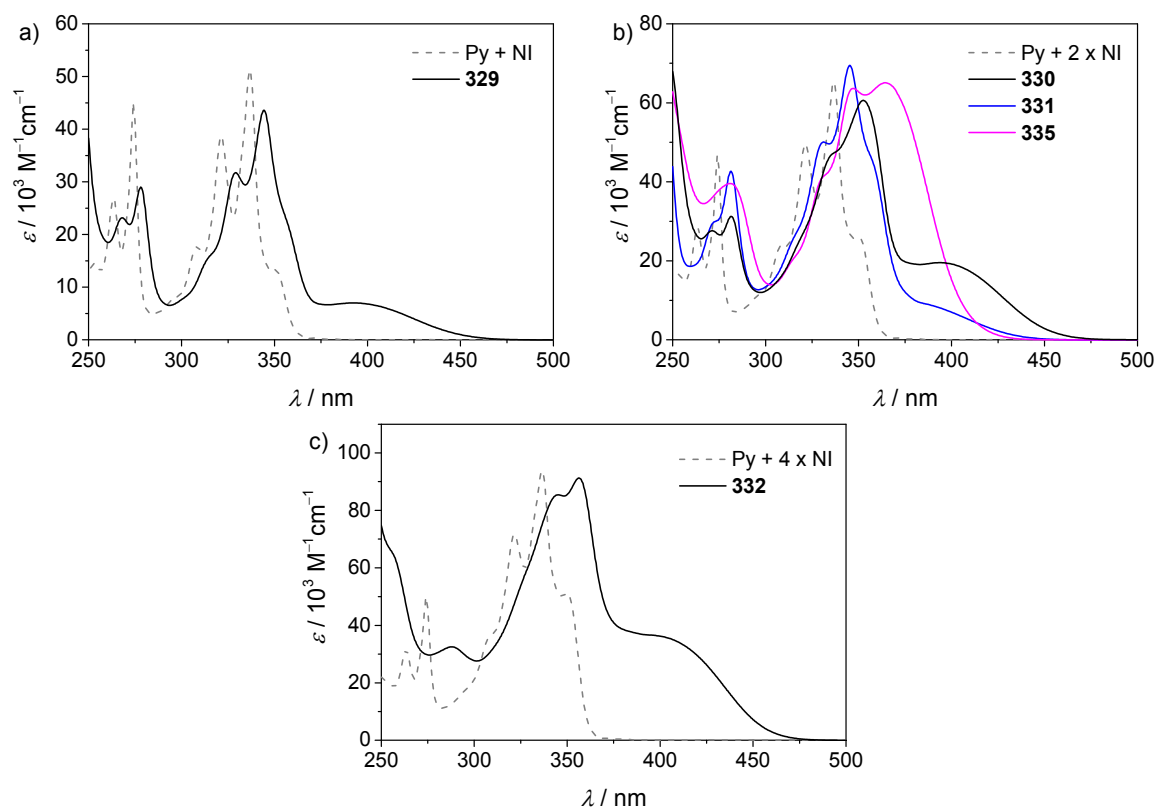


Figure 5 UV/Vis absorption spectra of a) mono-substituted pyrene **329** ($c = 3 \cdot 10^{-5}$ M), b) di-substituted compounds **330**, **331** and **335** ($c = 2-3 \cdot 10^{-5}$ M) and c) tetra-substituted pyrene **332** ($c = 1 \cdot 10^{-5}$ M) in dichloromethane at room temperature and the superposition of pyrene (Py) and naphthalimide (NI) spectra in appropriate ratios (dashed lines in grey).

The number of naphthalimide substituents attached to the pyrene core in 1, 3, 6 and 8 positions obviously enhances the intensity of this band as shown in Figure 5b, c. In contrast, the 4,9-substituted derivative **331** shows less intensity of this low energy absorption band. However, the bands at around 350 nm and 280 nm can similarly be attributed to the S_0 - S_2 and S_0 - S_3 transitions of the pyrene and the underlying S_0 - S_1 transition of the naphthalimide moieties. The spectral features of compound **335** substituted in 2,7-positions clearly differ from those of the 1,6- and 4,9-substituted derivatives **330** and **331** as we observe a maximum at 347 nm, which can be assigned to the S_0 - S_2 transition of the pyrene moiety, and an additional intense broad band at 364 nm, the latter might be assigned to a charge transfer transition with pronounced intramolecular interaction between the donor (Py) and acceptor (NI) moieties. These differences clearly reflect the influence of substitution pattern on the absorption properties of functionalized pyrenes, which are dependent on the orbital contributions to the different electronic transitions and their coefficients in the respective positions at the pyrene core.

The naphthalimide-substituted pyrenes **329-332** and **335** show broad emission spectra in the visible range with maxima between 521 and 560 nm in dichloromethane (Figure 6, Table 1). Interestingly, the addition of multiple naphthalimide substituents in positions 1, 6 or 1, 3, 6 and 8 leads to a blue shift of the emission maxima compared to that of mono-substituted **329** and an increase of the fluorescence quantum yield from 28 (**329**) to 33 (**330**) and 48 % (**332**). For the disubstituted regioisomeric derivatives **330**, **331** and **335** a blue shift of 12 and 25 nm is observed for 4,9-substituted **331** and 2,7-substituted **335**, respectively, compared to 1,6-substituted derivative **330**.

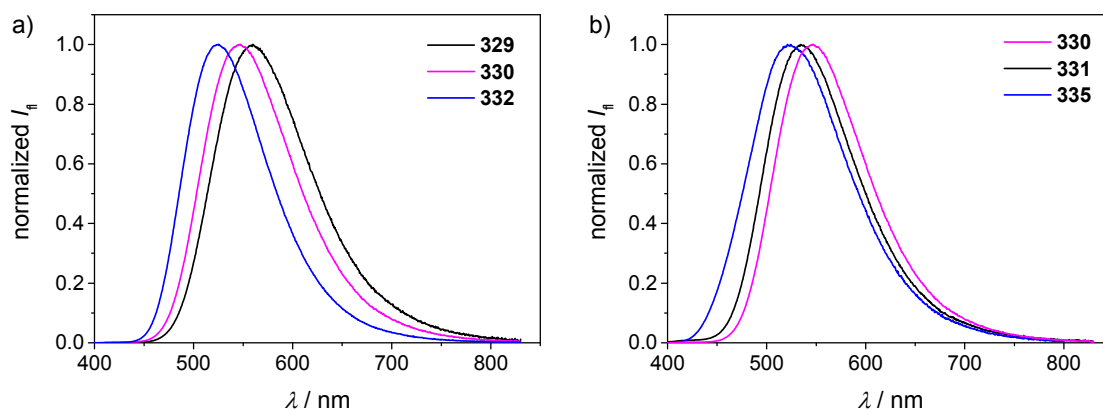


Figure 6 Emission spectra of a) 1-, 1,6- and 1,3,6,8-substituted derivatives **329**, **330** and **332** and b) disubstituted regioisomers **330**, **331** and **335** in dichloromethane at room temperature ($c \sim 1 \cdot 10^{-7}$ M, $\lambda_{\text{ex}} = 340$ nm).

Moreover, the quantum yields of the regioisomers are decreased from 33 (**330**) to 16 (**331**) and 4 % (**335**) clearly illustrating the effect of substitution pattern on the optical properties of pyrene derivatives. The fluorescence life times of compounds **329-332** and **335** show moderate alternations with values between 3.38 and 4.89 ns in dichloromethane (Table 1).

Table 1 Summary of the optical properties of compounds **329-332** and **335**.

Compd.	solvent	$\lambda_{\text{abs}} / \text{nm} (\epsilon / 10^3 \text{ M}^{-1} \text{ cm}^{-1})^a$	$\lambda_{\text{em}} / \text{nm}^a$	$\Delta\tilde{\nu} / \text{cm}^{-1}$	$\Phi_{\text{fl}} / \%$ ^{a,b}	$\tau / \text{ns}^{\text{a,c}}$
329	toluene	345 (41.1), 393 (7.2)	491	5079	52	3.62
	THF	278 (34.2), 343 (46.0), 387 (7.3)	534	7113	27	3.52
	DCM	278 (29.0), 344 (43.6), 393 (7.0)	560	7588	28	4.40
	DMSO	346 (44.5), 391 (6.7)	619	9420	20	6.12
330	DCM	281 (31.5), 353 (60.9), 394 (19.6)	546	7066	33	3.48
331	DCM	281 (42.7), 345 (69.4), 390 (sh, 8.6)	534	6914	16	4.89
332	DCM	288 (32.5), 356 (91.2), 397 (sh, 36.5)	525	6141	48	3.38
335	DCM	281 (39.6), 347 (63.7), 364 (65.1)	521	8279	4	1.92 (9 %), 4.61 (91 %)

^aMeasured at room temperature. ^bRelative fluorescence quantum yields measured by optical dilute method ($A < 0.05$)^[164] using quinine sulfate ($\Phi_{\text{fl}} = 59\%$ in 0.1 M HClO₄) as standard.^[165] ^cFor decay traces see Appendix Figure A1.

A broadening of the band shape of the lowest energy transition in absorption and emission spectra has also been reported for other aryl-substituted pyrenes^[147b, 149, 166] and can be attributed to intramolecular interactions between the constituent chromophores. In newly synthesized pyrene derivatives, these intramolecular interactions may lead to pronounced charge transfer character due to the electronic character of the individual chromophore moieties (as it can be seen from the frontier molecular orbitals, Figure 10). In addition, the new compounds show relatively large Stokes shifts ranging from 6141 to 8279 cm⁻¹ (in dichloromethane) that imply geometrical changes upon excitation. This geometric changes might be attributed to structures in which the individual chromophore moieties are arranged perpendicular or in-plane with respect to each other.^[167] Due to steric congestion between the chromophore moieties the ground state molecular structures exhibit a twisted geometry between the pyrene core and the naphthalimide groups (as shown for compound **329** in Figure 7, similar dihedral angles are anticipated for multi-substituted derivatives, which were not investigated by DFT calculations). Excitation might lead to a rotation around the common

single bond and thus conversion of a perpendicular arrangement into a more planar one.^[168] Assuming that this steric congestion prohibits a planar local excited state, the fluorescence might also be attributed to twisted intramolecular charge transfer (ICT) states.^[167]

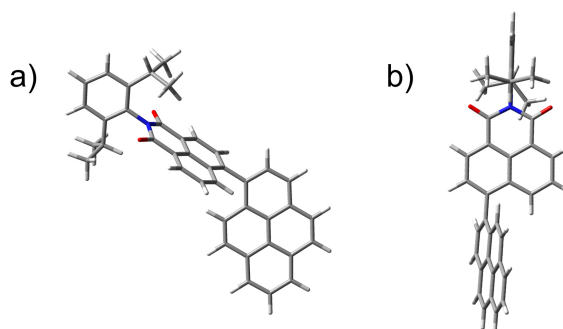


Figure 7 Geometry-optimized structure of **329** obtained from DFT calculations[†] (B3-LYP/6-31G*) with a measured dihedral angle of 72.6° between the NI and Py moieties. a) Top view on the pyrene moiety, b) top view on the naphthalimide moiety.

Solvent-dependent measurements for compound **329** revealed that the emission is largely influenced by the solvent polarity, while the absorption remains nearly unchanged (Figure 8). In less polar solvents like toluene an emission maximum at 491 nm with a quantum yield of 52 % is observed, while in more polar solvents such as DMSO a broader spectrum with a pronounced bathochromic shift of the emission maximum to 619 nm and a prolonged lifetime ($\tau = 6.12$ ns) and decreased quantum yield (20 %) was observed (Table 1).

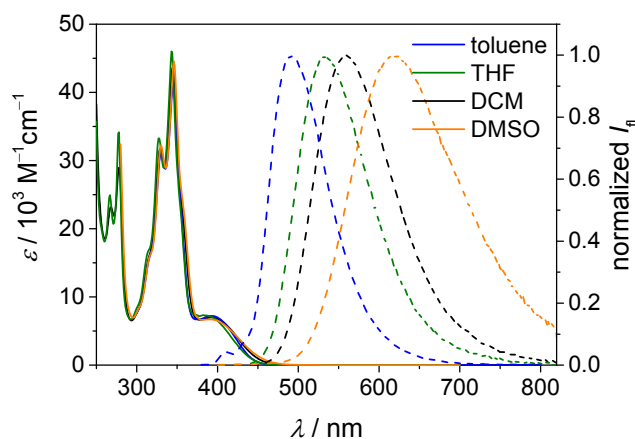


Figure 8 UV/Vis absorption (solid lines, $c = 3 \cdot 10^{-5}$ M) and emission spectra (dashed lines, $c \sim 1 \cdot 10^{-7}$ M, $\lambda_{\text{ex}} = 340$ nm) of **329** in solvents of different polarity at room temperature.

This solvent effect on the emission properties of **329** can be considered as an additional indication for an intramolecular charge transfer character, either twisted or more planar, in which the relaxation of surrounding polar solvent molecules define their formation kinetics and the equilibrium between local excited and intramolecular charge transfer states.^[167] The

[†] DFT calculations were performed by Dr. David Bialas.

large bathochromic shift in polar solvents indicates pronounced charge separation in the excited state. Due to significantly decreased solubility of di- and tetra-substituted pyrene derivatives **330**, **331**, **332** and **335** in toluene, THF and DMSO no reliable solvent-dependent measurements could be performed for these compounds and thus the data are not discussed here.

3.1.4 Electrochemical Properties

To assess the electronic character of naphthalimide-functionalized pyrenes **329-332** and **335**, cyclic and square wave voltammetry measurements were performed in dichloromethane with tetrabutylammonium hexafluorophosphate as supporting electrolyte (Figure 9).

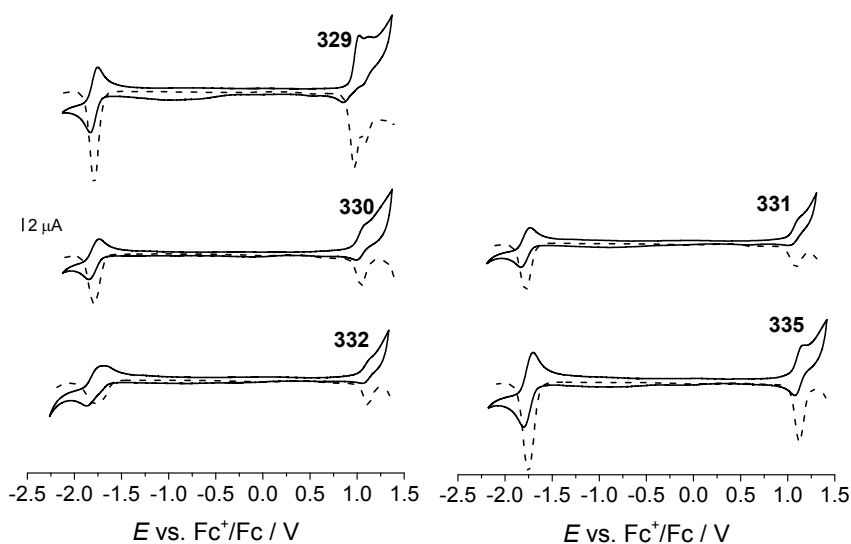


Figure 9 Cyclic (solid lines) and square wave voltammograms (dashed lines) of compounds **329-332** and **335** in dichloromethane ($c = 2-3 \cdot 10^{-4}$ M), 0.1 M TBAHFP as supporting electrolyte, scan rate 100 mVs^{-1} .

The redox properties of these compounds are summarized in Table 2. All of these naphthalimide-substituted pyrene derivatives showed reduction processes at nearly identical potentials in the range of -1.75 to -1.79 V and oxidation processes between 0.97 and 1.12 V. We assume that the reduction processes are due to the reduction of the naphthalimide moieties and the oxidation is taking place at the pyrene core, as the HOMO and LUMO orbitals are located on the individual chromophore moieties and show very little delocalization over the whole system (as illustrated for **329**, see Figure 10).

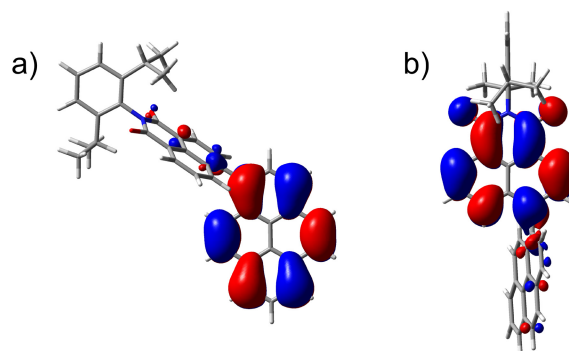


Figure 10 HOMO (a) and LUMO (b) of compound **329** obtained by DFT calculations (B3-LYP/6-31G*, isovalue 0.02 a.u.).

Table 2 Summary of the electrochemical properties of compounds **329-332** and **335**.

Compd.	$E_{\text{ox}} / \text{V}^a$	$E_{\text{red}} / \text{V}^a$	$\Delta E_{\text{red}}(E_{\text{pa}} - E_{\text{pc}}) / \text{mV}^b$
329	0.97, 1.09	-1.79 (-1.79) ^b	76
330	1.04	-1.79 (-1.79) ^b	115
331	1.09	-1.79 (-1.78) ^b	98
332	1.11	-1.80 (-1.78) ^b	176
335	1.12	-1.75 (-1.75) ^b	98

^aPotential obtained by square wave voltammetry, referenced against the ferrocenium/ferrocene redox couple.

^bHalf-wave potential obtained by cyclic voltammetry.

Only slight increase in the difference between anodic and cathodic peak potentials of the reduction was observed for multi-substituted pyrene derivatives compared with that of mono-substituted compound **329**. Moreover, the integrated currents of oxidation and reduction processes measured by square wave voltammetry indicate multiple-electron processes for the reduction of compounds **330-332** and **335**. Therefore, it can be assumed that all naphthalimide moieties are reduced almost simultaneously without considerable interaction due to weak electrostatic interactions between the quite distant naphthalimide moieties and only weak conjugation with the central pyrene core.

3.1.5 Conclusion

In summary, a series of mono-, di- and tetra-naphthalimide-substituted pyrenes was synthesized by Suzuki-Miyaura cross-coupling reactions in up to 98 % yield. The optical properties of these new pyrene derivatives are dependent on the number of substituents as well as substitution pattern at the pyrene core. The most significant spectroscopic feature of these pyrene derivatives functionalized with electron-poor naphthalimides is an intense, broad charge transfer transition in the range from 360 to 475 nm which differs in intensity depending on the number of naphthalimide substituents and their position at the pyrene core. Moreover, these pyrene derivatives show broad emission and their maxima are blue-shifted with increasing number of naphthalimide substituents. Solvent-dependent fluorescence spectra of mono-substituted derivative **329** indicate emission from a CT-state. In contrast, these naphthalimide-substituted pyrenes show nearly identical redox properties. Due to their interesting optical properties, these naphthalimide-substituted pyrenes might be of interest as organic optoelectronic materials. Therefore, further investigations on their photophysical properties in solution and in the solid state are initiated.

3.2 Palladium-Catalyzed C–C Coupling Cascade Reactions: An Efficient Route to Electron-Poor Polycyclic Aromatic Dicarboximides on the Nanoscale*

3.2.1 Introduction

Polycyclic aromatic hydrocarbons (PAHs) are a well-known class of organic molecules that are characterized by extended carbon-rich sp^2 -hybridized scaffolds with interesting electronic properties. Therefore, this type of compounds has attracted considerable interest as promising materials for organic electronics and photovoltaics.^[170] Since the first isolation of graphene,^[6] which is an infinite two dimensional material based on hexagonal connected sp^2 -hybridized carbon atoms, numerous graphene nanoribbons as well as graphene cutouts of different sizes and edge structures have been developed to deduce intrinsic structure-property relationships.^[10] The conventional synthetic strategies for the construction of such large sized PAHs are based on pioneering work by Scholl^[20a] and Clar,^[171] and usually include common C–C bond formation steps like Suzuki-Miyaura or Yamamoto cross-coupling, Diels-Alder cycloaddition or acetylene trimerizations to prepare oligoaromatic precursors. To ultimately annulate these multi aromatic building blocks for the construction of fully π -conjugated scaffolds, the final carbon-carbon bonds are commonly generated by oxidative dehydrogenation using Lewis acids or oxidants like $FeCl_3$, $MoCl_5$ or DDQ.^[10b, 20b] Although these multistep procedures are well established for electron-rich PAHs and nanographenes bearing no additional functional groups, the synthetic access to larger electron-poor systems as required for n-type semiconduction remains limited presumably due to the instability of carbocation intermediates that are formed from electron-deficient precursors under oxidative conditions. Examples accomplished in the past are particularly given for archetype electron-poor rylene bisimides, which could be obtained by oxidative dehydrogenation under strongly basic conditions.^[35, 172] Attempts to extend this structural motive towards nano-sized molecules, the groups of Wang^[14a, c] and Nuckolls^[15b, 173] reported on oligo rylene bisimides,

* This chapter was published in: [160] S. Seifert, K. Shoyama, D. Schmidt, F. Würthner, *Angew. Chem. Int. Ed.* **2016**, 55, 6390; and [169] S. Seifert, D. Schmidt, F. Würthner, *Org. Chem. Front.* **2016**, 3, 1435.

Reproduced and adopted with permission. Copyright 2016 Wiley-VCH Verlag GmbH & Co. KGaA, Weinheim and Royal Society of Chemistry.

Single-crystal structure analysis was performed by Dr. David Schmidt, DFT calculations were performed by Dr. David Bialas and Dr. Vincenzo Grande.

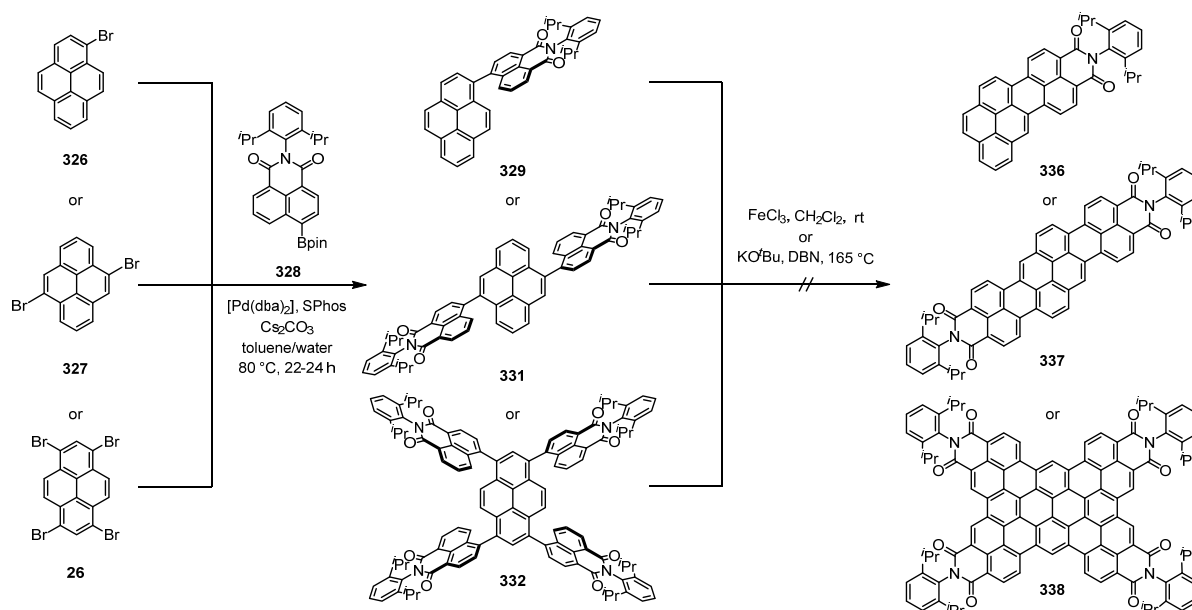
where the pre-synthesized monomeric units were connected by Stille or Ullmann coupling, followed by Mallory photocyclization or dehydrohalogenation. A somewhat more general synthetic approach towards electron-poor PAHs bearing more than two electron-withdrawing imide groups is concerned with the preconstruction of anhydride or carboxylic acid ester functionalized PAHs and their post-imidization to generate the respective electron-deficient imide analogues.^[16b, 114a]

In this chapter, we report on the attempt to planarize the multichromophoric precursors introduced in *Chapter 3.1* by oxidative dehydrogenation similar to previously described literature known procedures. Furthermore, an alternative direct and highly efficient one-pot synthesis of electron-poor polycyclic aromatic dicarboximides bearing up to four electron-withdrawing naphthalimide groups that are annulated to a pyrene core *via* six-membered rings is presented. Up to ten carbon-carbon bonds were created in a single chemical operation by palladium-catalyzed Suzuki-Miyaura cross-coupling, dehydrohalogenation and dehydrogenation leading to the formation of planar two-dimensional, electron-poor polycyclic aromatic dicarboximides (PADIs), which can be regarded as electron-poor nanographenes. Moreover, the molecular structures of these π -extended systems have been elucidated by single-crystal X-ray analysis confirming the formation of multiple C–C bonds by these cascade coupling reactions and the planar geometry of the synthesized scaffolds. Additionally, UV/Vis absorption and emission spectroscopy as well as cyclic and square wave voltammetry was performed to deduce their molecular properties.

3.2.2 Synthesis and Mechanistic Rationale

In our initial attempts to synthesize the electron-poor polycyclic aromatic dicarboximides **336**, **337** and **338**, we followed a frequently applied stepwise strategy that includes C–C bond formation by palladium-catalyzed cross-coupling and subsequent oxidative dehydrogenation. Although, we could prepare the intermediates **329**, **331** and **332** as described in *Chapter 3.1* by Suzuki-Miyaura cross-coupling reaction, the subsequent oxidative dehydrogenation under the conditions described in the literature^[35, 174] to generate the annulated systems **336**, **337** and **338** either failed completely or gave only trace amounts of the desired products (Scheme 45). After the reaction of pyrene derivatives **329** and **332** with iron(III) chloride as an oxidant the starting materials were recovered without any noticeable conversion. Obviously, the oxidation strength of FeCl₃ is not sufficient to dehydrogenate these electron-poor molecules to π -extended frameworks. Another explanation might be that the propensity for the formation of new carbon-carbon bonds is significantly reduced at the 4-, 5-, 9- and 10-

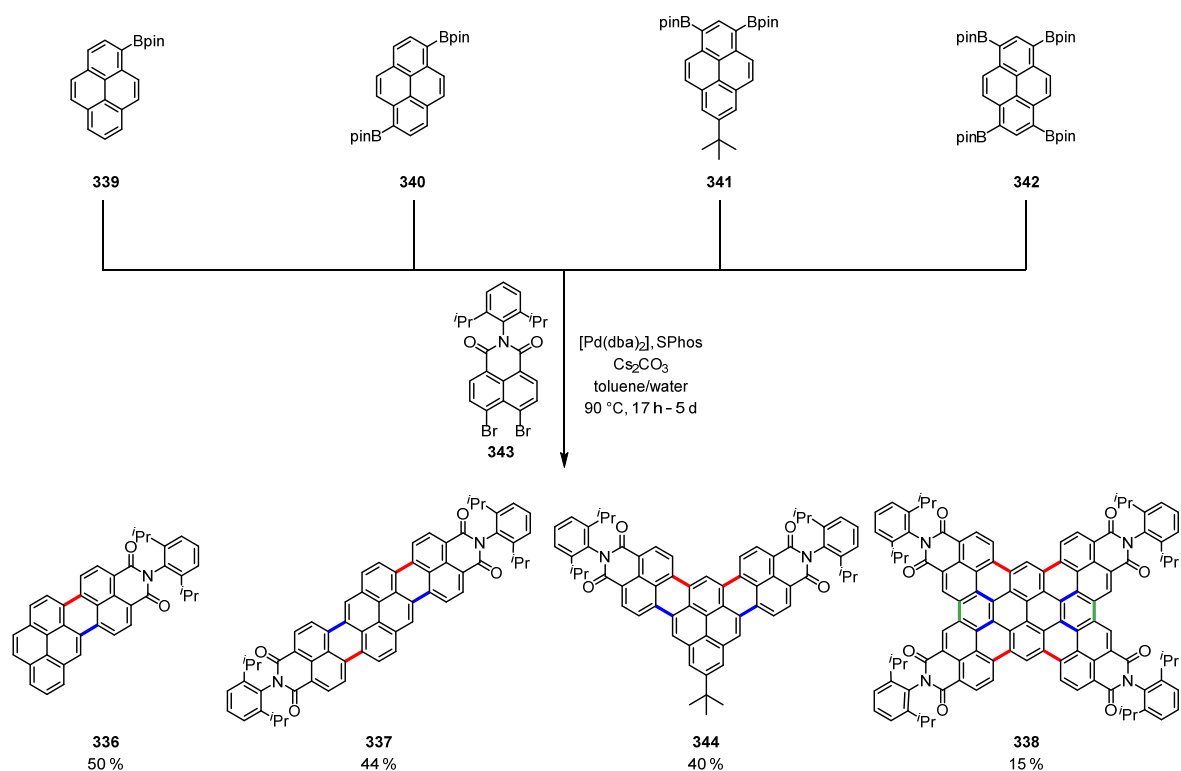
positions of the pyrene radical cations as suggested by Lorbach *et al.*^[52] based on their quantum-chemical calculations of spin density distribution in such species. Therefore, we tested the 4,9-substituted **331** for oxidative cyclization under the same conditions. However, no annulation to **337** could be detected. Likewise, the dehydrogenation of **329**, **331** and **332** under strongly basic conditions, which were previously applied for C–C bond formation for imide-containing systems,^[35] gave only minor amounts of the respective ring-fused products along with some partially cyclized side products, which could not be separated from each other.



Scheme 45 Attempts for the oxidative cyclization of compounds **329**, **331** and **332**.

To increase the driving force for the intramolecular cyclization reaction, we have changed our strategy and introduced an additional halogen atom next to the reaction center for Suzuki-Miyaura cross-coupling in the naphthalimide precursor and thus we used 4,5-dibromonaphthalimide **343**, anticipating a subsequent facile dehydrohalogenation reaction similar to literature-known procedures for pyrenes and other polyarenes.^[29, 59a] Therefore, we had to change the activating group on the pyrene core to boronate esters and thus the pyrene boronic acid pinacol esters **339-342** were synthesized from the respective brominated pyrene derivatives by Miyaura borylation^[175] with bis(pinacolato)diboron (B_2pin_2) as boronic acid ester source and isolated in 77–83 % yields after chromatographic purification. The precursor *N*-(2,6-diisopropylphenyl)-4,5-dibromo-1,8-naphthalimide **343** was synthesized in two steps by Hunsdiecker reaction of naphthalene bisanhydride^[176] and subsequent imidization with 2,6-diisopropylaniline under acidic conditions.^[132a] Indeed, the palladium-catalyzed coupling reaction of dibromonaphthalimide **343** with the mono- and di-boronate esters **339**, **340** and

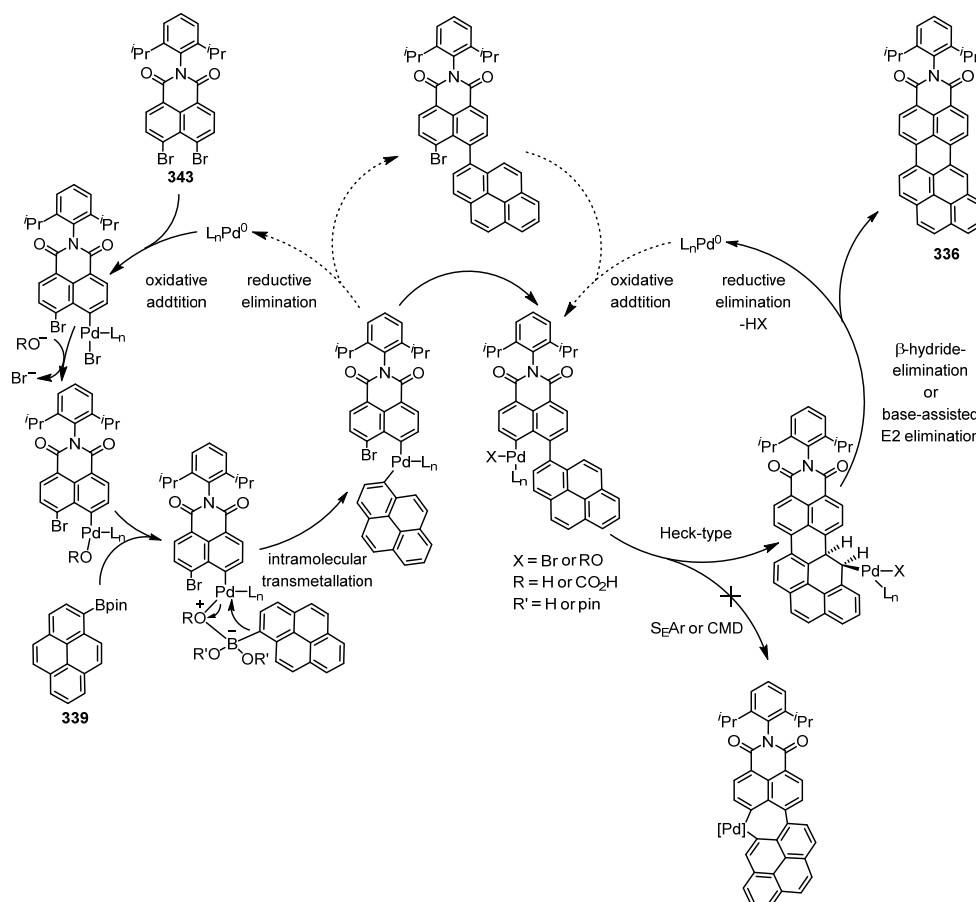
341 using $[\text{Pd}(\text{dba})_2]$ as Pd^0 source and SPhos (2-dicyclohexylphosphino-2',6'-dimethoxybiphenyl) as ligand led to the formation of the fully conjugated six-membered ring annulated polycyclic aromatic dicarboximides **336**, **337** and **344**, respectively, in 40–50 % isolated yields (Scheme 46). Most interestingly, the coupling reaction of pyrene tetra-boronic acid pinacol ester **342** with naphthalimide **343** under similar reaction conditions, as applied for **336**, **337** and **344**, afforded the dicarboximide-functionalized nanographene **338** by C–C bond formation cascade in a, for such extended two-dimensional scaffold, reasonably high yield of 15 %. Up to ten new C–C bonds were formed in this coupling cascade reaction by Suzuki-Miyaura cross-coupling (highlighted in red), intramolecular dehydrohalogenation (highlighted in blue), and, more intriguingly, additional C–C bond formation (compound **338**, highlighted in green) between adjacent naphthalimide moieties formally by oxidative dehydrogenation.



Scheme 46 Synthetic routes to new polycyclic aromatic dicarboximides **336**, **337**, **338** and **344** (dba: dibenzylideneacetone, SPhos: 2-dicyclohexylphosphino-2',6'-dimethoxybiphenyl).

Although by this Pd-catalyzed coupling reaction a five-membered ring annulation is in principle possible, such products were not detected. We have applied typical conditions for Suzuki-Miyaura cross-coupling reactions,^[43a, 177] thus we assume an initial C–C bond formation by Suzuki cross-coupling, which might lead to a mono-halogenated intermediate that can undergo further activation by palladium and rapid direct C–H arylation (Scheme 47). While different mechanisms have been discussed in the literature for direct C–H

arylations,^[26a, b] we consider a Suzuki-Heck-type coupling cascade to be the most likely pathway for the present case. A plausible mechanistic rationale is illustrated in Scheme 47, where the initial C–C coupling takes place *via* Suzuki-Miyaura cross-coupling (left cycle) and a second C–C bond formation by Pd-catalyzed Heck-type C–H arylation (right cycle). One possible explanation for a favored Heck-type coupling might be that a competing mechanism by electrophilic aromatic substitution ($S_{\text{E}}\text{Ar}$) or concerted metalation deprotonation (CMD) would lead to a seven-membered palladacycle intermediate. Such an intermediate would entail a drastic deformation of the aromatic cores and should accordingly be disfavored.

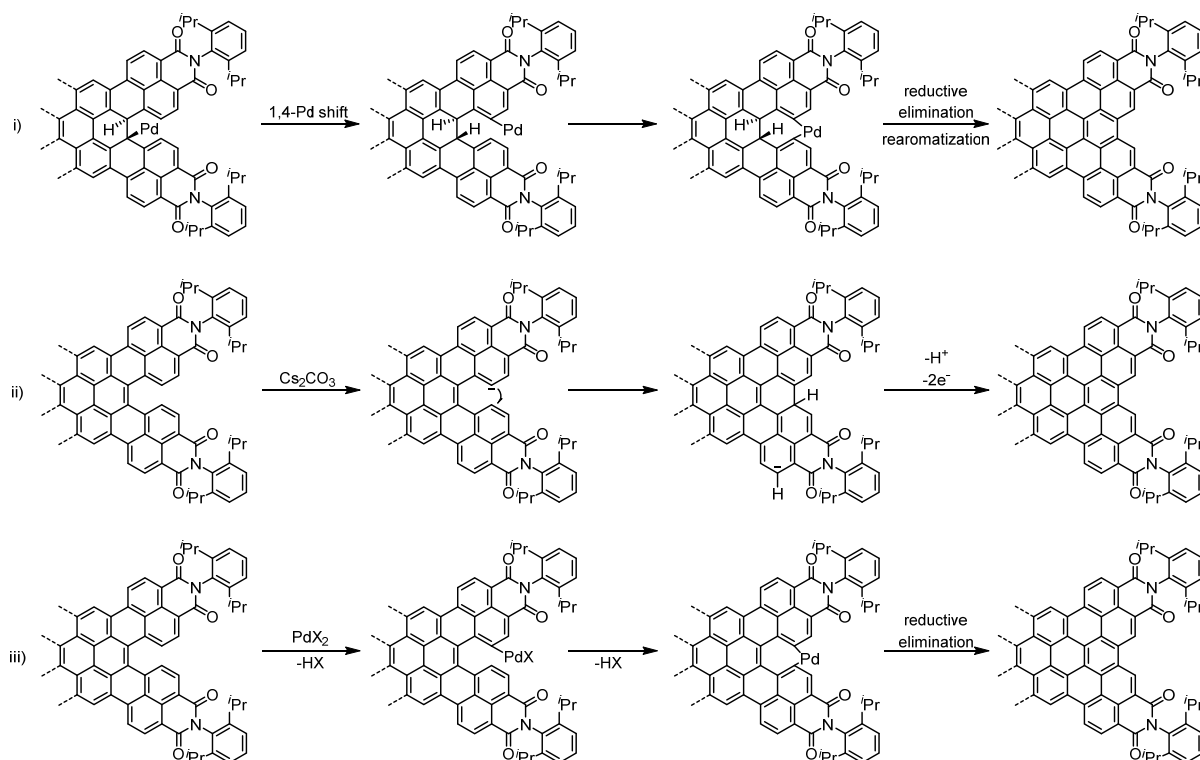


Scheme 47 A mechanistic proposal for the Pd-catalyzed cross-coupling-annulation cascade illustrated for the formation of compound **336** as an example.

Indeed, Rice and coworkers have observed the formation of cyclopenta-fused PAHs by intramolecular coupling of two naphthalene moieties through a six-membered palladacycle intermediate, which is of less steric constraint.^[57a] However, we could not detect any cyclopenta-fused systems under the reaction conditions applied. Moreover, the possibility of a Heck-type mechanism was proposed for several Pd-catalyzed arylations in the past.^[45a, 47c, 178] As illustrated in Scheme 47 (right cycle) the oxidative addition of the aryl-halide bond to the Pd-center takes place in the first step. Then the halide might be exchanged by another

anionic ligand (*i.e.* OH^- or CO_3H^-), followed by carbopalladation. In the last step of the catalytic cycle, an *anti*- β -hydride elimination or a base-assisted E2 elimination^[47c, 178b] leads to a cyclohexa-fused product. For di- and tetra-boronated pyrenes **340-342**, which lead to annulation of two or four naphthalimide moieties, similar repeating catalytic cycles are anticipated.

For the final C–C bond formation between adjacent naphthalimide moieties in case of nanographene **338** different possible scenarios might be considered (Scheme 48): □) A 1,4-Pd-migration proceeding from the carbopalladated species, formed by above described Suzuki-Miyaura cross-coupling and Heck-type carbopalladation, activating position 3 of one naphthalimide subunit that successively reacts with the naphthalimide unit in close proximity and finally undergoes rearomatization. However, this procedure is hardly imaginable due to the formation of a highly strained seven-membered palladacycle as intermediate and the absence of sacrificial oxidants for rearomatization. □) Another option may be an oxidative coupling induced by deprotonation of the electron-deficient π -core by the carbonate base. After nucleophilic attack on the neighboring naphthalimide moiety and release of a second proton a quinoidal structure might be formed, the latter has to undergo two one electron oxidation steps to form the conjugated aromatic structure, which might occur during workup under ambient conditions. However, the basicity of Cs_2CO_3 might not be sufficient for the deprotonation of the π -scaffold.



Scheme 48 Proposed mechanistic scenarios for the C–C bond formation between adjacent naphthalimide moieties leading to the formation of compound **338**.

□) The third possible scenario is a C–H activation by a Pd[□]-species, which can easily be formed by side reactions of the catalyst, leading to so called catalytic oxidative dehydrogenation as described in *Chapter 2.1.2* to generate the planar aromatic scaffold **338**. However, as for pathway □) also here a strained seven-membered palladacycle has to be considered as an intermediate.

3.2.3 Structural Elucidation

The new two-dimensional PADIs **336**, **337**, **338** and **344** were characterized by ¹H, ¹³C NMR spectroscopy and high-resolution mass spectrometry. Moreover, the structural assignment of these compounds was confirmed by single-crystal X-ray analysis. Their structure dependent optical and electrochemical properties were characterized by UV/Vis absorption and fluorescence spectroscopy and cyclic and square wave voltammetry.

Single crystals of **336**, **337** and **338** suitable for X-ray analysis could be grown by slow diffusion of non-polar solvents into their dichloromethane or chloroform solutions and thus their molecular structures could be unambiguously confirmed. Due to its comparatively high dipole moment of 7.0 Debye (obtained by DFT calculations), the solid state packing arrangement of **336** (Figure 11a-c) is characterized by tightly stacked antiparallel dimers with average π - π -distances of approximately 3.55 Å and the crystallographic inversion centers are located in the centers of gravity. These dimers are further interconnected by multiple short C–H \cdots O contacts (< sum of van der Waals radii, 2.68 Å) between adjacent molecules. However, the sterically demanding imide substituents force the individual dimers to be displaced laterally and longitudinally against each other, giving rise to voids that are filled with dichloromethane molecules. In contrast, the centrosymmetric PADI **337** (Figure 11d-f) exhibits a slipped stacked solid-state packing with intermolecular π - π -distances of 6.99 Å and C–H \cdots π as well as C–H \cdots O hydrogen bonding interactions between neighboring molecules. The large π -surfaces of **337** are additionally solvated by two toluene molecules each, whereas the voids between two slipped stacked chromophores are filled with dichloromethane molecules. Owing to the four bulky diisopropylphenyl substituents, nanographene **338** displays a large longitudinal and transversal intermolecular displacement of approximately 14 Å, whereas each individual molecule is intercalated by four symmetry equivalents through C–H \cdots π interactions (Figure 11h). As a consequence of the intercalation of the diisopropylphenyl substituents between the π -surfaces, a large π - π -distance of 13.30 Å was observed, giving rise to a brickwall-type packing arrangement in which the individual layers are separated by chloroform molecules (Figure 11j,k). Furthermore, several solvent

accessible voids exist within these layers, which describe the squeezed electron density of highly disordered chloroform molecules and could not be modeled satisfactorily.

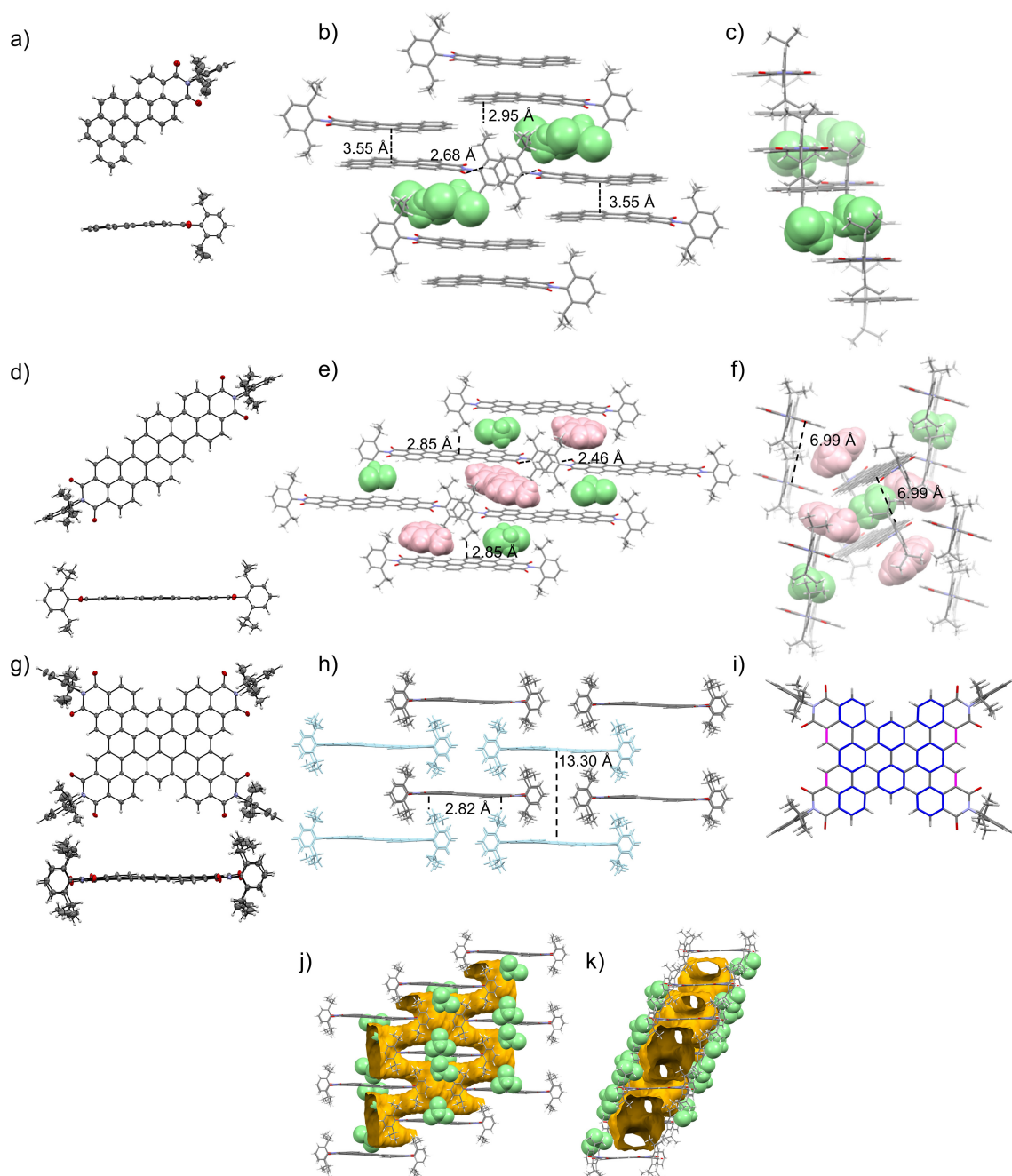


Figure 11 Solid-state molecular structures of compounds **336** (a), **337** (d) and **338** (g) determined by single-crystal X-ray diffraction (top: front view, bottom: side view; solvent molecules are omitted for clarity, ellipsoids set at 50 % probability); b) and c) packing arrangement of **336** in the solid state with included dichloromethane molecules (green); e) and f) packing arrangement of **337** in the solid state with included dichloromethane (green) and toluene molecules (rose); h) the packing arrangement of **338** (solvent molecules are omitted for clarity), i) visualization of the different C–C bonds (bonds within benzenoid rings (in blue): 1.382–1.436 Å (avg. 1.409 Å) and olefinic bonds (in magenta): 1.363 Å); j) and k) packing arrangement of **338** with included chloroform molecules (green) and solvent accessible voids (illustrated in dark yellow).

In contrast to other graphene cutouts like teranthene or quarteranthene,^[179] in which quinoidal resonance structures with biradicaloid character are established by the propensity of the π -scaffold to increase the number of Clar sextets,^[180] compounds **336**, **337** and **338** do not exhibit a systematic C–C bond length alternation. All crystallographically characterized molecules exhibit almost perfectly planar π -scaffolds with C–C bond length between 1.342–1.479 Å (**336**), 1.368–1.474 Å (**337**) and 1.363–1.483 Å (**338**), corroborating their polycyclic aromatic character. Interestingly, in compounds **336** and **337** the shortest C–C bonds are located in the 4–5 and 9–10 positions of the central pyrene core. Therefore, these positions have the most olefinic character in the molecule that might influence their reactivity towards additional annulation by the proposed Heck-type mechanism *via* a Pd- π complex. In contrast, compound **338** exhibits the shortest C–C bonds within the naphthalimide subunits (1.36 Å, Figure 11i marked in magenta). Furthermore, this molecule is characterized by benzenoid C–C bonds (Figure 11i, highlighted in blue, $\bar{\phi} = 1.409$ Å) that are somewhat shorter than the interconnecting carbon-carbon bonds ($\bar{\phi} = 1.436$ Å). Similar bond length characteristics have been observed for disc-shaped nanographenes^[181] and coronenes^[182] by X-ray analysis. With an almost coplanar π -surface of approximately 118 Å² that is generated by 64 fully conjugated carbon and 4 nitrogen atoms, compound **338** is one of the largest planar PAHs whose molecular structure has been determined by X-ray analysis. Somewhat smaller-sized and electron-rich flat nanographene derivatives were crystallographically characterized by Kubo^[179] and Yamada^[183] with sp² carbon atom counts of C₄₂ (teranthene, ca. 71 Å²) and C₅₆ (quarteranthene and tetrabenzoperipentacene, ca. 98 Å²). In contrast, nanographenes with an even higher carbon content of C₈₀^[184] or C₉₆^[181] that have been reported so far showed strongly distorted π -scaffolds due to the incorporation of odd-membered rings or sterically constraints at the edges of disc-shaped molecules.

3.2.4 Optical and Electrochemical Properties

The optical properties of the naphthalimide-annulated scaffolds **336**, **337**, **338** and **344** were characterized by UV/Vis absorption and emission spectroscopy in dichloromethane at room temperature (Figure 12). Distinct absorption spectral features are displayed by these π -extended PADIs **336**, **337**, **338** and **344** with remarkably high molar absorptivities in the visible range (Table 3). Compound **336** exhibits a broad S₀-S₁ absorption band with a maximum at 547 nm ($\epsilon = 44200$ M⁻¹cm⁻¹) without any well-defined vibronic fine structure, which is shifted about 77 nm to higher wavelength compared to the parent molecule without dicarboximide moieties, naphtho[8,1,2-*bcd*]perylene ($\lambda_{\max} = 470$ nm),^[133a] and about 38 nm

compared to the analogous perylene monoimide ($\lambda_{\max} = 509 \text{ nm}$).^[185] These observations can be attributed to the extension of the π -system by the core structure and the electron-withdrawing effect of the imide substituent. In contrast, the symmetric PADI **337** displays a S_0 - S_1 transition with well resolved vibronic progression from aromatic C–C stretching vibrations and an absorption maximum at 663 nm ($\epsilon = 152200 \text{ M}^{-1}\text{cm}^{-1}$). Compared to its analogue without dicarboximide groups, dibenzo[*lm,yz*]pyranthrene ($\lambda_{\max} = 575 \text{ nm}$),^[133a] the absorption is again shifted by 88 nm to higher wavelength due to the electron-withdrawing imide groups. Interestingly, this bis(dicarboximide) **337** shows a similar spectral shape as terrylene bis(dicarboximide) ($\lambda_{\max} = 650 \text{ nm}$)^[186] or zethrene bis(dicarboximide) ($\lambda_{\max} = 648 \text{ nm}$)^[132c] but the absorption is of higher intensity and red-shifted by 13 and 15 nm, respectively. The emission spectra of monoimide **336** and bisimide **337** reveal a mirror image relationship with their respective absorption spectra with Stokes shifts of 1559 (**336**) and 399 cm^{-1} (**337**) and fluorescence quantum yields of 79 % (**336**) and 40 % (**337**). While the quantum yield of **336** is very close to that of perylene monoimide (90 %),^[185] the quantum yield of **337** is lower than the value of the analogous perylene and terrylene bisimides (100 and 90 %)^[186-187] but in the similar range of zethrene bisimide (53 %).^[132c]

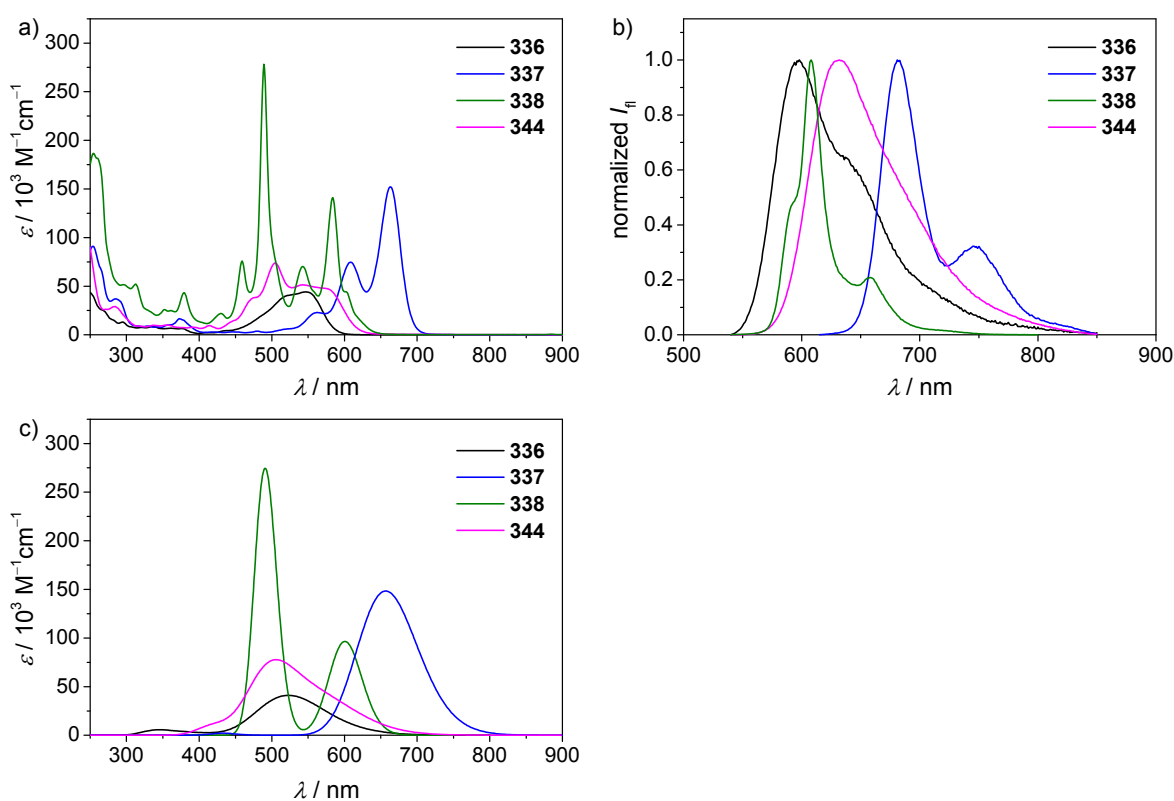


Figure 12 UV/Vis absorption ($c = 4 \cdot 10^{-6} - 5 \cdot 10^{-5} \text{ M}$) (a) and emission spectra ($c \sim 1 \cdot 10^{-7} \text{ M}$) (b) of compounds **336** (black, $\lambda_{\text{ex}} = 530 \text{ nm}$), **337** (blue, $\lambda_{\text{ex}} = 640 \text{ nm}$), **338** (olive, $\lambda_{\text{ex}} = 530 \text{ nm}$) and **344** (magenta, $\lambda_{\text{ex}} = 530 \text{ nm}$) measured in CH_2Cl_2 at room temperature and calculated absorption spectra (c) by TD-DFT (B3LYP/def2-SVP, half-width: 0.25 (**336**), 0.14 (**337**), 0.09 (**338**), 0.2 eV (**344**)).

While the optical signatures of **336** and **337** obviously relate to those of core-unsubstituted rylene mono- and bisimides,^[122, 185-187] which show intense S_0 - S_1 transitions, the absorption and emission properties of the angular bisimide **344** and tetraimide **338** differ considerably from those of **336** and **337** as a consequence of a different symmetry. Therefore, compound **344** exhibits optical transitions not only to the first excited state but also to higher excited states displaying a maximum at 504 ($\epsilon = 73700 \text{ M}^{-1}\text{cm}^{-1}$) and a broad shoulder with a maximum at 575 nm. Similarly, the absorption spectrum of **338** is not dominated anymore by the lowest-energy S_0 - S_1 transition ($\lambda_{\text{max}} = 584 \text{ nm}$, $\epsilon_{\text{max}} = 141200 \text{ M}^{-1}\text{cm}^{-1}$) but by a higher-energy absorption band at $\lambda_{\text{max}} = 489 \text{ nm}$, which is characterized by well-resolved vibronic progressions and a very high molar extinction coefficient of $278300 \text{ M}^{-1}\text{cm}^{-1}$. These observations are in good agreement with the TD-DFT calculated spectra (Figure 12c). According to these calculations, the transition dipole moments of these two main transitions of **338** and **344** are aligned along the short and long molecular axes of their central pyrene core (Figure 13).

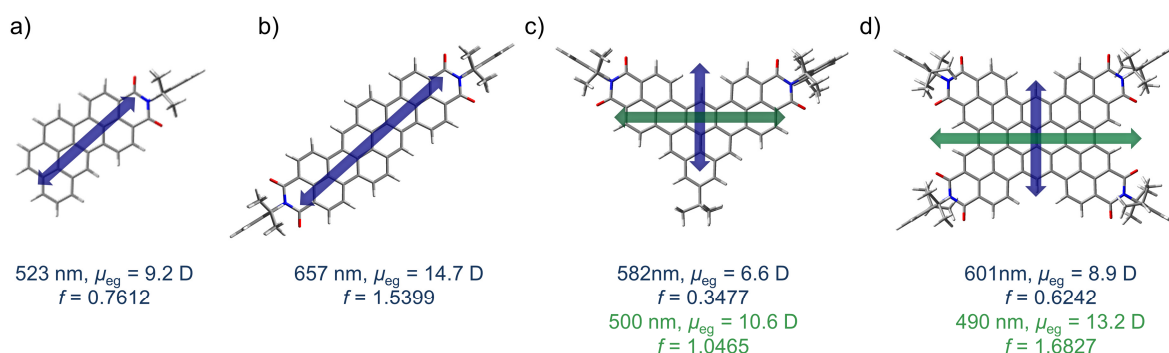


Figure 13 Energy minimized structures of a) **336**, b) **337**, c) **344** and d) **338** with the visualization of their most prominent transitions and their transition dipole moments (μ_{eg}) as well as oscillator strengths (f) obtained by (TD-)DFT calculations (B3LYP/def2-SVP).

Most interestingly, despite the inferior oscillator strength of the lowest-energy transition of compounds **344** and **338**, bright fluorescence with quantum yields of 79 % (**344**) and 67 % (**338**) occurs from their first excited singlet states at 632 (**344**) and 608 nm (**338**) with a mirror-image-like band shape. This high fluorescence quantum yields for the 2D fluorophores **344** and **338** can be explained by a prolonged fluorescence lifetime of 6.6 and 13.4 ns which is significantly longer than that of conventional fluorescent dyes such as perylene bisimides (ca. 4–6 ns).^[85a] The high fluorescence quantum yield and lifetime accordingly appear as promising properties of 2D core-expanded electron-poor polycyclic hydrocarbons that warrant further exploration.

Table 3 Summary of the optical properties of compounds **336**, **337**, **338** and **344**.

Compd.	$\lambda_{\text{abs}} / \text{nm} (\epsilon / 10^3 \text{M}^{-1} \text{cm}^{-1})^a$	$\lambda_{\text{em}} / \text{nm}^a$	$\Phi_{\text{fl}} / \%^{a,b}$	$\tau / \text{ns}^{a,d}$
336	547 (44.2)	598	79	4.87
337	563 (23.0), 608 (74.6), 663 (152.2)	681	40	4.75
338	459 (75.9), 489 (278.3), 543 (70.1), 584 (141.2)	608	67 ^c	13.38
344	504 (73.7), 543 (51.4), 575 (sh, 47.7)	632	79	6.61

^aMeasured in dichloromethane at room temperature. ^bRelative fluorescence quantum yields measured by optical dilute method ($A < 0.05$)^[164] using rhodamine 101 ($\Phi_{\text{fl}} = 91.5\%$ in ethanol) and oxazine 1 ($\Phi_{\text{fl}} = 15\%$ in ethanol) as standards.^[165] ^cAbsolute quantum yield. ^dFor decay traces see Appendix Figure A2.

To experimentally assess the electronic character of **336**, **337**, **338** and **344**, cyclic and square wave voltammetry (Figure 15) was performed. Multiple redox processes are observed for the PADIs **336**, **337**, **338** and **344**. Thus, compound **336** exhibits two well separated and reversible reduction processes at -1.35 and -1.79 V vs. the ferrocenium/ferrocene (Fc^+/Fc) redox couple, besides one reversible oxidation at $+0.75$ V. Compared to unsubstituted perylene monoimide (-1.46 , -1.95 V and $+0.95$ V)^[185] these potentials are shifted to less negative and less positive values, what goes in hand with a smaller HOMO-LUMO gap which is in accordance with the redshift of the absorption maximum of **336** compared to perylene monoimide. Compound **337** bearing two electron-withdrawing naphthalimide subunits can be reduced twice at identical potentials (-1.13 V) that are, however, cathodically shifted by 220 and 660 mV compared to those of **336**. Additionally, one single oxidation at $+0.67$ V can clearly be observed for **337**, whose integrated current is approximately the half of the anionic reduction.

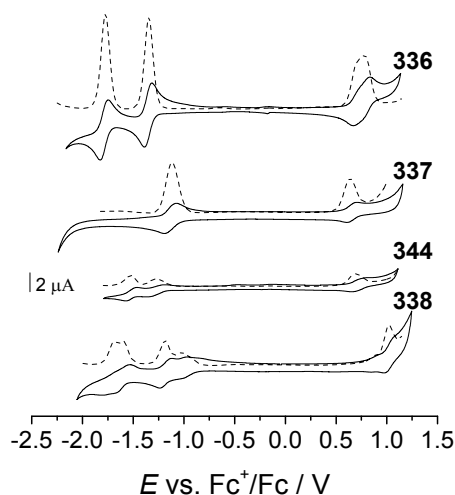


Figure 14 Cyclic (solid line) and square wave (dashed line) voltammograms of **336**, **337**, **338** and **344** in dichloromethane solutions ($c = 2\text{--}3 \cdot 10^{-4}$ M, 0.1 M TBAHFP, scan rate 100 mVs^{-1}).

The overlap of both reduction processes can be explained by the large distance between the two naphthalimide moieties, which reduces Coulomb repulsion. A similar behavior has been reported for higher rylene bisimides like terrylene and quarterylene bisimides.^[122] Compound **344**, however, shows again two separated reduction events at -1.28 and -1.52 V and one oxidation at $+0.73$ V indicating a slightly smaller HOMO-LUMO gap (see Figure 15) than that of **336** which is in good agreement with the optical data (Figure 12a). Interestingly, one oxidation and four not fully separated reduction processes are observed for tetraimide **338**, which could only be resolved by square wave voltammetry. These redox events with potentials of $+1.03$, -0.99 , -1.18 , -1.59 and -1.68 V exhibit roughly the same integrated current, indicating single-electron transfer processes.

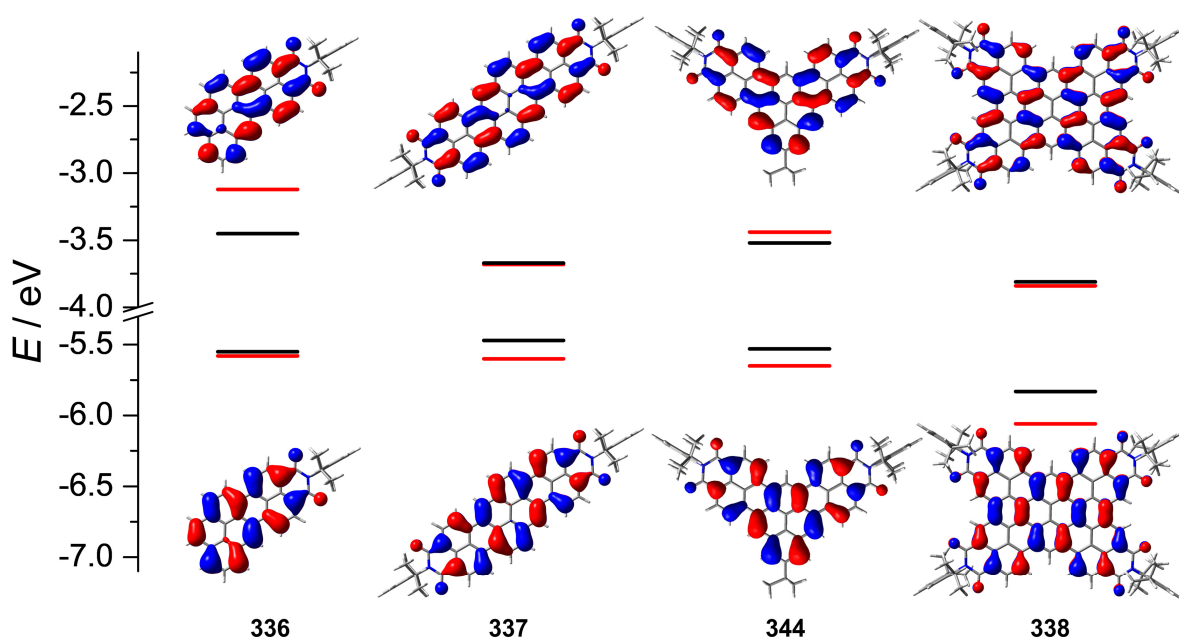


Figure 15 Calculated HOMOs and LUMOs of **336**, **337**, **338** and **344** by DFT (B3-LYP/def2-SVP, isovalue: 0.02 a.u.) and their experimentally determined energy levels (black, calculated by $E_{\text{LUMO}} = -[E_{\text{red1}} + 4.8 \text{ eV}]$ and $E_{\text{HOMO}} = -[E_{\text{ox}} + 4.8 \text{ eV}]$ and the energy level of Fc^+/Fc with respect to the vacuum level (-4.8 eV)^[188]) and DFT calculated values (red).

Considering the energy level of ferrocenium/ferrocene (Fc^+/Fc) with respect to the vacuum level (-4.8 eV)^[188] the HOMO and LUMO energy levels of **336**, **337**, **338** and **344** can be estimated using their experimentally determined redox potentials. The values thus obtained are in good agreement with our DFT calculations (see Figure 15) and exhibit energy levels at -3.45 eV (**336**), -3.67 eV (**337**), -3.81 eV (**338**) and -3.52 eV (**344**) for the LUMO and -5.55 eV (**336**), -5.47 eV (**337**), -5.83 eV (**338**) and -5.53 eV (**344**) for the HOMO levels (Table 4).

Table 4 Summary of electrochemical properties of compounds **336**, **337**, **338** and **344**.

Compd.	$E_{\text{ox}} / \text{V}^a$	$E_{\text{red1}} / \text{V}^a$	$E_{\text{red2}} / \text{V}^a$	$E_{\text{red3}} / \text{V}^a$	$E_{\text{red4}} / \text{V}^a$	$E_{\text{HOMO}} / \text{eV}^b$	$E_{\text{LUMO}} / \text{eV}^b$	$E_{\text{HOMO}} / \text{eV}^c$	$E_{\text{LUMO}} / \text{eV}^c$
336	0.75	-1.35	-1.79	-	-	-5.55	-3.45	-5.58	-3.12
337	0.67	-1.13*	-1.13*	-	-	-5.47	-3.67	-5.60	-3.68
338	1.03	-0.99	-1.18	-1.59	-1.68	-5.83	-3.81	-6.06	-3.84
344	0.73	-1.28	-1.52	-	-	-5.53	-3.52	-5.65	-3.44

^aHalf-wave potentials were determined by cyclic or square wave voltammetry measured in DCM (0.1 M TBAHFP) vs. Fc^+/Fc . *This reduction is, according to the integration from square wave data, a two electron process. ^bCalculated according to literature know procedure using the experimentally determined redox potentials ($E_{\text{LUMO}} = -[E_{\text{red1}} + 4.8 \text{ eV}]$ and $E_{\text{HOMO}} = -[E_{\text{ox}} + 4.8 \text{ eV}]$) and the energy level of Fc^+/Fc with respect to the vacuum level (-4.8 eV).^[188] ^cDFT calculated values (B3-LYP/def2-SVP).

Comparable LUMO levels were reported for other electron-poor π -conjugated systems like chlorinated nanographenes (-3.37 to -4.01 eV),^[181] dicarboximide-based systems like perylene bisimides (-3.79 eV)^[187] or higher rylene bisimides (-3.65 eV for a terrylene bisimide)^[122] and fullerene derivatives like PC₆₀BM (-3.91 eV).^[189] Therefore, we are convinced that derivatives of the newly synthesized dyes **336**, **337**, **338** and **344** have potential as electron-accepting or ambipolar charge transport materials that should be of interest for (opto)electronic devices.

3.2.4 Conclusion

In summary, we have reported here an efficient synthetic route towards electron-poor nanometer sized polycyclic aromatic dicarboximides by combining palladium-catalyzed Suzuki-Miyaura cross coupling, dehydrohalogenation and, in the case of nanographene **338**, dehydrogenation in a cascade reaction. Thus, up to ten carbon-carbon bonds were created in a single chemical operation to yield planar π -conjugated systems with a size of up to 118 Å² for the nanographene **338**. The optical properties of the newly synthesized PADIs are comparable to rylene mono- and bisimides if the core is extended in only one direction of the parent pyrene core. In the case of angular core annulation leading to a V- or square-shaped π -system, absorption to higher excited states also takes place as the overall geometry of the molecules changes and transitions to higher excited states become allowed. Redox properties reveal the potential of the new dicarboximide-functionalized PAHs as electron-accepting materials as they show similar LUMO energies as hitherto extensively studied rylene bisimides.

3.3 Base-Selective Six- versus Five-Membered Ring Annulation in Palladium-Catalyzed C–C Coupling Cascade Reactions: Synthesis of New Polycyclic Aromatic Dicarboximides and Mechanistic Rationale*

3.3.1 Introduction

Aromatic dicarboximides are an important class of compounds, which inherit low lying frontier molecular orbitals that are of significance for n-type semiconductors^[13, 83] and afford materials of high resistance against thermal, chemical and photooxidative degradation. As discussed in *Chapter 2*, only a limited number of innovative synthetic approaches toward polycyclic aromatic dicarboximides (PADIs) based on carbon-carbon bond formation reactions are available to date.^[14, 15b, 16, 87, 126, 131-132] This is rather surprising if we consider that carbon-carbon coupling reactions of aromatic molecules have been intensively investigated over the last decades and broadly applied for the synthesis of diverse polycyclic aromatic hydrocarbons (PAHs),^[18a, 20b, 29, 191] but have not been explored as a method of general scope for PADIs. Besides the studies on transition-metal-catalyzed cross-coupling reactions of two activated aromatic components, initially developed by Stille, Suzuki, Negishi, Hiyama and Kumada, much efforts have been invested to explore the direct arylation of C–H bonds.^[26] Not only intermolecular, but also intramolecular C–H arylation reactions have been extensively studied to develop new π -conjugated polycycles.^[29]

Despite this enormous development in the field of metal-catalyzed C–H arylation, there is apparently no report in the literature where the reaction mode of C–C coupling of individual coupling systems has been modulated by the applied auxiliary base to achieve selectively either six- or five-membered ring annulation. In *Chapter 3.2* we reported that cesium carbonate (Cs_2CO_3) assisted palladium-catalyzed C–C coupling cascade reactions of pyrene boronate esters with *peri*-dibromonaphthalimide led to the formation of novel electron-poor PADIs by six-membered ring annulation. In this chapter, we show that the mode of ring annulation in Pd-catalyzed C–C coupling cascade reactions of *peri*-dibromonaphthalimide with different aryl boronic acid pinacol esters can be directed by variation of the base to

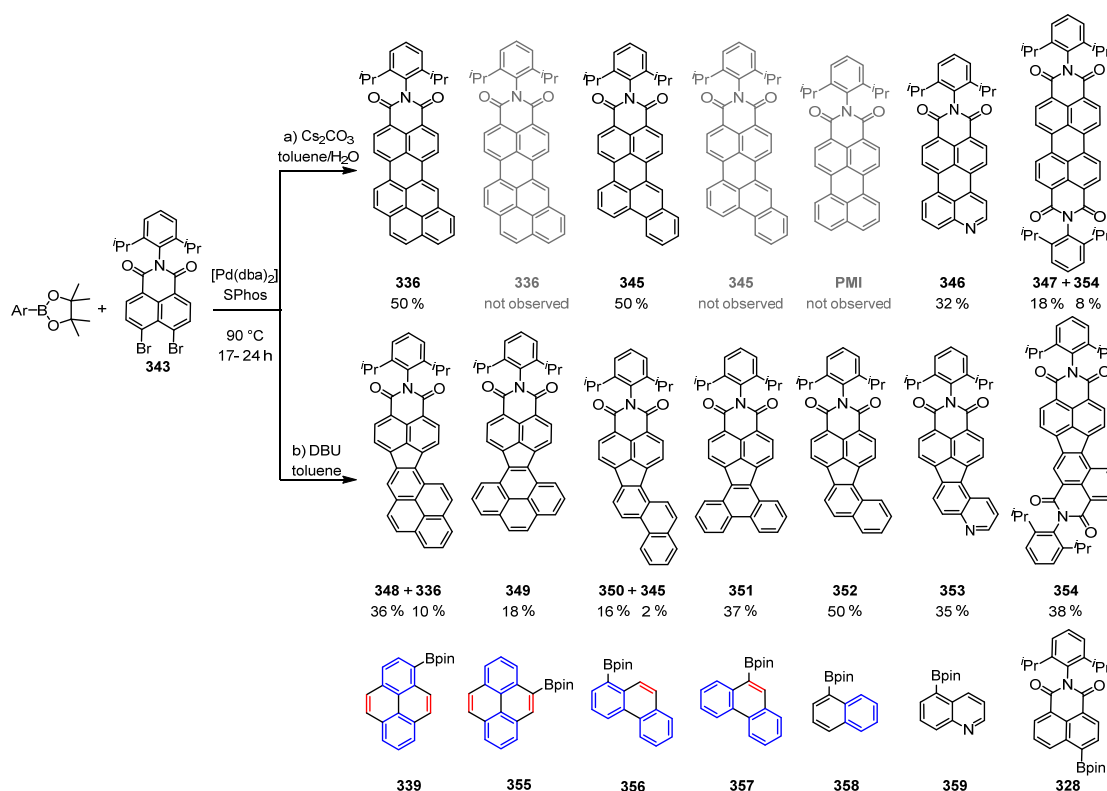
* This chapter was published in parts in: [190] S. Seifert, D. Schmidt, K. Shoyama, F. Würthner, *Angew. Chem. Int. Ed.* **2017**, *56*, 7595.

Reproduced and adopted with permission. Copyright 2017 Wiley-VCH Verlag GmbH & Co. KGaA, Weinheim. Single-crystal structure analysis was performed by Dr. David Schmidt, DFT calculations were performed by Dr. Kazutaka Shoyama.

achieve predominantly either six- or five-membered ring annulated products. Furthermore, the molecular properties of the newly synthesized PADIs were investigated by absorption and emission spectroscopy, cyclic voltammetry, DFT calculations and X-ray diffraction experiments.

3.3.2 Synthesis and Mechanistic Rationale

We have investigated the Pd-catalyzed cross-coupling reaction of dibrominated naphthalimide **343**^[132a] with aryl pinacol boronic acid esters **328**, **339** and **355-359** in the presence of either cesium carbonate (Cs₂CO₃) or 1,8-diazabicyclo[5.4.0]undec-7-ene (DBU) as an auxiliary base, otherwise under very similar reaction conditions (Scheme 49). The reaction of pyrene boronate ester **339** with dibromonaphthalimide **343** in the presence of Cs₂CO₃ led to the exclusive formation of the six-membered annulated PADI **336** in 50 % yield as already reported in *Chapter 3.2*. In contrast, DBU-assisted coupling reaction of these substrates formed the corresponding five-membered ring annulated compound **348** as a major product (36 % yield) along with **336** as a minor product (10 %). Interestingly, the regioisomeric pyrene boronic acid pinacol ester **355** afforded under DBU-mediation only the five-membered ring annulated product **349** in 18 % yield, whereas the Cs₂CO₃-mediated reaction gave neither the possible six-membered ring annulated compound **336** nor PADI **349**. Very similar reaction behavior was observed for the regioisomeric phenanthrene boronic acid pinacol esters **356** and **357** as the Cs₂CO₃-mediated reaction of **356** gave the six-membered product **345** in 50 % yield, while regioisomer **357** did not form **345** under identical reaction conditions. On the other hand, DBU-mediated reaction of **356** and **357** afforded the respective five-membered ring annulated products **350** and **351** in 16 % and 37 % yield, respectively. The naphthalene derivative **358** behaves similar like the pyrene and phenanthrene derivatives **355** and **357** as its Pd-catalyzed C–C coupling reaction in presence of DBU afforded the five-membered ring annulated PADI **352** in 50 % yield, whereas for Cs₂CO₃ as auxiliary base no ring annulation reaction was observed. Surprisingly the comparatively more electron-poor substrates **359** and **328** show again similar reaction behavior like substrates **339** and **356** giving rise to six-membered ring annulated compounds **346** and **347** in 32 and 18 % yield for the coupling reaction in the presence of cesium carbonate, while the five-membered ring annulated products **353** and **354** could be isolated in 35 and 38 % yield by using DBU as auxiliary base.



Scheme 49 Syntheses of electron-poor PADIIs **336** and **345-354** (dba: dibenzylideneacetone; SPhos: 2-dicyclohexylphosphino-2',6'-dimethoxybiphenyl; DBU: 1,8-diazabicyclo[5.4.0]undec-7-ene).

To assess whether other bases can be used for the selective ring annulation reaction, we have tested different inorganic bases such as carbonates, phosphates, hydroxides, alkoxides or fluorides and organic bases like diisopropylethylamine (Hünig's base), triethylamine, 1,5-diazabicyclo[4.3.0]non-5-ene (DBN) and 4-dimethylaminopyridine (DMAP) in Pd-catalyzed cross-coupling reaction of dibromonaphthalimide **343** with pyrene derivative **339** as model compound (Table 5). For all the tested inorganic bases, except potassium *tert*-butoxide, the six-membered ring annulated product **336** could be obtained, however, in lower yields (22–35 %) compared to that obtained with Cs_2CO_3 . On the other hand, for the applied organic bases the five-membered ring annulated compound **348** could only be obtained with DBU (36 %) and DBN (21 %), whereas for Hünig's base ($(iPr)_2NEt$), triethylamine and DMAP no ring annulation was observed. Moreover, Pd^{\square} sources like $[Pd(OAc)_2]$ and $[PdCl_2(MeCN)_2]$, instead of $[Pd(dba)_2]$ as Pd^0 source, have been tested. However, no improvement compared with the Pd^0 -catalyzed reaction could be observed (see Table 5). To increase the solubility of the inorganic bases, the reactions were carried out in a biphasic solvent mixture of toluene/water. Control experiments were performed without addition of water, which led to lower yields but showed no significant influence on the chemoselectivity (six- versus five-membered ring annulation) of the Pd-catalyzed reaction cascade. In the case of DBU-mediated reaction, the addition of water led to a decrease of the isolated yield, which might

be attributed to the fact that the basicity and the coordination ability of DBU is decreased upon addition of water to the organic solution.

Table 5 Overview of the isolated products in the presence of different inorganic and organic bases and different Pd sources for the C–C coupling reaction of **339** with **343**.^a

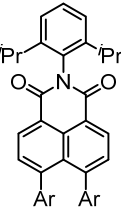
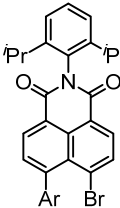
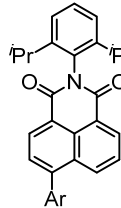
Entry	Catalyst	Base	Solvent	Isolated yields / %	
				Product 336	Product 348
1	[Pd(dba) ₂]/SPhos	Cs ₂ CO ₃	toluene/water	50	-
2	[Pd(dba) ₂]/SPhos	Cs ₂ CO ₃	toluene	31	-
3	[Pd(dba) ₂]/SPhos	K ₂ CO ₃	toluene/water	35	-
4	[Pd(dba) ₂]/SPhos	K ₃ PO ₄	toluene/water	31	-
5	[Pd(dba) ₂]/SPhos	KO ^t Bu	toluene/water	-	-
6	[Pd(dba) ₂]/SPhos	CsOH·H ₂ O	toluene/water	22	-
7	[Pd(dba) ₂]/SPhos	CsF	toluene/water	25	-
8	[Pd(dba) ₂]/SPhos	DBU	toluene	10	36
9	[Pd(dba) ₂]/SPhos	DBU	toluene/water	2	20
10	[Pd(dba) ₂]/SPhos	DBN	toluene	1	21
11	[Pd(dba) ₂]/SPhos	DMAP	toluene	-	-
12	[Pd(dba) ₂]/SPhos	(ⁱ Pr) ₂ NEt	toluene	-	-
13	[Pd(dba) ₂]/SPhos	NEt ₃	toluene	-	-
14	[Pd(OAc) ₂]/SPhos	Cs ₂ CO ₃	toluene/water	39	-
15	[Pd(OAc) ₂]/SPhos	DBU	toluene	traces	10
16	[PdCl ₂ (MeCN) ₂]/SPhos	Cs ₂ CO ₃	toluene/water	12	-
17	[PdCl ₂ (MeCN) ₂]/SPhos	DBU	toluene	-	-

^aReaction conditions: 90 °C, overnight; purification by column chromatography over silica, gradient of hexane/dichloromethane from 3:2 to 100 % dichloromethane.

The moderate isolated yields of the ring annulated products obtained by these C–C coupling cascade reactions (shown in Scheme 49) are apparently due to incomplete conversion of the coupling components and the formation of side products since up to about 30 % of the applied quantity of dibromonaphthalimide **343** was reisolated, along with considerable amounts of the boronate ester precursors or the corresponding hydrodeborylated derivatives. In addition, different mono- and di-arylated naphthalimides were detected by MALDI-ToF mass spectrometry (Table 6).

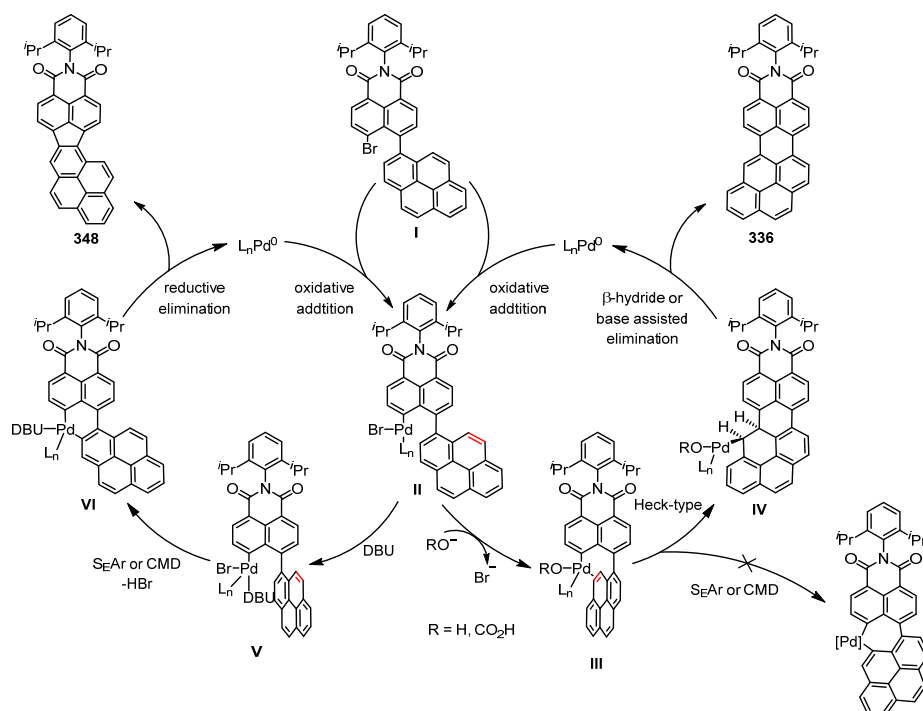
Our present studies have clearly shown that, depending on the applied auxiliary base, the pathway of the intramolecular C–H arylation in Pd-catalyzed C–C coupling reactions can be controlled to yield preferentially either five- or six-membered ring annulated polycyclic aromatic dicarboximides. Whilst the ring annulation reaction in the presence of cesium carbonate is substrate dependent as only for the aryl boronate esters **328**, **339**, **356** and **359** the respective six-membered ring annulated products were formed, with the organic base DBU all the applied substrates formed the corresponding five-membered ring annulated products **348-354**.

Table 6 Overview of isolated or detected (side) products of the coupling cascade reactions.

Coupling components	Reaction conditions	Reisolated starting materials / %		Hydrode-borylation ^c	Side products / %			Isolated and corrected ^e yields / %	
		Boronic ester	343					Six-membered annulation	Five-membered annulation
343 + 339	<i>a</i>	-	23	50	<i>d</i>	-	-	50	-
343 + 339	<i>b</i>	21	8	-	-	<i>d</i>	-	10 (11)	36 (39)
343 + 355	<i>a</i>	-	44	76	<i>d</i>	-	-	-	-
343 + 355	<i>b</i>	62	22	-	<i>d</i>	<i>d</i>	<i>d</i>	-	18 (24)
343 + 356	<i>a</i>	-	18	27	<i>d</i>	-	-	50	-
343 + 356	<i>b</i>	33	31	-	<i>d</i>	-	-	2 (3)	16 (23)
343 + 357	<i>a</i>	-	48	17	<i>d</i>	-	-	-	-
343 + 357	<i>b</i>	-	13	16	<i>d</i>	<i>d</i>	-	-	37
343 + 358	<i>a</i>	-	55	48	<i>d</i>	-	-	-	-
343 + 358	<i>b</i>	39	29	-	-	<i>d</i>	-	-	50 (70)
343 + 359	<i>a</i>	-	30	-	-	-	-	32	-
343 + 359	<i>b</i>	-	13	-	-	-	-	-	36
343 + 328	<i>a</i>	-	10	11	-	-	-	18	8*
343 + 328	<i>b</i>	-	19	5	-	<i>d</i>	-	-	38

^a[Pd(dba)₂], SPhos, Cs₂CO₃, toluene/H₂O, 90 °C; ^b[Pd(dba)₂], SPhos, DBU, toluene, 90 °C; ^ccorresponding hydrodeborylated compounds (pyrene, phenanthrene, naphthalene or naphthalimide); ^ddetected only by mass spectrometry; ^eyield corrected for the converted amount of starting material **343** is indicated in brackets; *determined by NMR.

The above discussed base-selective formation of six- and five-membered ring annulated products in Pd-catalyzed C–C coupling reactions in the presence of cesium carbonate or DBU can be rationalized by two different mechanistic pathways for the intramolecular C–C bond formation step as illustrated in Scheme 50. Since we have applied typical reaction conditions for Suzuki-Miyaura cross-coupling, we assume a common initial C–C bond formation for both catalytic cycles leading to the monoarylated bromonaphthalimide intermediate (I), which functions as a precursor for the palladium-catalyzed C–H arylation reaction. As already discussed in *Chapter 3.2*, we consider a Heck-type coupling reaction in the presence of Cs_2CO_3 (Scheme 50, right cycle) to be the most likely process for the formation of cyclohexa-fused PADIs because the competing mechanistic pathways like electrophilic aromatic substitution ($\text{S}_{\text{E}}\text{Ar}$), concerted metalation deprotonation (CMD) or oxidative C–H bond addition (see *Chapter 2.1*) would involve the formation of seven-membered palladacycles. However, the formation of such strained intermediates are highly unlikely due to steric constraints and substantial deformation of the rigid aromatic cores as it has already been discussed by the groups of Rice and Scott for the intramolecular C–H arylation of two naphthalene subunits.^[57a, 60] After oxidative addition of the aryl-bromide bond to a Pd^0 species (I), halide exchange by other anionic ligands like OH^- or HCO_3^- may occur prior to an intermediate π -complex (II) formation between the former substrate and the palladium center.



Scheme 50 Proposed mechanistic rationale for the base-selective six- versus five-membered ring annulation exemplarily illustrated for the formation of products **336** and **348**.

After carbopalladation (\square) by olefin insertion, *anti*- β -hydride elimination or, more likely, base-assisted E2 elimination, as described in literature,^[47c, 178b] closes the catalytic cycle under liberation of the final products (e.g. **336** as shown in Scheme 50). The initial formation of a π -complex (\square) as a key intermediate for the subsequent C–C bond formation step is thereby highly dependent on the olefinic character of the coordinated π -system. Consequently, for substrates **339** and **356** with a pronounced olefinic bond character at the γ -position of the boronate ester substituent (Scheme 49, highlighted in red), the respective six-membered ring-annulated products **336** and **345** were obtained in good yields, while for regioisomers **355**, **357** and the naphthalene derivative **358** with the coordinating C–C double bond formally embedded into aromatic Clar-sextets (Scheme 49, highlighted in blue) no ring annulation was observed. Electron deficient substrates like **328** and **359** seem to stabilize the intermediate π -complex, facilitating Heck-type C–H arylation even for isoelectronic derivatives with comparatively low double bond character at the γ -position. Apparently, the substitution of the anionic carbonate base by DBU changes the mechanism for the intramolecular C–H arylation resulting in the formation of cyclopenta-fused PADIs as constitutional isomers of the six-membered ring-annulated products (Scheme 50, left cycle). Unlike Cs_2CO_3 , the amidine base DBU potentially acts as competitive neutral σ -donor ligand (\square) preventing the formation of an intermediate π -complex. Therefore, Heck-type carbopalladation and subsequent elimination of the cyclohexa-fused PADIs is effectively suppressed and thus alternative mechanistic pathways like those discussed before become operational. After formation of a six-membered palladacycle intermediate (\square) by electrophilic aromatic substitution ($\text{S}_{\text{E}}\text{Ar}$) or concerted metalation deprotonation (CMD), reductive elimination takes place to generate the cyclopenta-fused products (e.g. **348** as shown in Scheme 50). Since both mechanisms illustrated in Scheme 50 are competitive, minor amounts of the corresponding five- or six-membered PADIs are formed in few cases by the respectively opposite mechanism.

3.3.3 Structural Elucidation

The new electron-poor PADIs were unambiguously characterized by ^1H and ^{13}C NMR spectroscopy, high-resolution mass spectrometry, elemental analysis and crystallographic analyses. Single crystals suitable for X-ray structural analysis could be grown by slow evaporation of chloroform or dichloromethane solutions of **336**, **345**, **346**, **349** and **351-354** (Figure 16). All polycyclic aromatic dicarboximides containing one naphthalimide moiety

(**336**, **345**, **346**, **349** and **351-353**) exhibit solid state packing arrangements that are characterized by antiparallel oriented π -dimers with close interplanar distances of 3.42–3.56 Å due to their comparatively high ground state dipole moments (3.0–7.0 D obtained by DFT calculations). Within these dimers, the aromatic π -surfaces of PADIs **336**, **345**, **349** and **351** are perfectly stacked on top of each other without any significant lateral displacement of the longitudinal pseudo- C_2 symmetry axis passing through the individual naphthalimide subunits (indicated by arrows in Figure 16). In contrast, those of molecules **346**, **352** and **353** are laterally displaced by approximately 1.2, 2.1 and 0.6 Å, respectively, with further close π -contacts of 3.31, 3.49 and 3.41 Å between adjacent dimer subunits that are longitudinally shifted against each other. Such extended π - π -stacking interactions are absent in the case of **336**, **345**, **349** and **351** where multiple short C–H \cdots O and C–H \cdots π contacts (< sum of van der Waals radii) interconnect the loosely packed centrosymmetric dimers. For compound **354** with sterically demanding diisopropylphenyl substituents on both sides of the molecule, π - π -interactions are efficiently suppressed in the solid state resulting in isolated chromophores that are separated by hexane or chloroform molecules. Solvent accessible voids inside the other structures (except for compound **352**) are likewise filled with dichloromethane or chloroform making all crystals sensitive towards solvent evaporation. All the investigated PADIs with one dicarboximide-functionality exhibit nearly coplanar π -scaffolds with torsion angles between the annulated aromatic moieties in the range from 0.21 to 4.55° and C–C bond lengths of 1.34–1.49 Å like they are typically found in sp^2 -hybridized carbon rich materials. A slightly more distorted π -core with torsion angles of 2.45 and 7.78° was observed for compound **354** bearing two dicarboximide moieties. Similar to compound **336** as discussed in *Chapter 3.2*, the phenanthrene-naphthalimide conjugate **345** exhibits the shortest C–C bond distance (1.37 Å) at the 9–10 position of the phenanthrene subunit, indicating an increased olefinic character of this carbon-carbon double bond. These structural findings support our mechanistic considerations on the base-selective formation of five or six-membered ring-annulated PADIs, in which the potential formation of an intermediate π -complex determines the mechanistic pathway but is highly dependent on the position of the olefinic double bond inside the substrate.

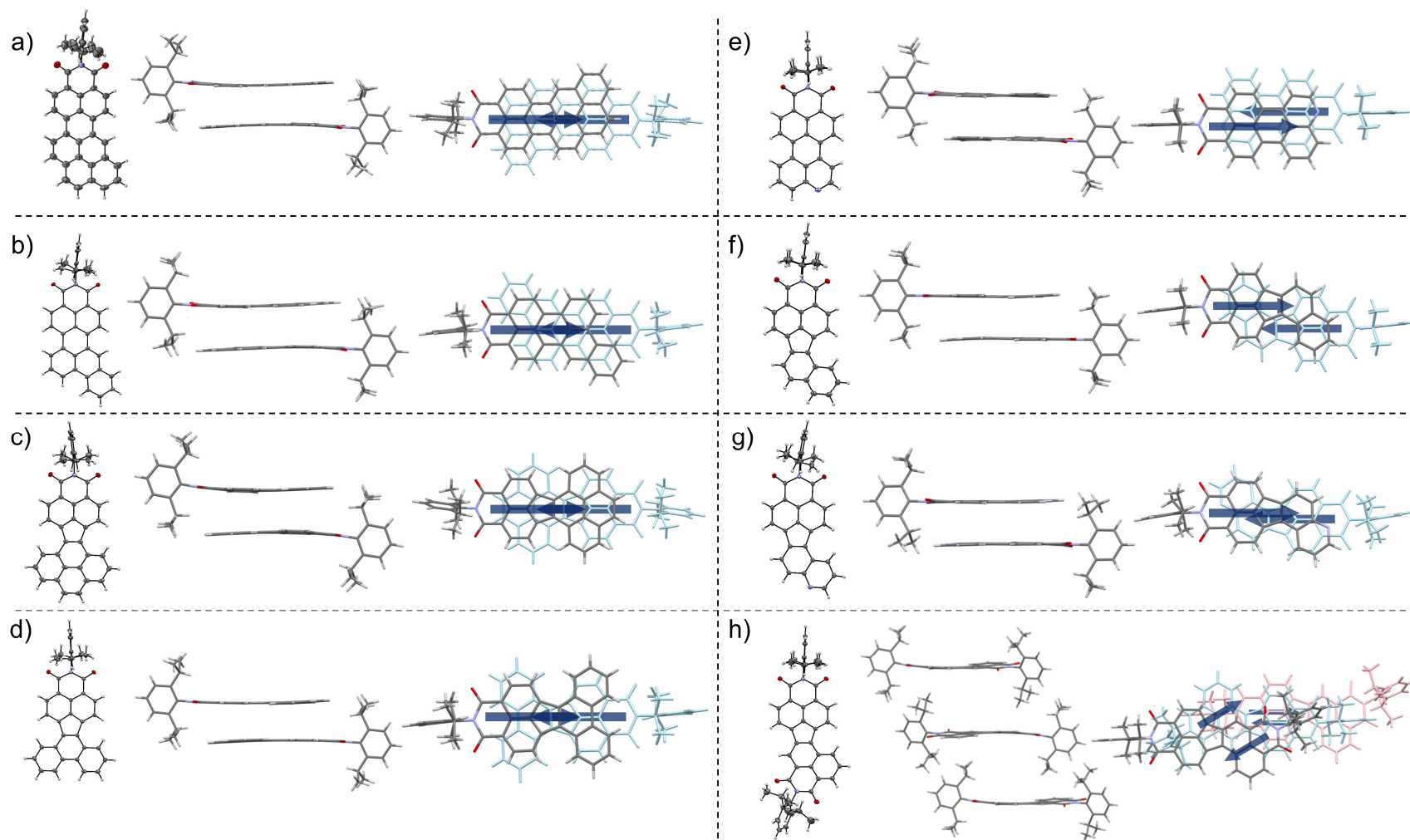


Figure 16 Solid-state molecular structures of a) **336**, b) **345**, c) **349**, d) **351**, e) **346**, f) **352**, g) **353** and h) **354** determined by single-crystal X-ray diffraction (ellipsoids set at 50 % probability) and visualization of their packing arrangement (solvent molecules are omitted for clarity, arrows indicate longitudinal pseudo- C_2 symmetry axis passing through the individual naphthalimide subunits).

3.3.4 Optical and Electrochemical Properties

The optical properties of the naphthalimide conjugates **336**, **345**, **346** and **348-354** were characterized by UV/Vis absorption and emission spectroscopy in dichloromethane solutions at room temperature (Figure 17). Obviously, the six-membered ring annulated compounds **336**, **345** and **346** exhibit similar absorption and emission spectral features like perylene monoimides ($\lambda_{\text{abs}} = 509 \text{ nm}$; $\lambda_{\text{em}} = 539 \text{ nm}$, $\Phi_{\text{fl}} = 90 \%$ in chloroform)^[185] and azaperylene monoimides ($\lambda_{\text{abs}} = 484 \text{ nm}$; $\lambda_{\text{em}} = 544 \text{ nm}$, $\Phi_{\text{fl}} = 89 \%$ in chloroform)^[192] with high molar absorptivities in the visible range and S_0 - S_1 absorption maxima located at 547 nm (**336**, $\epsilon = 44200 \text{ M}^{-1}\text{cm}^{-1}$), 508 nm (**345**, $\epsilon = 38700 \text{ M}^{-1}\text{cm}^{-1}$) and 488 nm (**346**, $\epsilon = 34900 \text{ M}^{-1}\text{cm}^{-1}$). Bright fluorescence with relative quantum yields of 79 % (**336**), 89 % (**345**) and 96 % (**346**) occurs from the first excited singlet state at 598 (**336**), 546 (**345**) and 510 nm (**346**) with mirror image like band shapes relative to their absorption spectra. The corresponding cyclopenta-fused PADIs can be divided into three groups with structurally different motives and distinct optical properties.

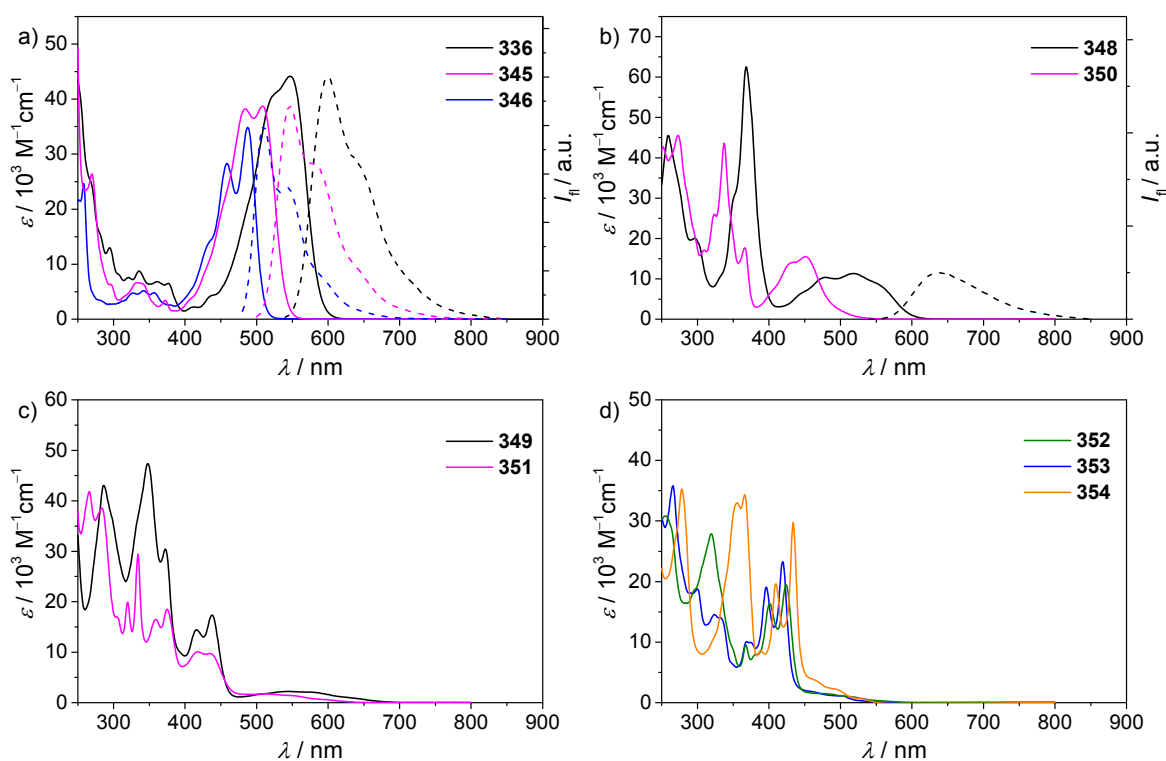


Figure 17 UV/Vis absorption (solid lines, $c = 2\text{--}3 \cdot 10^{-5} \text{ M}$) and emission spectra (dashed lines, $c \sim 1 \cdot 10^{-7} \text{ M}$) of PADIs **336** ($\lambda_{\text{ex}} = 530 \text{ nm}$), **345** ($\lambda_{\text{ex}} = 490 \text{ nm}$), **346** ($\lambda_{\text{ex}} = 450 \text{ nm}$), **348** ($\lambda_{\text{ex}} = 510 \text{ nm}$) and **349-354** in dichloromethane at room temperature.

Thus, the absorption spectra of compounds **348** and **350** with C_S symmetry and unsymmetrically annulated pyrene or phenanthrene moieties are not predominated anymore by the lowest energetic S_0 - S_1 transitions but by higher energetic absorption bands below 400 nm (see Table 7) with extinction coefficients up to $62500 \text{ M}^{-1}\text{cm}^{-1}$. Similar absorption spectra were reported for acenaphtho[1,2-*a*]pyrene and naphtho[1,2-*j*]fluoranthene derivatives,^[193] with hypsochromically shifted UV/Vis transitions, however, due to the absence of electron-withdrawing imide moieties. The constitutional C_{2v} symmetric isomers **349** and **351** exhibit broad and featureless transitions with low intensities centered around 500–650 nm next to multiple higher energy absorption bands between 250 and 450 nm that are comparable to those of undecorated dibenzo[*j,l*]fluoranthene^[194] and acenaphtho[1,2-*e*]pyrene.^[195] Likewise, the optical properties of PADIs **352**-**354** are consistent with those of parent benzo[*j*]fluoranthene^[196] exhibiting absorption bands at 424 (**352**), 419 (**353**) and 434 nm (**354**) with partially resolved vibronic progressions and broad shoulders of low intensity up to 550 nm. These experimental findings could be verified by time-dependent DFT calculations (Figure 18).

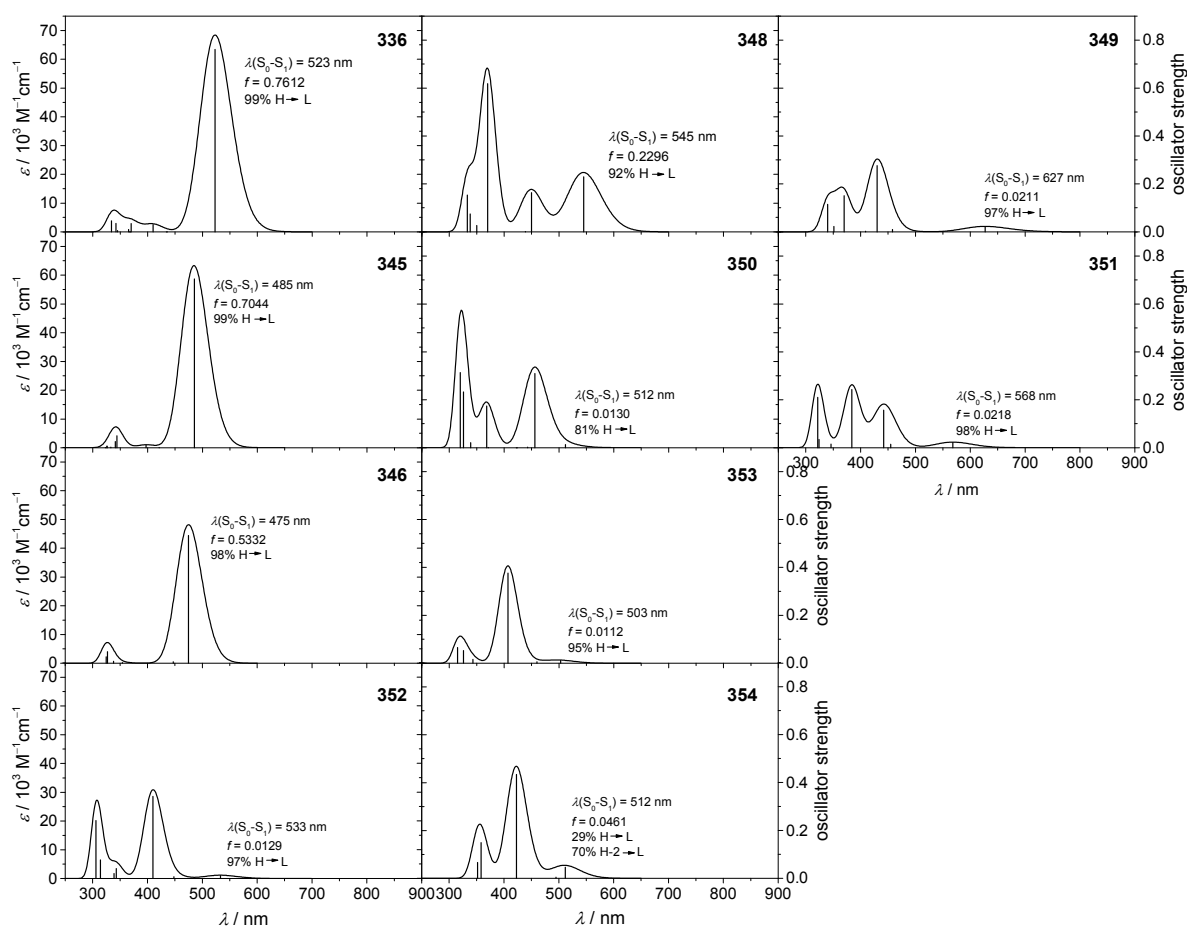


Figure 18 Calculated absorption spectra of PADIs **336**, **345**, **346** and **348**-**354** by TD-DFT (B3LYP/def2-SVP, half-width 0.15 eV).

These calculations revealed high oscillator strength for the S_0 - S_1 -transition of the six-membered ring annulated compounds **336**, **345** and **346** (0.76, 0.70 and 0.53), while the oscillator strength for the lowest energy transition of all five-membered annulated PADIs stays below a value of 0.05, except for compound **348** that shows an oscillator strength of 0.23 (Figure 18). Regarding the fluorescence properties of the five-membered ring annulated PADIs, only compound **348** shows emission with a moderate quantum yield of 23 % and a maximum at 637 nm (Figure 17b), while for all other cyclopenta-fused derivatives no fluorescence could be detected, presumably due to the low oscillator strength of their S_0 - S_1 transition. Moreover, the S_0 - S_1 transitions of all cyclopenta-fused compounds **348-354** possess a pronounced charge transfer character compared to the respective six-membered ring annulated PADIs as revealed by TD-DFT calculated charge density differences that describe the change of static charge distribution upon excitation (Figure 19). Therefore, the pyrene, phenanthrene or naphthalene subunit in the respective compounds can be regarded as electron donor that transfers electron density to the electron-poor naphthalimide moiety. This effect is even preserved in the comparatively more electron-poor compounds **353** and **354**, because the electron density in the respective molecular orbitals of these compounds contributing to the S_0 - S_1 transition is not delocalized to the same extent as in their cyclohexa-fused analogs.

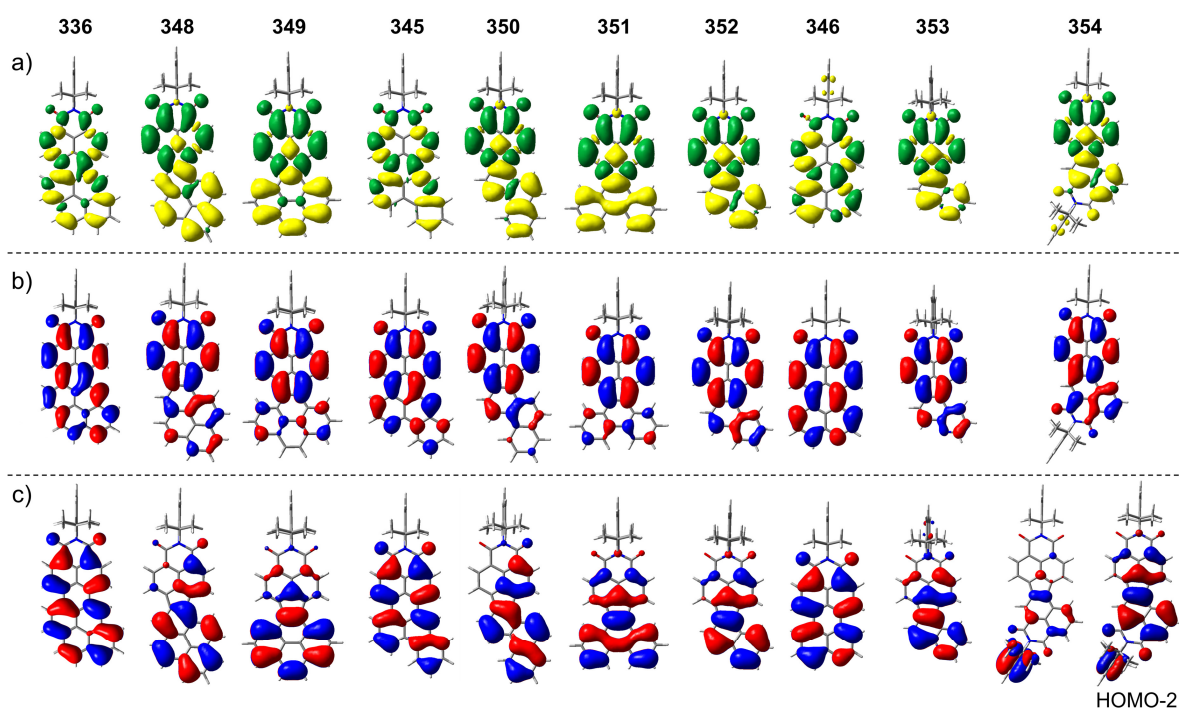


Figure 19 a) Calculated charge density differences for the S_0 - S_1 transition by TD-DFT (B3-LYP/def2-SVP, isovalue 0.0004 a.u.); b) calculated LUMOs (B3-LYP/def2-SVP, isovalue 0.02 a.u.); c) calculated HOMOs and HOMO-2 (B3-LYP/def2-SVP, isovalue 0.02 a.u.) for compounds **336**, **345**, **346** and **348-354**.

The orbital contributions to the lowest energy transition can be assigned in most cases to the excitation of an electron from the HOMO to the respective LUMO with > 80 %. Only compound **354** has a low contribution of only 29 % of these orbitals, while the major contribution of 70 % originates from the excitation of an electron of the HOMO-2 into the LUMO. This can be rationalized by having a closer look onto these molecular orbitals that are very close in energy (-6.55 and -6.63 eV). While the HOMO of compound **354** has large coefficients on one diisopropylphenyl substituent and low coefficients centered on the π -conjugated core, the HOMO-2 shows reverse electron density distribution (Figure 19).

To characterize the electrochemical properties of the newly synthesized aromatic dicarboximides cyclic voltammetry measurements of **336**, **345**, **346** and **348-354** were performed in dichloromethane containing tetrabutylammonium hexafluorophosphate as supporting electrolyte (Figure 20). Two reversible and well separated reduction processes and one oxidation process, except for compound **346**, could be observed for each of the six-membered ring annulated compounds **336**, **345** and **346** (Table 7).

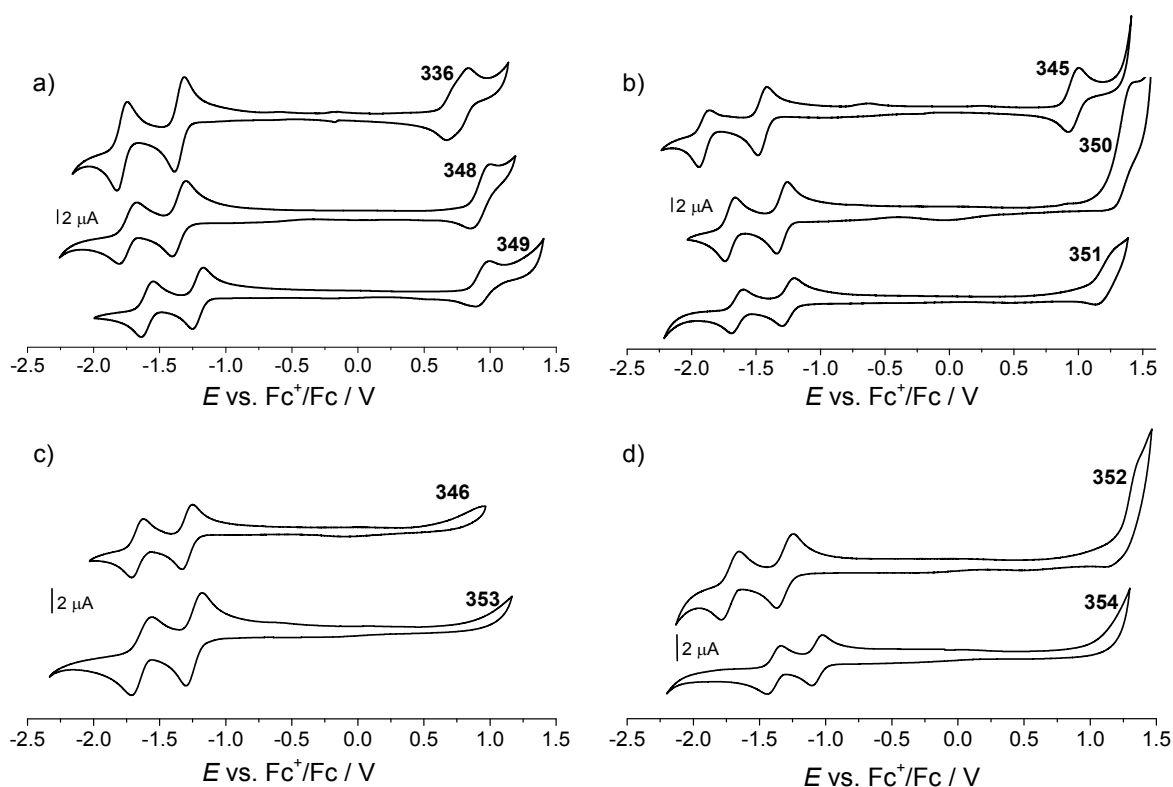


Figure 20 Cyclic voltammograms of a) pyrene containing derivatives **336**, **348** and **349**, b) phenanthrene containing derivatives **345**, **350** and **351**, c) quinoline containing derivatives **346** and **353** and d) compounds **352** and **354**. Scan rate 100 mVs^{-1} , 0.1 M TBAHFP in dichloromethane ($c = 2\text{--}3 \cdot 10^{-4} \text{ M}$).

Due to their structural similarity, the potentials of the first reduction processes of the six-membered ring annulated products **336**, **345** and **346** are comparable to the one of unsubstituted perylene monoimide (-1.46 V)^[185] with cathodically shifted values for **336** (-1.35 V) and **346** (-1.29 V), the latter caused apparently by the extension of the aromatic π -core (compound **336**) or the introduction of electronegative heteroatoms into the π -conjugated scaffold (compound **346**). Although the reduction potentials of their constitutional isomers **348**, **349**, **350**, **351** and **353** are not considerably affected by different connectivity, all cyclopenta-fused derivatives can generally be reduced at the same or less negative potentials. Thus, compounds **348** and **349** show each two reversible reductions at -1.35 and -1.74 V (for **348**) or -1.29 and -1.59 V (for **349**). Additionally, the oxidation is shifted towards more positive values by 0.17 and 0.20 V, respectively, compared to that of **336**. These subtle changes in redox potentials are well reflected by the DFT-calculated energy levels of the HOMOs and LUMOs (Figure 21).

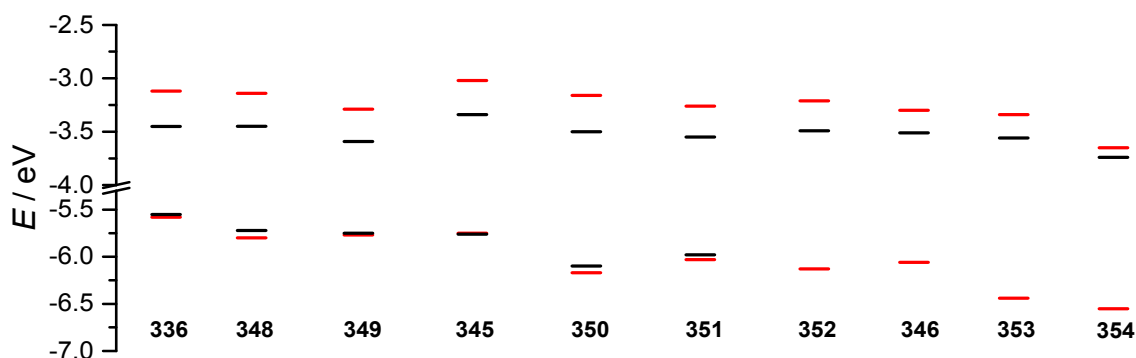


Figure 21 Schematic representation of the energy levels of the frontier molecular orbitals of PADIs **336**, **345**, **346** and **348-354** obtained by DFT calculations (red lines, B3-LYP/def2-SVP) and experimentally determined values (black lines, calculated by $E_{\text{LUMO}} = -[E_{\text{red1}} + 4.8 \text{ eV}]$ and $E_{\text{HOMO}} = -[E_{\text{ox}} + 4.8 \text{ eV}]$ using the experimentally determined redox potentials and the energy level of Fc^+/Fc with respect to the vacuum level (-4.8 eV)^[188]).

For compounds **350**, **351** and **353** a similar trend is observed. The potentials of the first reduction are shifted by 0.16 (**350**), 0.21 (**351**) and 0.05 V (**353**) to less negative values, while the oxidation potentials of **350** and **351** are shifted by 0.34 and 0.22 V to higher potentials compared to those of the respective six-membered ring annulated compounds **345** or **346**. This stabilization of the reduced species might be due to the formation of 6π -electron cyclopentadienide sub-structures upon reduction. Similar stabilization effects have been reported by Jenneskens and coworkers who investigated a series of non-alternant polycyclic aromatic hydrocarbons containing annulated peripheral pentagons.^[197]

Table 7 Summary of the electrochemical and optical properties of compounds **336**, **345-354**.

Compd.	$E_{\text{ox}} / \text{V}^a$	$E_{\text{red1}} / \text{V}^a$	$E_{\text{red2}} / \text{V}^a$	$\lambda_{\text{abs}} / \text{nm} (\epsilon / 10^3 \text{M}^{-1} \text{cm}^{-1})^b$	$\lambda_{\text{em}} / \text{nm}^b$	$\Phi_{\text{fl}} / \%^c$
336	0.75	-1.35	-1.79	547 (44.2)	598	79
345	0.96	-1.46	-1.90	484 (38.2), 508 (38.7)	546	89
346		-1.29	-1.67	459 (28.3), 488 (34.9)	510	96
347 ^[187]	1.29	-1.01	-1.24	526 (94.9)	531	100
348	0.92	-1.35	-1.74	368 (62.5), 518 (11.3)	637	23
349	0.95	-1.21	-1.59	348 (47.4), 438 (17.3)		
350	1.30 ^d	-1.30	-1.71	337 (43.6), 451 (15.5)		
351	1.18 ^d	-1.25	-1.63	334 (29.4), 375 (18.5), 435 (9.7)		
352		-1.31	-1.71	319 (27.9), 401 (16.4), 424 (19.5)		
353		-1.24	-1.64	396 (19.1), 419 (23.3)		
354		-1.06	-1.39	366 (34.4), 410 (19.6), 434 (29.7)		

^aHalf-wave potentials were determined by cyclic voltammetry measured in dichloromethane (0.1 M TBAHFP) vs. Fc^+/Fc . ^bMeasured in dichloromethane at room temperature. ^cRelative fluorescence quantum yields were measured by optical dilute method ($A < 0.05$)^[164] using rhodamin 101 ($\Phi_{\text{fl}} = 91.5\%$ in ethanol) and fluorescein ($\Phi_{\text{fl}} = 89\%$ in 0.1 M NaOH) as standards.^[165] ^dPotentials were determined by square wave voltammetry under otherwise identical experimental conditions.

Regarding the naphthalene derivative **352**, the potential for the first reduction process is again shifted by 0.15 V to less negative values compared to its six-membered ring annulated analogue perylene monoimide (-1.46 V).^[185] Moreover, the second imide functionality of compound **354** shifts the reduction potentials significantly to less negative potentials of -1.06 and -1.39 V, closely resembling those of perylene bisimides (-1.01 and -1.24 V).^[187]

3.3.5 Conclusion

In summary, we have accomplished the synthesis of a series of new cyclohexa- and cyclopenta-fused polycyclic aromatic dicarboximides by base-modulated Pd-catalyzed C-C coupling cascade reactions in which Suzuki-Miyaura cross-coupling and direct C-H arylation are combined. We have shown that, depending on the coordination properties of the auxiliary base, the mechanism of the intramolecular C-H arylation step can be modulated by switching from a Heck-type coupling to a sequential C-H activation/reductive elimination pathway. This simplicity of the mechanistic control in Pd-catalyzed C-C coupling cascade reactions by proper selection of the auxiliary base, opens up new perspectives for the synthesis of highly desirable electron-poor dicarboximide-functionalized PAHs, including non-alternant aromatic systems.

3.4 An Ambient Stable Core-Substituted Perylene Bisimide Dianion*

3.4.1 Introduction

In the preceding chapters new approaches for the synthesis of different types of polycyclic aromatic dicarboximides based on palladium-catalyzed C–C coupling cascade reactions are discussed. In this chapter, we deal with another prominent class of polycyclic aromatic dicarboximides, namely perylene bisimides (PBIs). PBIs are one of the most widely studied organic colorants and may be considered as the archetype for an electron-poor π -conjugated aromatic scaffold.^[13b, 85a] More recently, the interest in this class of compounds as an organic alternative for the common inorganic semiconducting materials has grown tremendously.^[13, 200] Interestingly, the first application of these unique molecules as vat dyes^[89, 201] - similar to indigo^[202] - has already been based on the possibility to reduce the water insoluble PBI derivatives to the corresponding water soluble anions (leuko bases). Related to this initial coloration process the most recent implementation of PBIs in organic field effect transistors (OFETs)^[203] and organic photovoltaics (OPV)^[200, 204] benefits in a similar way from the appreciable stability of reduced PBI species^[205] where charge carriers are either injected from the source electrode or generated by photoinduced electron transfer processes at a dielectric interface. Moreover, there are some current efforts to use multiple reduced rylene bisimide derivatives as rechargeable supramolecular materials or as organic alternatives for common lithium-ion batteries.^[206] Regarding the importance of reduced PBI species in all these applications, it is rather surprising that only very recently the first stable and completely characterized PBI radical anion could be achieved.^[207] Moreover, Rybtchinski and coworkers have reported that a core-unsubstituted PBI containing polyethylene glycol chains at the imide positions was reduced with sodium dithionite in water to its dianion, which was stable for months in deoxygenated aqueous solution.^[205c, d] Similarly, Brochsztain and coworkers have investigated the aggregation behavior of a PBI dianion that was generated by Na₂S₂O₄ titration in water ethanol mixtures.^[205a, b] Although PBI anions and/or dianions are discussed to be sufficiently stable in solution and within the (opto)electronic device by virtue of a

* This chapter was published in: [198] S. Seifert, D. Schmidt, F. Würthner, *Chem. Sci.* **2015**, *6*, 1663. Reproduced and adopted with permission. Copyright 2015 Royal Society of Chemistry.

The synthesis of PBIs **361** and **362** are reported in [199] S. Seifert, Master Thesis, Julius-Maximilians-Universität Würzburg, **2013**.

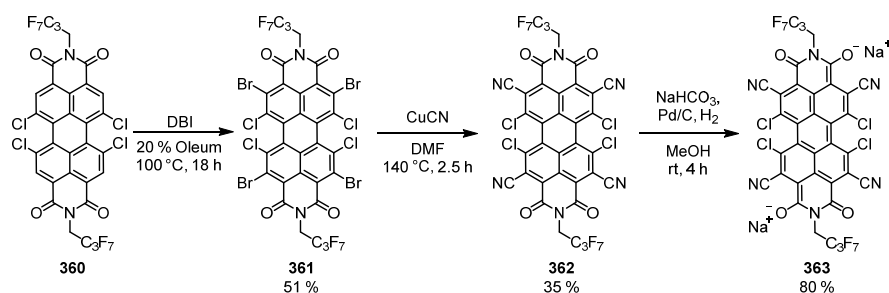
Single crystal structure analysis was performed by Dr. David Schmidt, DFT calculations were performed by Dr. David Bialas.

robust and protecting environment, the isolation of such an ambient stable compound appears to be rather difficult as reduced PBI species are prone to react with moderate oxidants. In this regard we thought that recently reported highly electron deficient PBIs such as octachloro-,^[208] tetracyano-^[209] and in particular tetrachlorotetracyano-PBI,^[210] bearing multiple electron-withdrawing substituents should be suitable to stabilize the respective PBI anions and/or dianions. Indeed, Wang and coworkers have recently reported that tetrachlorotetracyano-PBI exhibits two reversible reduction processes with potentials of $E_{\text{red}1} = -0.20$ V and $E_{\text{red}2} = -0.54$ V (vs. ferrocenium/ferrocene) for the first and second reduction, respectively, that are shifted about 800–900 mV to more positive values than those for the parent PBI.^[210] Therefore, such highly electron deficient PBIs are promising precursors for stable PBI dianions.

In this chapter, we report the synthesis and isolation of an ambient stable PBI dianion disodium salt from a tetrachlorotetracyano-PBI derivative. Moreover, we have investigated the optical and electrochemical properties by UV/Vis absorption and fluorescence spectroscopy and square wave voltammetry. The solid-state structural features of this PBI dianion were studied by X-ray analysis.

3.4.2 Synthesis

Starting from 1,6,7,12-tetrachloroperylene-3,4:9,10-tetracarboxylic acid bisanhydride the PBI dianion disodium salt **363** was synthesized in four steps (Scheme 51). After imidization of this bisanhydride with heptafluorobutylamine,^[203b] the obtained PBI **360** was brominated using dibromoisocyanuric acid (DBI) in oleum (20 %) to give the tetrachlorotetrabromo-substituted PBI **361** in 51 %. Subsequent nucleophilic substitution of all four bromine atoms in PBI **361** with cyano groups using CuCN as the cyanide source, following a slightly modified literature procedure,^[210] afforded the tetrachlorotetracyano-substituted PBI **362** in 35 % yield. Finally, PBI **362** was reduced by hydrogen in the presence of 10 % (wt) palladium on activated charcoal (Pd/C) and an excess of sodium hydrogen carbonate to the desired PBI dianion disodium salt **363**. Immediately after replacing the nitrogen atmosphere by hydrogen an intensive color change of the reaction mixture from orange to dark blue was observed. After filtration of the residual catalyst and precipitation of the product out of an acetone solution by adding pentane, **363** could be isolated as analytically pure material in 80 % yield.



Scheme 51 Syntheses of the core-substituted PBIs **360-362** and the PBI dianion disodium salt **363**.

Although this mild catalytic procedure has initially been introduced for the reductive dehalogenation of aryl halides,^[211] a simultaneous dechlorination during the reduction of PBI **362** to **363** was not observed under the applied reaction conditions. This finding is in contrast to our observation made in analogous reduction experiments with PBI **360** and **361** under the same reaction conditions. Although a similar color change from orange to blue was observed in both cases, PBI **360** was reisolated after the reaction, whereas for PBI **361** debromination to **360** was observed. These significant differences regarding the reactivity of PBIs **360**, **361** and **362** towards reduction indicate that the proper choice of electron-withdrawing substituents in PBIs is of great importance for the stabilization of reduced species of perylene bisimides.

3.4.3 Structural Elucidation

The dianion disodium salt **363** was unequivocally characterized by multinuclear NMR spectroscopy, high resolution mass spectrometry, elemental analysis as well as single-crystal X-ray diffraction experiments.

Crystallographic Analysis

Single crystals of perylene bisimide dianion disodium salt **363** were grown by slow diffusion of pentane into its 1 mM acetone solution to unambiguously determine the structure and the connectivities of this novel compound in the solid state. This dianion disodium salt crystallizes in the triclinic space group $P\bar{1}$ including both atropo-enantiomers (*P* and *M*) within the asymmetric unit (Figure 22). The packing motif of **363** is characterized by bridging sodium cations that are coordinated by the carbonyl and cyano groups of up to three PBI molecules and a varying amount of solvent molecules (acetone) which help to saturate the coordination sphere of the sodium cations.

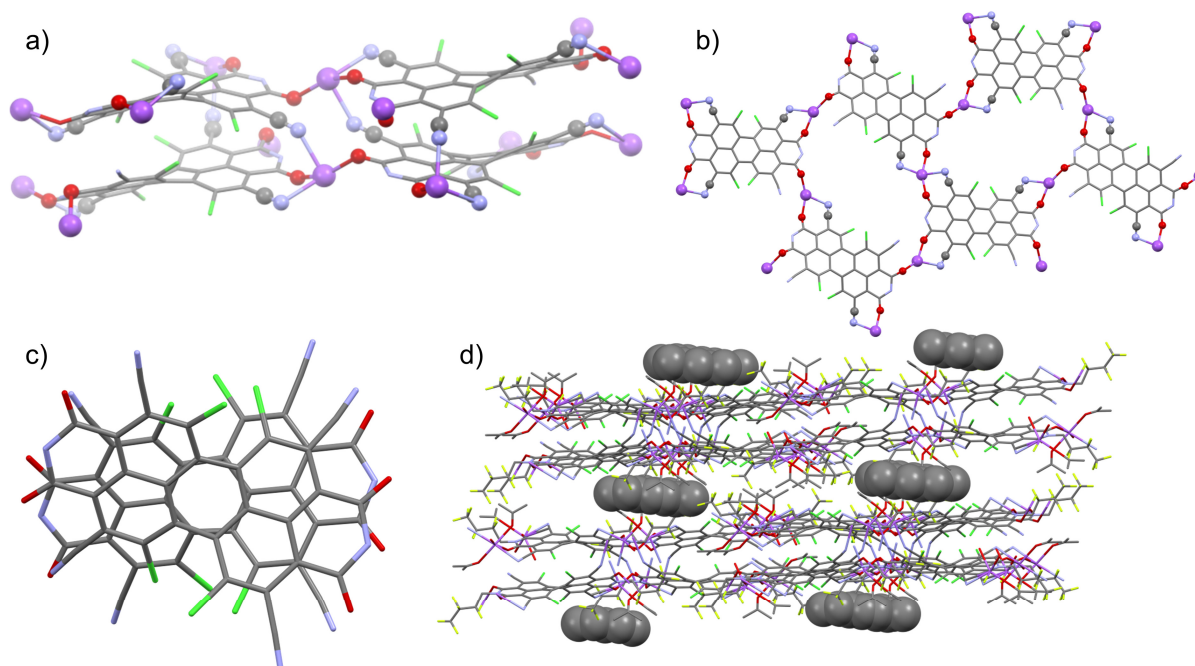


Figure 22 a) Molecular structure of the PBI dianion disodium salt **363** in the solid state, b) top view on the perylene cores illustrating the connectivity, c) visualization of the rotational displacement (fluorinated alkyl chains and solvent molecules are omitted for clarity) and d) visualization of the molecular packing of compound **363** within the solid state, pentane molecules (grey) are incorporated between every PBI bilayer.

Since every PBI molecule is equipped with four carbonyl oxygen atoms that are all orientated in different directions, the coordination of sodium by the carbonyl groups of **363** results in a two-dimensional sheet-like structure (Figure 22b). Each two of these sheets are further interconnected by the additional coordination of cyano groups of the adjacent layer to the sodium cations forming a dimeric layer-type structure (Figure 22a) with a π - π -distance of 4.33 Å between the PBI centroids. Within these bilayers the PBI molecules are arranged parallel with a rotational displacement of 22° between each two PBI dianions (Figure 22c). Such an arrangement in the solid state of core-twisted PBIs is rather rare since commonly a transversal displacement along the short and the long axes is observed.^[203b, 212] For the present PBI salt an extended three dimensional interconnection is prevented by the incorporation of pentane molecules between every bilayer (Figure 22d). Comparing all bond lengths and angles of the PBI dianion disodium salt **363** with a neutral dibutyl-substituted tetrachlorotetracyano-PBI derivative^[210] only minor deviations can be ascertained (Figure 23 and Table 8).

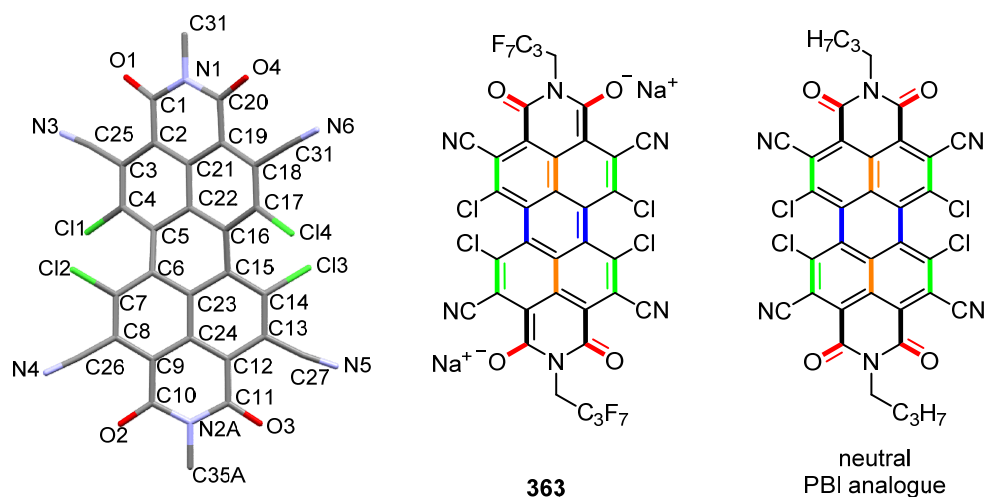


Figure 23 Molecular structure of dianion **363** in the solid state (fluorinated alkyl chains, counter ions and solvent molecules have been omitted for clarity) and schematic illustration of the most deviating bond length of compound **363** compared to a neutral tetracyanotetrachloro-PBI analogue with *n*-butyl chains in imide positions that was synthesized in the group of Wang.^[210]

However, all these very small changes that affect particularly the carbonyl bonds and the peripheral carbon-carbon bonds of the aromatic core are in very good agreement with theoretical considerations made by Rybtchinski and coworkers for the parent core-unsubstituted PBI dianion.^[205c, d]

Table 8 Comparison of bond distances and torsion angles of the PBI dianion disodium salt **363** with bond distances and angles of a neutral PBI analogue with *n*-butyl chains in imide positions.

Bonds ^a	PBI dianion disodium salt 363	<i>n</i> -butyl-substituted CN ₄ Cl ₄ PBI analogue ^[210]
C=O	1.224–1.240 Å	1.189–1.229 Å
C=C (C15-C16, C5-C6)	1.429–1.437 Å	1.478–1.484 Å
C=C (C3-C4, C17-C18, C7-C8, C13-C14)	1.378–1.382 Å	1.401–1.449 Å
C=C (C21-C22, C23-C24)	1.433–1.439 Å	1.392–1.425 Å
C–C (C1-C2, C9-C10, C11-C12, C19-C20)	1.437–1.446 Å	1.470–1.500 Å
C–C (C2-C3, C8-C9, C12-C13, C18-C19)	1.417–1.431 Å	1.380–1.392 Å
C–C (C9-C24, C12-C24, C2-C21, C19-C21)	1.409–1.412 Å	1.377–1.438 Å
C–C (C4-C5, C6-C7, C14-C15, C16-C17)	1.421–1.431 Å	1.361–1.400 Å
C–C (C6-C23, C15-C23, C5-C22, C16-C22)	1.423–1.430 Å	1.396–1.440 Å
C–N (in imide rings)	1.395–1.403 Å	1.385–1.416 Å
C–Cl	1.726–1.735 Å	1.716–1.729 Å
C–C (to CN groups)	1.436–1.446 Å	1.421–1.470 Å
CN triple bond	1.144–1.151 Å	1.119–1.174 Å
torsion angle	32.9° to 33.9°	35.0° to 36.4°

^aFor the numbering of atoms see Figure 23 (left).

According to their theoretical investigations on a simplified model system, the peripheral C=C bonds of perylene bisimide dianions should possess alternating bond distances as it is indeed observed for **363** in the solid state. Whereas the C=C bonds that are arranged longitudinal to the long axis of the PBI core are slightly shortened compared with the neutral dibutyl-substituted tetrachlorotetracyano analogue, in the latter the C=C bonds that are aligned transversal to this axis are somewhat elongated. Furthermore, upon reduction of the neutral PBI to the corresponding dianion disodium salt **363** the twist of the aromatic core is reduced about 2.3° from 35.0 and 36.4° for the neutral dibutyl tetrachlorotetracyano-PBI derivative^[210] to 32.9° and 33.9° in **363**. The contraction of the peripheral C=C bonds in PBI dianions (longitudinal ones) has been attributed to the additional amount of electron density that is partially localized on these bonds and is consistent with the calculated HOMO (Figure 24) of a simplified model system of **363** (heptafluorobutyl chains were replaced by methyl groups, sodium cations were omitted), in which the maximum orbital coefficients can be found on the relevant bonds.^[205c, d]

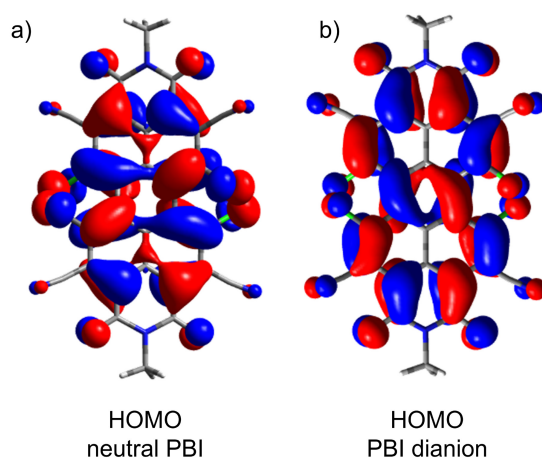


Figure 24 HOMOs of simplified structures of PBI **362** (a) and PBI dianion **363** (b) calculated by DFT (B3-LYP/6-31G*, isovalue: 0.02 a.u., fluorinated alkyl chains were replaced by methyl groups, sodium cations are omitted).

Furthermore, some of the additional electron density of **363** is localized in the C=O and C≡N π^* orbitals as derived from IR spectroscopy (Figure 25). Upon reduction, both C=O and C≡N stretch vibrations of **362** are somewhat shifted from 2227 ($\tilde{\nu}_{\text{C}\equiv\text{N}}$), 1733 and 1724 ($\tilde{\nu}_{\text{C}=\text{O}}$) cm^{-1} to 2222 ($\tilde{\nu}_{\text{C}\equiv\text{N}}$), 1631 and 1620 ($\tilde{\nu}_{\text{C}=\text{O}}$) cm^{-1} in **363**. This characteristic shift to lower wavenumbers is accompanied by a significantly increased intensity for the C≡N stretch vibration.

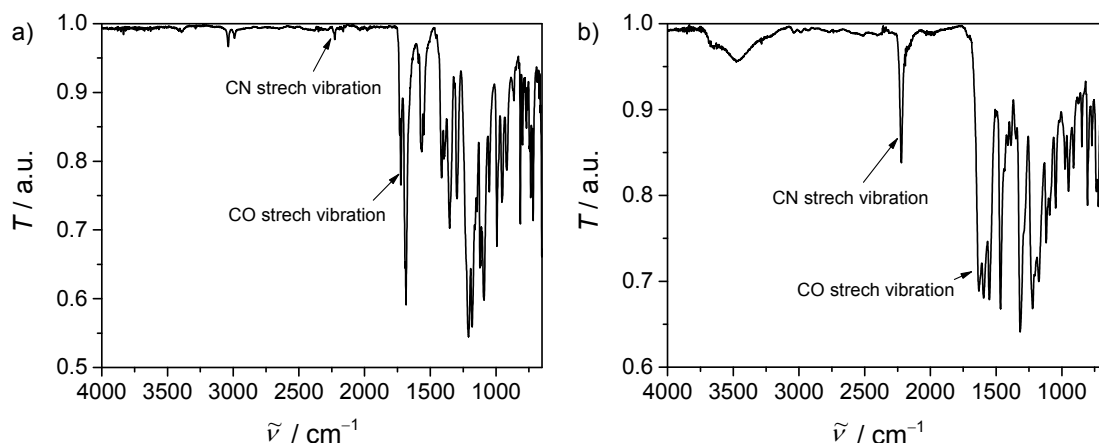


Figure 25 a) IR spectrum (transmission) of compound **362** in the range of 650 up to 4000 cm^{-1} and b) IR spectrum (transmission) of the PBI dianion disodium salt **363** in the range of 650 up to 4000 cm^{-1} .

UV/Vis Absorption and Fluorescence Spectra

Absorption spectra of all neutral PBIs were measured in dichloromethane at room temperature (Figure 26) and revealed intensive absorption in the visible range with maxima located at 520 nm (**360**, $\epsilon = 38400 \text{ M}^{-1}\text{cm}^{-1}$),^[203b] 523 nm (**361**, $\epsilon = 29900 \text{ M}^{-1}\text{cm}^{-1}$) and 528 nm (**362**, $\epsilon = 34100 \text{ M}^{-1}\text{cm}^{-1}$) that can be attributed to the S_0 - S_1 transition of the chromophores. The small bathochromic shift of the absorption maxima is apparently due to the additional electron-withdrawing bromo or cyano substituents. Compared to unsubstituted perylene bisimides the intensity of the S_0 - S_1 transition is decreased, while that of the S_0 - S_2 transition is enhanced, resulting in an overall broadening of the spectral band shape and decreased extinction coefficients. This effect can be attributed to the core-twist of *bay*-substituted PBIs, which increases the intensity of the S_0 - S_2 transition that is aligned transversal to the long axis of the π -core.^[13b] The UV/Vis/NIR absorption spectrum of the PBI dianion **363** in acetone features a very intensive absorption band within the NIR region with a maximum at 793 nm that is significantly shifted to longer wavelength compared with the neutral starting material **362** (Figure 26). This very characteristic absorption band is in excellent agreement with electrochemically generated dianion **362**²⁻ (see Figure 28b) but significantly shifted to higher wavelength in comparison to core-unsubstituted PBI dianions.^[205b, d] Since a gradual bathochromic shift of the absorption maxima of PBI dianions can be observed with an increasing number of electron-withdrawing groups at the aromatic core,^[205e, 207] the red-shift of the absorption bands of compound **363** can be attributed to the four chlorine and four cyano substituents. Whereas the absorption band of **363** exhibits a vibronic fine structure, that is well resolved like the one of parent PBI **362**, the extinction coefficient of the dianion disodium salt **363** is considerably increased from $34100 \text{ M}^{-1}\text{cm}^{-1}$

(PBI **362**) to $91300 \text{ M}^{-1}\text{cm}^{-1}$. Unchanged spectral features can be obtained by dissolving isolated **363** in acetone after exposing the solid material for approximately 5 months to air and moisture (ambient conditions). The acetone solution itself also remains stable for at least one week under ambient conditions since no spectral changes were observed after this time course. These findings corroborate the remarkable stability of the PBI dianion disodium salt in solution as well as in the solid state under ambient conditions.

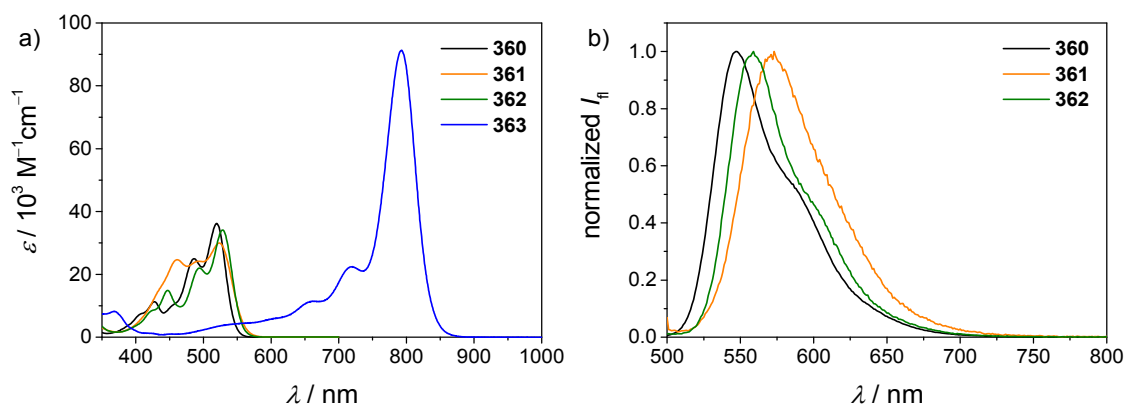


Figure 26 UV/Vis/NIR absorption ($c = 2 \cdot 10^{-5} \text{ M}$) (a) and emission ($c \sim 1 \cdot 10^{-7} \text{ M}$, $\lambda_{\text{ex}} = 490 \text{ nm}$) (b) spectra of the neutral PBIs **360-362** in dichloromethane and the dianion disodium salt **363** in acetone at room temperature.

Furthermore, the neutral PBIs **360-362** show fluorescence with maxima at 547, 559 and 573 nm, respectively, while for the PBI dianion **363** no fluorescence could be detected. While the tetrachloro-substituted derivative **360** exhibits a high quantum yield of 89 %, ^[203b] the introduction of additional electron withdrawing substituents in *ortho*-position leads to a drastic decrease of the quantum yield with values of 11 (**362**) and 2 % (**361**), respectively.

3.4.4 Electrochemical Studies

Cyclic voltammetry studies were performed for PBIs **361** and **362** in dichloromethane to elucidate the influence of the four additional electron-withdrawing substituents on the electron accepting properties of heptafluorobutyl-substituted perylene bisimides (Figure 27) in comparison to PBI **360**. ^[203b] Two reversible reduction waves with potentials of -0.74 and -0.95 V (vs. ferrocenium/ferrocene) are observed for PBI **360** ^[203b] that are significantly shifted to more positive potentials for the fourfold brominated PBI **361** (-0.49 and -0.67 V). In the case of the tetrachlorotetracyano-PBI **362** a further shift of both reversible reduction waves to -0.07 and -0.41 V could be recognized, confirming the highly electron deficient character of **362**. Both reduction potentials of **362** are even more positive than the ones reported by Wang and coworkers (*vide supra*) and confirm the electron withdrawing effect of

the fluorinated butyl substituent on the redox behavior of PBIs.^[203b, 210] To the best of our knowledge, PBI **362** can be regarded as one of the most electron-poor rylene bisimide derivatives that have been reported to date.^[13c, 210]

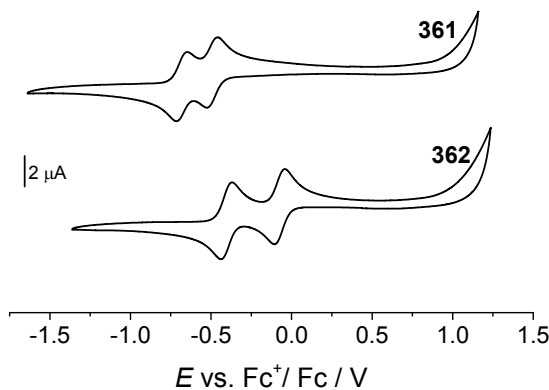


Figure 27 Cyclic voltammograms of PBIs **361** and **362** in dichloromethane ($c = 2 \cdot 10^{-4}$ M, 0.1 M TBAHFP, scan rate 100 mVs^{-1}).

Based on these electrochemical investigations the reduction of PBI **362** to the corresponding PBI radical anion $\mathbf{362}^{\cdot-}$ and dianion $\mathbf{362}^{2-}$ has also been monitored by spectroelectrochemistry (Figure 28). Upon applying a negative potential, the characteristic absorption bands at around 528 nm for the neutral PBI **362** slowly decrease whereas new equally characteristic absorption bands in the NIR region at around 1241, 1046, 948, 815 and 715 nm increase, which can be attributed to the formation of the radical anion $\mathbf{362}^{\cdot-}$. However, upon the second electrochemical reduction to generate the corresponding dianion $\mathbf{362}^{2-}$, absorption bands at 804, 728 and 661 nm increase at the expense of $\mathbf{362}^{\cdot-}$, which are perfectly consistent with the ones of the isolated PBI dianion disodium salt **363** (Figure 26).

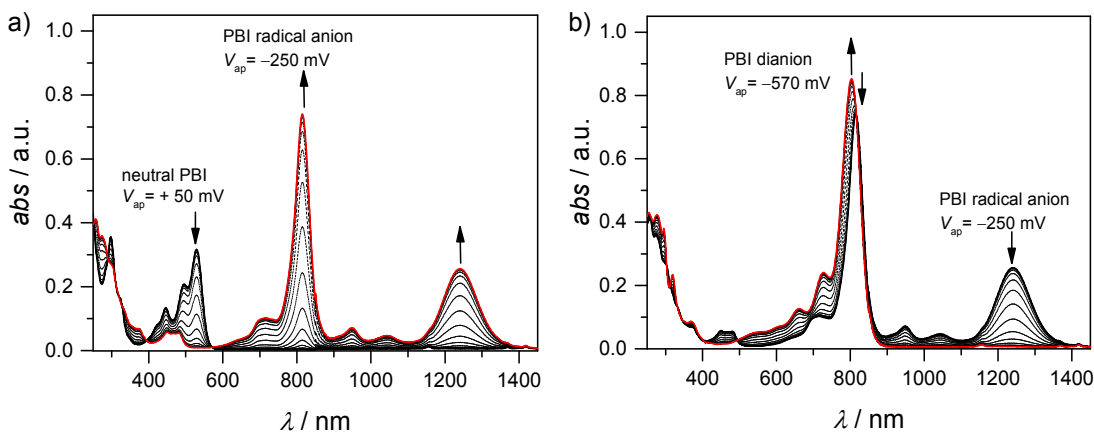


Figure 28 a) UV/Vis/NIR absorption changes upon electrochemical reduction of PBI **362** to PBI $\mathbf{362}^{\cdot-}$ (in steps of 20 mV) at potentials from +50 to -250 mV and b) UV/Vis/NIR absorption changes upon electrochemical reduction of PBI $\mathbf{362}^{\cdot-}$ to PBI $\mathbf{362}^{2-}$ (in steps of 20 mV) at potentials from -250 to -570 mV ($c = 1 \cdot 10^{-3}$ M, 0.2 M TBAHFP, dichloromethane).

Both distinct reduction processes are characterized by several isosbestic points, indicating the reasonable stability of both radical anion and dianion in moderately polar solvents like dichloromethane under inert conditions. Even though the data obtained by cyclic voltammetry and spectroelectrochemistry suggest that the corresponding radical anion should, in principle, be isolable in non-polar solvents, we could just recover the neutral PBI **362** under the same reaction conditions for the reduction of PBI **362** as discussed above using dichloromethane as a solvent. Apparently, the radical anion $362^{\cdot-}$ is not stable under ambient conditions. To gain some insights into the stability of PBI radical anions, we became interested in a quantitative analysis of the thermodynamic stability of reduced species of PBI **362**. Based on the work of Hünig and coworkers^[213] and the theory of Michaelis and Schubert^[214] that concern the determination of semiquinone formation constants K to quantify the stability of semiquinones with regard to their disproportionation into quinones and hydroquinone anions in solution, we performed solvent-dependent square wave voltammetry to estimate K for the radical anion $362^{\cdot-}$ in different solvents (Figure 29).

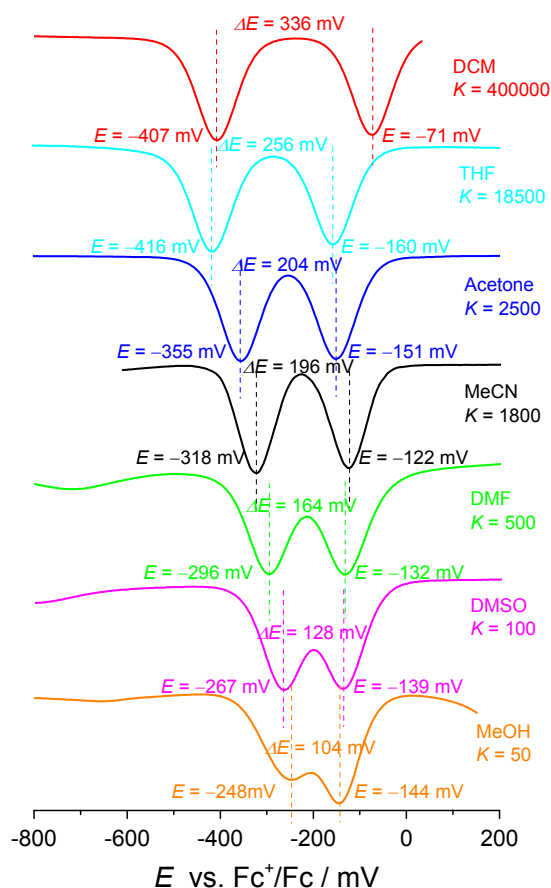


Figure 29 Square wave voltammograms of PBI **362** in solvents of different polarity. The dianion disodium salt **363** was used in the case of MeOH due to solubility reasons. Reference electrode: Ag/AgCl, working and auxiliary electrode: Pt; $c = 2 \cdot 10^{-4}$ M, 0.1 M TBAHFP, vs. Fc^+/Fc .

Due to the fact that both reduction processes are reversible and the different redox states have similar diffusion coefficients, the Nernst equation (1) can be used to describe the relationship between redox potential and standard electrode potential. For redox systems that take up two electrons, equations 2-4 can be used to describe the two electron transfer process and the individual one electron transfer processes.

$$E = E_0 + \frac{RT}{nF} \times \ln \frac{[Ox]}{[Red]} \quad (1)$$

$$E = E_m + \frac{RT}{2F} \times \ln \frac{[Ox]}{[Red]} \quad (2)$$

$$E = E_1 + \frac{RT}{F} \times \ln \frac{[Sem]}{[Red]} \quad (3)$$

$$E = E_2 + \frac{RT}{F} \times \ln \frac{[Ox]}{[Sem]} \quad (4)$$

$$E_m - E_1 = \frac{RT}{2F} \times \ln \frac{[Sem]^2}{[Red][Ox]} \quad (5)$$

In our case the fully reduced state (Red) is related to the PBI dianion, while the semiquinone (Sem) is represented by the PBI radical anion and the fully oxidized species (Ox) by the neutral PBI. In equilibrium the disproportionation of the radical anion into the dianion and the neutral PBI are described by the equilibrium constant, or semiquinone formation constant K (equation 6). By applying this relationship to equation 5, the semiquinone formation constant can be calculated from the experimentally determined redox potentials of the two-electron transfer process (E_m), which is in general the center between the potentials of the individual one-electron transfer processes (E_1 and E_2), and the latter ones (equation 7).



$$K = \frac{[Sem]^2}{[Red][Ox]} \quad (6)$$

$$K = e^{\frac{2F}{RT}(E_m - E_1)} = e^{\frac{2F}{RT}(E_2 - E_m)} \quad (7)$$

Using the redox potentials obtained in dichloromethane solution a semiquinone formation constant K of 400000 was calculated, which is consistent with two well separated reduction processes. However, the formation of the radical anion $\mathbf{362}^{\cdot-}$ becomes less favored by increasing the polarity of the solvent as demonstrated by a continuously decreased semiquinone formation constant ($K = 18500$ (THF) > 2500 (acetone) > 1800 (acetonitrile) >

500 (DMF) > 100 (DMSO)). These findings are in very good agreement with the direct formation of the PBI dianion disodium salt **363** in methanol (used as solvent in synthesis) where both reduction processes with a semiquinone formation constant of $K = 50$ (determined using **363** due to solubility reasons) are obviously superimposed (Figure 29).

3.4.5 Conclusion

In summary, we have reported a straightforward synthetic procedure for the preparation of an ambient stable perylene bisimide dianion disodium salt using a highly electron deficient perylene bisimide derivative for the stabilization of the additional negative charges. This unprecedented molecule has been fully characterized by UV/Vis/NIR absorption and NMR spectroscopy as well as single crystal X-ray analysis. Semiquinone formation constants that have been investigated by square wave voltammetry for the PBI radical anion in different solvents reveal that the formation of dianionic perylene bisimides is generally preferred in more polar solvents, whereas the generation of PBI radical anions should be favored in less polar solvents. The enhanced thermodynamic stability of the PBI dianion in polar media sheds light on the formation and persistence of leuco bases in aqueous media which might also apply to other vat dyes such as BASF's famous indanthrene dyes and indigo.^[202, 215]

Chapter 4

Summary

The aim of the current thesis was the development of new synthetic strategies towards planar nanometer-sized and *electron-deficient* polycyclic aromatic dicarboximides, which are rather unexplored compared with the large variety of *electron-rich* polycyclic aromatic hydrocarbons and nanographenes. Thus, new polycyclic aromatic systems containing a different number of dicarboximide groups were designed since this class of compounds has revealed its significance in the past due to a range of desirable molecular properties and its high thermal and photochemical stability. The synthetic concept towards these systems includes different C–C coupling techniques that were combined within coupling cascade reactions. Therefore, this thesis provides new insights into the reactivity of aromatic substrates and elucidates mechanistic aspects of C–C coupling cascade reactions to facilitate the precise design of new and desirable materials based on polycyclic aromatic dicarboximides. Furthermore, structure-property relationships as well as the optical and electrochemical properties were investigated by UV/Vis absorption and fluorescence spectroscopy and cyclic or square wave voltammetry. Insights into the molecular structures in the solid state were obtained by single-crystal X-ray analysis. In subsequent studies, highly electron-deficient perylene bisimides and their reduced species have been investigated in detail. Thus, core-functionalized perylene bisimides (PBIs) were synthesized and UV/Vis absorption spectroscopy, spectroelectrochemistry and cyclic or square wave voltammetry were used to determine their optical properties and the stability of the individual reduced species.

Chapter 2 provides a brief overview on C–C coupling methods that are frequently applied for the construction of polycyclic aromatic molecules. In the first part, some mechanistic aspects for different C–C coupling reactions are discussed, which are prerequisite for the interpretation of the results that are presented in *Chapter 3*. Furthermore, an overview on polycyclic aromatic dicarboximides synthesized by C–C coupling reactions is provided

including synthetic procedures for the core-expansion of rylene imides as well as for the preparation of polycyclic systems containing multiple dicarboximide groups.

In the first part of *Chapter 3*, multichromophoric systems based on a pyrene core and several naphthalimide substituents are described that were designed as potential precursors for the preparation of planar π -conjugated multidicarboximides that are discussed in *Chapter 3.2*. The synthesis of these molecules was achieved by Suzuki-Miyaura cross-coupling of the respectively boronated and brominated derivatives of pyrene and naphthalimide in high yields. To gain insights into the structure-dependent molecular properties, UV/Vis absorption and emission spectroscopy as well as cyclic and square wave voltammetry was performed in dichloromethane solutions. The UV/Vis absorption studies revealed, that the spectral properties of the individual pyrene and naphthalimide subunits are maintained with an additional broad and structureless transition appearing at higher wavelength that can be assigned to a transition with pronounced intramolecular charge transfer. The intensity and exact energetic position of this lowest energy transition is mainly influenced by the number of attached naphthalimide subunits and their position on the pyrene core (see Figure 30).

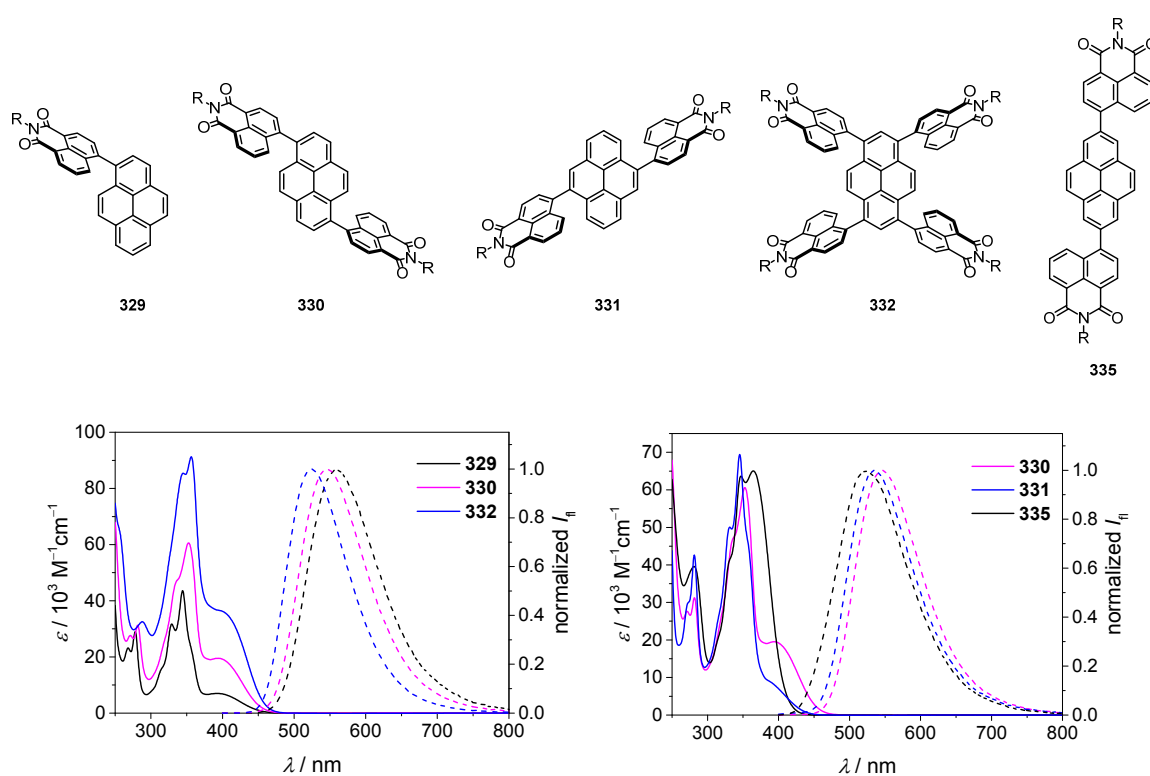
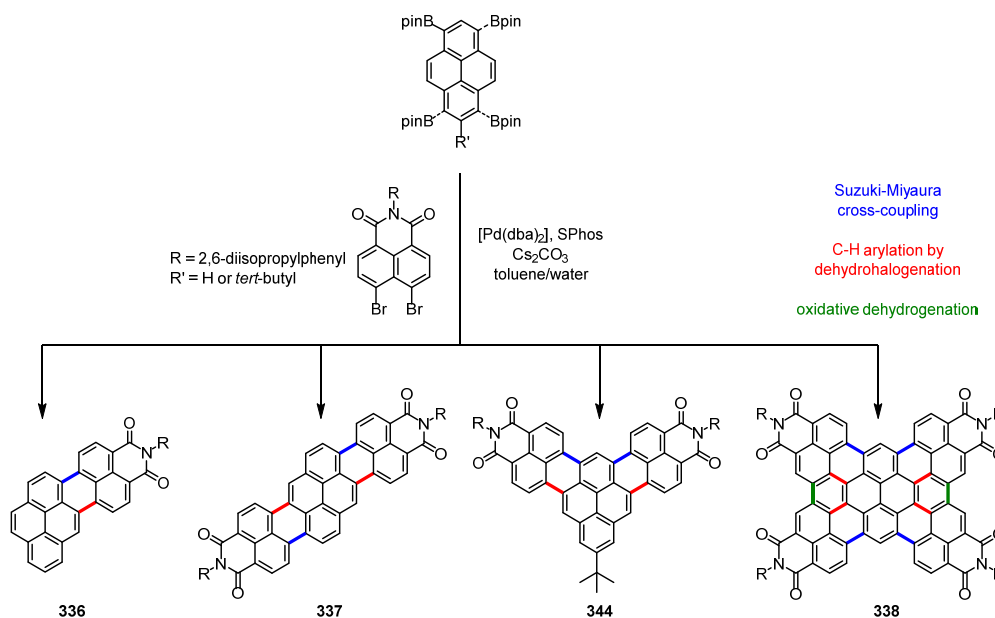


Figure 30 Overview of the multichromophoric systems presented in *Chapter 3.1* and their UV/Vis absorption (solid lines) and emission spectra (dashed lines) measured in dichloromethane at room temperature (R = 2,6-diisopropylphenyl).

Furthermore, the structural features affect the fluorescence properties and emission occurs from intramolecular charge transfer states with quantum yields and lifetimes in the range of 4–48 % and 3.38–4.89 ns, respectively. In contrast, the substitution pattern has almost no influence on the redox properties, which were investigated by cyclic and square wave voltammetry and reveal reduction processes around -1.8 V and oxidation processes in the range of 1.0 to 1.1 V vs. the ferrocenium/ferrocene redox couple.

Since the ring annulation and planarization of the multichromophoric systems **329**, **331** and **332** failed by oxidative cyclodehydrogenation (presumably due to low reactivity of these systems towards oxidative coupling), a new synthetic strategy was developed in *Chapter 3.2*, which combines different C–C coupling methodologies in a one pot reaction procedure. Hence, a second bromine substituent was introduced next to the reaction center of Suzuki–Miyaura cross-coupling and thus a *peri*-dibromonaphthalimide was used for the first time as coupling component for the reaction with pyrene mono-, di- or tetra-boronate esters. The subsequent formation of up to ten new C–C bonds for tetraimide **338** in a single chemical operation could be explained by plausible mechanisms for the individual C–C coupling reactions. Accordingly, Suzuki–Miyaura cross-coupling, C–H arylation *via* a Heck-type annulation and oxidative dehydrogenation (see Scheme 52) can occur in a cascade-like reaction cycle leading to the annulated extended π -scaffolds.

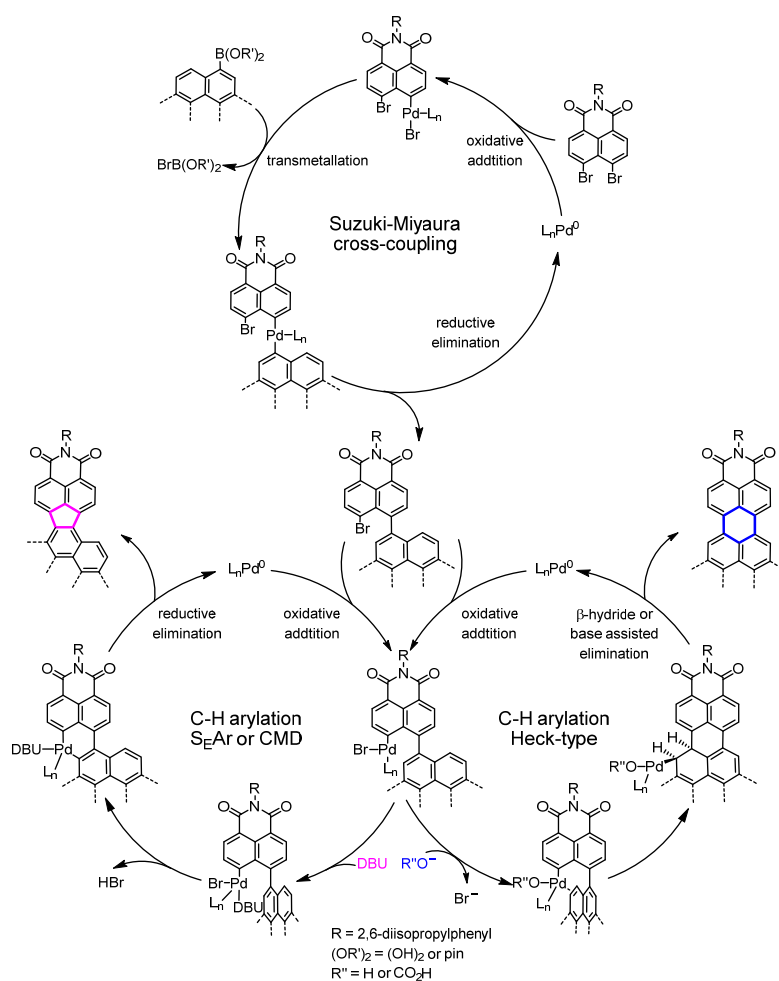


Scheme 52 Overview of electron-poor 2D scaffolds presented in *Chapter 3.2*.

UV/Vis absorption and emission spectroscopy performed on the newly synthesized polycyclic aromatic dicarboximides in dichloromethane solutions revealed intense absorption and fluorescence over a broad range of the visible spectral range. Interestingly, the angular

annulated compounds **338** and **344** exhibit additional transitions to higher excited states while the optical spectra of the linearly annulated systems **336** and **337** are predominated by very intense S_0 - S_1 transitions. Furthermore, DFT calculations and electrochemical investigations revealed their potential as electron acceptors, as the electron density is delocalized over the whole π -scaffold and all molecules possess similar LUMO levels (-3.45 to -3.81 eV) like those of frequently applied electron acceptor materials such as rylene bisimides (~ -3.8 eV). Due to the planar geometry of the π -scaffolds, determined by single-crystal X-ray analysis, a desirable packing arrangement into extended π -stacks can be anticipated for derivatives containing imide substituents which are less sterically demanding.

In *Chapter 3.3* a detailed description of the mechanism is provided together with investigations on the scope of the substrates for such C–C coupling cascade reactions between aryl boronate esters and *peri*-dibromonaphthalimides. Therefore, C–C coupling cascade reactions were performed with substrates possessing different olefinic double bond character in the γ -position to the boronic ester group and in the presence of different auxiliary bases (see Scheme 53).



Scheme 53 Illustration of the proposed mechanistic pathways for the cascade annulation towards five- and six-membered polycyclic aromatic dicarboximides.

These experiments proved, that the regioselectivity of the second C–C bond formation step, that leads to the annulated products, is highly dependent on the nature of the auxiliary base. Thereby inorganic bases like carbonates enable a Heck-type C–H arylation resulting in six-membered ring annulated products, while the application of organic amidine-bases leads to the respective five-membered annulated systems. This observation can be explained by formation of a six-membered palladacycle intermediate by electrophilic aromatic substitution or a concerted metalation deprotonation pathway. The resulting five- and six-membered ring annulated systems (see Chart 4) possess different optical and electrochemical properties despite their equal atomic composition.

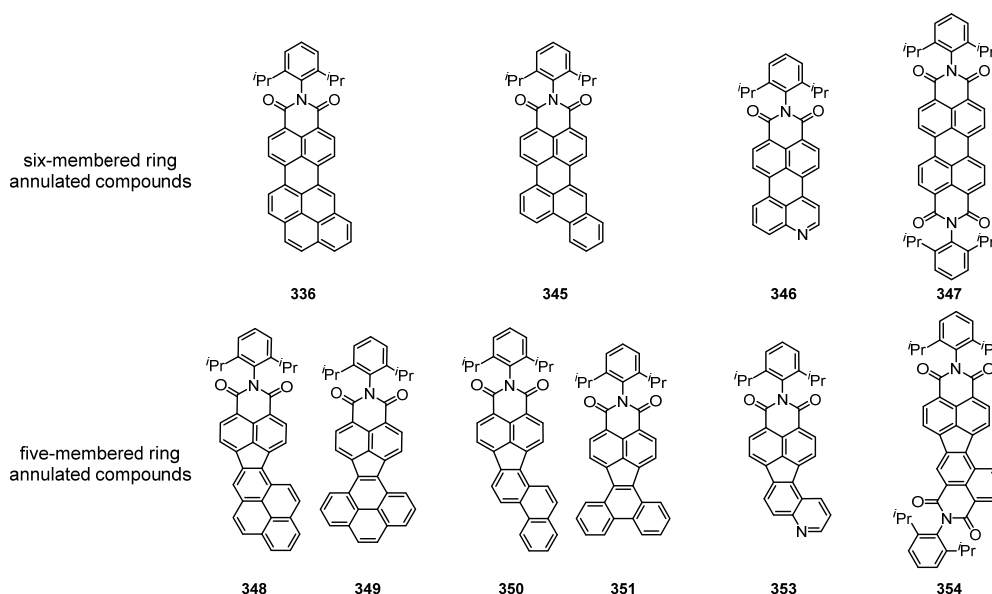


Chart 4 Structures of the six-membered ring annulated systems and their five-membered ring annulated analogues.

While the six-membered ring annulated compounds are characterized by intense absorption and emission originating from the S_0 - S_1 transitions, their five-membered ring annulated analogues exhibit multiple transitions to higher excited states and possess decreased or no fluorescence. Furthermore, the π -electron density is highly delocalized for all six-membered ring annulated systems but is clearly separated for the five-membered annulated analogues onto the electron-rich PAH-part (in the HOMO) and onto the electron-poor naphthalimide-part (in the LUMO). Furthermore, a slight stabilization could be elaborated for the reduced species of the five-membered ring annulated products, which exhibit similar or less negative reduction potentials compared with their hexagonally connected counterparts. The influence of the annulation mode on electrochemical and optical properties and the control on six- vs. five-membered ring annulation can facilitate the development of new electron acceptor materials.

In the last part of this thesis (*Subchapter 3.4*) the stabilization and structural characterization of reduced species of perylene bisimides was evaluated. For this purpose, a PBI core was functionalized with highly electron-withdrawing chloro and cyano substituents, which stabilize the reduced species against oxidation under ambient conditions due to the extremely low LUMO level of -4.73 eV. Therefore, the chemical reduction of this PBI could easily be achieved under mild reaction conditions and the PBI dianion could be isolated as its disodium salt. The dianion was unambiguously characterized by UV/Vis/NIR absorption and IR spectroscopy, DFT calculations and its solid state molecular structure was determined by X-ray analysis. Those results prove the delocalization of the additional electron density of the PBI dianion over the whole molecule, resulting in shortened C–C bond length along the long molecular axes and additional electron density located on C=O and C \equiv N moieties compared to the neutral analogue. The additional electron density at these particular positions leads to the coordination of the sodium cations, which stabilizes the reduced species in the solid state (as shown in Figure 31). Further electrochemical investigations showed that the stability of the intermediate PBI radical anion towards disproportionation into the fully reduced and fully oxidized species is highly dependent on the polarity of the solvent.

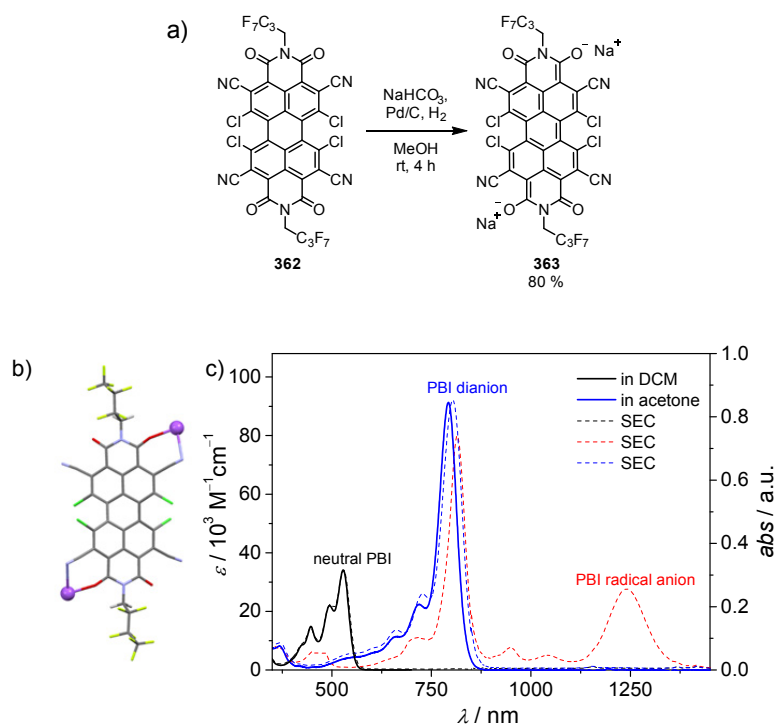


Figure 31 Synthesis of the PBI dianion disodium salt (a), molecular structure of the PBI dianion disodium salt **363** obtained by X-ray analysis (b) and UV/Vis/NIR absorption spectra (c) of the neutral PBI **362** (solid black line), its electrochemically generated reduced species (by SEC, dashed lines, 0.2 M TBAHFP in DCM) and the isolated dianion **363** (solid blue line).

In conclusion, this thesis describes new synthetic strategies for the preparation of various polycyclic aromatic dicarboximides including electron-poor graphene-type molecules and cyclopenta-fused aromatic systems. Furthermore, the reactivity of aromatic systems in C–C coupling cascade reactions and the mechanistic aspects of the individual C–C coupling pathways has been elucidated, which facilitates the design of new organic materials with particular optical and electronic properties. Electrochemical investigations on these systems clearly demonstrate that the reduced species can be stabilized by incorporation of five-membered rings into the polycyclic aromatic structure or by introduction of highly electron-withdrawing substituents. Thus an ambient stable perylene bisimide dianion salt could even be isolated, which is of great importance for the application of such materials as n-type semiconductors or in energy storage devices. Based on the knowledge on the synthesis and structure related molecular properties of new polycyclic aromatic hydrocarbons gained in this thesis, the development of new innovative (opto)electronic materials based on polycyclic aromatic multi-dicarboximides seems particularly promising.

Chapter 5

Zusammenfassung

Das Ziel der vorliegenden Arbeit war die Entwicklung neuer Synthesestrategien für planare und *elektronenarme* polyzyklische aromatische Dicarboximide in der Größenskala weniger Nanometer, welche im Vergleich zu der Vielzahl an *elektronenreichen* polyzyklischen aromatischen Kohlenwasserstoffen und Nanographenen weitaus weniger erforscht sind. Daher wurden neue polyzyklische aromatische Systeme entworfen, welche eine unterschiedliche Anzahl von Dicarboximid-Einheiten enthalten, da diese Klasse von Verbindungen ihre Bedeutsamkeit in der Vergangenheit aufgrund einer Reihe vorteilhafter molekularer Eigenschaften und ihrer hohen thermischen und photochemischen Stabilität gezeigt hat. Das synthetische Konzept für diese Systeme umfasst dabei verschiedene C–C-Knüpfungstechniken, die zu Kaskadenreaktionen kombiniert wurden. Daher werden in dieser Arbeit neue Einblicke in die Reaktivität von aromatischen Substraten aufgezeigt und mechanistische Aspekte von C–C-Kupplungskaskadenreaktionen erläutert, um eine präzise Gestaltung neuer und erstrebenswerter Materialien auf der Basis von polyzyklischen aromatischen Dicarboximiden zu erleichtern. Darüber hinaus wurden Struktur-Eigenschafts-Beziehungen sowie die optischen und elektrochemischen Eigenschaften durch UV/Vis-Absorptions- und Fluoreszenzspektroskopie sowie Cyclo- oder Square Wave Voltammetrie untersucht. Einblicke in die molekularen Strukturen im Festkörper wurden durch Einkristallstrukturanalyse erhalten. In nachfolgenden Studien wurden stark elektronenarme Perylenbisimide und ihre reduzierten Spezies detailliert untersucht. Dazu wurden kernfunktionalisierte Perylenbisimide (PBIs) synthetisiert. Um deren optische Eigenschaften und die Stabilität der reduzierten Spezies zu bestimmen wurden UV/Vis-Absorptionsspektroskopie, Spektroelektrochemie und Cyclo- oder Square Wave Voltammetrie verwendet.

Kapitel 2 gibt einen kurzen Überblick über C–C-Kupplungsstrategien, welche häufig für die Darstellung polyzyklischer aromatischer Moleküle verwendet werden. Im ersten Teil werden einige mechanistische Aspekte für verschiedene C–C-Kupplungsreaktionen diskutiert, die für

die Interpretation der in *Kapitel 3* vorgestellten Ergebnisse notwendig sind. Weiterhin wird ein Überblick über polyzyklische aromatische Dicarboximide, welche über C–C-Kupplungsreaktionen synthetisiert wurden, aufgeführt. Dabei sind synthetische Verfahren zur Kernerweiterung von Rylenimiden sowie zur Herstellung von polyzyklischen Systemen mit mehreren Dicarboximid-Einheiten enthalten.

Im ersten Teil des *Kapitels 3* werden Systeme auf Basis eines Pyrenkerns und mehrerer Naphthalimidsubstituenten beschrieben. Diese wurden als potentielle Vorläufer für die Herstellung von planaren π -konjugierten Multidicarboximiden, welche in *Kapitel 3.2* behandelt wurden, entworfen. Die Synthese dieser Moleküle konnte durch Suzuki-Miyaura-Kreuzkupplung der jeweils borylierten und bromierten Pyren- und Naphthalimid-Derivate in hohen Ausbeuten erreicht werden. Um Einblicke in die strukturabhängigen molekularen Eigenschaften zu erhalten, wurden UV/Vis-Absorptions- und Emissionsspektroskopie sowie Cyclo- oder Square Wave Voltammetrie in Dichlormethan Lösungen durchgeführt. Die UV/Vis-Absorptionsstudien zeigten, dass die spektralen Eigenschaften der einzelnen Pyren- und Naphthalimid-Untereinheiten erhalten bleiben und ein zusätzlicher breiter und strukturloser Übergang bei höheren Wellenlängen auftritt (siehe Abbildung 32, Figure 32).

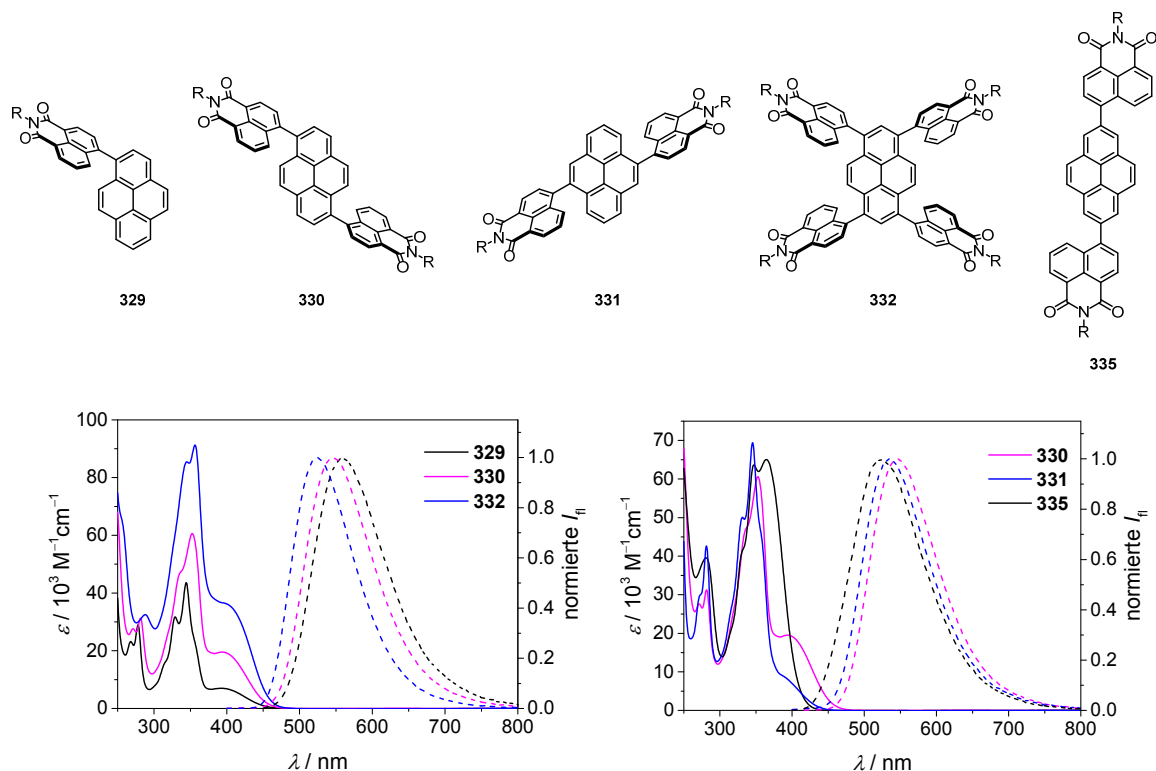
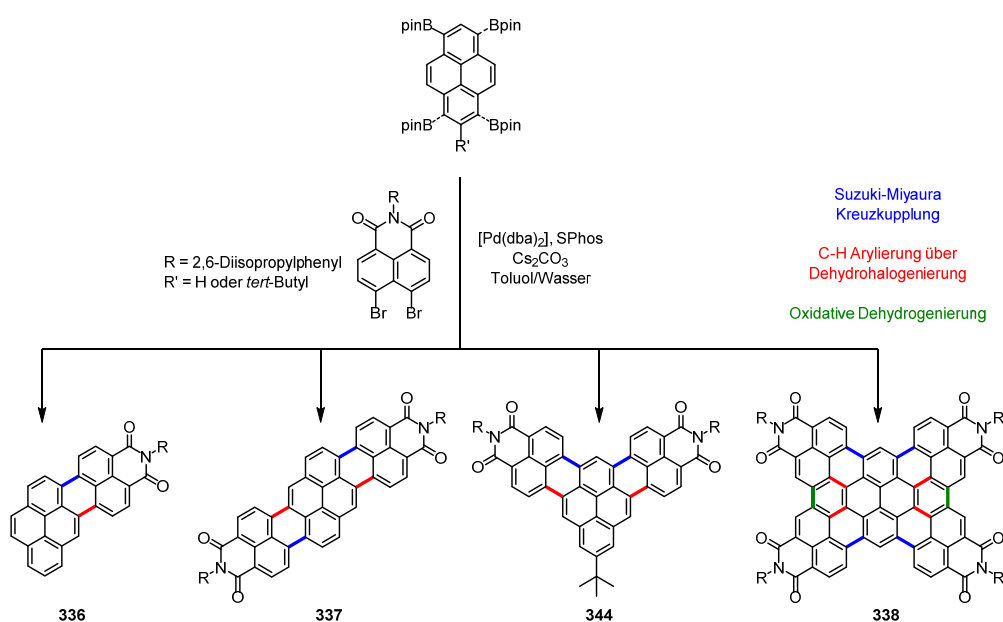


Figure 32 Überblick der in *Kapitel 3.1* vorgestellten Systeme und deren UV/Vis Absorptions- (durchgezogene Linien) und Fluoreszenzspektren (gestrichelte Linien), welche in Dichlormethan bei Raumtemperatur aufgenommen wurden (R = 2,6-Diisopropylphenyl).

Dieser kann einem Übergang mit ausgeprägtem intramolekularem Ladungstransfer zugeordnet werden. Die Intensität und die genaue energetische Lage dieses niederenergetischen Übergangs wird hauptsächlich durch die Anzahl der Naphthalimid-Einheiten und deren Position am Pyrenkern beeinflusst. Weiterhin haben diese Strukturmerkmale einen Einfluss auf die Fluoreszenzeigenschaften und daher wird Emission aus Zuständen mit intramolekularem Ladungstransfer und Quantenausbeuten sowie Lebensdauern im Bereich von 4–48 % bzw. 3.38–4.89 ns beobachtet. Im Gegensatz dazu hat das Substitutionsmuster nahezu keinen Einfluss auf die Redoxeigenschaften, welche durch Cyclo- und Square Wave Voltammetrie untersucht wurden. Es wurden Reduktionsprozesse bei etwa -1.8 V und Oxidationsprozesse im Bereich von 1.0 bis 1.1 V gegenüber dem Ferrocenium/Ferrocen-Redoxpaar beobachtet.

Da die Ringannulierung und Planarisierung der Systeme **329**, **331** und **332** mittels oxidativer Cyclodehydrogenierung nicht gelang (vermutlich wegen der geringen Reaktivität der Systeme bei einer oxidativen Kupplung), wurde in *Kapitel 3.2* eine neue Synthesestrategie entwickelt, welche verschiedene C–C Kupplungsmethoden in einer Eintopfreaktion kombiniert. Deshalb wurde ein zweiter Brom-Substituent neben dem Reaktionszentrum der Suzuki-Miyaura Kreuzkupplung eingeführt und damit erstmals *peri*-Dibromnaphthalimid als Kupplungskomponente für die Reaktion mit Mono-, Di- und Tetraboronsäureestern des Pyrens verwendet (siehe Schema 54, Scheme 54). Die daraus folgende Bildung von bis zu zehn neuen C–C Bindungen im Fall von Tetraimid **338** in einer einzelnen chemischen Umsetzung konnte anhand plausibler Mechanismen für die einzelnen C–C Kupplungsreaktionen erklärt werden.

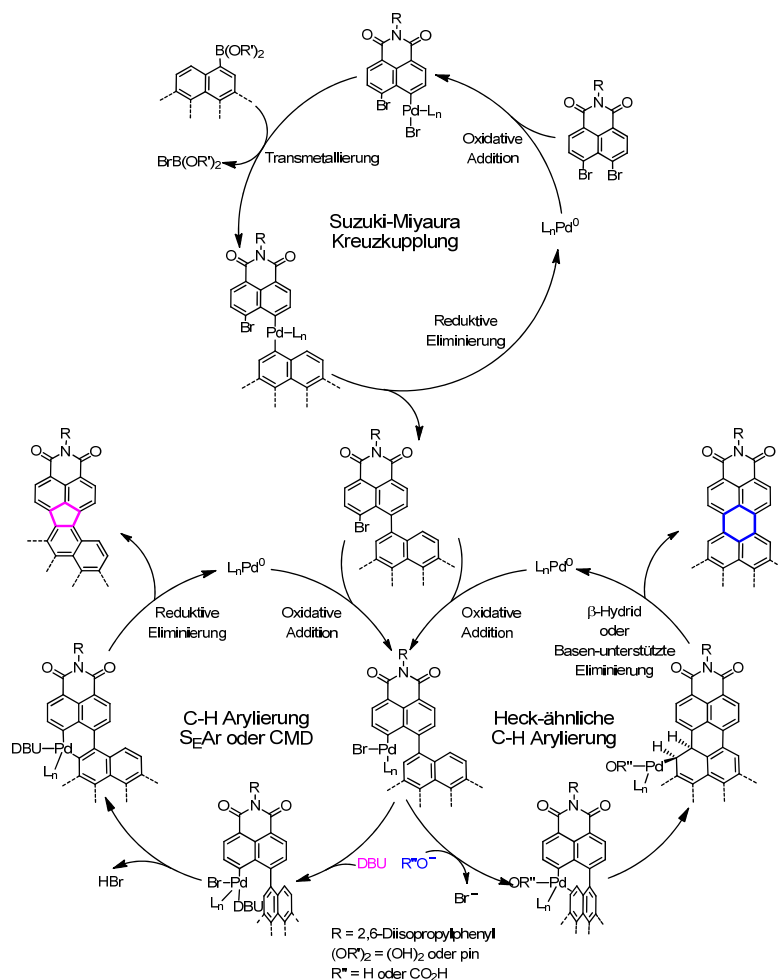


Scheme 54 Überblick über die in *Kapitel 3.2* vorgestellten 2D elektronenarmen π -Systeme.

Demnach können Suzuki-Miyaura Kreuzkupplung, C–H Arylierung über eine Heck-artige Annullierung und oxidative Dehydrogenierung in einem kaskadenartigen Reaktionszyklus stattfinden, was zu den annullierten ausgedehnten π -Systemen führt.

Die UV/Vis Absorptions- und Emissionsspektren der neu hergestellten polyzyklischen aromatischen Dicarboximide in Dichlormethan Lösung zeigten starke Absorption und Fluoreszenz über einen weiten Bereich des sichtbaren Spektralbereichs. Interessanterweise zeigen die verwinkelt annullierten Verbindungen **338** und **344** zusätzliche Übergänge zu höher angeregten Zuständen, während die optischen Spektren der linear annullierten Systeme **336** und **337** von sehr intensiven S_0 - S_1 -Übergängen dominiert werden. Weiterhin zeigten DFT-Rechnungen und elektrochemische Untersuchungen deren Potential als Elektronenakzeptoren auf, da die Elektronendichte über die gesamte π -Fläche delokalisiert ist und alle Moleküle ähnliche LUMO-Niveaus (-3.45 bis -3.81 eV) wie jene von häufig verwendeten Elektronenakzeptor Materialien wie Rylenbisimidinen besitzen (~ -3.8 eV). Durch die mittels Einkristallstrukturanalyse festgestellte planare Geometrie der π -Systeme wird eine wünschenswerte Packung in ausgedehnte π -Stapel für Derivate mit weniger sterisch anspruchsvollen Imidsubstituenten erwartet.

In *Kapitel 3.3* wird eine detaillierte Beschreibung des Mechanismus sowie Untersuchungen zum Anwendungsbereich von Substraten für solche C–C Kupplungskaskadenreaktionen zwischen aromatischen Boronsäureestern und *peri*-Dibromnaphthalimiden vorgestellt. Dazu wurden C–C Kupplungskaskadenreaktionen mit Substraten durchgeführt, welche einen unterschiedlich starken Doppelbindungscharakter in γ -Position zur Boronsäureesterfunktion besitzen. Außerdem wurden die Reaktionen in Gegenwart unterschiedlicher Hilfs-Basen durchgeführt. Diese Versuche bestätigten, dass die Regioselektivität der zweiten C–C-Bindungsbildung, welche gleichzeitig zu den annullierten Produkten führt, stark von der Art der Base abhängig ist. Dabei ermöglichen anorganische Basen wie Carbonate eine Heck-ähnliche C–H Arylierung, welche zu Sechsring-annullierten Produkten führt, während die Verwendung von organischen Amidinbasen zu den entsprechenden Fünfring-annullierten Systemen führt. Diese Beobachtung kann durch die Bildung eines sechsgliedrigen zyklischen Palladiumintermediats erklärt werden, welches über eine elektrophile aromatische Substitution oder einen konzertierten Metallierungs-Deprotonierungs-Pfad entstehen kann (siehe Schema 55, Scheme 55).



Scheme 55 Darstellung des vorgeschlagenen mechanistischen Verlaufs der kaskadenartigen Annullierung zu Fünf- und Sechsring enthaltenden polyzyklischen aromatischen Dicarboximiden.

Die resultierenden fünf- bzw. sechsgliedrig annullierten Systeme (siehe Tafel 5, Chart 5) besitzen trotz ihrer gleichen atomaren Zusammensetzung unterschiedliche optische und elektrochemische Eigenschaften.

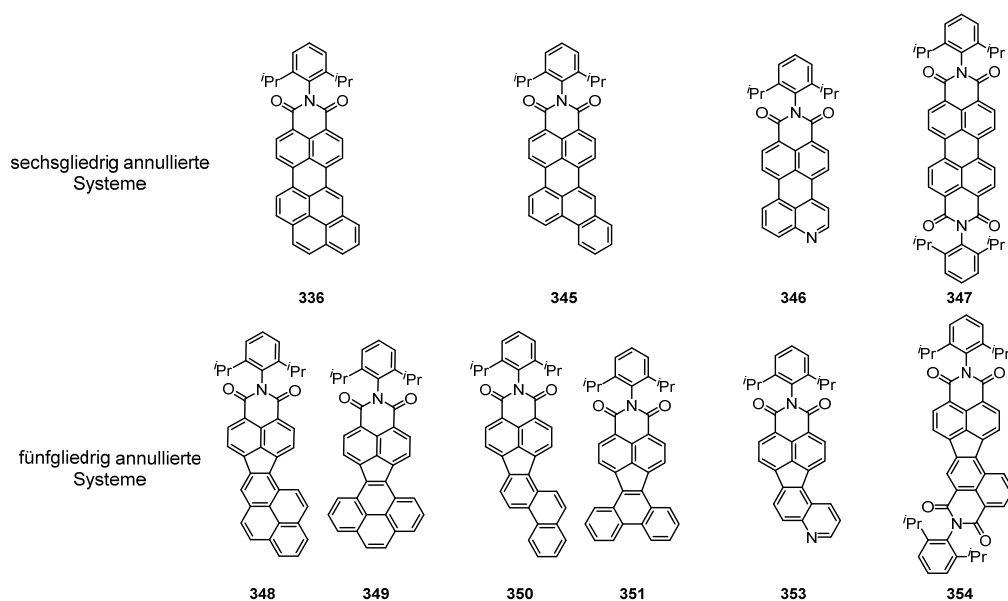


Chart 5 Strukturen der sechsgliedrig annullierten Systeme und deren fünfgliedrig annullierten Analoga.

Während die sechsgliedrigen Verbindungen durch intensive Absorption und Emission aus einem S_0 - S_1 -Übergang charakterisiert werden, zeigen die fünfgliedrigen Analoga mehrere Übergänge zu höher angeregten Zuständen und besitzen niedrigere oder keine Fluoreszenz. Außerdem ist die π -Elektronendichte für alle Sechsring-annullierten Systeme stark delokalisiert, während diese bei den Fünfring-annullierten Systemen eine klare Trennung auf den elektronenreichen PAH-Bereich (innerhalb des HOMOs) und auf den elektronenarmen Naphthalimid-Teil (innerhalb des LUMOs) aufweist. Zusätzlich konnte eine leichte Stabilisierung der reduzierten Spezies der Fünfring-annullierten Verbindungen festgestellt werden, welche sich durch gleiche oder weniger negative Reduktionspotentiale gegenüber den hexagonal verknüpften Pendants widerspiegelte. Der Einfluss des Annullierungstypus auf die elektrochemischen und optischen Eigenschaften sowie die Kontrolle über Sechs- bzw. Fünfring-Annullierung können die Entwicklung neuer Elektronenakzeptor Materialien erleichtern.

Im letzten Teil dieser Arbeit (*Unterkapitel 3.4*) wird die Stabilisierung und strukturelle Charakterisierung reduzierter Spezies von Perylenbisimiden diskutiert. Zu diesem Zweck wurde ein PBI-Kern mit stark elektronenziehenden Chlor- und Cyano-Substituenten versehen, welche die reduzierten Spezies gegenüber Oxidation an Luft durch ein extrem niedrig liegendes LUMO-Niveau von -4.73 eV stabilisieren. Dadurch konnte die chemische Reduktion dieses PBIs unter milden Reaktionsbedingungen erreicht werden und das PBI Dianion konnte als Dinatriumsalz isoliert werden. Das Dianion wurde eindeutig mittels UV/Vis/NIR Absorptions- und IR-Spektroskopie sowie DFT Rechnungen charakterisiert. Außerdem wurde die molekulare Struktur im Festkörper durch Einkristallstrukturanalyse bestimmt. Diese Ergebnisse bestätigten die Delokalisierung der zusätzlichen Elektronendichte des PBI-Dianions über das gesamte Molekül, was zu verkürzten C–C Bindungslängen entlang der molekularen Längsachse führte. Weiterhin konnte eine erhöhte Elektronendichte auf den C=O und C \equiv N Gruppen nachgewiesen werden, was zur Koordination dieser Einheiten an die Natrium-Kationen führt und damit zur Stabilisierung der reduzierten Spezies im Festkörper beiträgt (siehe Abbildung 33, Figure 33). Weitergehende elektrochemische Untersuchungen zeigten, dass die Stabilität des intermediären PBI-Radikalions gegenüber der Disproportionierung in die entsprechenden vollständig reduzierte und oxidierte Spezies stark von der Polarität des Lösungsmittels abhängig ist.

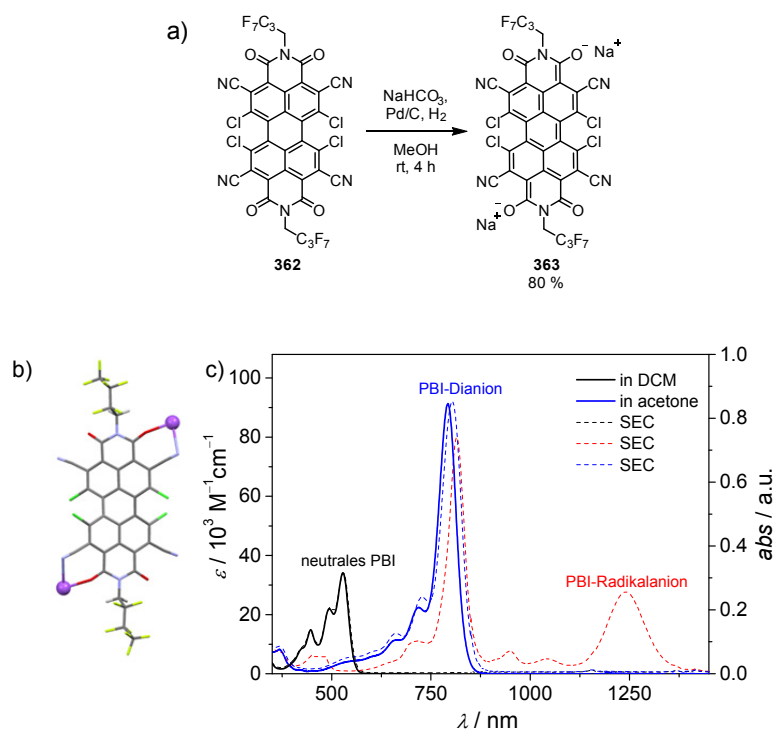


Figure 33 Synthese des PBI-Dianions als Dinatriumsalz (a), die durch Einkristallstrukturanalyse erhaltene molekulare Struktur des PBI-Dianions **363** (b) sowie die UV/Vis/NIR Absorptionsspektren (c) des neutralen PBIs **362** (durchgezogene schwarze Linie), dessen elektrochemisch generierten reduzierten Spezies (SEC, gestrichelte Linien, 0.2 M TBAHFP in DCM) und des isolierten Dianions **363** (durchgezogene blaue Linie).

Zusammenfassend beschreibt diese Arbeit neue Synthesestrategien für die Herstellung verschiedener polyzyklischer aromatischer Dicarboximide einschließlich elektronenarmer graphenartiger Moleküle und Fünfring-verknüpfter aromatischer Systeme. Weiterhin wurde die Reaktivität aromatischer Systeme bezüglich C–C Kupplungskaskadenreaktionen und die mechanistischen Aspekte der einzelnen C–C Kupplungspfade diskutiert, wodurch die Gestaltung neuer organischer Materialien mit bestimmten optischen und elektronischen Eigenschaften erleichtert werden kann. Elektrochemische Untersuchungen dieser Systeme zeigen deutlich eine Stabilisierung von reduzierten Spezies durch die Eingliederung von Fünfringen in polyzyklische aromatische Strukturen oder durch die Einführung von stark elektronenziehenden Substituenten. Dadurch konnte sogar ein Luft-stabiles Perylenbisimid Dianion isoliert werden. Dieser Schritt ist von großer Bedeutung für die Anwendung solcher Materialien als n-Halbleiter oder in der Energiespeicherung. Durch die in dieser Arbeit gewonnenen Erkenntnisse zur Synthese sowie zu Struktur-basierten molekularen Eigenschaften von neuen polyzyklischen aromatischen Kohlenwasserstoffen scheint die Entwicklung neuer innovativer (opto)elektronischer Materialien basierend auf polyzyklischen aromatischen Multi-Dicarboximiden besonders vielversprechend.

Chapter 6

Experimental Part

6.1 Materials and Methods

Chemicals:

N-(2,6-Diisopropylphenyl)-1,8-dicarboxylic acid imide (NI),^[172] 1,6-dibromopyrene (**312**),^[158] 4,9-dibromopyrene (**327**),^[154b] 4-bromopyrene,^[154c] pyrene-2,7-diboronic acid pinacol ester (**333**),^[151] *N*-(2,6-diisopropylphenyl)-4-bromonaphthalene-1,8-dicarboxylic acid imide (**334**),^[216] *N*-(2,6-diisopropylphenyl)-4,5-dibromonaphthalene-1,8-dicarboxylic acid imide (**343**),^[132a] *N,N'*-bis(heptafluorobutyl)-1,6,7,12-tetrachloroperylene-3,4:9,10-tetracarboxylic acid bisimide (**360**)^[203b] and dibromoisocyanuric acid (DBI)^[217] were synthesized according to literature known procedures. The commercially available reagents used in this work were of reagent grade and applied without further purification. Solvents were dried by a commercial solvent purification system (Pure Solv MD-5, Innovative Technology) and applied where necessary.

Chromatography:

Column chromatography was performed in glass columns of appropriate size with silica gel (particle size 0.040–0.063 mm) as stationary phase and freshly distilled solvents as eluents. Preparative size-exclusion chromatography was performed using Bio-Beads S-X3 (mesh size: 200–400, molar mass operation range: up to 2000 g/mol) swollen with a 9:1 dichloromethane/methanol solvent mixture.

Melting points:

Melting points (Mp) were determined on an Olympus BX41 polarization microscope or a Büchi Melting Point B-545 device and are uncorrected.

IR spectroscopy:

IR spectra were recorded on a JASCO FT/IR-4100 spectrometer using an ATR unit.

NMR spectroscopy:

NMR spectra were recorded on a Bruker Avance III HD 400 or Bruker Avance III HD 600 spectrometer in deuterated solvents. ^{13}C NMR spectra were broad-band proton-decoupled. Chemical shifts (δ) are listed in parts per million (ppm) and are reported relative to tetramethylsilane (TMS) or CFCl_3 . Coupling constants (J) are quoted in Hertz (Hz). ^1H and ^{13}C spectra are referenced internally to residual proton solvent resonances or natural-abundance carbon resonances. The following abbreviations were used to describe nuclear spin coupling: s = singlet, d = doublet, t = triplet, sept = septet and m = multiplet.

Mass spectrometry:

MALDI-TOF mass spectra were recorded on a autoflex II mass spectrometer (Bruker Daltronik GmbH). High-resolution ESI-TOF mass spectrometry was carried out on a microTOF focus instrument (Bruker Daltronik GmbH).

Elemental analysis:

Elemental analyses were performed with an Elementar vario micro cube at the Institute for Inorganic Chemistry, University of Würzburg.

UV/Vis/NIR absorption spectroscopy:

Absorption spectra were recorded on Perkin Elmer Lambda 950, Lambda 35 or a JASCO V-670 spectrophotometers in 1 cm quartz cuvettes at room temperature. The solvents for the spectroscopic measurements were of spectroscopic grade and used without further purification.

Fluorescence spectroscopy:

Steady-state and time-dependent fluorescence spectra were recorded in 1 cm quartz cuvettes at room temperature in spectroscopic grade solvents on a PTI QM4-2003 or a FLS980 Edinburgh Instruments fluorescence spectrometer and corrected against photomultiplier and lamp intensity. Relative fluorescence quantum yields were determined by optical dilute method^[164] ($A < 0.05$) using *N,N'*-bis(2,6-diisopropylphenyl)-perylene-3,4:9,10-tetracarboxylic acid bisimide (Lumogen orange) ($\Phi_{\text{fl}} = 1.00$ in chloroform),^[218] fluorescein ($\Phi_{\text{fl}} = 0.89$ in 0.1 M NaOH), rhodamine 101 ($\Phi_{\text{fl}} = 0.915$ in ethanol), oxazine 1 ($\Phi_{\text{fl}} = 0.15$ in ethanol) or quinine sulfate ($\Phi_{\text{fl}} = 0.59$ in 0.1 M HClO_4) as reference.^[165] The absolute

fluorescence quantum yield of **338** was determined with an integrating sphere of Hamamatsu (A10094, C8849, C10027-01, E7536).

Cyclic and square wave voltammetry:

For cyclic and square wave voltammetry, a standard commercial electrochemical analyzer (EC epsilon, BAS Instruments, UK) with a three-electrode single-compartment cell was used. The supporting electrolyte tetrabutylammonium hexafluorophosphate (TBAHFP) was recrystallized from ethanol/water and dried in vacuum. The measurements were carried out using ferrocenium/ferrocene (Fc^+/Fc) as an internal standard for the calibration of the potential. An Ag/AgCl reference electrode, a Pt disc and a Pt wire were used as working and auxiliary electrodes, respectively. For all measurements dry solvents were used and degassed with argon prior to the measurements.

Spectroelectrochemical measurements:

The set-up for spectroelectrochemistry consists of a cylindrical quartz cell with an optically transparent and polished bottom, a platinum disc working electrode (6 mm diameter), a gold-coated metal plate as counter electrode and an Ag/AgCl pseudo-reference electrode. An EG & G Princeton Applied Research Model 283 potentiostat was used. UV/Vis/NIR spectra (JASCO V-670 spectrophotometer) were recorded in reflection at the polished working electrode, with 100 μm distance between the cell bottom and the surface of the working electrode (adjusted with a micrometer screw).

DFT calculations:

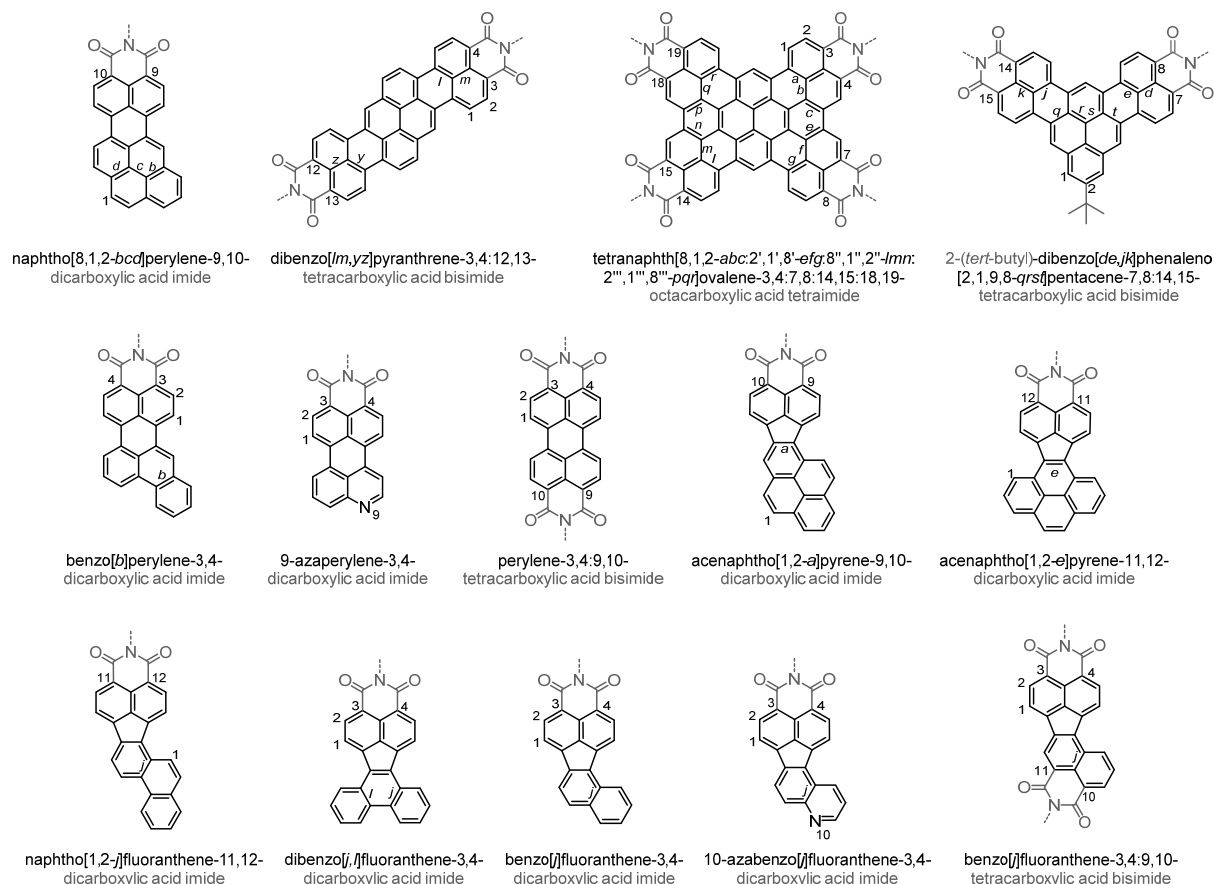
DFT calculations were performed by using the Gaussian 09 program package^[219] with B3-LYP^[220] as functional and 6-31G* (for **329**, PBI **362** and dianion **363**) or def2-SVP^[221] (for all other compounds) as basis set. The structures were geometry optimized, followed by frequency calculations on the optimized structures. Small imaginary frequencies of 11i and 15i cm^{-1} were obtained for compounds **348** and **352**, respectively. Imaginary frequencies $<100\text{i cm}^{-1}$ are considered most likely to be an artefact of the calculation,^[222] thus the resulting geometries can be seen as real minima. The molecular orbitals, charge density differences and the calculated absorption spectra were simulated with the help of the GaussView 5 visualization software package^[223] using the data obtained from (TD-)DFT calculations. For PBI **362** and the PBI dianion **363** simplified structures (fluorinated alkyl

chains were replaced by methyl groups and sodium cations were omitted) were used for calculations.

Crystal structure determination:

Single-crystal X-ray diffraction data for **336**, **338**, **345**, **346**, **351**, **352**, **353**, **354**, **363** were collected at 100 K or 200K (for **336**) on a Bruker D8 Quest Kappa diffractometer with a Photon100 CMOS detector and multi-layered mirror monochromated $\text{CuK}\alpha$ radiation. Single-crystal X-ray diffraction data for **337** and **349** were collected at 100K (**337**) or 296 K (**349**) on a Bruker X8APEX-II diffractometer with a CCD area detector and multi-layer mirror monochromated $\text{MoK}\alpha$ radiation. The structures were solved using direct methods (SHELXS), expanded with Fourier techniques and refined with SHELXL.^[224] All non-hydrogen atoms were refined anisotropically. Hydrogen atoms were included in the structure factor calculation on geometrically idealized positions.

Illustration of atom and bond positions applied for the nomenclature of the synthesized PADIs:



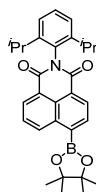
6.2 Synthesis and Characterization

6.2.1 Synthesis of Aryl Boronic Acid Pinacol Esters

General procedure for the synthesis of aryl boronic acid pinacol esters

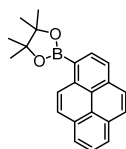
The respective aryl bromide and bis(pinacolato)diboron (B_2pin_2) were suspended in degassed 1,4-dioxane under a nitrogen atmosphere. Afterwards, $[PdCl_2(dppf)]$ and KOAc were added and the mixture was heated at 80 °C for 20 to 23 h. After being cooled down to room temperature, the solution was filtered through a short pad of silica and washed with dichloromethane. The filtrate was concentrated under reduced pressure and the crude product was purified by column chromatography (silica gel, gradient of dichloromethane/hexane 1/1 to 3/1; or gradient of pure dichloromethane to dichloromethane/methanol 99/1 for the quinoline derivative).

***N*-(2,6-Diisopropylphenyl)-4-(4,4,5,5-tetramethyl-1,3,2-dioxaborolan-2-yl)-naphthalene-1,8-dicarboxylic acid imide (328)**: Compound **328** was synthesized according to the general procedure by reaction of *N*-(2,6-diisopropylphenyl)-4-bromonaphthalene-1,8-dicarboxylic acid imide (**334**) (1.00 g, 2.29 mmol, 1.0 eq), B_2pin_2 (873 mg, 3.44 mmol, 1.5 eq), $[PdCl_2(dppf)]$ (83.8 mg, 115 μ mol, 5 mol%) and KOAc (674 mg, 6.87 mmol, 3.0 eq) in 20 mL of dioxane.



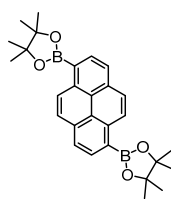
Yield: 720 mg (1.49 mmol, 65 %) colorless solid. 1H NMR ($CDCl_3$, 400 MHz, 298 K): δ = 9.21 (dd, $^3J = 8.5$ and $^4J = 1.2$ Hz, 1H), 8.67 (dd, $^3J = 7.3$ and $^4J = 1.2$ Hz, 1H), 8.63 (d, $^3J = 7.3$ Hz, 1H), 8.35 (d, $^3J = 7.3$ Hz, 1H), 7.84 (dd, $^3J = 8.4$ and $^3J = 7.3$ Hz, 1H), 7.47 (t, $^3J = 7.8$ Hz, 1H), 7.32 (d, $^3J = 7.8$ Hz, 2H), 2.73 (sept, $^3J = 6.9$ Hz, 2H), 1.49 (s, 12H), 1.15 (d, $^3J = 6.9$ Hz, 12H). The analytical data correspond to those reported in the literature.^[159b]

Pyrene-1-boronic acid pinacol ester (339): Compound **339** was synthesized according to the general procedure by reaction of 1-bromopyrene (500 mg, 1.78 mmol, 1.0 eq), B_2pin_2 (903 mg, 3.56 mmol, 2.0 eq), $[PdCl_2(dppf)]$ (195 mg, 267 μ mol, 15 mol%) and KOAc (349 mg, 3.56 mmol, 2.0 eq) in 20 mL of dioxane.



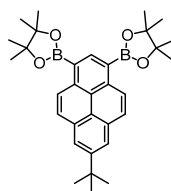
Yield: 475 mg (1.45 mmol, 81 %) colorless solid. ^1H NMR (CDCl_3 , 400 MHz, 298 K): δ = 9.10 (d, $^3J = 9.3$ Hz, 1H), 8.56 (d, $^3J = 7.7$ Hz, 1H), 8.24–8.07 (m, 6H), 8.02 (t, $^3J = 7.7$ Hz, 1H), 1.51 (s, 12H). The analytical data correspond to those reported in the literature.^[225]

Pyrene-1,6-diboronic acid pinacol ester (340): Compound **340** was synthesized according to the general procedure by reaction of 1,6-dibromopyrene (100 mg, 278 μmol , 1.0 eq), B_2pin_2 (212 mg, 834 μmol , 3.0 eq), $[\text{PdCl}_2(\text{dppf})]$ (30.5 mg, 41.7 μmol , 15 mol%) and KOAc (82 mg, 834 μmol , 3.0 eq) in 10 mL of dioxane.



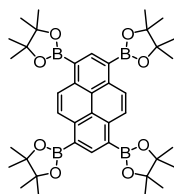
Yield: 105 mg (231 μmol , 83 %) colorless solid. ^1H NMR (CDCl_3 , 400 MHz, 298 K): δ = 9.12 (d, $^3J = 9.2$ Hz, 2H), 8.54 (d, $^3J = 7.7$ Hz, 2H), 8.20 (d, $^3J = 7.7$ Hz, 2H), 8.13 (d, $^3J = 9.3$ Hz, 2H), 1.49 (s, 24H). The analytical data correspond to those reported in the literature.^[226]

7-(tert-Butyl)-pyrene-1,3-diboronic acid pinacol ester (341): Compound **341** was synthesized according to the general procedure by reaction of 1,3-dibromo-7-*tert*-butylpyrene (500 mg, 1.20 mmol, 1.0 eq), B_2pin_2 (915 mg, 3.60 mmol, 3.0 eq), $[\text{PdCl}_2(\text{dppf})]$ (147 mg, 180 μmol , 15 mol%) and KOAc (353 mg, 3.60 mmol, 3.0 eq) in 20 mL of dioxane.



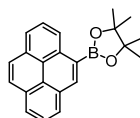
Yield: 474 mg (929 μmol , 77 %) colorless solid. ^1H NMR (CDCl_3 , 400 MHz, 298 K): δ = 9.04 (d, $^3J = 9.2$ Hz, 2H), 8.97 (s, 1H), 8.25 (s, 2H), 8.15 (d, $^3J = 9.2$ Hz, 1H), 1.60 (s, 9H), 1.51 (s, 24H). The analytical data correspond to those reported in the literature.^[150a]

Pyrene-1,3,6,8-tetraboronic acid pinacol ester (342): Compound **342** was synthesized according to the general procedure by reaction of 1,3,6,8-tetrabromopyrene (2.00 g, 3.86 mmol, 1.0 eq), B_2pin_2 (5.88 g, 23.2 mmol, 6.0 eq), $[\text{PdCl}_2(\text{dppf})]$ (570 mg, 772 μmol , 20 mol%) and KOAc (3.03 g, 30.9 mmol, 8.0 eq) in 40 mL of dioxane.



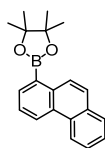
Yield: 1.94 g (2.74 mmol, 71 %) colorless solid. ^1H NMR (CDCl_3 , 400 MHz, 298 K): δ = 9.16 (s, 4H), 8.99 (s, 2H), 1.50 (s, 48H). The analytical data correspond to those reported in the literature.^[227]

Pyrene-4-boronic acid pinacol ester (355): Compound **355** was synthesized according to the general procedure by reaction of 4-bromopyrene (1.24 g, 4.41 mmol, 1.0 eq), B_2pin_2 (2.24 g, 8.82 mmol, 2.0 eq), $[\text{PdCl}_2(\text{dppf})]$ (484 mg, 662 μmol , 15 mol%) and KOAc (866 mg, 8.82 mmol, 2.0 eq) in 40 mL of dioxane.



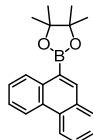
Yield: 959 mg (2.92 mmol, 66 %) colorless solid. ^1H NMR (CDCl_3 , 400 MHz, 298 K): δ = 9.14 (dd, $^3J = 7.9$ and $^4J = 1.0$ Hz, 1H), 8.77 (s, 1H), 8.26–8.19 (m, 3H), 8.10–8.04 (m, 3H), 8.01 (t, $^3J = 7.6$ Hz, 1H), 1.53 (s, 12H). The analytical data correspond to those reported in the literature.^[52]

Phenanthrene-1-boronic acid pinacol ester (356): Compound **356** was synthesized according to the general procedure by reaction of 1-bromophenanthrene (894 mg, 3.48 mmol, 1.0 eq), B_2pin_2 (1.32 g, 5.22 mmol, 1.5 eq), $[\text{PdCl}_2(\text{dppf})]$ (127 mg, 174 μmol , 5 mol%) and KOAc (1.02 g, 10.4 mmol, 3.0 eq) in 40 mL of dioxane.



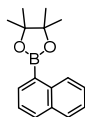
Yield: 846 mg (2.78 mmol, 80 %) colorless solid. Mp.: 99–101 °C. ^1H NMR (CDCl_3 , 400 MHz, 298 K): δ = 8.84 (d, $^3J = 8.4$ Hz, 1H), 8.74–8.70 (m, 2H), 8.18 (dd, $^3J = 7.0$ and $^4J = 1.2$ Hz, 1H), 7.90 (dd, $^3J = 7.7$ and $^4J = 1.2$ Hz, 1H), 7.80 (d, $^3J = 9.2$ Hz, 1H), 7.68–7.58 (m, 3H), 1.45 (s, 12H). ^{13}C NMR (CDCl_3 , 101 MHz, 298 K): δ = 136.3, 135.9, 131.8, 130.7, 130.1, 128.5, 127.4, 127.3, 126.5, 126.4, 126.0, 125.7, 122.8, 84.0, 25.1. HRMS (ESI-TOF, positive mode, acetonitrile/chloroform): m/z calculated for $\text{C}_{20}\text{H}_{21}\text{BKO}_2$: 343.1266; found 343.1269; $[\text{M}+\text{K}]^+$. Elemental analysis: calculated (%) for $\text{C}_{20}\text{H}_{21}\text{BO}_2$: C 78.97, H 6.96; found: C 78.68, H 6.99.

Phenanthrene-9-boronic acid pinacol ester (357): Compound **357** was synthesized according to the general procedure by reaction of 9-bromophenanthrene (1.00 g, 3.89 mmol, 1.0 eq), B₂pin₂ (1.98 g, 7.78 mmol, 2.0 eq), [PdCl₂(dppf)] (476 mg, 583 μmol, 15 mol%) and KOAc (763 mg, 7.78 mmol, 2.0 eq) in 40 mL of dioxane.



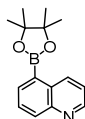
Yield: 760 mg (25.0 mmol, 64 %) colorless solid. ¹H NMR (CDCl₃, 400 MHz, 298 K): δ = 8.85–8.83 (m, 1H), 8.72–8.67 (m, 2H), 8.40 (s, 1H), 7.96–7.93 (m, 1H), 7.71–7.57 (m, 4H), 1.47 (s, 12H). The analytical data correspond to those reported in the literature.^[225]

Naphthalene-1-boronic acid pinacol ester (358): Compound **358** was synthesized according to the general procedure by reaction of 1-bromonaphthalene (1.00 g, 4.83 mmol, 1.0 eq), B₂pin₂ (1.84 g, 7.23 mmol, 1.5 eq), [PdCl₂(dppf)] (176 mg, 241 μmol, 5 mol%) and KOAc (1.42 g, 14.5 mmol, 3.0 eq) in 80 mL of dioxane.



Yield: 1.24 g (4.80 mmol, 99 %) colorless solid. ¹H NMR (CDCl₃, 400 MHz, 298 K): δ = 8.78–8.76 (m, 1H), 8.08 (dd, ³J = 6.9 and ⁴J = 1.3 Hz, 1H), 7.94 (d, ³J = 8.2 Hz, 1H), 7.85–7.82 (m, 1H), 7.56–7.52 (m, 1H), 7.49–7.45 (m, 2H), 1.43 (s, 12H). The analytical data correspond to those reported in the literature.^[228]

Quinoline-5-boronic acid pinacol ester (359): Compound **359** was synthesized according to the general procedure by reaction of 5-bromoquinoline (1.00 g, 4.81 mmol, 1.0 eq), B₂pin₂ (2.44 g, 9.61 mmol, 2.0 eq), [PdCl₂(dppf)] (435 mg, 533 μmol, 15 mol%) and KOAc (943 mg, 9.61 mmol, 2.0 eq) in 40 mL of dioxane.



Yield: 813 mg (3.19 mmol, 66 %) light brown waxy solid. ¹H NMR (CDCl₃, 400 MHz, 298 K): δ = 9.13–9.10 (m, 1H), 8.91 (dd, ³J = 4.2 and ⁴J = 1.7 Hz, 1H), 8.21–8.13 (m, 2H), 7.71 (dd, ³J = 8.4 and ³J = 6.8 Hz, 1H), 7.44 (dd, ³J = 8.5 and ³J = 4.2 Hz, 1H), 1.42 (s, 12H). The analytical data correspond to those reported in the literature.^[229]

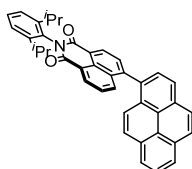
6.2.2 Synthesis of Naphthalimide-Substituted Pyrenes

General procedure for the synthesis of naphthalimide-substituted pyrenes

The respective aryl bromide and boronic acid pinacol ester were dissolved in a mixture of toluene/water (2:1). Afterwards, [Pd(dba)₂], 2-dicyclohexylphosphino-2',6'-dimethoxybiphenyl (SPhos) and Cs₂CO₃ were successively added and the mixture was stirred at 80 °C for 22–24 h under nitrogen atmosphere. After cooling to room temperature, the mixture was extracted three times with dichloromethane and the combined organic layers were washed with water. The organic layer was dried over MgSO₄ and the solvent was removed under reduced pressure.

1-((*N*-(2,6-Diisopropylphenyl)naphthalene-1,8-dicarboximide)-4-yl)pyrene (329):

Compound **329** was synthesized according to the general procedure by reaction of 1-bromopyrene (**326**) (1.00 g, 3.56 mmol, 1.0 eq), naphthalimide boronic ester **328** (2.07 g, 4.27 mmol, 1.2 eq), [Pd(dba)₂] (307 mg, 534 μmol, 15 mol%), SPhos (438 mg, 1.07 mmol, 30 mol%) and Cs₂CO₃ (11.6 g, 35.6 mmol, 10 eq) in 30 mL of a mixture of toluene/water (2:1). The crude product was purified by column chromatography on silica with dichloromethane as eluent. After column chromatography the product was dissolved in dichloromethane and precipitated by addition of hexane, filtered and dried in vacuum at 50 °C to give a yellow solid.

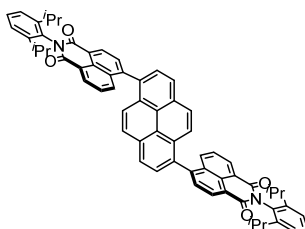


Yield: 1.95 g (3.50 mmol, 98 %) yellow solid. Mp.: >350 °C. ¹H NMR (CDCl₃, 400 MHz, 298 K): δ = 8.86 (d, ³J = 7.4 Hz, 1H), 8.71 (dd, ³J = 7.2 and ⁴J = 1.2 Hz, 1H), 8.36 (d, ³J = 7.8 Hz, 1H), 8.29 (dd, ³J = 7.6 and ⁴J = 1.0 Hz, 1H), 8.22–8.20 (m, 3H), 8.10–8.03 (m, 2H), 8.00–7.96 (m, 2H), 7.88 (dd, ³J = 8.5 and ⁴J = 1.2 Hz, 1H), 7.68 (d, ³J = 9.2 Hz, 1H), 7.60 (dd, ³J = 8.5 and ³J = 7.2 Hz, 1H), 7.52 (t, ³J = 7.8 Hz, 1H), 7.40–7.37 (m, 2H), 2.96–2.80 (m, 2H), 1.27–1.21 (m, 12H). ¹³C NMR (CDCl₃, 101 MHz, 298 K): δ = 164.5, 164.3, 146.4, 145.9, 145.8, 133.54, 133.50, 132.0, 131.8, 131.7, 131.6, 131.4, 131.0, 130.9, 129.75, 129.70, 129.3, 128.41, 128.39, 128.0, 127.5, 127.2, 126.6, 126.0, 125.7, 125.0, 124.9, 124.7, 124.2, 123.1, 122.4, 29.3, 24.3, 24.22, 24.18. HRMS (ESI-TOF, positive mode, acetonitrile/chloroform): *m/z* calculated for C₄₀H₃₂NO₂: 558.24276; found 558.24256; [M+H]⁺. Elemental analysis: calculated for C₄₀H₃₁NO₂·0.75CH₂Cl₂: C 78.77, H 5.27, N 2.25; found: C 78.73, H 5.34, N 2.19. UV/Vis (CH₂Cl₂): λ/nm (ε/M⁻¹cm⁻¹) = 278 (29000), 344

(43600), 393 (7000). Fluorescence (CH₂Cl₂): $\lambda/\text{nm} = 560$ ($\lambda_{\text{ex}} = 340$ nm), $\Phi_{\text{fl}} = 0.28 \pm 0.01$ (vs. quinine sulfate). SWV (CH₂Cl₂, 0.1 M TBAHFP, vs. Fc⁺/Fc): $E^{\text{ox}1} = 0.97$ V, $E^{\text{ox}2} = 1.09$ V, $E^{\text{red}} = -1.79$ V.

1,6-Bis-((N-(2,6-diisopropylphenyl)naphthalene-1,8-dicarboximide)-4-yl)-pyrene (330):

Compound **330** was synthesized according to the general procedure by reaction of 1,6-dibromopyrene (**312**) (100 mg, 278 μmol , 1.0 eq), naphthalimide boronic ester **328** (336 mg, 694 μmol , 2.5 eq), [Pd(dba)₂] (24.0 mg, 41.7 μmol , 15 mol%), SPhos (34.2 mg, 83.4 μmol , 30 mol%) and Cs₂CO₃ (906 mg, 2.78 mmol, 10 eq) in 7.5 mL of a mixture of toluene/water (2:1). The crude product was purified by column chromatography on silica with dichloromethane as eluent.

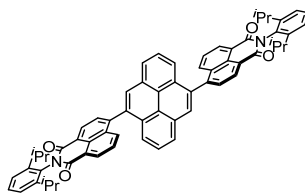


Yield: 241 mg (264 μmol , 95 %) yellow solid. Mp.: >350 °C. ¹H NMR (CDCl₃, 400 MHz, 298 K): $\delta = 8.88$ (d, ³J = 7.4 Hz, 2H), 8.73 (d, ³J = 7.2 Hz, 2H), 8.38 (d, ³J = 7.8 Hz, 2H), 8.11 (d, ³J = 8.3 Hz, 4H), 8.01 (t, ³J = 7.2 Hz, 2H), 7.89 (dd, ³J = 8.4 and ⁴J = 0.8 Hz, 2H), 7.81 (d, ³J = 9.2 Hz, 2H), 7.64 (dd, ³J = 8.4 and ³J = 7.4 Hz, 2H), 7.52 (t, ³J = 7.8 Hz, 2H), 7.40–7.37 (m, 4H), 2.96–2.80 (m, 4H), 1.28–1.20 (m, 24H). ¹³C NMR (CDCl₃, 101 MHz, 298 K): $\delta = 164.4, 164.3, 146.1, 145.8, 134.4, 133.4, 132.0, 131.9, 131.4, 131.0, 130.1, 129.8, 129.3, 128.6, 128.4, 127.4, 127.3, 125.9, 125.3, 124.9, 124.3, 123.2, 122.6, 29.4, 24.3, 24.24, 24.20$. HRMS (ESI-TOF, positive mode, acetonitrile/chloroform): m/z calculated for C₆₄H₅₂N₂NaO₄: 935.38193; found 935.38248; [M+Na]⁺. Elemental analysis: calculated (%) for C₆₄H₅₂N₂O₄: C 84.18, H 5.74, N 3.07; found: C 83.73, H 5.91, N 3.21. UV/Vis (CH₂Cl₂): λ/nm ($\epsilon/\text{M}^{-1}\text{cm}^{-1}$) = 281 (31500), 353 (60900), 394 (19600). Fluorescence (CH₂Cl₂): $\lambda/\text{nm} = 546$ ($\lambda_{\text{ex}} = 340$ nm), $\Phi_{\text{fl}} = 0.33 \pm 0.01$ (vs. quinine sulfate). SWV (CH₂Cl₂, 0.1 M TBAHFP, vs. Fc⁺/Fc): $E^{\text{ox}} = 1.04$ V, $E^{\text{red}} = -1.79$ V.

4,9-Bis-((N-(2,6-diisopropylphenyl)naphthalene-1,8-dicarboximide)-4-yl)-pyrene (331):

Compound **331** was synthesized according to the general procedure by reaction of 4,9-dibromopyrene (**327**) (100 mg, 278 μmol , 1.0 eq), naphthalimide boronic ester **328** (336 mg, 694 μmol , 2.5 eq), [Pd(dba)₂] (24.0 mg, 41.7 μmol , 15 mol%), SPhos (34.2 mg, 83.4 μmol , 30 mol%) and Cs₂CO₃ (906 mg, 2.78 mmol, 10 eq) in 15 mL of a toluene/water-mixture

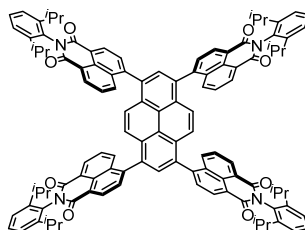
(2:1). The crude product was purified by column chromatography on silica with a gradient of DCM/Hexane 4/1 to 100 % DCM as eluent.



Yield: 182 mg (199 μmol , 72 %) light yellow solid. Mp.: $>350\text{ }^\circ\text{C}$. ^1H NMR (CDCl_3 , 400 MHz, 298 K): δ = 8.90 (d, 3J = 7.4 Hz, 2H), 8.73 (dt, 3J = 7.2 and 4J = 1.1 Hz, 2H), 8.33 (d, 3J = 7.1 Hz, 2H), 8.25 (s, 2H), 8.09–8.04 (m, 4H), 7.99 (t, 3J = 7.7 Hz, 2H), 7.84 (d, 3J = 7.9 Hz, 2H), 7.66–7.61 (m, 2H), 7.52 (t, 3J = 7.7 Hz, 2H), 7.41–7.37 (m, 4H), 2.94–2.81 (m, 4H), 1.27–1.21 (m, 24H). ^{13}C NMR (CDCl_3 , 151 MHz, 298 K): δ = 164.4, 164.3, 145.9, 145.8, 145.6, 136.3, 133.3, 132.14, 132.11, 131.86, 131.85, 131.7, 131.6, 131.01, 130.97, 130.7, 129.8, 129.6, 129.34, 129.31, 127.31, 127.27, 126.9, 126.41, 126.39, 125.0, 124.9, 124.3, 123.23, 123.20, 122.8, 29.4, 24.29, 24.25, 24.20. HRMS (ESI-TOF, positive mode, acetonitrile/chloroform): m/z calculated for $\text{C}_{64}\text{H}_{53}\text{N}_2\text{O}_4$: 913.39998; found 913.40001; $[\text{M}+\text{H}]^+$. Elemental analysis: calculated (%) for $\text{C}_{64}\text{H}_{52}\text{N}_2\text{O}_4 \cdot 0.17\text{CH}_2\text{Cl}_2$: C 83.09, H 5.69, N 3.02; found C 83.27, H 5.86, N 2.84. UV/Vis (CH_2Cl_2): λ/nm ($\epsilon/\text{M}^{-1}\text{cm}^{-1}$) = 281 (42700), 345 (69400), 390 (sh, 8600). Fluorescence (CH_2Cl_2): λ/nm = 534 (λ_{ex} = 340 nm), Φ_{fl} = 0.16 ± 0.01 (vs. quinine sulfate). SWV (CH_2Cl_2 , 0.1 M TBAHFP, vs. Fc^+/Fc): E^{ox} = 1.09 V, E^{red} = -1.79 V.

1,3,6,8-Tetrakis-((*N*-(2,6-diisopropylphenyl)naphthalene-1,8-dicarboximide)-4-yl)-pyrene (332): Compound **332** was synthesized according to the general procedure by

reaction of 1,3,6,9-tetrabromopyrene (510 mg, 0.98 mmol, 1.0 eq), naphthalimide boronic ester **328** (2.4 g, 4.9 mmol, 5.0 eq), $[\text{Pd}(\text{dba})_2]$ (85.0 mg, 148 μmol , 15 mol%), SPhos (120 mg, 292 μmol , 30 mol%) and Cs_2CO_3 (3.20 g, 9.82 mmol, 3.0 eq) in 15 mL of a mixture of toluene/water (2:1). The crude product was purified by column chromatography on silica with a gradient of dichloromethane/acetone from 1:0 to 15:1 as eluent.

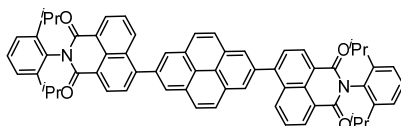


Yield: 580 g (357 μmol , 37 %) yellow solid. Mp.: $>350\text{ }^\circ\text{C}$. ^1H NMR ($\text{C}_2\text{D}_2\text{Cl}_4$, 600 MHz, 368 K): δ = 8.74–8.77 (m, 4H), 8.62–8.64 (m, 4H), 8.22–8.25 (m, 2H), 7.94–8.07 (m, 8H),

7.77–7.80 (m, 4H), 7.63–7.68 (m, 4H), 7.42 (t, $^3J = 7.8$ Hz, 4H), 7.26–7.29 (m, 8H), 2.68–2.77 (m, 8H), 1.10–1.16 (m, 48H). ^{13}C NMR ($\text{C}_2\text{D}_2\text{Cl}_4$, 151 MHz, 368 K): $\delta = 164.2, 164.0, 146.0, 144.9, 135.0, 134.9, 133.0, 132.8, 132.0, 131.9, 131.3, 131.2, 130.5, 130.1, 130.0, 129.9, 129.6, 129.4, 127.8, 127.7, 126.8, 125.6, 124.2, 123.6, 123.2, 120.6, 29.5, 24.3, 24.2$. HRMS (ESI-TOF, positive mode, acetonitrile/chloroform): m/z calculated for $\text{C}_{112}\text{H}_{95}\text{N}_4\text{O}_8$: 1623.71444; found 1623.71493; $[\text{M}+\text{H}]^+$. Elemental analysis: calculated (%) for $\text{C}_{112}\text{H}_{94}\text{N}_4\text{O}_8$: C 82.83; H 5.83, N 3.45; found: C 82.55; H 5.93, N 3.43. UV/Vis (CH_2Cl_2): λ/nm ($\epsilon/\text{M}^{-1}\text{cm}^{-1}$) = 288 (32500), 356 (91200), 397 (sh, 36500). Fluorescence (CH_2Cl_2): $\lambda/\text{nm} = 525$ ($\lambda_{\text{ex}} = 340$ nm), $\Phi_{\text{fl}} = 0.48 \pm 0.004$ (vs. quinine sulfate). SWV (CH_2Cl_2 , 0.1 M TBAHFP, vs. Fc^+/Fc): $E^{\text{ox}} = 1.11$ V, $E^{\text{red}} = -1.80$ V.

2,7-Bis-((*N*-(2,6-diisopropylphenyl)naphthalene-1,8-dicarboximide)-4-yl)-pyrene (335):

Compound **335** was synthesized according to the general procedure by reaction of pyrene-2,7-diboronic acid pinacol ester (**333**) (250 mg, 550 μmol , 1.0 eq), 4-bromonaphthalimide **334** (600 mg, 1.38 mmol, 2.5 eq), $[\text{Pd}(\text{dba})_2]$ (47.4 mg, 82.5 μmol , 15 mol%), SPhos (67.7 mg, 165 μmol , 30 mol%) and Cs_2CO_3 (1.79 g, 5.50 mmol, 10 eq) in 20 mL of a mixture of toluene/water (2:1). The crude product was purified by column chromatography on silica with dichloromethane as eluent.



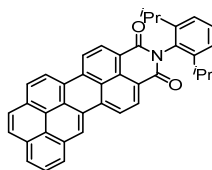
Yield: 476 mg (522 μmol , 95 %) beige solid. Mp.: >350 °C. ^1H NMR (CDCl_3 , 400 MHz, 298 K): $\delta = 8.84$ (d, $^3J = 7.5$ Hz, 2H), 8.77 (dd, $^3J = 7.2$ and $^4J = 1.1$ Hz, 2H), 8.46 (dd, $^3J = 8.6$ and $^4J = 1.1$ Hz, 2H), 8.44 (s, 4H), 8.30 (s, 4H), 8.03 (d, $^3J = 7.5$ Hz, 2H), 7.81 (dd, $^3J = 8.6$ and $^3J = 7.2$ Hz, 2H), 7.51 (t, $^3J = 7.7$ Hz, 2H), 7.38 (d, $^3J = 7.7$ Hz, 4H), 2.84 (sept, $^3J = 6.8$ Hz, 4H), 1.22 (d, $^3J = 6.8$ Hz, 12H), 1.21 (d, $^3J = 6.8$ Hz, 12H). ^{13}C NMR (CDCl_3 , 101 MHz, 298 K): $\delta = 164.5, 164.3, 147.4, 145.8, 137.2, 133.3, 132.0, 131.6, 131.5, 131.0, 130.9, 129.7, 129.6, 129.1, 128.5, 127.4, 126.8, 124.3, 124.2, 123.2, 122.3, 29.4, 24.20, 24.19$. HRMS (ESI-TOF, positive mode, acetonitrile/chloroform): m/z calculated for $\text{C}_{64}\text{H}_{53}\text{N}_2\text{O}_4$: 913.39998; found 913.39951; $[\text{M}+\text{H}]^+$. Elemental analysis: calculated (%) for $\text{C}_{64}\text{H}_{52}\text{N}_2\text{O}_4$: C 84.18, H 5.74, N 3.07; found: C 84.31, H 5.97, N 3.14. UV/Vis (CH_2Cl_2): λ/nm ($\epsilon/\text{M}^{-1}\text{cm}^{-1}$) = 281 (39600), 347 (63700), 364 (65100). Fluorescence (CH_2Cl_2): $\lambda/\text{nm} = 521$ ($\lambda_{\text{ex}} = 340$ nm), $\Phi_{\text{fl}} = 0.04 \pm 0.001$ (vs. quinine sulfate). SWV (CH_2Cl_2 , 0.1 M TBAHFP, vs. Fc^+/Fc): $E^{\text{ox}} = 1.12$ V, $E^{\text{red}} = -1.75$ V.

6.2.3 Synthesis of Six-Membered Ring Annulated Systems by C–C Coupling Cascade Reactions

General procedure for six-membered ring annulated systems by C–C coupling cascade reactions in the Presence of Cs₂CO₃

The respective aryl boronic acid pinacol esters, *N*-(2,6-diisopropylphenyl)-4,5-dibromo-1,8-naphthalimide **343**, [Pd(dba)₂] and 2-dicyclohexylphosphino-2',6'-dimethoxybiphenyl (SPhos) were dissolved in degassed toluene. Subsequently, a solution of Cs₂CO₃ in water was added and the reaction mixture was heated to 90 °C for 17 h up to 5 d under nitrogen atmosphere. After being cooled down to room temperature, water was added and the solution was extracted three times with dichloromethane. The combined organic layers were washed with water, dried over anhydrous MgSO₄ and concentrated under vacuum.

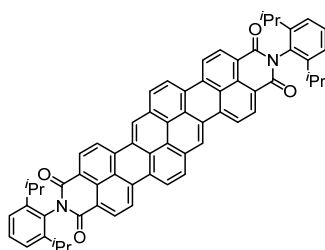
***N*-(2,6-Diisopropylphenyl)-naphtho[8,1,2-*bcd*]perylene-9,10-dicarboxylic acid imide (336)**: Compound **336** was synthesized according to the general procedure by reaction of pyrene-1-boronic acid pinacol ester (**339**) (57.8 mg, 176 μmol, 1.0 eq), *N*-(2,6-diisopropylphenyl)-4,5-dibromo-1,8-naphthalimide (**343**) (100 mg, 194 μmol, 1.1 eq), [Pd(dba)₂] (50.6 mg, 88.0 μmol, 50 mol%), SPhos (72.3 mg, 176 μmol, 100 mol%) and Cs₂CO₃ (172 mg, 528 μmol, 3.0 eq) in 6 mL toluene and 1 mL water. The crude product was purified by column chromatography (silica gel, gradient of hexane/dichloromethane from 3:2 to 100 % dichloromethane), concentrated under vacuum and washed further with methanol to yield **336** as a dark purple solid.



Yield: 53.8 mg (96.8 μmol, 50 %) dark purple solid. Mp.: > 350 °C. ¹H NMR (CDCl₃, 400 MHz, 298 K): δ = 9.09 (s, 1H), 8.87 (d, ³J = 8.4 Hz, 1H), 8.75–8.71 (m, 3H), 8.58 (d, ³J = 8.2 Hz, 1H), 8.32 (t, ³J = 8.2 Hz, 2H), 8.26 (d, ³J = 7.4 Hz, 1H), 8.17–8.11 (m, 2H), 8.06 (t, ³J = 7.6 Hz, 1H), 7.50 (t, ³J = 7.6 Hz, 1H), 7.36 (d, ³J = 7.7 Hz, 2H), 2.82 (sept_{vt}, ³J = 6.8 Hz, 2H), 1.21 (d, ³J = 6.8 Hz, 6H), 1.21 (d, ³J = 6.8 Hz, 6H). ¹³C NMR (CDCl₃, 151 MHz, 298 K): δ = 164.2, 145.9, 138.1, 137.6, 132.8, 132.5, 131.8, 131.5, 131.3, 131.1, 130.9, 129.6, 128.7, 128.4, 128.0, 127.8, 127.7, 127.3, 127.1, 126.8, 126.4, 126.0, 125.2, 125.0, 124.3, 124.2, 122.4, 121.3, 120.8, 120.7, 120.5, 29.3, 24.2. HRMS (ESI-TOF, positive mode, acetonitrile/chloroform): *m/z* calcd for C₄₀H₂₉NO₂: 555.21983; found 555.21891; [M]⁺. Elemental analysis: calculated (%) for C₄₀H₂₉NO₂: C 86.46, H 5.26, N 2.52; found:

C 86.38, H 5.37, 2.35. UV/Vis (CH₂Cl₂): λ/nm ($\epsilon/\text{M}^{-1}\text{cm}^{-1}$) = 547 (44200). Fluorescence (CH₂Cl₂): λ/nm = 598 (λ_{ex} = 530 nm), Φ_{fl} = 0.79±0.04 (vs. rhodamine 101). CV (CH₂Cl₂, 0.1 M TBAHFP, vs. Fc⁺/Fc): $E_{1/2}^{\text{ox}}$ = 0.75, $E_{1/2}^{\text{red1}}$ = -1.35 V, $E_{1/2}^{\text{red2}}$ = -1.79 V.

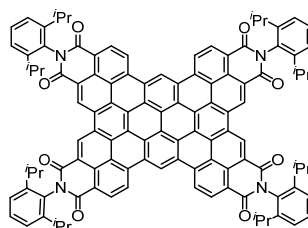
***N,N'*-Bis(2,6-diisopropylphenyl)-dibenzo[*lm,yz*]pyranthrene-3,4:12,13-tetracarboxylic acid bisimide (337)**: Compound **337** was synthesized according to the general procedure by reaction of pyrene-1,6-diboronic acid pinacol ester (**340**) (80.1 mg, 176 μmol , 1.0 eq), *N*-(2,6-diisopropylphenyl)-4,5-dibromo-1,8-naphthalimide (**343**) (200 mg, 388 μmol , 2.2 eq), [Pd(dba)₂] (101 mg, 176 μmol , 100 mol%), SPhos (145 mg, 352 μmol , 200 mol%) and Cs₂CO₃ (172 mg, 528 μmol , 3.0 eq) in 12 mL toluene and 2 mL water. The crude product was purified by column chromatography (silica gel, gradient of dichloromethane to dichloromethane/1 % methanol), followed by washing with methanol and subsequent size exclusion chromatography on Bio-Beads S-X3 (dichloromethane/methanol 9:1). The isolated solid was dissolved in chloroform and precipitated by addition of hexane, filtrated and dried in vacuum at 50 °C to yield **337** as a dark blue solid.



Yield: 70.2 mg (77.3 μmol , 44 %) dark blue solid. Mp.: > 350 °C. ¹H NMR (CDCl₃, 600 MHz, 298 K): δ = 9.22 (s, 2H), 9.00 (d, ³J = 8.8 Hz, 2H), 8.89 (d, ³J = 8.2 Hz, 2H), 8.83 (d, ³J = 7.9 Hz, 2H), 8.80 (d, ³J = 7.9 Hz, 2H), 8.72 (d, ³J = 8.3 Hz, 2H), 8.52 (d, ³J = 8.5 Hz, 2H), 7.51 (t, ³J = 7.9 Hz, 2H), 7.38 (d, ³J = 7.9 Hz, 4H), 2.81 (sept_{vt}, ³J = 6.8 Hz, 4H), 1.21 (d, ³J = 6.8 Hz, 12H), 1.21 (d, ³J = 6.8 Hz, 12H). ¹³C NMR (CDCl₃, 151 MHz, 298 K): δ = 164.1, 164.0, 145.8, 137.2, 136.8, 132.6, 132.0, 131.1, 130.9, 129.7, 129.5, 129.0, 128.9, 127.7, 127.1, 126.3, 125.6, 125.5, 124.3, 124.2, 123.8, 122.0, 121.7, 121.6, 29.9, 29.4, 24.2. HRMS (ESI-TOF, positive mode, acetonitrile/chloroform): *m/z* calculated for C₆₄H₄₈N₂NaO₄: 931.35063; found 931.35345; [M+Na]⁺. Elemental analysis: calculated (%) for C₆₄H₄₈N₂O₄: C 84.56, H 5.32, N 3.08; found: C 85.06, H 5.92, 2.29. UV/Vis (CH₂Cl₂): λ/nm ($\epsilon/\text{M}^{-1}\text{cm}^{-1}$) = 563 (23000), 608 (74600), 663 (152200). Fluorescence (CH₂Cl₂): λ/nm = 681 (λ_{ex} = 640 nm), Φ_{fl} = 0.40±0.05 (vs. oxazine 1). CV (CH₂Cl₂, 0.1 M TBAHFP, vs. Fc⁺/Fc): $E_{1/2}^{\text{ox}}$ = 0.67, $E_{1/2}^{\text{red1}}$ = -1.13 V, $E_{1/2}^{\text{red2}}$ = -1.13 V.

***N,N',N'',N'''*-Tetra(2,6-diisopropylphenyl)-tetranaphth[8,1,2-*abc*:2',1',8'-*efg*:8'',1'',2''-*lmn*:2''',1''',8'''-*pqr*]ovalene-3,4:7,8:14,15:18,19-octacarboxylic acid tetraimide (338):**

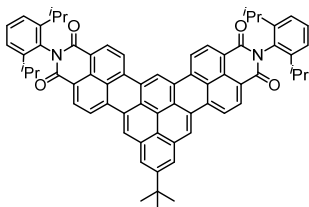
Compound **338** was synthesized according to the general procedure by reaction of pyrene-1,3,6,8-tetraboronic acid pinacol ester (**342**) (137 mg, 194 μmol , 1.0 eq), *N*-(2,6-diisopropylphenyl)-4,5-dibromo-1,8-naphthalimide (**343**) (450 mg, 873 μmol , 4.5 eq), [Pd(dba)₂] (223 mg, 388 μmol , 200 mol%), SPhos (318 mg, 776 μmol , 400 mol%) and Cs₂CO₃ (379 mg, 1.16 mmol, 6.0 eq) in 24 mL toluene and 6 mL water. The crude product was purified by column chromatography (silica gel, gradient of DCM to DCM/1 % MeOH), followed by washing with toluene and MeOH and finally size exclusion chromatography on Bio-Beads S-X3 (DCM/MeOH 9:1). The isolated solid was washed with hexane and dried in vacuum to yield **338** as a dark purple solid.



Yield: 48 mg (29.6 μmol , 15 %) dark purple solid. Mp.: >350 °C. ¹H NMR (CDCl₃, 600 MHz, 298 K): δ = 11.90 (s, 2H), 11.19 (s, 4H), 10.43 (broad m, 4H), 9.71 (broad m, 4H), 7.64 (t, ³J = 8.2 Hz, 4H), 7.50 (d, ³J = 8.2 Hz, 8H), 3.06 (broad m, 8H), 1.34 (broad m, 48H). ¹³C NMR (CDCl₃, 151 MHz, 298 K): δ = 164.5, 146.0, 138.0, 135.0, 130.9, 130.4, 130.1, 129.3, 129.2, 128.5, 128.4, 127.1, 125.4, 124.5, 123.6, 123.4, 122.2, 120.1, 29.6, 24.4. HRMS (ESI-TOF, positive mode, acetonitrile/chloroform): *m/z* calculated for C₁₁₂H₈₃N₄O₈: 1611.62054; found 1611.62137; [M+H]⁺. Elemental analysis: calculated (%) for C₁₁₂H₈₂N₄O₈: C 83.46, H 5.13, N 3.48; found: C 83.26, H 5.69, N 3.93. UV/Vis (CH₂Cl₂): λ/nm ($\epsilon/\text{M}^{-1}\text{cm}^{-1}$) = 459 (75900), 489 (278300), 543 (70100), 584 (141200). Fluorescence (CH₂Cl₂): λ/nm = 608 (λ_{ex} = 530 nm), Φ_{fl} = 0.67±0.01 (absolute). SWV (CH₂Cl₂, 0.1 M TBAHFP, vs. Fc⁺/Fc): E^{ox} = 1.03V, E^{red1} = -0.99 V, E^{red2} = -1.18 V, E^{red3} = -1.59 V, E^{red4} = -1.68 V.

***N,N'*-Bis(2,6-diisopropylphenyl)-2-(*tert*-butyl)-dibenzo[*de,jk*]phenaleno[2,1,9,8-*qrst*]pentacene-7,8:14,15-tetracarboxylic acid bisimide (344):** Compound **344** was synthesized according to the general procedure by reaction of 7-(*tert*-butyl)-pyrene-1,3-diboronic acid pinacol ester (**341**) (200 mg, 392 μmol , 1.0 eq), *N*-(2,6-diisopropylphenyl)-4,5-dibromo-1,8-naphthalimide (**343**) (444 mg, 862 μmol , 2.2 eq), [Pd(dba)₂] (225 mg, 392 μmol , 100 mol%), SPhos (322 mg, 784 μmol , 200 mol%) and Cs₂CO₃ (385 mg, 1.18 mmol,

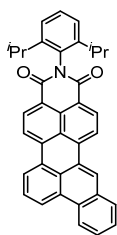
3.0 eq) in 24 mL toluene and 6 mL water. The crude product was purified by column chromatography (silica gel, gradient of dichloromethane to dichloromethane/1 % methanol), followed by washing with methanol and subsequent size exclusion chromatography on Bio-Beads S-X3 (dichloromethane/methanol 9:1). The isolated solid was dissolved in chloroform, precipitated by addition of methanol, filtrated and dried in vacuum at 50 °C to yield **344** as a dark purple solid.



Yield: 153 mg (159 μmol , 40 %) dark purple solid. Mp.: >350 °C. ^1H NMR ($\text{C}_2\text{D}_2\text{Cl}_4$, 600 MHz, 345 K): δ = 9.68 (s, 1H), 9.08 (s, 2H), 8.69–8.76 (m, 8H), 8.43 (s, 2H), 7.43 (t, 3J = 8.0 Hz, 2H), 7.29 (d, 3J = 7.9 Hz, 4H), 2.76 (sept, 3J = 6.8 Hz, 4H), 1.65 (s, 9H), 1.17 (d, 3J = 6.8 Hz, 24H). ^{13}C NMR ($\text{C}_2\text{D}_2\text{Cl}_4$, 151 MHz, 345 K): δ = 164.0, 152.5, 146.1, 137.3, 132.4, 132.0, 131.7, 131.6, 130.9, 129.5, 128.9, 127.9, 127.7, 127.5, 127.3, 126.8, 126.2, 124.2, 124.0, 123.9, 122.1, 121.6, 121.1, 120.6, 118.2, 99.9, 35.7, 31.9, 29.5, 24.3. HRMS (ESI-TOF, positive mode, acetonitrile/chloroform): m/z calcd for $\text{C}_{68}\text{H}_{56}\text{N}_2\text{NaO}_4$: 987.41323; found 987.41354; $[\text{M}+\text{Na}]^+$. UV/Vis (CH_2Cl_2): λ/nm ($\epsilon/\text{M}^{-1}\text{cm}^{-1}$) = 504 (73700), 543 (51400), 575 (sh, 47700). Fluorescence (CH_2Cl_2): λ/nm = 632 (λ_{ex} = 530 nm), Φ_{fl} = 0.79 \pm 0.05 (vs. rhodamine 101). CV (CH_2Cl_2 , 0.1 M TBAHFP, vs. Fc^+/Fc): $E_{1/2}^{\text{ox}}$ = 0.73, $E_{1/2}^{\text{red1}}$ = -1.28 V, $E_{1/2}^{\text{red2}}$ = -1.52 V.

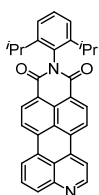
***N*-(2,6-Diisopropylphenyl)-benzo[*b*]perylene-3,4-dicarboxylic acid imide (**345**):**

Compound **345** was synthesized according to the general procedure by reaction of phenanthrene-1-boronic acid pinacol ester (**356**) (107 mg, 353 μmol , 1.0 eq), *N*-(2,6-diisopropylphenyl)-4,5-dibromo-1,8-naphthalimide (**343**) (200 mg, 388 μmol , 1.1 eq), $[\text{Pd}(\text{dba})_2]$ (101 mg, 177 μmol , 50 mol%), SPhos (145 mg, 353 μmol , 100 mol%) and Cs_2CO_3 (345 mg, 1.06 mmol, 3.0 eq) in 12 mL toluene and 2 mL water. The crude product was purified by column chromatography (silica gel, gradient of hexane/dichloromethane from 2:3 to 100 % dichloromethane). After precipitation of **345** by addition of hexane to a concentrated dichloromethane solution, the orange solid was collected by filtration and dried in vacuum at 50 °C.



Yield: 93.2 mg (175 μmol , 50 %) orange solid. Mp.: $>350\text{ }^\circ\text{C}$. ^1H NMR (CDCl_3 , 400 MHz, 298 K): δ = 8.77 (d, 3J = 8.0 Hz, 1H), 8.74 (s, 1H), 8.70–8.65 (m, 3H), 8.58 (d, 3J = 8.2 Hz, 1H), 8.56 (d, 3J = 7.3 Hz, 1H), 8.48 (d, 3J = 8.2 Hz, 1H), 8.03 (dd, 3J = 7.8 and 4J = 1.4 Hz, 1H), 7.82 (t, 3J = 8.0 Hz, 1H), 7.77–7.73 (m, 1H), 7.71–7.67 (m, 1H), 7.49 (t, 3J = 7.8 Hz, 1H), 7.36 (d, 3J = 7.8 Hz, 2H), 2.80 (sept_{vt}, 3J = 6.9 Hz, 2H), 1.20 (d, 3J = 6.9 Hz, 6H), 1.20 (d, 3J = 6.9 Hz, 6H). ^{13}C NMR (CDCl_3 , 101 MHz, 298 K): δ = 164.20, 164.17, 145.8, 137.8, 137.6, 132.4, 132.0, 131.9, 131.4, 131.22, 131.19, 130.6, 130.0, 129.6, 129.4, 128.8, 127.9, 127.6, 127.3, 126.80, 126.78, 125.9, 125.3, 124.2, 123.8, 123.0, 121.14, 121.12, 120.53, 120.46, 29.3, 24.2. HRMS (ESI-TOF, positive mode, acetonitrile/chloroform): m/z calculated for $\text{C}_{38}\text{H}_{30}\text{NO}_2$: 532.2271; found 532.2267; $[\text{M}+\text{H}]^+$. Elemental analysis: calculated (%) for $\text{C}_{38}\text{H}_{29}\text{NO}_2$: C 85.85, H 5.50, N 2.63; found: C 85.91, H 5.71, N 2.80. UV/Vis (CH_2Cl_2): λ/nm ($\epsilon/\text{M}^{-1}\text{cm}^{-1}$) = 484 (38200), 508 (38700). Fluorescence (CH_2Cl_2): λ/nm = 546 (λ_{ex} = 490 nm), Φ_{fl} = 0.89 ± 0.07 (vs. fluorescein). CV (CH_2Cl_2 , 0.1 M TBAHFP, vs. Fc^+/Fc): $E_{1/2}^{\text{ox}}$ = 0.96 V, $E_{1/2}^{\text{red1}}$ = -1.46 V, $E_{1/2}^{\text{red2}}$ = -1.90 V.

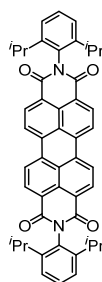
***N*-(2,6-Diisopropylphenyl)-9-azaperylene-3,4-dicarboxylic acid imide (346)**: Compound **346** was synthesized according to the general procedure by reaction of quinoline-5-boronic acid pinacol ester (**359**) (44.9 mg, 176 μmol , 1.0 eq), *N*-(2,6-diisopropylphenyl)-4,5-dibromo-1,8-naphthalimide (**343**) (100 mg, 194 μmol , 1.1 eq), $[\text{Pd}(\text{dba})_2]$ (50.6 mg, 88.0 μmol , 50 mol%), SPhos (72.2 mg, 176 μmol , 100 mol%) and Cs_2CO_3 (172 mg, 528 μmol , 3.0 eq) in 6 mL toluene and 1 mL water. The crude product was purified by column chromatography (silica gel, gradient of pure dichloromethane to dichloromethane with 1 % MeOH). After evaporation of the solvent under reduced pressure the residue was washed with MeOH and subjected to size exclusion chromatography on bio beads S-X3 (dichloromethane/methanol 9:1). After precipitation of **346** by addition of hexane to a concentrated dichloromethane solution, the orange solid was collected by filtration and dried in vacuum at $50\text{ }^\circ\text{C}$.



Yield: 27.1 mg (56.2 μmol , 32 %) orange solid. Mp.: >350 °C. ^1H NMR (CD_2Cl_2 , 400 MHz, 298 K): δ = 9.04 (d, 3J = 4.8 Hz, 1H), 8.71–8.68 (m, 2H), 8.63 (d, 3J = 8.0 Hz, 1H), 8.57 (d, 3J = 8.1 Hz, 1H), 8.52 (dd, 3J = 7.6 and 4J = 0.9 Hz, 1H), 8.20 (d, 3J = 4.8 Hz, 1H), 8.15 (dd, 3J = 8.4 and 4J = 0.8 Hz, 1H), 7.88 (dd, 3J = 8.4 and 3J = 7.6 Hz, 1H), 7.51 (t, 3J = 7.8 Hz, 1H), 7.36 (d, 3J = 7.8 Hz, 2H), 2.75 (sept, 3J = 6.9 Hz, 2H), 1.14 (d, 3J = 6.9 Hz, 12H). ^{13}C NMR (CD_2Cl_2 , 101 MHz, 298 K): δ = 164.20, 164.17, 151.9, 150.1, 146.5, 136.9, 136.7, 135.1, 132.5, 132.2, 132.0, 131.6, 130.6, 130.5, 129.8, 127.4, 124.4, 123.9, 123.8, 123.6, 122.7, 122.0, 121.8, 116.1, 29.5, 24.1. HRMS (ESI-TOF, positive mode, acetonitrile/chloroform): m/z calculated for $\text{C}_{33}\text{H}_{27}\text{N}_2\text{O}_2$: 483.20670; found 483.20671; $[\text{M}+\text{H}]^+$. Elemental analysis: calculated (%) for $\text{C}_{33}\text{H}_{26}\text{N}_2\text{O}_2$: C 82.13, H 5.43, N 5.81; found: C 81.72, H 5.65, N 5.59. UV/Vis (CH_2Cl_2): λ/nm ($\epsilon/\text{M}^{-1}\text{cm}^{-1}$) = 459 (28300), 488 (34900). Fluorescence (CH_2Cl_2): λ/nm = 510 (λ_{ex} = 450 nm), Φ_{fl} = 0.96 ± 0.04 (vs. fluorescein). CV (CH_2Cl_2 , 0.1 M TBAHFP, vs. Fc^+/Fc): $E_{1/2}^{\text{red1}}$ = -1.29 V, $E_{1/2}^{\text{red2}}$ = -1.67 V.

***N,N'*-Bis(2,6-diisopropylphenyl)-perylene-3,4:9,10-tetracarboxylic acid bisimide (347):**

Compound **347** was synthesized according to the general procedure by reaction of *N*-(2,6-diisopropylphenyl)-4-(4,4,5,5-tetramethyl-1,3,2-dioxaborolan-2-yl)-naphthalene-1,8-dicarboxylic acid imide (**328**) (85.1 mg, 176 μmol , 1.0 eq), *N*-(2,6-diisopropylphenyl)-4,5-dibromo-1,8-naphthalimide (**343**) (100 mg, 194 μmol , 1.1 eq), $[\text{Pd}(\text{dba})_2]$ (50.6 mg, 88.0 μmol , 50 mol%), SPhos (72.2 mg, 176 μmol , 100 mol%) and Cs_2CO_3 (172 mg, 528 μmol , 3.0 eq) in 6 mL toluene and 1 mL water. The crude product was purified by column chromatography (silica gel, dichloromethane). The solvent was evaporated under reduced pressure to yield product **347** as an orange solid.



Yield: 22.0 mg (30.9 μmol , 18 %) orange solid. ^1H NMR (CDCl_3 , 400 MHz, 298 K): δ = 8.80 (d, 3J = 8.0 Hz, 4H), 8.75 (d, 3J = 8.0 Hz, 4H), 7.51 (t, 3J = 7.8 Hz, 2H), 7.36 (d, 3J = 7.8 Hz, 4H), 2.76 (sept, 3J = 6.8 Hz, 4H), 1.19 (d, 3J = 6.8 Hz, 24H). MS (MALDI, negative mode, DCTB in chloroform): m/z calculated for $\text{C}_{48}\text{H}_{42}\text{N}_2\text{O}_4$: 710.31; found 710.41; $[\text{M}]^-$.

The analytical data correspond to those reported in the literature.^[218]

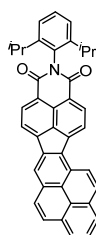
6.2.4 Synthesis of Five-Membered Ring Annulated Systems by C–C Coupling Cascade Reactions

General procedure for five-membered ring annulated systems by C–C coupling cascade reactions in the presence of DBU

The respective aryl boronic acid pinacol ester, *N*-(2,6-diisopropylphenyl)-4,5-dibromo-1,8-naphthalimide **343**, [Pd(dba)₂] and SPhos were dissolved in degassed toluene. Subsequently, DBU was added and the reaction mixture was heated to 90 °C for 19–24 h. After being cooled down to room temperature, water was added and the solution was extracted three times with dichloromethane. The combined organic layers were washed with water, dried over anhydrous MgSO₄ and concentrated under vacuum.

N-(2,6-Diisopropylphenyl)-acenaphtho[1,2-*a*]pyrene-9,10-dicarboxylic acid imide (**348**):

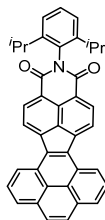
Compound **348** was synthesized according to the general procedure by reaction of pyrene-1-boronic acid pinacol ester (**339**) (57.7 mg, 176 μmol, 1.0 eq), *N*-(2,6-diisopropylphenyl)-4,5-dibromo-1,8-naphthalimide (**343**) (100 mg, 194 μmol, 1.1 eq), [Pd(dba)₂] (50.6 mg, 88.0 μmol, 50 mol%), SPhos (72.2 mg, 176 μmol, 100 mol%) and DBU (78.8 μL, 528 μmol, 3.0 eq) in 6 mL toluene. The crude product was purified by column chromatography (silica gel, gradient of hexane/dichloromethane from 2:3 to 100 % dichloromethane). The residue was washed with MeOH and hexane and dried in vacuum at 50 °C to yield compound **348** as a dark purple solid.



Yield: 34.9 mg (62.8 μmol, 36 %) dark purple solid. Mp.: >350 °C. ¹H NMR (CDCl₃, 600 MHz, 298 K): δ = 8.75 (d, ³J = 9.1 Hz, 1H), 8.63–8.59 (m, 3H), 8.53 (d, ³J = 7.6 Hz, 1H), 8.24–8.20 (m, 4H), 8.15 (s, 2H), 8.02 (t, ³J = 7.6 Hz, 1H), 7.50 (t, ³J = 7.9 Hz, 1H), 7.35 (d, ³J = 7.9 Hz, 2H), 2.86 (sept_{vt}, ³J = 6.9 Hz, 2H), 1.20 (d, ³J = 6.9, 6H), 1.20 (d, ³J = 6.9, 6H). ¹³C NMR (CDCl₃, 151 MHz, 298 K): δ = 164.2, 164.1, 146.0, 144.1, 143.3, 138.1, 133.6, 133.4, 133.1, 132.7, 132.4, 131.9, 131.2, 131.0, 130.3, 129.6, 129.4, 129.1, 128.2, 127.0, 126.8, 126.6, 126.23, 126.22, 125.4, 124.1, 123.8, 123.4, 122.5, 121.7, 121.0, 120.2, 29.3, 24.2. HRMS (ESI-TOF, positive mode, acetonitrile/chloroform): *m/z* calculated for C₄₀H₃₀NO₂: 556.22711; found 556.22609; [M+H]⁺. Elemental analysis: calculated (%) for

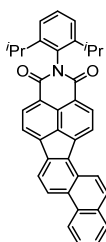
C₄₀H₂₉NO₂: C 86.46, H 5.26, N 2.52; found: C 85.83, H 5.61, N 2.61. UV/Vis (CH₂Cl₂): λ/nm ($\epsilon/M^{-1}cm^{-1}$) = 368 (62500), 518 (11300). Fluorescence (CH₂Cl₂): λ/nm = 637 (λ_{ex} = 510 nm), Φ_{fl} = 0.23±0.01 (vs. rhodamine 101). CV (CH₂Cl₂, 0.1 M TBAHFP, vs. Fc⁺/Fc): $E_{1/2}^{ox}$ = 0.92 V, $E_{1/2}^{red1}$ = -1.35 V, $E_{1/2}^{red2}$ = -1.74 V.

***N*-(2,6-Diisopropylphenyl)-acenaphtho[1,2-*e*]pyrene-11,12-dicarboxylic acid imide (349)**: Compound **349** was synthesized according to the general procedure by reaction of pyrene-4-boronic acid pinacol ester (**355**) (57.7 mg, 176 μ mol, 1.0 eq), *N*-(2,6-diisopropylphenyl)-4,5-dibromo-1,8-naphthalimide (**343**) (100 mg, 194 μ mol, 1.1 eq), [Pd(dba)₂] (50.6 mg, 88.0 μ mol, 50 mol%), SPhos (72.2 mg, 176 μ mol, 100 mol%) and DBU (78.8 μ L, 528 μ mol, 3.0 eq) in 6 mL toluene. The crude product was purified by column chromatography (silica gel, gradient of hexane/dichloromethane from 1:2 to 100 % dichloromethane). After precipitation of the product by addition of hexane to a concentrated dichloromethane solution, the green-brown solid was collected by filtration and dried in vacuum at 50 °C.



Yield: 18.0 mg (32.4 μ mol, 18 %) green-brown solid. Mp.: >350 °C. ¹H NMR (CDCl₃, 600 MHz, 298 K): δ = 8.95 (d, ³J = 7.6 Hz, 2H), 8.58 (d, ³J = 7.4 Hz, 2H), 8.56 (d, ³J = 7.4 Hz, 2H), 8.26 (dd, ³J = 7.6 and ⁴J = 0.7 Hz, 2H), 8.16 (t, ³J = 7.6, 2H), 8.11 (s, 2H), 7.51 (t, ³J = 7.9 Hz, 1H), 7.37 (d, ³J = 7.9 Hz, 2H), 2.90 (sept, ³J = 6.9 Hz, 2H), 1.23 (d, ³J = 6.9, 12H). ¹³C NMR (CDCl₃, 151 MHz, 298 K): δ = 164.0, 146.1, 143.7, 136.1, 132.8, 132.1, 131.4, 131.1, 129.7, 128.5, 128.1, 126.9, 126.7, 125.6, 125.5, 125.1, 124.1, 122.7, 122.3, 29.3, 24.2. HRMS (ESI, positive mode, acetonitrile/chloroform): *m/z* calculated for C₄₀H₂₉KNO₂: 594.1830; found 594.1831; [M+K]⁺. Elemental analysis: calculated (%) for C₄₀H₂₉NO₂: C 86.46, H 5.26, N 2.52; found: C 86.36, H 5.58, N 2.60. UV/Vis (CH₂Cl₂): λ/nm ($\epsilon/M^{-1}cm^{-1}$) = 348 (47400), 438 (17300). CV (CH₂Cl₂, 0.1 M TBAHFP, vs. Fc⁺/Fc): $E_{1/2}^{ox}$ = 0.95 V, $E_{1/2}^{red1}$ = -1.21 V, $E_{1/2}^{red2}$ = -1.59 V.

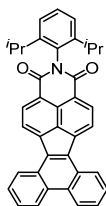
***N*-(2,6-Diisopropylphenyl)-naphtho[1,2-*j*]fluoranthene-11,12-dicarboxylic acid imide (350):** Compound **350** was synthesized according to the general procedure by reaction of phenanthrene-1-boronic acid pinacol ester (**356**) (107 mg, 353 μmol , 1.0 eq), *N*-(2,6-diisopropylphenyl)-4,5-dibromo-1,8-naphthalimide (**343**) (200 mg, 388 μmol , 1.1 eq), $[\text{Pd}(\text{dba})_2]$ (101 mg, 177 μmol , 50 mol%), SPhos (145 mg, 353 μmol , 100 mol%) and DBU (156 μL , 1.06 mmol, 3.0 eq) in 12 mL toluene. The crude product was purified by column chromatography (silica gel, gradient of hexane/dichloromethane from 3:7 to 100 % dichloromethane). After precipitation of the product by addition of hexane to a concentrated dichloromethane solution, the orange-red solid was collected by filtration and dried in vacuum at 50 $^{\circ}\text{C}$.



Yield: 29.4 mg (55.3 μmol , 16 %) orange-red solid. Mp.: $>350\text{ }^{\circ}\text{C}$. ^1H NMR (CDCl_3 , 400 MHz, 298 K): δ = 8.80 (d, 3J = 8.4 Hz, 1H), 8.78 (d, 3J = 8.0 Hz, 1H), 8.61 (d, 3J = 7.4 Hz, 1H), 8.58–8.53 (m, 3H), 8.18 (d, 3J = 8.4 Hz, 1H), 8.12 (d, 3J = 7.2 Hz, 1H), 7.95 (d, 3J = 9.1 Hz, 2H), 7.75–7.65 (m, 2H), 7.49 (t, 3J = 7.7 Hz, 1H), 7.34 (d, 3J = 7.8 Hz, 2H), 2.90 (sept_{vt}, 3J = 6.9 Hz, 2H), 1.19 (d, 3J = 6.9, 6H), 1.18 (d, 3J = 6.9, 6H). ^{13}C NMR (CDCl_3 , 101 MHz, 298 K): δ = 164.1, 164.0, 146.0, 142.9, 139.0, 136.3, 133.2, 133.0, 132.2, 132.0, 131.2, 130.9, 130.2, 129.8, 129.6, 129.1, 127.7, 127.6, 125.9, 124.8, 124.1, 123.3, 122.7, 122.5, 122.3, 121.5, 121.2, 29.3, 24.2. HRMS (ESI-TOF, positive mode, acetonitrile/chloroform): m/z calculated for $\text{C}_{38}\text{H}_{30}\text{NO}_2$: 532.2271; found 532.2267; $[\text{M}+\text{H}]^+$. Elemental analysis: calculated (%) for $\text{C}_{38}\text{H}_{29}\text{NO}_2$: C 85.85, H 5.50, N 2.63; found: C 85.64, H 5.66, N 2.64. UV/Vis (CH_2Cl_2): λ/nm ($\epsilon/\text{M}^{-1}\text{cm}^{-1}$) = 337 (43600), 451 (15500). CV (CH_2Cl_2 , 0.1 M TBAHFP, vs. Fc^+/Fc): $E_{1/2}^{\text{ox}}$ = 1.30 V, $E_{1/2}^{\text{red1}}$ = -1.30 V, $E_{1/2}^{\text{red2}}$ = -1.71 V.

***N*-(2,6-Diisopropylphenyl)-dibenzo[*j,l*]fluoranthene-3,4-dicarboxylic acid imide (351):** Compound **351** was synthesized according to the general procedure by reaction of phenanthrene-9-boronic acid pinacol ester (**357**) (53.5 mg, 176 μmol , 1.0 eq), *N*-(2,6-diisopropylphenyl)-4,5-dibromo-1,8-naphthalimide (**343**) (100 mg, 194 μmol , 1.1 eq), $[\text{Pd}(\text{dba})_2]$ (50.6 mg, 88.0 μmol , 50 mol%), SPhos (72.2 mg, 176 μmol , 100 mol%) and DBU (78.8 μL , 528 μmol , 3.0 eq) in 6 mL toluene. The crude product was purified by column

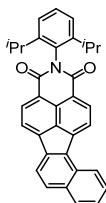
chromatography (silica, dichloromethane/hexane 3:1). The residue was washed with MeOH and hexane and dried in vacuum at 50 °C to yield compound **351** as a brown solid.



Yield: 35.0 mg (65.8 μmol , 37 %) brown solid. Mp.: >350 °C. ^1H NMR (CDCl_3 , 400 MHz, 298 K): δ = 8.74–8.66 (m, 4H), 8.50 (d, $^3J = 7.4$ Hz, 2H), 8.45 (d, $^3J = 7.4$ Hz, 2H), 7.76–7.69 (m, 4H), 7.50 (t, $^3J = 7.8$ Hz, 1H), 7.36 (d, $^3J = 7.8$ Hz, 2H), 2.87 (sept, $^3J = 6.8$ Hz, 2H), 1.21 (d, $^3J = 6.8$ Hz, 12H). ^{13}C NMR (CDCl_3 , 101 MHz, 298 K): δ = 164.0, 146.0, 143.6, 135.5, 132.8, 131.7, 131.3, 131.0, 129.7, 129.4, 128.0, 127.6, 125.5, 125.1, 125.0, 124.1, 123.9, 122.6, 29.3, 24.2. HRMS (ESI-TOF, positive mode, acetonitrile/chloroform): m/z calculated for $\text{C}_{38}\text{H}_{30}\text{NO}_2$: 532.22711; found 532.22551 $[\text{M}+\text{H}]^+$. Elemental analysis: calculated (%) for $\text{C}_{38}\text{H}_{29}\text{NO}_2$: C 85.85, H 5.50, N 2.63; found: C 85.22, H 5.51, N 2.88. UV/Vis (CH_2Cl_2): λ/nm ($\epsilon/\text{M}^{-1}\text{cm}^{-1}$) = 334 (29400), 375 (18500), 435 (9700). CV (CH_2Cl_2 , 0.1 M TBAHFP, vs. Fc^+/Fc): $E_{1/2}^{\text{ox}}$ = 1.18 V, $E_{1/2}^{\text{red1}}$ = -1.25 V, $E_{1/2}^{\text{red2}}$ = -1.63 V.

***N*-(2,6-Diisopropylphenyl)-benzo[*j*]fluoranthene-3,4-dicarboxylic acid imide (352):**

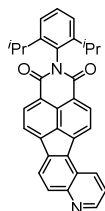
Compound **352** was synthesized according to the general procedure by reaction of naphthalene-1-boronic acid pinacol ester (**358**) (44.7 mg, 176 μmol , 1.0 eq), *N*-(2,6-diisopropylphenyl)-4,5-dibromo-1,8-naphthalimide (**343**) (100 mg, 194 μmol , 1.1 eq), $[\text{Pd}(\text{dba})_2]$ (50.6 mg, 88.0 μmol , 50 mol%), SPhos (72.2 mg, 176 μmol , 100 mol%) and DBU (78.8 μL , 528 μmol , 3.0 eq) in 6 mL toluene. The crude product was purified by column chromatography (silica, dichloromethane/hexane 3:1). The residue was washed with MeOH and hexane, and dried in vacuum at 50 °C to yield compound **352** as a red solid.



Yield: 42.1 mg (87.4 μmol , 50 %) red solid. Mp.: >350 °C. ^1H NMR (CDCl_3 , 400 MHz, 298 K): δ = 8.60 (d, $^3J = 8.4$ Hz, 1H), 8.58 (d, $^3J = 7.4$ Hz, 1H), 8.53 (d, $^3J = 7.2$ Hz, 1H), 8.48 (d, $^3J = 7.4$ Hz, 1H), 8.07 (d, $^3J = 7.2$ Hz, 1H), 8.02 (d, $^3J = 8.3$ Hz, 1H), 7.95–7.93 (m, 2H), 7.70–7.66 (m, 1H), 7.57–7.53 (m, 1H), 7.48 (t, $^3J = 7.8$ Hz, 1H), 7.34 (d, $^3J = 7.8$ Hz, 2H), 2.83 (sept_{vr}, $^3J = 6.9$ Hz, 2H), 1.18 (d, $^3J = 6.9$, 6H), 1.18 (d, $^3J = 6.9$, 6H). ^{13}C NMR

(CDCl₃, 101 MHz, 298 K): δ = 164.1, 164.0, 146.0, 143.6, 143.1, 138.8, 135.8, 135.1, 133.1, 132.9, 131.4, 131.1, 131.0, 130.7, 129.7, 129.6, 128.3, 126.8, 125.6, 124.8, 124.3, 124.1, 122.8, 122.3, 121.8, 120.7, 29.3, 24.2. HRMS (ESI-TOF, positive mode, acetonitrile/chloroform): m/z calculated for C₃₄H₂₈NO₂: 482.21146; found 482.21113; [M+H]⁺. Elemental analysis: calculated (%) for C₃₄H₂₇NO₂: C 84.80, H 5.65, N 2.91; found: C 84.50, H 5.67, N 3.26. UV/Vis (CH₂Cl₂): λ/nm ($\epsilon/M^{-1}cm^{-1}$) = 319 (27900), 401 (16400), 424 (19500). CV (CH₂Cl₂, 0.1 M TBAHFP, vs. Fc⁺/Fc): $E_{1/2}^{red1}$ = -1.31 V, $E_{1/2}^{red2}$ = -1.71 V.

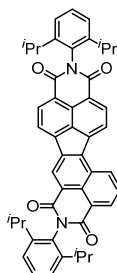
***N*-(2,6-Diisopropylphenyl)-10-azabenzol[j]fluoranthene-3,4-dicarboxylic acid imide (353)**: Compound **353** was synthesized according to the general procedure by reaction of quinoline-5-boronic acid pinacol ester (**359**) (44.9 mg, 176 μ mol, 1.0 eq), *N*-(2,6-diisopropylphenyl)-4,5-dibromo-1,8-naphthalimide (**343**) (100 mg, 194 μ mol, 1.1 eq), [Pd(dba)₂] (50.6 mg, 88.0 μ mol, 50 mol%), SPhos (72.2 mg, 176 μ mol, 100 mol%) and DBU (78.8 μ L, 528 μ mol, 3.0 eq) in 6 mL toluene. The crude product was purified by column chromatography (silica gel, gradient of pure dichloromethane to dichloromethane with 1 % MeOH). After evaporation of the solvent under reduced pressure the residue was washed with MeOH and subjected to size exclusion chromatography on bio beads S-X3 (dichloromethane/methanol 9:1). After precipitation of the product by addition of hexane to a concentrated dichloromethane solution, the orange solid was collected by filtration and dried in vacuum at 50 °C.



Yield: 30.1 mg (62.3 μ mol, 35 %) orange solid. Mp.: >350 °C. ¹H NMR (CDCl₃, 400 MHz, 298 K): δ = 8.99 (dd, ³*J* = 4.2 and ⁴*J* = 1.6 Hz, 1H), 8.91 (dd, ³*J* = 8.6 and ⁴*J* = 0.9 Hz, 1H), 8.59 (d, ³*J* = 7.4 Hz, 1H), 8.56 (d, ³*J* = 7.2 Hz, 1H), 8.44 (d, ³*J* = 7.4 Hz, 1H), 8.25 (d, ³*J* = 8.7 Hz, 1H), 8.20 (d, ³*J* = 8.7 Hz, 1H), 8.13 (d, ³*J* = 7.2 Hz, 1H), 7.58 (dd, ³*J* = 8.6 and ³*J* = 4.2 Hz, 1H), 7.49 (t, ³*J* = 7.8 Hz, 1H), 7.34 (d, ³*J* = 7.8 Hz, 2H), 2.82 (sept, ³*J* = 6.9 Hz, 2H), 1.18 (d, ³*J* = 6.9 Hz, 12H). ¹³C NMR (CDCl₃, 101 MHz, 298 K): δ = 163.92, 163.86, 151.2, 149.5, 146.0, 142.6, 142.3, 139.1, 135.9, 133.0, 132.3, 132.0, 131.5, 131.0, 129.7, 126.4, 125.7, 124.6, 124.1, 124.0, 123.1, 122.8, 122.7, 122.5, 29.3, 24.2. HRMS (ESI-TOF, positive mode, acetonitrile/chloroform): m/z calculated for C₃₃H₂₇N₂O₂: 483.20670; found 483.20695; [M+H]⁺. Elemental analysis: calculated (%) for C₃₃H₂₆N₂O₂·H₂O: C 79.18, H 5.64, N 5.60;

found: C 79.40, H 5.65, N 5.40. UV/Vis (CH₂Cl₂): λ/nm ($\epsilon/\text{M}^{-1}\text{cm}^{-1}$) = 396 (19100), 419 (23300). CV (CH₂Cl₂, 0.1 M TBAHFP, vs. Fc⁺/Fc): $E_{1/2}^{\text{red}1} = -1.24$ V, $E_{1/2}^{\text{red}2} = -1.64$ V.

***N,N'*-Bis(2,6-diisopropylphenyl)-benzo[*j*]fluoranthene-3,4:10,11-tetracarboxylic acid bisimide (354)**: Compound **354** was synthesized according to the general procedure by reaction of *N*-(2,6-diisopropylphenyl)-4-(4,4,5,5-tetramethyl-1,3,2-dioxaborolan-2-yl)-naphthalene-1,8-dicarboxylic acid imide (**328**) (85.1 mg, 176 μmol , 1.0 eq), *N*-(2,6-diisopropylphenyl)-4,5-dibromo-1,8-naphthalimide (**343**) (100 mg, 194 μmol , 1.1 eq), [Pd(dba)₂] (50.6 mg, 88.0 μmol , 50 mol%), SPhos (72.2 mg, 176 μmol , 100 mol%) and DBU (78.8 μL , 528 μmol , 3.0 eq) in 6 mL toluene. The crude product was purified by column chromatography (silica gel, dichloromethane). After precipitation of **354** by addition of hexane to a concentrated dichloromethane solution, the orange solid was collected by filtration and dried in vacuum at 50 °C.

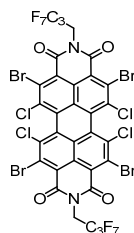


Yield: 47.0 mg (66.1 μmol , 38 %) orange solid. Mp.: >350 °C. ¹H NMR (CDCl₃, 400 MHz, 298 K): δ = 9.22 (s, 1H), 9.10 (dd, ³*J* = 8.5 and ⁴*J* = 1.1 Hz, 1H), 8.76 (dd, ³*J* = 7.2 and ⁴*J* = 1.1 Hz, 1H), 8.72 (s, 2H), 8.67 (d, ³*J* = 7.2 Hz, 1H), 8.32 (d, ³*J* = 7.2 Hz, 1H), 8.01 (dd, ³*J* = 8.5 and ³*J* = 7.2 Hz, 1H), 7.54–7.49 (m, 2H), 7.38–7.34 (m, 4H), 2.85–2.76 (m, 4H), 1.21–1.18 (m, 24H). ¹³C NMR (CDCl₃, 101 MHz, 298 K): δ = 164.1, 164.0, 163.6, 146.0, 145.8, 141.3, 141.2, 141.1, 139.2, 133.4, 132.9, 132.5, 131.7, 130.8, 130.7, 130.6, 130.3, 129.9, 129.8, 129.5, 128.8, 126.4, 126.1, 125.8, 124.3, 124.2, 124.09, 124.06, 123.63, 123.62, 123.5, 29.4, 29.3, 24.19, 24.16. HRMS (ESI-TOF, positive mode, acetonitrile/chloroform): *m/z* calculated C₄₈H₄₃N₂O₄: 711.32173; found 711.32352; [M+H]⁺. Elemental analysis: calculated (%) for C₄₈H₄₂N₂O₄: C 81.10, H 5.96, N 3.94; found: C 81.14, H 6.17, N 4.00. UV/Vis (CH₂Cl₂): λ/nm ($\epsilon/\text{M}^{-1}\text{cm}^{-1}$) = 366 (34400), 410 (19600), 434 (29700). CV (CH₂Cl₂, 0.1 M TBAHFP, vs. Fc⁺/Fc): $E_{1/2}^{\text{red}1} = -1.06$ V, $E_{1/2}^{\text{red}2} = -1.39$ V.

6.2.5 Synthesis of Core-Functionalized Perylene Bisimides

N,N'-Bis(heptafluorobutyl)-2,5,8,11-tetrabromo-1,6,7,12-tetrachloroperylene-3,4:9,10-tetracarboxylic acid bisimide (361)

A solution of PBI **360** (1.00 g, 1.12 mmol, 1.0 eq) and dibromoisocyanuric acid (DBI) (1.12 g, 3.92 mmol, 3.5 eq) in 40 mL of oleum (20 % SO₃) was stirred at 100 °C for 18 h. After cooling to room temperature, the mixture was poured slowly onto 150 g of ice. 150 mL water were added and the precipitate was collected by filtration, washed several times with water and dried in vacuum. The crude product was purified by column chromatography using dichloromethane as the eluent to give a red solid.



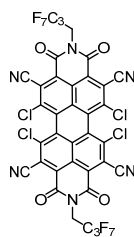
Yield: 667 mg (552 μmol, 51 %) red solid. Mp.: >350 °C. ¹H NMR (CDCl₃, 400 MHz, 298 K): δ = 5.24–5.03 (m, 4H). ¹³C NMR (CDCl₃, 101 MHz, 298 K): δ = 160.0, 139.5, 132.2, 129.7, 128.1, 125.5, 121.7, 39.4. ¹⁹F NMR (CDCl₃, 376 MHz, 298 K): δ = –80.4 (t, ³J_{FF} = 9.4 Hz, 6F), –116.0 (m, 4F), –127.5 (m, 4F). HRMS (ESI-TOF, positive mode, acetonitrile/chloroform 1/1): *m/z* calculated for C₃₂H₅Br₄Cl₄F₁₄N₂O₄: 1208.5438; found 1208.5427; [M+H]⁺. Elemental analysis: calculated (%) for C₃₂H₄Br₄Cl₄F₁₄N₂O₄: C 31.82, H 0.33, N 2.32; found C 32.09, H 0.43, N 2.53. UV/Vis (CH₂Cl₂): λ/nm (ε/M⁻¹cm⁻¹) = 523 (29900), 493 (24200), 461 (24700). Fluorescence (CH₂Cl₂): λ/nm = 573 (λ_{ex} = 490 nm), Φ_{fl} = 0.02±0.01 (vs. lumogen orange). CV (CH₂Cl₂, 0.1 M TBAHFP, vs. Fc⁺/Fc): E_{1/2}^{red1} = –0.49 V, E_{1/2}^{red2} = –0.67 V.

N,N'-Bis(heptafluorobutyl)-2,5,8,11-tetracyano-1,6,7,12-tetrachloroperylene-3,4:9,10-tetracarboxylic acid bisimide (362)

The synthesis was adapted to a literature known procedure for alkyl-substituted PBIs.^[210]

PBI **361** (300 mg, 248 μmol, 1.0 eq) and copper cyanide (133 mg, 1.49 mmol, 10 eq) were mixed in 15 mL of dry DMF under argon and heated at 140 °C for 2.5 h. After cooling down to room temperature, the mixture was poured onto 150 mL of water. The precipitate was separated by filtration, washed with water and dissolved in dichloromethane. The solution was dried over MgSO₄ and concentrated under reduced pressure. The crude product was

purified by repeated column chromatography (silica, dichloromethane/ethyl acetate (95/5)) to give an orange-red solid.

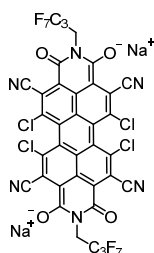


Yield: 86.4 mg (87.1 μmol , 35 %) orange-red solid. Mp.: $>350\text{ }^\circ\text{C}$ decomposition. ^1H NMR (D_2SO_4 , 400 MHz, 298 K): $\delta = 5.10$ (broad m, 4H). ^{19}F NMR (D_2SO_4 , 376 MHz, 298 K): $\delta = -80.0$ (t, $^3J_{\text{FF}} = 8.1$ Hz, 6F), -115.3 (m, 4F), -126.9 (m, 4F). HRMS (ESI-TOF, negative mode, acetone): m/z calculated for $\text{C}_{36}\text{H}_4\text{Cl}_4\text{F}_{14}\text{N}_6\text{O}_4$: 989.88301; found 989.88244; $[\text{M}]^-$. Elemental analysis: calculated (%) for $\text{C}_{36}\text{H}_4\text{Cl}_4\text{F}_{14}\text{N}_6\text{O}_4$: C 43.58, H 0.41, N 8.47; found C 44.01, H 0.44, N 8.27. UV/Vis (CH_2Cl_2): λ/nm ($\epsilon/\text{M}^{-1}\text{cm}^{-1}$) = 528 (34100), 494 (22000), 447 (14900). Fluorescence (CH_2Cl_2): $\lambda/\text{nm} = 559$ ($\lambda_{\text{ex}} = 490$ nm), $\Phi_{\text{fl}} = 0.11 \pm 0.01$ (vs. lumogen orange). CV (CH_2Cl_2 , 0.1 M TBAHFP, vs. Fc^+/Fc): $E_{1/2}^{\text{red1}} = -0.07$ V, $E_{1/2}^{\text{red2}} = -0.41$ V.

Due to the low solubility of this compound in all organic solvents as well as in D_2SO_4 , no ^{13}C resonances could be detected.

Dianion disodium salt of *N,N'*-Bis(heptafluorobutyl)-2,5,8,11-tetracyano-1,6,7,12-tetrachloroperylene-3,4:9,10-tetracarboxylic acid bisimide (**363**)

PBI **362** (20.0 mg, 20.2 μmol , 1.0 eq), NaHCO_3 (20.0 mg, 238 μmol , 11.8 eq) and Pd/C (2 mg, 10 wt%) were mixed in 10 mL of dry methanol under nitrogen atmosphere. Once nitrogen was replaced by hydrogen, a colour change from orange to blue was observed within few minutes. The solution stirred for additional 4 h at room temperature and the residual catalyst was filtered off through a pad of celite. After removing the solvent under reduced pressure, the residue was dissolved in 20 mL acetone and the product was precipitated by addition of 100 mL pentane. This mixture was cooled to $5\text{ }^\circ\text{C}$ and the product was separated by filtration, washed with pentane and dried under vacuum at $50\text{ }^\circ\text{C}$ to yield **363** as a blue solid.



Yield: 17.3 mg (16.1 μmol , 80 %) blue solid. Mp.: $>350\text{ }^\circ\text{C}$. ^1H NMR (acetone- D_6 , 400 MHz, 298 K): $\delta = 5.07$ (broad m, 4H). ^{13}C NMR (acetone- D_6 , 101 MHz, 298 K): $\delta = 38.9$, quaternary carbons and CF_2 , CF_3 groups were not visible, even at extended acquisition time. ^{19}F NMR (acetone- D_6 , 376 MHz): -81.4 (t, $^3J_{\text{FF}} = 9.7$ Hz, 6F), -115.8 (m, 4F), -128.5 (m, 4F). HRMS (ESI-TOF, negative mode, acetone): m/z calculated for $\text{C}_{36}\text{H}_4\text{Cl}_4\text{F}_{14}\text{N}_6\text{O}_4$: 989.88301; found 989.88361; $[\text{M}]^-$. Sodium cations cannot be detected by this method. Elemental analysis: calculated (%) for $\text{Na}_2[\text{C}_{36}\text{H}_4\text{Cl}_4\text{F}_{14}\text{N}_6\text{O}_4]\cdot 2\text{H}_2\text{O}$: C 40.25, H 0.75, N 7.82; found: C 40.67, H 0.94, N 7.58. UV/Vis (acetone): λ/nm ($\epsilon/\text{M}^{-1}\text{cm}^{-1}$) = 793 (91300), 718 (22400). CV (acetone, 0.1 M TBAHFP, vs. Fc^+/Fc): $E_{1/2}^{\text{ox}1} = -0.35$ V, $E_{1/2}^{\text{ox}2} = -0.15$ V.

6.3 Single Crystal Data

Single crystals of **336** suitable for X-ray structural analysis were grown by slow diffusion of hexane into a solution of **336** in dichloromethane at room temperature.

Crystal data for 336 ($C_{40}H_{29}NO_2 \cdot CH_2Cl_2$): $M_r = 640.57$, $0.23 \times 0.14 \times 0.05 \text{ mm}^3$, triclinic space group $P\bar{1}$, $a = 9.1392(2) \text{ \AA}$, $\alpha = 77.6080(10)^\circ$, $b = 13.2716(3) \text{ \AA}$, $\beta = 76.0260(10)^\circ$, $c = 13.7699(3) \text{ \AA}$, $\gamma = 84.9090(10)^\circ$, $V = 1581.79(6) \text{ \AA}^3$, $Z = 2$, $\rho(\text{calcd}) = 1.345 \text{ g}\cdot\text{cm}^{-3}$, $\mu = 2.145 \text{ mm}^{-1}$, $F_{(000)} = 668$, $\text{Goof}(F^2) = 1.035$, $R_I = 0.0737$, $wR^2 = 0.2179$ for $I > 2\sigma(I)$, $R_1 = 0.0802$, $wR^2 = 0.2253$ for all data, 6207 unique reflections [$\theta \leq 72.225^\circ$] with a completeness of 99.8% and 486 parameters, 8 restraints.

Single crystals of **337** suitable for X-ray structural analysis were grown by slow diffusion of toluene into a solution of **337** in dichloromethane at room temperature.

Crystal data for 337 ($C_{64}H_{48}N_2O_4 \cdot 2 C_7H_8 \cdot CH_2Cl_2$): $M_r = 1178.23$, $0.23 \times 0.07 \times 0.05 \text{ mm}^3$, monoclinic space group $P2_1/c$, $a = 13.3641(12) \text{ \AA}$, $\alpha = 90^\circ$, $b = 15.7960(14) \text{ \AA}$, $\beta = 112.839(2)^\circ$, $c = 14.8901(13) \text{ \AA}$, $\gamma = 90^\circ$, $V = 2896.9(4) \text{ \AA}^3$, $Z = 2$, $\rho(\text{calcd}) = 1.351 \text{ g}\cdot\text{cm}^{-3}$, $\mu = 0.171 \text{ mm}^{-1}$, $F_{(000)} = 1240$, $\text{Goof}(F^2) = 1.035$, $R_I = 0.0494$, $wR^2 = 0.1334$ for $I > 2\sigma(I)$, $R_1 = 0.0651$, $wR^2 = 0.1459$ for all data, 5776 unique reflections [$\theta \leq 26.145^\circ$] with a completeness of 100.0% and 420 parameters, 0 restraints.

Single crystals of **338** for X-ray structural analysis were grown by slow diffusion of hexane into a solution of **338** in chloroform at room temperature. The single crystals thus obtained were highly sensitive towards temperature. Therefore, the crystalline material was directly immersed (from the remaining solution) into a film of perfluoropolyether which was precooled to 200 K on a copper substrate. Subsequently, the investigated single crystal was transferred on a Teflon loop to a Bruker D8 Quest Kappa diffractometer continuously cooled by evaporated liquid nitrogen. The refinement showed at least 3 more disordered chloroform molecules which could not be modelled satisfactorily. Therefore, the SQUEEZE routine of PLATON was used to remove the respective electron density.^[230] The remaining structure could be refined properly.

Crystal data for 338 ($C_{112}H_{82}N_4O_8 \cdot 4 CHCl_3$): $M_r = 2089.28$, $0.35 \times 0.22 \times 0.22 \text{ mm}^3$, triclinic space group $P\bar{1}$, $a = 14.8784(4) \text{ \AA}$, $\alpha = 74.7990(10)^\circ$, $b = 15.1215(4) \text{ \AA}$, $\beta = 87.9040(10)^\circ$, $c = 16.8294(4) \text{ \AA}$, $\gamma = 62.1650(10)^\circ$, $V = 3214.70(15) \text{ \AA}^3$, $Z = 1$, $\rho(\text{calcd}) = 1.079 \text{ g}\cdot\text{cm}^{-3}$, $\mu = 2.753 \text{ mm}^{-1}$, $F_{(000)} = 1078$, $\text{Goof}(F^2) = 1.073$, $R_I = 0.0702$, $wR^2 = 0.1825$

for $I > 2\sigma(I)$, $R_1 = 0.0773$, $wR^2 = 0.1883$ for all data, 12636 unique reflections [$\theta \leq 72.319^\circ$] with a completeness of 99.8 % and 765 parameters, 13 restraints.

Single crystals of **345** suitable for X-ray structural analysis were grown by slow evaporation of a solution of **345** in chloroform at room temperature.

Crystal data for 345 ($C_{38}H_{29}NO_2 \cdot CHCl_3$): $M_r = 650.99$, $0.291 \times 0.097 \times 0.036 \text{ mm}^3$, triclinic space group $P\bar{1}$, $a = 9.1191(3) \text{ \AA}$, $\alpha = 80.596(2)^\circ$, $b = 13.2405(4) \text{ \AA}$, $\beta = 84.690(2)^\circ$, $c = 13.3105(4) \text{ \AA}$, $\gamma = 75.229(2)^\circ$, $V = 1530.95(8) \text{ \AA}^3$, $Z = 2$, $\rho(\text{calcd}) = 1.412 \text{ g}\cdot\text{cm}^{-3}$, $\mu = 3.008 \text{ mm}^{-1}$, $F_{(000)} = 676$, $\text{Goof}(F^2) = 1.050$, $R_I = 0.0491$, $wR^2 = 0.1230$ for $I > 2\sigma(I)$, $R_1 = 0.0565$, $wR^2 = 0.1288$ for all data, 5988 unique reflections [$\theta \leq 72.263^\circ$] with a completeness of 99.3 % and 441 parameters, 6 restraints.

Single crystals of **346** suitable for X-ray structural analysis were grown by slow evaporation of a solution of **346** in dichloromethane at room temperature.

Crystal data for 346 ($C_{33}H_{26}N_2O_2 \cdot CH_2Cl_2$): $M_r = 567.48$, $0.198 \times 0.135 \times 0.043 \text{ mm}^3$, triclinic space group $P\bar{1}$, $a = 8.3071(4) \text{ \AA}$, $\alpha = 74.563(2)^\circ$, $b = 11.0789(6) \text{ \AA}$, $\beta = 87.663(2)^\circ$, $c = 15.5551(8) \text{ \AA}$, $\gamma = 83.862(2)^\circ$, $V = 1371.92(12) \text{ \AA}^3$, $Z = 2$, $\rho(\text{calcd}) = 1.374 \text{ g}\cdot\text{cm}^{-3}$, $\mu = 2.407 \text{ mm}^{-1}$, $F_{(000)} = 592$, $\text{Goof}(F^2) = 1.039$, $R_I = 0.0463$, $wR^2 = 0.1228$ for $I > 2\sigma(I)$, $R_1 = 0.0505$, $wR^2 = 0.1264$ for all data, 5402 unique reflections [$\theta \leq 72.271^\circ$] with a completeness of 99.8 % and 375 parameters, 7 restraints.

Single crystals of **349** suitable for X-ray structural analysis were grown by slow evaporation of a solution of **349** in chloroform at room temperature.

Crystal data for 349 ($C_{40}H_{29}NO_2 \cdot CHCl_3$): $M_r = 675.01$, $0.149 \times 0.136 \times 0.074 \text{ mm}^3$, triclinic space group $P\bar{1}$, $a = 9.2621(7) \text{ \AA}$, $\alpha = 73.209(2)^\circ$, $b = 12.9315(9) \text{ \AA}$, $\beta = 73.716(2)^\circ$, $c = 14.4917(10) \text{ \AA}$, $\gamma = 80.652(2)^\circ$, $V = 1588.8(2) \text{ \AA}^3$, $Z = 2$, $\rho(\text{calcd}) = 1.411 \text{ g}\cdot\text{cm}^{-3}$, $\mu = 0.328 \text{ mm}^{-1}$, $F_{(000)} = 700$, $\text{Goof}(F^2) = 1.038$, $R_I = 0.0515$, $wR^2 = 0.1232$ for $I > 2\sigma(I)$, $R_1 = 0.0777$, $wR^2 = 0.1363$ for all data, 6263 unique reflections [$\theta \leq 26.054^\circ$] with a completeness of 100.0 % and 450 parameters, 6 restraints.

Single crystals of **351** suitable for X-ray structural analysis were grown by slow evaporation of a solution of **351** in chloroform at room temperature.

Crystal data for 351 ($C_{38}H_{29}NO_2 \cdot CHCl_3$): $M_r = 650.99$, $0.389 \times 0.147 \times 0.119 \text{ mm}^3$, triclinic space group $P\bar{1}$, $a = 10.1191(4) \text{ \AA}$, $\alpha = 93.4090(10)^\circ$, $b = 12.9620(5) \text{ \AA}$, $\beta = 103.6290(10)^\circ$, $c = 13.0407(5) \text{ \AA}$, $\gamma = 110.4260(10)^\circ$, $V = 1538.81(10) \text{ \AA}^3$, $Z = 2$, $\rho(\text{calcd}) =$

1.405 g·cm⁻³, $\mu = 2.993 \text{ mm}^{-1}$, $F_{(000)} = 676$, $\text{Goof}(F^2) = 1.030$, $R_I = 0.0320$, $wR^2 = 0.0837$ for $I > 2\sigma(I)$, $R_I = 0.0338$, $wR^2 = 0.0852$ for all data, 6037 unique reflections [$\theta \leq 72.264^\circ$] with a completeness of 99.5 % and 473 parameters, 19 restraints.

Single crystals of **352** suitable for X-ray structural analysis were grown by slow evaporation of a solution of **352** in chloroform at room temperature.

Crystal data for 352 (C₃₄H₂₇NO₂): $M_r = 481.56$, 0.183 x 0.142 x 0.080 mm³, triclinic space group P $\bar{1}$, $a = 8.4240(3) \text{ \AA}$, $\alpha = 97.2420(10)^\circ$, $b = 8.4292(3) \text{ \AA}$, $\beta = 92.7110(10)^\circ$, $c = 18.6552(6) \text{ \AA}$, $\gamma = 110.3620(10)^\circ$, $V = 1226.05(7) \text{ \AA}^3$, $Z = 2$, $\rho(\text{calcd}) = 1.304 \text{ g}\cdot\text{cm}^{-3}$, $\mu = 0.629 \text{ mm}^{-1}$, $F_{(000)} = 508$, $\text{Goof}(F^2) = 1.051$, $R_I = 0.0388$, $wR^2 = 0.1012$ for $I > 2\sigma(I)$, $R_I = 0.0415$, $wR^2 = 0.1033$ for all data, 4798 unique reflections [$\theta \leq 72.115^\circ$] with a completeness of 99.6 % and 338 parameters, 0 restraints.

Single crystals of **353** suitable for X-ray structural analysis were grown by slow diffusion of hexane into a solution of **353** in chloroform at room temperature.

Crystal data for 353 (C₃₃H₂₆N₂O₂ · CHCl₃): $M_r = 601.92$, 0.347 x 0.096 x 0.088 mm³, monoclinic space group P2₁/c, $a = 8.8745(6) \text{ \AA}$, $\alpha = 90^\circ$, $b = 9.9783(7) \text{ \AA}$, $\beta = 95.378(2)^\circ$, $c = 31.832(2) \text{ \AA}$, $\gamma = 90^\circ$, $V = 2806.4(3) \text{ \AA}^3$, $Z = 4$, $\rho(\text{calcd}) = 1.425 \text{ g}\cdot\text{cm}^{-3}$, $\mu = 3.242 \text{ mm}^{-1}$, $F_{(000)} = 1248$, $\text{Goof}(F^2) = 1.071$, $R_I = 0.0338$, $wR^2 = 0.0885$ for $I > 2\sigma(I)$, $R_I = 0.0352$, $wR^2 = 0.0895$ for all data, 5518 unique reflections [$\theta \leq 72.191^\circ$] with a completeness of 99.9 % and 393 parameters, 21 restraints.

Single crystals of **354** suitable for X-ray structural analysis were grown by slow diffusion of hexane into a solution of **354** in chloroform at room temperature.

Crystal data for 354 (C₄₈H₄₂N₂O₄ · 0.855 C₆H₁₄ · 0.219 CHCl₃): $M_r = 810.67$, 0.439 x 0.427 x 0.065 mm³, triclinic space group P $\bar{1}$, $a = 9.1488(7) \text{ \AA}$, $\alpha = 79.5750(17)^\circ$, $b = 15.2616(11) \text{ \AA}$, $\beta = 75.9515(17)^\circ$, $c = 16.5098(12) \text{ \AA}$, $\gamma = 82.6270(18)^\circ$, $V = 2190.7(3) \text{ \AA}^3$, $Z = 2$, $\rho(\text{calcd}) = 1.229 \text{ g}\cdot\text{cm}^{-3}$, $\mu = 0.958 \text{ mm}^{-1}$, $F_{(000)} = 863$, $\text{Goof}(F^2) = 1.026$, $R_I = 0.0378$, $wR^2 = 0.1015$ for $I > 2\sigma(I)$, $R_I = 0.0394$, $wR^2 = 0.1031$ for all data, 8598 unique reflections [$\theta \leq 72.301^\circ$] with a completeness of 99.7 % and 644 parameters, 25 restraints.

Single crystals of **363** suitable for X-ray diffraction experiments were grown by slow diffusion of pentane into a 1mM solution of dianion **363** in acetone at room temperature.

Crystal data for 363 (C_{89.40}H_{44.52}Cl₈F₂₈N₁₂Na₄O_{14.43}): $M_r = 2425.21$, 0.307 x 0.156 x 0.095 mm³, triclinic space group P $\bar{1}$, $a = 14.6741(9) \text{ \AA}$, $\alpha = 91.946(2)^\circ$, $b = 15.8676(10) \text{ \AA}$, $\beta =$

106.327(2)°, $c = 24.1918(15)$ Å, $\gamma = 115.228(2)$ °, $V = 4812.8(5)$ Å³, $Z = 2$, $\rho(\text{calcd}) = 1.674$ g cm⁻³, $\mu = 3.447$ mm⁻¹, $F_{(000)} = 2425$, $\text{Goof}(F^2) = 1.015$, $R_I = 0.0485$, $wR^2 = 0.1285$ for $I > 2\sigma(I)$, $R_I = 0.0580$, $wR^2 = 0.1370$ for all data, 82373 unique reflections [$\theta \leq 67.679^\circ$] with a completeness of 99.9 % and 1669 parameters, 527 restraints.

Crystallographic data have been deposited with the Cambridge Crystallographic Data Centre no. CCDC 1497040 (**336**), CCDC 1497041 (**337**), CCDC 1452370 (**338**), CCDC 1537962 (**345**), CCDC 1537961 (**349**), CCDC 1537964 (**351**) and CCDC 1537963 (**352**), CCDC 1032959 (**363**). These data can be obtained free of charge from The Cambridge Crystallographic Data Centre *via* www.ccdc.ac.uk/data.request/cif.

Appendix

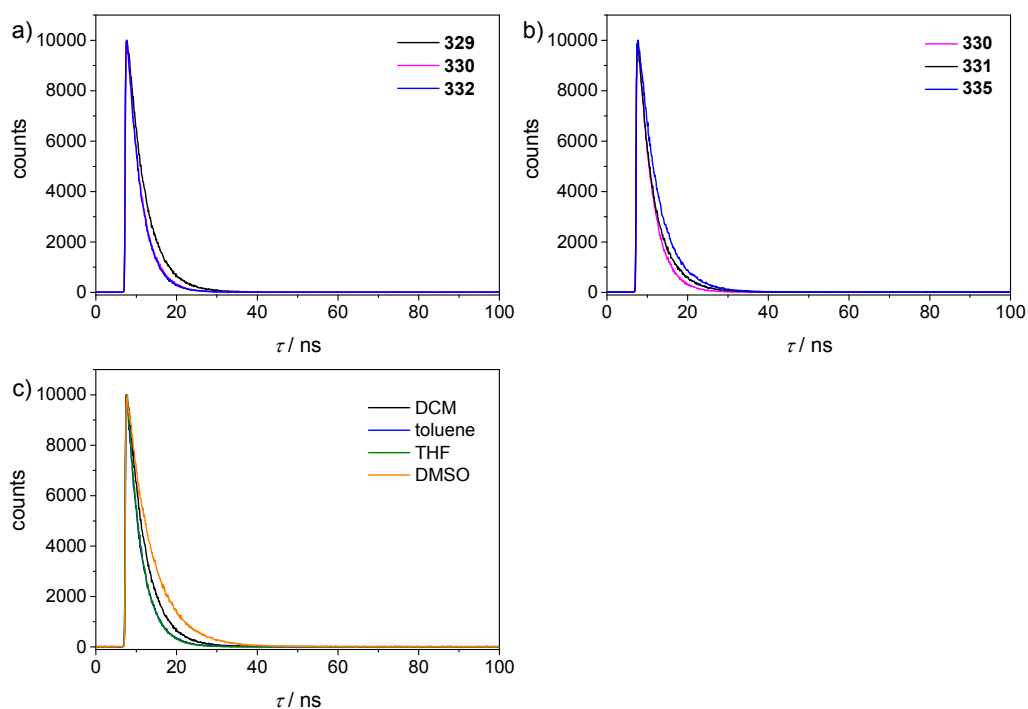


Figure A1 Decay traces of compounds **329**, **330** and **332** (a), decay of di-substituted derivatives **330**, **331** and **335** (b) in dichloromethane and decay of compound **329** in solvents of different polarity (c); $\lambda_{\text{ex}} = 405$ nm, $\lambda_{\text{det}} =$ respective emission maxima (see Table1).

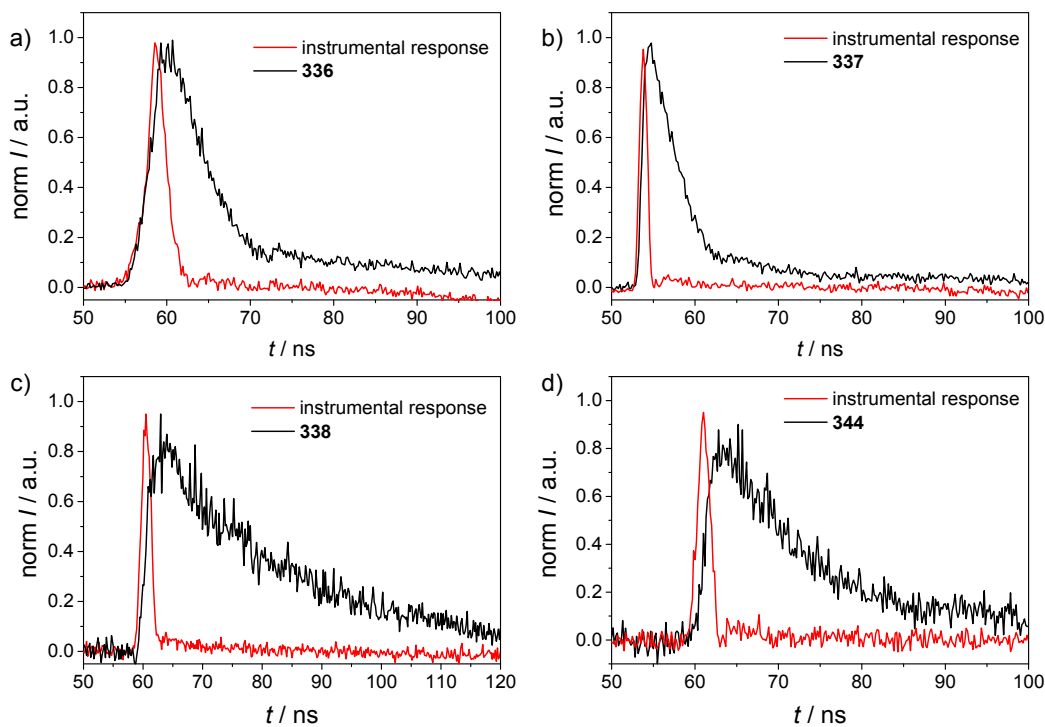


Figure A2 Time-resolved fluorescence decay of **336** (a, $\lambda_{\text{ex}} = 490$ nm, $\lambda_{\text{det}} = 598$ nm), of **337** (b, $\lambda_{\text{ex}} = 649$ nm, $\lambda_{\text{det}} = 681$ nm), for **338** (c, $\lambda_{\text{ex}} = 572$ nm, $\lambda_{\text{det}} = 608$ nm) and for **344** (d, $\lambda_{\text{ex}} = 572$ nm, $\lambda_{\text{det}} = 632$ nm) in DCM.

Literature

- [1] *Nanotechnologie aktuell*, Nanoinitiative Bayern GmbH, **2016**.
- [2] a) D. H. Bamford, *Curr. Biol.* **2000**, *10*, R558; b) R. F. Service, *Science* **2002**, *298*, 2322.
- [3] a) V. Balzani, A. Credi, F. M. Raymo, J. F. Stoddart, *Angew. Chem. Int. Ed.* **2000**, *39*, 3348; b) J.-P. Sauvage, *Acc. Chem. Res.* **1998**, *31*, 611; c) S. Kassem, T. van Leeuwen, A. S. Lubbe, M. R. Wilson, B. L. Feringa, D. A. Leigh, *Chem. Soc. Rev.* **2017**, *46*, 2592.
- [4] a) V. Balzani, *Small* **2005**, *1*, 278; b) G. M. Whitesides, *Small* **2005**, *1*, 172.
- [5] K. Müllen, *ACS Nano* **2014**, *8*, 6531.
- [6] K. S. Novoselov, A. K. Geim, S. V. Morozov, D. Jiang, Y. Zhang, S. V. Dubonos, I. V. Grigorieva, A. A. Firsov, *Science* **2004**, *306*, 666.
- [7] a) K. S. Novoselov, *Angew. Chem. Int. Ed.* **2011**, *50*, 6986; b) A. K. Geim, *Angew. Chem. Int. Ed.* **2011**, *50*, 6966.
- [8] M. J. Allen, V. C. Tung, R. B. Kaner, *Chem. Rev.* **2010**, *110*, 132.
- [9] <https://graphene-flagship.eu/>, 22/09/2017.
- [10] a) L. Chen, Y. Hernandez, X. Feng, K. Müllen, *Angew. Chem. Int. Ed.* **2012**, *51*, 7640; b) A. Narita, X.-Y. Wang, X. Feng, K. Müllen, *Chem. Soc. Rev.* **2015**, *44*, 6616.
- [11] a) https://apps.webofknowledge.com/WOS_GeneralSearch_input.do?product=WOS&search_mode=GeneralSearch&SID=Y2tMI9a7FchhqxjgSON&preferencesSaved=, topic: nanoscience, refined by: document types: article, create citation report, 22/09/2017;
- b) https://apps.webofknowledge.com/WOS_GeneralSearch_input.do?product=WOS&search_mode=GeneralSearch&SID=Y2tMI9a7FchhqxjgSON&preferencesSaved=, topic: nanographene, refined by: document types: article, create citation report, 22/09/2017.

- [12] a) F. Morgenroth, C. Kübel, M. Müller, U. M. Wiesler, A. J. Berresheim, M. Wagner, K. Müllen, *Carbon* **1998**, *36*, 833; b) C. D. Simpson, G. Mattersteig, K. Martin, L. Gherghel, R. E. Bauer, H. J. Räder, K. Müllen, *J. Am. Chem. Soc.* **2004**, *126*, 3139.
- [13] a) X. W. Zhan, A. Facchetti, S. Barlow, T. J. Marks, M. A. Ratner, M. R. Wasielewski, S. R. Marder, *Adv. Mater.* **2011**, *23*, 268; b) C. Huang, S. Barlow, S. R. Marder, *J. Org. Chem.* **2011**, *76*, 2386; c) F. Würthner, M. Stolte, *Chem. Commun.* **2011**, *47*, 5109; d) Z. Liu, G. Zhang, Z. Cai, X. Chen, H. Luo, Y. Li, J. Wang, D. Zhang, *Adv. Mater.* **2014**, *26*, 6965.
- [14] a) H. Qian, F. Negri, C. Wang, Z. Wang, *J. Am. Chem. Soc.* **2008**, *130*, 17970; b) H. Qian, Z. Wang, W. Yue, D. Zhu, *J. Am. Chem. Soc.* **2007**, *129*, 10664; c) W. Yue, A. Lv, J. Gao, W. Jiang, L. Hao, C. Li, Y. Li, L. E. Polander, S. Barlow, W. Hu, S. Di Motta, F. Negri, S. R. Marder, Z. Wang, *J. Am. Chem. Soc.* **2012**, *134*, 5770.
- [15] a) N. J. Schuster, D. W. Paley, S. Jockusch, F. Ng, M. L. Steigerwald, C. Nuckolls, *Angew. Chem. Int. Ed.* **2016**, *55*, 13519; b) Y. Zhong, B. Kumar, S. Oh, M. T. Trinh, Y. Wu, K. Elbert, P. Li, X. Zhu, S. Xiao, F. Ng, M. L. Steigerwald, C. Nuckolls, *J. Am. Chem. Soc.* **2014**, *136*, 8122; c) P. E. Hartnett, H. S. S. R. Matte, N. D. Eastham, N. E. Jackson, Y. Wu, L. X. Chen, M. A. Ratner, R. P. H. Chang, M. C. Hersam, M. R. Wasielewski, T. J. Marks, *Chem. Sci.* **2016**, *7*, 3543; d) D. Meng, H. Fu, C. Xiao, X. Meng, T. Winands, W. Ma, W. Wei, B. Fan, L. Huo, N. L. Doltsinis, Y. Li, Y. Sun, Z. Wang, *J. Am. Chem. Soc.* **2016**, *138*, 10184.
- [16] a) X. Cui, C. Xiao, L. Zhang, Y. Li, Z. Wang, *Chem. Commun.* **2016**, *52*, 13209; b) T. V. Pho, F. M. Toma, M. L. Chabinyk, F. Wudl, *Angew. Chem. Int. Ed.* **2013**, *52*, 1446; c) M. Żyła-Karwowska, H. Zhylitskaya, J. Cybińska, T. Lis, P. J. Chmielewski, M. Stępień, *Angew. Chem. Int. Ed.* **2016**, *55*, 14658.
- [17] T. M. Figueira-Duarte, K. Müllen, *Chem. Rev.* **2011**, *111*, 7260.
- [18] a) J. Hassan, M. Sévignon, C. Gozzi, E. Schulz, M. Lemaire, *Chem. Rev.* **2002**, *102*, 1359; b) F. Ullmann, J. Bielecki, *Ber. Dtsch. Chem. Ges.* **1901**, *34*, 2174.
- [19] a) R. Pummerer, E. Cherbuliez, *Ber. Dtsch. Chem. Ges.* **1914**, *47*, 2957; b) R. Pummerer, F. Frankfurter, *Ber. Dtsch. Chem. Ges.* **1914**, *47*, 1472; c) J. Löwe, *J. Prakt. Chem.* **1868**, *103*, 464.
- [20] a) R. Scholl, J. Mansfeld, *Ber. Dtsch. Chem. Ges.* **1910**, *43*, 1734; b) M. Grzybowski, K. Skonieczny, H. Butenschön, D. T. Gryko, *Angew. Chem. Int. Ed.* **2013**, *52*, 9900.
- [21] J. K. Stille, *Angew. Chem. Int. Ed.* **1986**, *25*, 508.
- [22] T. Y. N. Miyaura, A. Suzuki, *Synth. Commun.* **1981**, *11*, 513.

- [23] E. Negishi, A. O. King, N. Okukado, *J. Org. Chem.* **1977**, *42*, 1821.
- [24] Y. Hatanaka, T. Hiyama, *J. Org. Chem.* **1988**, *53*, 918.
- [25] K. Tamao, K. Sumitani, M. Kumada, *J. Am. Chem. Soc.* **1972**, *94*, 4374.
- [26] a) D. Alberico, M. E. Scott, M. Lautens, *Chem. Rev.* **2007**, *107*, 174; b) L. Ackermann, R. Vicente, A. R. Kapdi, *Angew. Chem. Int. Ed.* **2009**, *48*, 9792; c) G. P. McGlacken, L. M. Bateman, *Chem. Soc. Rev.* **2009**, *38*, 2447.
- [27] M. Berthelot, *Liebigs Ann.* **1867**, *141*, 173.
- [28] W. Reppe, W. J. Schweckendiek, *Liebigs Ann.* **1948**, *560*, 104.
- [29] T. Jin, J. Zhao, N. Asao, Y. Yamamoto, *Chem. – Eur. J.* **2014**, *20*, 3554.
- [30] A. P. Dianin, *Zh. Russ. Fiz.-Khim. O-va.* **1874**, 183.
- [31] *Modern Arene Chemistry*, Wiley-VCH, Weinheim, **2002**.
- [32] a) G. Baddeley, *J. Chem. Soc.* **1950**, 994; b) C. D. Nenitzescu, A. Balaban, *Chem. Ber.* **1958**, *91*, 2109.
- [33] L. Zhai, R. Shukla, S. H. Wadumethrige, R. Rathore, *J. Org. Chem.* **2010**, *75*, 4748.
- [34] a) M. Kardos, **1913**, DE276956; b) M. Kardos, **1913**, DE276357.
- [35] T. Sakamoto, C. Pac, *J. Org. Chem.* **2001**, *66*, 94.
- [36] a) D. R. Stuart, K. Fagnou, *Science* **2007**, *316*, 1172; b) R. Li, L. Jiang, W. Lu, *Organometallics* **2006**, *25*, 5973.
- [37] T. Yamamoto, S. Wakabayashi, K. Osakada, *J. Organomet. Chem.* **1992**, *428*, 223.
- [38] M. F. Semmelhack, P. M. Helquist, L. D. Jones, *J. Am. Chem. Soc.* **1971**, *93*, 5908.
- [39] *Metal-Catalyzed Cross-Coupling Reactions*, Vol. 1, 2 ed., Wiley-VCH, Weinheim, **2004**.
- [40] U. Christmann, R. Vilar, *Angew. Chem. Int. Ed.* **2005**, *44*, 366.
- [41] J. Louie, J. F. Hartwig, *J. Am. Chem. Soc.* **1995**, *117*, 11598.
- [42] a) A. L. Casado, P. Espinet, *J. Am. Chem. Soc.* **1998**, *120*, 8978; b) A. L. Casado, P. Espinet, A. M. Gallego, *J. Am. Chem. Soc.* **2000**, *122*, 11771; c) J. A. Casares, P. Espinet, G. Salas, *Chem. – Eur. J.* **2002**, *8*, 4843.
- [43] a) R. Martin, S. L. Buchwald, *Acc. Chem. Res.* **2008**, *41*, 1461; b) N. Miyaura, *J. Organomet. Chem.* **2002**, *653*, 54.
- [44] D. Lapointe, K. Fagnou, *Chem. Lett.* **2010**, *39*, 1118.
- [45] a) B. Glover, K. A. Harvey, B. Liu, M. J. Sharp, M. F. Tymoschenko, *Org. Lett.* **2003**, *5*, 301; b) Y. Su, H. Zhou, J. Chen, J. Xu, X. Wu, A. Lin, H. Yao, *Org. Lett.* **2014**, *16*, 4884.

- [46] a) S. R. Neufeldt, M. S. Sanford, *Acc. Chem. Res.* **2012**, *45*, 936; b) K. M. Engle, T.-S. Mei, M. Wasa, J.-Q. Yu, *Acc. Chem. Res.* **2012**, *45*, 788.
- [47] a) S. Yanagisawa, K. Ueda, H. Sekizawa, K. Itami, *J. Am. Chem. Soc.* **2009**, *131*, 14622; b) K. Ueda, S. Yanagisawa, J. Yamaguchi, K. Itami, *Angew. Chem. Int. Ed.* **2010**, *49*, 8946; c) S.-Y. Tang, Q.-X. Guo, Y. Fu, *Chem. – Eur. J.* **2011**, *17*, 13866; d) I. A. Sanhueza, A. M. Wagner, M. S. Sanford, F. Schoenebeck, *Chem. Sci.* **2013**, *4*, 2767.
- [48] a) M. D. Watson, A. Fechtenkötter, K. Müllen, *Chem. Rev.* **2001**, *101*, 1267; b) M. Quernheim, F. E. Golling, W. Zhang, M. Wagner, H.-J. Räder, T. Nishiuchi, K. Müllen, *Angew. Chem. Int. Ed.* **2015**, *54*, 10341; c) X. Feng, J. Wu, M. Ai, W. Pisula, L. Zhi, J. P. Rabe, K. Müllen, *Angew. Chem. Int. Ed.* **2007**, *46*, 3033; d) A. Narita, I. A. Verzhbitskiy, W. Frederickx, K. S. Mali, S. A. Jensen, M. R. Hansen, M. Bonn, S. De Feyter, C. Casiraghi, X. Feng, K. Müllen, *ACS Nano* **2014**, *8*, 11622; e) J. Wu, Z. Tomovic, V. Enkelmann, K. Müllen, *J. Org. Chem.* **2004**, *69*, 5179.
- [49] a) Z. Wang, Ž. Tomović, M. Kastler, R. Pretsch, F. Negri, V. Enkelmann, K. Müllen, *J. Am. Chem. Soc.* **2004**, *126*, 7794; b) J. Liu, B.-W. Li, Y.-Z. Tan, A. Giannakopoulos, C. Sanchez-Sanchez, D. Beljonne, P. Ruffieux, R. Fasel, X. Feng, K. Müllen, *J. Am. Chem. Soc.* **2015**, *137*, 6097.
- [50] a) A. Fechtenkötter, K. Saalwächter, M. A. Harbison, K. Müllen, H. W. Spiess, *Angew. Chem. Int. Ed.* **1999**, *38*, 3039; b) S. Ito, M. Wehmeier, J. D. Brand, C. Kübel, R. Epsch, J. P. Rabe, K. Müllen, *Chem. – Eur. J.* **2000**, *6*, 4327.
- [51] Y. Fogel, L. Zhi, A. Rouhanipour, D. Andrienko, H. J. Räder, K. Müllen, *Macromolecules* **2009**, *42*, 6878.
- [52] D. Lorbach, M. Wagner, M. Baumgarten, K. Müllen, *Chem. Commun.* **2013**, *49*, 10578.
- [53] Y. Avlasevich, C. Kohl, K. Müllen, *J. Mater. Chem. C* **2006**, *16*, 1053.
- [54] a) D. E. Ames, A. Opalko, *Synthesis* **1983**, 234; b) D. E. Ames, A. Opalko, *Tetrahedron* **1984**, *40*, 1919; c) D. E. Ames, D. Bull, *Tetrahedron* **1982**, *38*, 383.
- [55] a) L.-C. Campeau, M. Parisien, M. Leblanc, K. Fagnou, *J. Am. Chem. Soc.* **2004**, *126*, 9186; b) M. Lafrance, D. Lapointe, K. Fagnou, *Tetrahedron* **2008**, *64*, 6015; c) L.-C. Campeau, M. Parisien, A. Jean, K. Fagnou, *J. Am. Chem. Soc.* **2006**, *128*, 581; d) S. I. Gorelsky, D. Lapointe, K. Fagnou, *J. Org. Chem.* **2012**, *77*, 658.
- [56] a) P. de Mendoza, A. M. Echavarren, in *Modern Arylation Methods*, Wiley-VCH, **2009**, pp. 363; b) D. García-Cuadrado, P. de Mendoza, A. A. C. Braga, F. Maseras, A.

- M. Echavarren, *J. Am. Chem. Soc.* **2007**, *129*, 6880; c) B. Gómez-Lor, E. González-Cantalapiedra, M. Ruiz, Ó. de Frutos, D. J. Cárdenas, A. Santos, A. M. Echavarren, *Chem. – Eur. J.* **2004**, *10*, 2601; d) S. Pascual, P. de Mendoza, A. A. C. Braga, F. Maseras, A. M. Echavarren, *Tetrahedron* **2008**, *64*, 6021; e) D. García-Cuadrado, A. A. C. Braga, F. Maseras, A. M. Echavarren, *J. Am. Chem. Soc.* **2006**, *128*, 1066.
- [57] a) J. E. Rice, Z.-W. Cai, *J. Org. Chem.* **1993**, *58*, 1415; b) J. E. Rice, Z.-W. Cai, *Tetrahedron Lett.* **1992**, *33*, 1675; c) J. E. Rice, Z.-W. Cai, Z.-M. He, E. J. LaVoie, *J. Org. Chem.* **1995**, *60*, 8101.
- [58] a) A. M. Echavarren, B. Gómez-Lor, J. J. González, Ó. de Frutos, *Synlett* **2003**, *2003*, 0585; b) E. A. Jackson, B. D. Steinberg, M. Bancu, A. Wakamiya, L. T. Scott, *J. Am. Chem. Soc.* **2007**, *129*, 484; c) H. A. Reisch, M. S. Bratcher, L. T. Scott, *Org. Lett.* **2000**, *2*, 1427; d) L. Wang, P. B. Shevlin, *Org. Lett.* **2000**, *2*, 3703; e) N.-h. Chang, X.-c. Chen, H. Nonobe, Y. Okuda, H. Mori, K. Nakajima, Y. Nishihara, *Org. Lett.* **2013**, *15*, 3558; f) N.-h. Chang, H. Mori, X.-c. Chen, Y. Okuda, T. Okamoto, Y. Nishihara, *Chem. Lett.* **2013**, *42*, 1257; g) K. Kamikawa, I. Takemoto, S. Takemoto, H. Matsuzaka, *J. Org. Chem.* **2007**, *72*, 7406; h) M. A. Campo, Q. Huang, T. Yao, Q. Tian, R. C. Larock, *J. Am. Chem. Soc.* **2003**, *125*, 11506.
- [59] a) H. A. Wegner, H. Reisch, K. Rauch, A. Demeter, K. A. Zachariasse, A. de Meijere, L. T. Scott, *J. Org. Chem.* **2006**, *71*, 9080; b) H. A. Wegner, L. T. Scott, A. de Meijere, *J. Org. Chem.* **2003**, *68*, 883.
- [60] J. M. Quimby, L. T. Scott, *Adv. Synth. Catal.* **2009**, *351*, 1009.
- [61] M. Shimizu, T. Hiyama, *Eur. J. Org. Chem.* **2013**, *2013*, 8069.
- [62] Z.-h. Zhou, T. Yamamoto, *J. Organomet. Chem.* **1991**, *414*, 119.
- [63] E. C. Rüdiger, M. Porz, M. Schaffroth, F. Rominger, U. H. F. Bunz, *Chem. – Eur. J.* **2014**, *20*, 12725.
- [64] a) A. Jančařík, J. Rybáček, K. Cocq, J. Vacek Chocholoušová, J. Vacek, R. Pohl, L. Bednářová, P. Fiedler, I. Císařová, I. G. Stará, I. Starý, *Angew. Chem. Int. Ed.* **2013**, *52*, 9970; b) F. Teplý, I. G. Stará, I. Starý, A. Kollárovič, D. Šaman, L. Rulišek, P. Fiedler, *J. Am. Chem. Soc.* **2002**, *124*, 9175.
- [65] a) Y.-T. Wu, A. Linden, J. S. Siegel, *Org. Lett.* **2005**, *7*, 4353; b) Y.-T. Wu, T. Hayama, K. K. Baldridge, A. Linden, J. S. Siegel, *J. Am. Chem. Soc.* **2006**, *128*, 6870.
- [66] a) D. Wu, H. Ge, S. H. Liu, J. Yin, *RSC Advances* **2013**, *3*, 22727; b) D. Pérez, D. Peña, E. Guitián, *Eur. J. Org. Chem.* **2013**, *2013*, 5981; c) E. Yoshikawa, K. V. Radhakrishnan, Y. Yamamoto, *J. Am. Chem. Soc.* **2000**, *122*, 7280; d) E. Yoshikawa,

- Y. Yamamoto, *Angew. Chem. Int. Ed.* **2000**, *39*, 173; e) D. Peña, S. Escudero, D. Pérez, E. Guitián, L. Castedo, *Angew. Chem. Int. Ed.* **1998**, *37*, 2659.
- [67] B. Schuler, S. Collazos, L. Gross, G. Meyer, D. Pérez, E. Guitián, D. Peña, *Angew. Chem. Int. Ed.* **2014**, *53*, 9004.
- [68] Y.-H. Kung, Y.-S. Cheng, C.-C. Tai, W.-S. Liu, C.-C. Shin, C.-C. Ma, Y.-C. Tsai, T.-C. Wu, M.-Y. Kuo, Y.-T. Wu, *Chem. – Eur. J.* **2010**, *16*, 5909.
- [69] L. Kaplan, S. P. Walch, K. E. Wilzbach, *J. Am. Chem. Soc.* **1968**, *90*, 5646.
- [70] A. H. A. Tinnemans, W. H. Laarhoven, *Tetrahedron Lett.* **1973**, *14*, 817.
- [71] a) A. H. A. Tinnemans, W. H. Laarhoven, *J. Chem. Soc., Perkin Trans. 2* **1976**, 1115; b) A. H. A. Tinnemans, W. H. Laarhoven, *J. Chem. Soc., Perkin Trans. 2* **1976**, 1111.
- [72] a) F. B. Mallory, C. S. Wood, J. T. Gordon, *J. Am. Chem. Soc.* **1964**, *86*, 3094; b) K. B. Jørgensen, *Molecules* **2010**, *15*, 4334.
- [73] a) T.-A. Chen, T.-J. Lee, M.-Y. Lin, S. M. A. Sohel, E. W.-G. Diao, S.-F. Lush, R.-S. Liu, *Chem. – Eur. J.* **2010**, *16*, 1826; b) T.-A. Chen, R.-S. Liu, *Chem. – Eur. J.* **2011**, *17*, 8023.
- [74] T. Yao, M. A. Campo, R. C. Larock, *Org. Lett.* **2004**, *6*, 2677.
- [75] T.-A. Chen, R.-S. Liu, *Org. Lett.* **2011**, *13*, 4644.
- [76] R. Grigg, P. Kennewell, A. Teasdale, V. Sridharan, *Tetrahedron Lett.* **1993**, *34*, 153.
- [77] a) H. Dang, M. A. Garcia-Garibay, *J. Am. Chem. Soc.* **2001**, *123*, 355; b) H. Dang, M. Levitus, M. A. Garcia-Garibay, *J. Am. Chem. Soc.* **2002**, *124*, 136.
- [78] C. Lütke Eversloh, Y. Avlasevich, C. Li, K. Müllen, *Chem. – Eur. J.* **2011**, *17*, 12756.
- [79] a) Z. U. Levi, T. D. Tilley, *J. Am. Chem. Soc.* **2009**, *131*, 2796; b) T. Kawase, T. Fujiwara, C. Kitamura, A. Konishi, Y. Hirao, K. Matsumoto, H. Kurata, T. Kubo, S. Shinamura, H. Mori, E. Miyazaki, K. Takimiya, *Angew. Chem. Int. Ed.* **2010**, *49*, 7728; c) T. Kawase, A. Konishi, Y. Hirao, K. Matsumoto, H. Kurata, T. Kubo, *Chem. – Eur. J.* **2009**, *15*, 2653.
- [80] T.-C. Wu, C.-H. Chen, D. Hibi, A. Shimizu, Y. Tobe, Y.-T. Wu, *Angew. Chem. Int. Ed.* **2010**, *49*, 7059.
- [81] T. Maekawa, Y. Segawa, K. Itami, *Chem. Sci.* **2013**, *4*, 2369.
- [82] J. Zhao, K. Oniwa, N. Asao, Y. Yamamoto, T. Jin, *J. Am. Chem. Soc.* **2013**, *135*, 10222.
- [83] a) S.-L. Suraru, F. Würthner, *Angew. Chem. Int. Ed.* **2014**, *53*, 7428; b) W. Jiang, Y. Li, Z. Wang, *Acc. Chem. Res.* **2014**, *47*, 3135.

- [84] F. Röhrscheid, in *Ullmann's Encyclopedia of Industrial Chemistry*, Wiley-VCH, **2000**.
- [85] a) F. Würthner, *Chem. Commun.* **2004**, 1564; b) M. A. Kobaisi, S. V. Bhosale, K. Latham, A. M. Raynor, S. V. Bhosale, *Chem. Rev.* **2016**, *116*, 11685.
- [86] F. Würthner, C. R. Saha-Möller, B. Fimmel, S. Ogi, P. Leowanawat, D. Schmidt, *Chem. Rev.* **2016**, *116*, 962.
- [87] L. Chen, C. Li, K. Müllen, *J. Mater. Chem. C* **2014**, *2*, 1938.
- [88] T. Weil, T. Vosch, J. Hofkens, K. Peneva, K. Müllen, *Angew. Chem. Int. Ed.* **2010**, *49*, 9068.
- [89] W. Herbst, K. Hunger, *Industrial Organic Pigments*, 2 ed., Wiley-VCH, Weinheim, **1997**.
- [90] Y. Fukutomi, M. Nakano, J.-Y. Hu, I. Osaka, K. Takimiya, *J. Am. Chem. Soc.* **2013**, *135*, 11445.
- [91] J. Gao, Y. Li, Z. Wang, *Org. Lett.* **2013**, *15*, 1366.
- [92] a) S.-L. Suraru, U. Zschieschang, H. Klauk, F. Würthner, *Chem. Commun.* **2011**, *47*, 11504; b) S.-L. Suraru, C. Burschka, F. Würthner, *J. Org. Chem.* **2014**, *79*, 128.
- [93] a) W. Yue, J. Gao, Y. Li, W. Jiang, S. Di Motta, F. Negri, Z. Wang, *J. Am. Chem. Soc.* **2011**, *133*, 18054; b) Q. Ye, J. Chang, K.-W. Huang, C. Chi, *Org. Lett.* **2011**, *13*, 5960.
- [94] a) H. Langhals, G. Schönmann, K. Polborn, *Chem. – Eur. J.* **2008**, *14*, 5290; b) T. Suzuki, T. Okamoto, A. Saeki, S. Seki, H. Sato, Y. Matsuo, *ACS Appl. Mater. Interfaces* **2013**, *5*, 1937; c) T. Okamoto, T. Suzuki, H. Tanaka, D. Hashizume, Y. Matsuo, *Chem. – Asian J.* **2012**, *7*, 105.
- [95] a) S. Katsuta, K. Tanaka, Y. Maruya, S. Mori, S. Masuo, T. Okujima, H. Uno, K.-i. Nakayama, H. Yamada, *Chem. Commun.* **2011**, *47*, 10112; b) A. R. Mohebbi, C. Munoz, F. Wudl, *Org. Lett.* **2011**, *13*, 2560.
- [96] a) U. Rohr, P. Schlichting, A. Böhm, M. Gross, K. Meerholz, C. Bräuchle, K. Müllen, *Angew. Chem. Int. Ed.* **1998**, *37*, 1434; b) A. Böhm, H. Arms, G. Henning, P. Blaschka, **1997**, DE19547210.
- [97] U. Rohr, C. Kohl, K. Müllen, A. van de Craats, J. Warman, *J. Mater. Chem. C* **2001**, *11*, 1789.
- [98] Q. Yan, K. Cai, C. Zhang, D. Zhao, *Org. Lett.* **2012**, *14*, 4654.
- [99] C. Zhang, K. Shi, K. Cai, J. Xie, T. Lei, Q. Yan, J.-Y. Wang, J. Pei, D. Zhao, *Chem. Commun.* **2015**, *51*, 7144.

- [100] a) S. Müller, K. Müllen, *Chem. Commun.* **2005**, 4045; b) Y. Avlasevich, S. Müller, P. Erk, K. Müllen, *Chem. – Eur. J.* **2007**, *13*, 6555.
- [101] C. Lütke Eversloh, C. Li, K. Müllen, *Org. Lett.* **2011**, *13*, 4148.
- [102] W. Jiang, Y. Li, W. Yue, Y. Zhen, J. Qu, Z. Wang, *Org. Lett.* **2010**, *12*, 228.
- [103] H. Usta, C. Newman, Z. Chen, A. Facchetti, *Adv. Mater.* **2012**, *24*, 3678.
- [104] a) W. Zhou, F. Jin, X. Huang, X.-M. Duan, X. Zhan, *Macromolecules* **2012**, *45*, 7823; b) W. Zhou, Z.-G. Zhang, L. Ma, Y. Li, X. Zhan, *Sol. Energy Mater. Sol. Cells* **2013**, *112*, 13.
- [105] a) J. Kelber, M.-F. Achard, F. Durola, H. Bock, *Angew. Chem. Int. Ed.* **2012**, *51*, 5200; b) J. Vollbrecht, H. Bock, C. Wiebeler, S. Schumacher, H. Kitzerow, *Chem. – Eur. J.* **2014**, *20*, 12026; c) Y. Yang, Y. Wang, Y. Xie, T. Xiong, Z. Yuan, Y. Zhang, S. Qian, Y. Xiao, *Chem. Commun.* **2011**, *47*, 10749.
- [106] X. Zhan, J. Zhang, S. Tang, Y. Lin, M. Zhao, J. Yang, H.-L. Zhang, Q. Peng, G. Yu, Z. Li, *Chem. Commun.* **2015**, *51*, 7156.
- [107] a) Z. Lin, C. Li, D. Meng, Y. Li, Z. Wang, *Chem. – Asian J.* **2016**, *11*, 2695; b) Y. Li, L. Xu, T. Liu, Y. Yu, H. Liu, Y. Li, D. Zhu, *Org. Lett.* **2011**, *13*, 5692.
- [108] a) Z. Zhao, Y. Zhang, Y. Xiao, *J. Org. Chem.* **2013**, *78*, 5544; b) A. H. Endres, M. Schaffroth, F. Paulus, H. Reiss, H. Wadepohl, F. Rominger, R. Krämer, U. H. F. Bunz, *J. Am. Chem. Soc.* **2016**, *138*, 1792.
- [109] Z. Zhang, T. Lei, Q. Yan, J. Pei, D. Zhao, *Chem. Commun.* **2013**, *49*, 2882.
- [110] Y. Xie, X. Zhang, Y. Xiao, Y. Zhang, F. Zhou, J. Qi, J. Qu, *Chem. Commun.* **2012**, *48*, 4338.
- [111] Y. Li, C. Wang, C. Li, S. Di Motta, F. Negri, Z. Wang, *Org. Lett.* **2012**, *14*, 5278.
- [112] Y. Zhong, M. T. Trinh, R. Chen, W. Wang, P. P. Khlyabich, B. Kumar, Q. Xu, C.-Y. Nam, M. Y. Sfeir, C. Black, M. L. Steigerwald, Y.-L. Loo, S. Xiao, F. Ng, X. Y. Zhu, C. Nuckolls, *J. Am. Chem. Soc.* **2014**, *136*, 15215.
- [113] Y. Zhen, W. Yue, Y. Li, W. Jiang, S. Di Motta, E. Di Donato, F. Negri, S. Ye, Z. Wang, *Chem. Commun.* **2010**, *46*, 6078.
- [114] a) S. Alibert-Fouet, I. Seguy, J.-F. Bobo, P. Destruel, H. Bock, *Chem. – Eur. J.* **2007**, *13*, 1746; b) H. Langhals, B. Böck, T. Schmid, A. Marchuk, *Chem. – Eur. J.* **2012**, *18*, 13188.
- [115] a) J. H. Yao, C. Chi, J. Wu, K.-P. Loh, *Chem. – Eur. J.* **2009**, *15*, 9299; b) D. Désilets, P. M. Kazmaier, R. A. Burt, G. K. Hamer, *Can. J. Chem.* **1995**, *73*, 325.

- [116] Chaolumen, H. Enno, M. Murata, A. Wakamiya, Y. Murata, *Chem. – Asian J.* **2014**, *9*, 3136.
- [117] a) Q. Bai, B. Gao, Q. Ai, Y. Wu, X. Ba, *Org. Lett.* **2011**, *13*, 6484; b) Y. Li, W. Xu, S. D. Motta, F. Negri, D. Zhu, Z. Wang, *Chem. Commun.* **2012**, *48*, 8204.
- [118] C. Lütke Eversloh, Z. Liu, B. Müller, M. Stangl, C. Li, K. Müllen, *Org. Lett.* **2011**, *13*, 5528.
- [119] H. Langhals, S. Poxleitner, *Eur. J. Org. Chem.* **2008**, *2008*, 797.
- [120] Y. Avlasevich, K. Müllen, *Chem. Commun.* **2006**, 4440.
- [121] Y. Avlasevich, C. Li, K. Müllen, *J. Mater. Chem. C* **2010**, *20*, 3814.
- [122] S. K. Lee, Y. Zu, A. Herrmann, Y. Geerts, K. Müllen, A. J. Bard, *J. Am. Chem. Soc.* **1999**, *121*, 3513.
- [123] a) Z. Yuan, S.-L. Lee, L. Chen, C. Li, K. S. Mali, S. De Feyter, K. Müllen, *Chem. – Eur. J.* **2013**, *19*, 11842; b) X. Zhao, Y. Xiong, J. Ma, Z. Yuan, *J. Phys. Chem. A* **2016**, *120*, 7554.
- [124] M. Adachi, Y. Nagao, *Chem. Mater.* **2001**, *13*, 662.
- [125] T. V. Pho, F. M. Toma, B. J. Tremolet de Villers, S. Wang, N. D. Treat, N. D. Eisenmenger, G. M. Su, R. C. Coffin, J. D. Douglas, J. M. J. Fréchet, G. C. Bazan, F. Wudl, M. L. Chabinyk, *Adv. Energy Mater.* **2014**, *4*, 1301007.
- [126] H. Zhylitskaya, J. Cybińska, P. Chmielewski, T. Lis, M. Stępień, *J. Am. Chem. Soc.* **2016**, *138*, 11390.
- [127] a) A. Sanguineti, M. Sassi, R. Turrisi, R. Ruffo, G. Vaccaro, F. Meinardi, L. Beverina, *Chem. Commun.* **2013**, *49*, 1618; b) P. de Echegaray, M. J. Mancheño, I. Arrechea-Marcos, R. Juárez, G. López-Espejo, J. T. López Navarrete, M. M. Ramos, C. Seoane, R. P. Ortiz, J. L. Segura, *J. Org. Chem.* **2016**, *81*, 11256.
- [128] R. Ponce Ortiz, H. Herrera, M. J. Mancheño, C. Seoane, J. L. Segura, P. Mayorga Burrezo, J. Casado, J. T. López Navarrete, A. Facchetti, T. J. Marks, *Chem. – Eur. J.* **2013**, *19*, 12458.
- [129] a) H. Herrera, P. de Echegaray, M. Urdanpilleta, M. J. Mancheno, E. Mena-Osteritz, P. Bäuerle, J. L. Segura, *Chem. Commun.* **2013**, *49*, 713; b) H. Li, F. S. Kim, G. Ren, E. C. Hollenbeck, S. Subramaniyan, S. A. Jenekhe, *Angew. Chem. Int. Ed.* **2013**, *52*, 5513.
- [130] D. Wu, H. Ge, Z. Chen, J. Liang, J. Huang, Y. Zhang, X. Chen, X. Meng, S. H. Liu, J. Yin, *Org. Biomol. Chem.* **2014**, *12*, 8902.
- [131] L. Duan, Y. Xu, X. Qian, Y. Zhang, Y. Liu, *Tetrahedron Lett.* **2009**, *50*, 22.

- [132] a) Z. Sun, K.-W. Huang, J. Wu, *Org. Lett.* **2010**, *12*, 4690; b) Z. Sun, K.-W. Huang, J. Wu, *J. Am. Chem. Soc.* **2011**, *133*, 11896; c) Z. Sun, J. Wu, *J. Org. Chem.* **2013**, *78*, 9032.
- [133] a) E. Clar, O. Kühn, *Liebigs Ann.* **1956**, *601*, 181; b) E. Clar, M. Zander, *J. Chem. Soc.* **1957**, 4616.
- [134] H. Langhals, S. Grundner, *Chem. Ber.* **1986**, *119*, 2373.
- [135] J. Li, J.-J. Chang, H. S. Tan, H. Jiang, X. Chen, Z. Chen, J. Zhang, J. Wu, *Chem. Sci.* **2012**, *3*, 846.
- [136] L. Shan, Z. Liang, X. Xu, Q. Tang, Q. Miao, *Chem. Sci.* **2013**, *4*, 3294.
- [137] L. Minuti, A. Taticchi, A. Marrocchi, E. Gacs-Baitz, *Tetrahedron* **1997**, *53*, 6873.
- [138] H. Sakai, T. Kubota, J. Yuasa, Y. Araki, T. Sakanoue, T. Takenobu, T. Wada, T. Kawai, T. Hasobe, *J. Phys. Chem. C* **2016**, *120*, 7860.
- [139] a) P. Sarkar, F. Durola, H. Bock, *Chem. Commun.* **2013**, *49*, 7552; b) H. Bock, D. Subervie, P. Mathey, A. Pradhan, P. Sarkar, P. Dechambenoit, E. A. Hillard, F. Durola, *Org. Lett.* **2014**, *16*, 1546; c) H. Bock, S. Huet, P. Dechambenoit, E. A. Hillard, F. Durola, *Eur. J. Org. Chem.* **2015**, *2015*, 1033; d) M. Ferreira, E. Giroto, A. Bentaleb, E. A. Hillard, H. Gallardo, F. Durola, H. Bock, *Chem. – Eur. J.* **2015**, *21*, 4391; e) R. Wang, K. Shi, K. Cai, Y. Guo, X. Yang, J.-Y. Wang, J. Pei, D. Zhao, *New J. Chem.* **2016**, *40*, 113.
- [140] Z. Wang, C. Kim, A. Facchetti, T. J. Marks, *J. Am. Chem. Soc.* **2007**, *129*, 13362.
- [141] a) J. Yin, H. Qu, K. Zhang, J. Luo, X. Zhang, C. Chi, J. Wu, *Org. Lett.* **2009**, *11*, 3028; b) D. Wu, H. Zhang, S. H. Liu, J. Yin, *Chem. – Asian J.* **2015**, *10*, 602.
- [142] H. Qu, W. Cui, J. Li, J. Shao, C. Chi, *Org. Lett.* **2011**, *13*, 924.
- [143] F. Ilhan, D. S. Tyson, M. A. Meador, *Org. Lett.* **2006**, *8*, 577.
- [144] a) Z. Zhao, F. Zhang, X. Zhang, X. Yang, H. Li, X. Gao, C.-a. Di, D. Zhu, *Macromolecules* **2013**, *46*, 7705; b) D. Zhao, Q. Wu, Z. Cai, T. Zheng, W. Chen, J. Lu, L. Yu, *Chem. Mater.* **2016**, *28*, 1139.
- [145] L. Zou, X.-Y. Wang, X.-X. Zhang, Y.-Z. Dai, Y.-D. Wu, J.-Y. Wang, J. Pei, *Chem. Commun.* **2015**, *51*, 12585.
- [146] a) T. Förster, K. Kasper, *Z. Elektrochem.* **1955**, *59*, 976; b) K. Kalyanasundaram, J. K. Thomas, *J. Am. Chem. Soc.* **1977**, *99*, 2039.
- [147] a) J. N. Moorthy, P. Natarajan, P. Venkatakrishnan, D.-F. Huang, T. J. Chow, *Org. Lett.* **2007**, *9*, 5215; b) J.-Y. Hu, X. Feng, H. Tomiyasu, N. Seto, U. Rayhan, M. R. J. Elsegood, C. Redshaw, T. Yamato, *J. Mol. Struct.* **2013**, *1047*, 194; c) Z.-Q. Liang,

- Y.-X. Li, J.-X. Yang, Y. Ren, X.-T. Tao, *Tetrahedron Lett.* **2011**, *52*, 1329; d) F. Liu, J.-h. Zou, Q.-y. He, C. Tang, L.-h. Xie, B. Peng, W. Wei, Y. Cao, W. Huang, *J. Polym. Sci., Part A: Polym. Chem.* **2010**, *48*, 4943; e) R. R. Reghu, J. V. Grazulevicius, J. Simokaitiene, A. Miasojedovas, K. Kazlauskas, S. Jursenas, P. Data, K. Karon, M. Lapkowski, V. Gaidelis, V. Jankauskas, *J. Phys. Chem. C* **2012**, *116*, 15878; f) P. Sonar, M. S. Soh, Y. H. Cheng, J. T. Henssler, A. Sellinger, *Org. Lett.* **2010**, *12*, 3292; g) Z. Zhao, S. Chen, J. W. Y. Lam, P. Lu, Y. Zhong, K. S. Wong, H. S. Kwok, B. Z. Tang, *Chem. Commun.* **2010**, *46*, 2221; h) C.-H. Yang, T.-F. Guo, I. W. Sun, *J. Lumin.* **2007**, *124*, 93; i) K. C. Wu, P. J. Ku, C. S. Lin, H. T. Shih, F. I. Wu, M. J. Huang, J. J. Lin, I. C. Chen, C. H. Cheng, *Adv. Funct. Mater.* **2008**, *18*, 67; j) K. Suzuki, A. Seno, H. Tanabe, K. Ueno, *Synth. Met.* **2004**, *143*, 89; k) S. L. Tao, Z. K. Peng, X. H. Zhang, P. F. Wang, C. S. Lee, S. T. Lee, *Adv. Funct. Mater.* **2005**, *15*, 1716; l) S. Jiao, Y. Liao, X. Xu, L. Wang, G. Yu, L. Wang, Z. Su, S. Ye, Y. Liu, *Adv. Funct. Mater.* **2008**, *18*, 2335; m) C. Tang, F. Liu, Y.-J. Xia, J. Lin, L.-H. Xie, G.-Y. Zhong, Q.-L. Fan, W. Huang, *Org. Electron.* **2006**, *7*, 155; n) C. He, Q. He, Q. Chen, L. Shi, H. Cao, J. Cheng, C. Deng, T. Lin, *Tetrahedron Lett.* **2010**, *51*, 1317.
- [148] a) G. Venkataramana, P. Dongare, L. N. Dawe, D. W. Thompson, Y. Zhao, G. J. Bodwell, *Org. Lett.* **2011**, *13*, 2240; b) S. Diring, F. Camerel, B. Donnio, T. Dintzer, S. Toffanin, R. Capelli, M. Muccini, R. Ziessel, *J. Am. Chem. Soc.* **2009**, *131*, 18177; c) H. Maeda, T. Maeda, K. Mizuno, K. Fujimoto, H. Shimizu, M. Inouye, *Chem. – Eur. J.* **2006**, *12*, 824; d) Z. Wang, C. Xu, W. Wang, W. Fu, L. Niu, B. Ji, *Solid-State Electron.* **2010**, *54*, 524.
- [149] T. M. Figueira-Duarte, S. C. Simon, M. Wagner, S. I. Druzhinin, K. A. Zachariasse, K. Müllen, *Angew. Chem. Int. Ed.* **2008**, *47*, 10175.
- [150] a) M. A. Zwijnenburg, G. Cheng, T. O. McDonald, K. E. Jelfs, J.-X. Jiang, S. Ren, T. Hasell, F. Blanc, A. I. Cooper, D. J. Adams, *Macromolecules* **2013**, *46*, 7696; b) T. M. Figueira-Duarte, P. G. Del Rosso, R. Trattnig, S. Sax, E. J. W. List, K. Müllen, *Adv. Mater.* **2010**, *22*, 990; c) D. Lorbach, A. Keerthi, T. M. Figueira-Duarte, M. Baumgarten, M. Wagner, K. Müllen, *Angew. Chem. Int. Ed.* **2016**, *55*, 418.
- [151] D. N. Coventry, A. S. Batsanov, A. E. Goeta, J. A. K. Howard, T. B. Marder, R. N. Perutz, *Chem. Commun.* **2005**, 2172.
- [152] a) A. G. Crawford, A. D. Dwyer, Z. Liu, A. Steffen, A. Beeby, L.-O. Pålsson, D. J. Tozer, T. B. Marder, *J. Am. Chem. Soc.* **2011**, *133*, 13349; b) A. G. Crawford, Z. Liu, I. A. I. Mkhallid, M.-H. Thibault, N. Schwarz, G. Alcaraz, A. Steffen, J. C. Collings,

- A. S. Batsanov, J. A. K. Howard, T. B. Marder, *Chem. – Eur. J.* **2012**, *18*, 5022; c) Y. Qiao, J. Zhang, W. Xu, D. Zhu, *Tetrahedron* **2011**, *67*, 3395.
- [153] a) H. Lee, R. G. Harvey, *J. Org. Chem.* **1986**, *51*, 2847; b) D. Rausch, C. Lambert, *Org. Lett.* **2006**, *8*, 5037.
- [154] a) V. V. Filichev, I. V. Astakhova, A. D. Malakhov, V. A. Korshun, E. B. Pedersen, *Chem. – Eur. J.* **2008**, *14*, 9968; b) J. Lee, J. Park, *Org. Lett.* **2015**, *17*, 3960; c) R. Pratap, Y. Tominaga, M. L. Lee, R. N. Castle, *J. Heterocycl. Chem.* **1981**, *18*, 973.
- [155] a) L. Meng, T. Fujikawa, M. Kuwayama, Y. Segawa, K. Itami, *J. Am. Chem. Soc.* **2016**, *138*, 10351; b) W. Han, J. Tran, H. Zhang, S. Jeffrey, D. Swartling, G. P. Ford, E. Biehl, *Synthesis* **1995**, *1995*, 827.
- [156] J. Hu, D. Zhang, F. W. Harris, *J. Org. Chem.* **2005**, *70*, 707.
- [157] T. Yamato, M. Fujimoto, A. Miyazawa, K. Matsuo, *J. Chem. Soc., Perkin Trans. 1* **1997**, 1201.
- [158] J.-Y. Hu, X. Feng, N. Seto, J.-H. Do, X. Zeng, Z. Tao, T. Yamato, *J. Mol. Struct.* **2013**, *1035*, 19.
- [159] a) W. Sun, W. Li, J. Li, J. Zhang, L. Du, M. Li, *Tetrahedron* **2012**, *68*, 5363; b) G.-F. Zhang, H. Wang, M. P. Aldred, T. Chen, Z.-Q. Chen, X. Meng, M.-Q. Zhu, *Chem. Mater.* **2014**, *26*, 4433.
- [160] S. Seifert, K. Shoyama, D. Schmidt, F. Würthner, *Angew. Chem. Int. Ed.* **2016**, *55*, 6390.
- [161] Z. Liu, Y. Wang, Y. Chen, J. Liu, Q. Fang, C. Kleeberg, T. B. Marder, *J. Org. Chem.* **2012**, *77*, 7124.
- [162] a) S.-i. Kawano, C. Yang, M. Ribas, S. Balushev, M. Baumgarten, K. Müllen, *Macromolecules* **2008**, *41*, 7933; b) L. Zöphel, V. Enkelmann, R. Rieger, K. Müllen, *Org. Lett.* **2011**, *13*, 4506.
- [163] T. Weil, E. Reuther, K. Müllen, *Angew. Chem. Int. Ed.* **2002**, *41*, 1900.
- [164] J. R. Lakowicz, *Principles of Fluorescence Spectroscopy*, Kluwer Academic/Plenum, New York, **1999**.
- [165] C. Würth, M. Grabolle, J. Pauli, M. Spieles, U. Resch-Genger, *Nat. Protoc.* **2013**, *8*, 1535.
- [166] F. Liu, W.-Y. Lai, C. Tang, H.-B. Wu, Q.-Q. Chen, B. Peng, W. Wei, W. Huang, Y. Cao, *Macromol. Rapid Commun.* **2008**, *29*, 659.
- [167] a) W. Rettig, *Angew. Chem. Int. Ed.* **1986**, *25*, 971; b) W. Rettig, *Appl. Phys. B* **1988**, *45*, 145.

- [168] P. Emele, D. U. Meyer, N. Holl, H. Port, H. C. Wolf, F. Würthner, P. Bäuerle, F. Effenberger, *Chem. Phys.* **1994**, *181*, 417.
- [169] S. Seifert, D. Schmidt, F. Würthner, *Org. Chem. Front.* **2016**, *3*, 1435.
- [170] a) C. Wang, H. Dong, W. Hu, Y. Liu, D. Zhu, *Chem. Rev.* **2012**, *112*, 2208; b) J. Wu, *Curr. Org. Chem.* **2007**, *11*, 1220.
- [171] E. Clar, *Chem. Ber.* **1948**, *81*, 52.
- [172] F. Nolde, J. Qu, C. Kohl, N. G. Pschierer, E. Reuther, K. Müllen, *Chem. – Eur. J.* **2005**, *11*, 3959.
- [173] Y. Zhong, M. T. Trinh, R. Chen, G. E. Purdum, P. P. Khlyabich, M. Sezen, S. Oh, H. Zhu, B. Fowler, B. Zhang, W. Wang, C.-Y. Nam, M. Y. Sfeir, C. T. Black, M. L. Steigerwald, Y.-L. Loo, F. Ng, X. Y. Zhu, C. Nuckolls, *Nat. Commun.* **2015**, *6*.
- [174] Y. Avlasevich, K. Müllen, *J. Org. Chem.* **2007**, *72*, 10243.
- [175] T. Ishiyama, M. Murata, N. Miyaura, *J. Org. Chem.* **1995**, *60*, 7508.
- [176] H. Wonneberger, H. Reichelt, Y. Zagranjarski, C. Li, K. Müllen, L. Chen, **2014**, WO2014033620A2.
- [177] T. E. Barder, S. D. Walker, J. R. Martinelli, S. L. Buchwald, *J. Am. Chem. Soc.* **2005**, *127*, 4685.
- [178] a) E. J. Hennessy, S. L. Buchwald, *J. Am. Chem. Soc.* **2003**, *125*, 12084; b) C. Colletto, S. Islam, F. Juliá-Hernández, I. Larrosa, *J. Am. Chem. Soc.* **2016**, *138*, 1677.
- [179] a) A. Konishi, Y. Hirao, K. Matsumoto, H. Kurata, R. Kishi, Y. Shigeta, M. Nakano, K. Tokunaga, K. Kamada, T. Kubo, *J. Am. Chem. Soc.* **2013**, *135*, 1430; b) A. Konishi, Y. Hirao, M. Nakano, A. Shimizu, E. Botek, B. Champagne, D. Shiomi, K. Sato, T. Takui, K. Matsumoto, H. Kurata, T. Kubo, *J. Am. Chem. Soc.* **2010**, *132*, 11021.
- [180] E. Clar, *The Aromatic Sextet*, Wiley, London, **1972**.
- [181] Y.-Z. Tan, B. Yang, K. Parvez, A. Narita, S. Osella, D. Beljonne, X. Feng, K. Müllen, *Nat. Commun.* **2013**, *4*.
- [182] Q. Zhang, H. Peng, G. Zhang, Q. Lu, J. Chang, Y. Dong, X. Shi, J. Wei, *J. Am. Chem. Soc.* **2014**, *136*, 5057.
- [183] A. Matsumoto, M. Suzuki, D. Kuzuhara, H. Hayashi, N. Aratani, H. Yamada, *Angew. Chem. Int. Ed.* **2015**, *54*, 8175.
- [184] K. Kawasumi, Q. Zhang, Y. Segawa, L. T. Scott, K. Itami, *Nat. Chem.* **2013**, *5*, 739.
- [185] J. Cremer, E. Mena-Osteritz, N. G. Pschierer, K. Müllen, P. Bäuerle, *Org. Biomol. Chem.* **2005**, *3*, 985.

- [186] F. O. Holtrup, G. R. J. Müller, H. Quante, S. De Feyter, F. C. De Schryver, K. Müllen, *Chem. – Eur. J.* **1997**, *3*, 219.
- [187] C.-C. You, R. Dobrawa, C. R. Saha-Möller, F. Würthner, in *Supramolecular Dye Chemistry*, Springer, Berlin, Heidelberg, **2005**, pp. 39.
- [188] I. Seguy, P. Jolinat, P. Destruel, R. Mamy, H. Allouchi, C. Courseille, M. Cotrait, H. Bock, *ChemPhysChem* **2001**, *2*, 448.
- [189] Y. He, Y. Li, *Phys. Chem. Chem. Phys.* **2011**, *13*, 1970.
- [190] S. Seifert, D. Schmidt, K. Shoyama, F. Würthner, *Angew. Chem. Int. Ed.* **2017**, *56*, 7595.
- [191] Y. Segawa, T. Maekawa, K. Itami, *Angew. Chem. Int. Ed.* **2015**, *54*, 66.
- [192] a) T. L. Andrew, B. VanVeller, T. M. Swager, *Synlett* **2010**, 3045; b) Y. Nagao, E. Shimokoshi, K. Kozawa, *Heterocycles* **2004**, *62*, 821; c) Y. Nagao, T. Yoshida, K. Arimitsu, K. Kozawa, *Heterocycles* **2010**, *80*, 1197.
- [193] a) S. Toyota, K. Kaneko, M. Kurokawa, K. Wakamatsu, *Tetrahedron Lett.* **2006**, *47*, 7349; b) X. Huang, L. Zeng, Z. Zeng, J. Wu, *Chem. – Eur. J.* **2011**, *17*, 14907.
- [194] H.-G. Franck, H. Buffleb, *Liebigs Ann.* **1967**, *701*, 53.
- [195] Y.-H. Lai, P. Chen, Y. X. Cui, *J. Chem. Soc., Perkin Trans. 2* **1996**, 1655.
- [196] a) M. Orchin, L. Reggel, *J. Am. Chem. Soc.* **1947**, *69*, 505; b) M. Orchin, L. Reggel, *J. Am. Chem. Soc.* **1951**, *73*, 436.
- [197] C. Koper, M. Sarobe, L. W. Jenneskens, *Phys. Chem. Chem. Phys.* **2004**, *6*, 319.
- [198] S. Seifert, D. Schmidt, F. Würthner, *Chem. Sci.* **2015**, *6*, 1663.
- [199] S. Seifert, Master Thesis, Julius-Maximilians-Universität Würzburg, **2013**.
- [200] C. Li, H. Wonneberger, *Adv. Mater.* **2012**, *24*, 613.
- [201] M. P. Schmidt, W. Neugebauer, **1929**, US1715430A.
- [202] E. D. Głowacki, G. Voss, N. S. Sariciftci, *Adv. Mater.* **2013**, *25*, 6783.
- [203] a) B. A. Jones, A. Facchetti, M. R. Wasielewski, T. J. Marks, *J. Am. Chem. Soc.* **2007**, *129*, 15259; b) R. Schmidt, J. H. Oh, Y. S. Sun, M. Deppisch, A. M. Krause, K. Radacki, H. Braunschweig, M. Könemann, P. Erk, Z. A. Bao, F. Würthner, *J. Am. Chem. Soc.* **2009**, *131*, 6215.
- [204] X. Zhan, Z. a. Tan, B. Domercq, Z. An, X. Zhang, S. Barlow, Y. Li, D. Zhu, B. Kippelen, S. R. Marder, *J. Am. Chem. Soc.* **2007**, *129*, 7246.
- [205] a) R. O. Marcon, S. Brochsztain, *Langmuir* **2007**, *23*, 11972; b) R. O. Marcon, S. Brochsztain, *J. Phys. Chem. A* **2009**, *113*, 1747; c) M. A. Iron, R. Cohen, B. Rybtchinski, *J. Phys. Chem. A* **2011**, *115*, 2047; d) E. Shirman, A. Ustinov, N. Ben-

- Shitrit, H. Weissman, M. A. Iron, R. Cohen, B. Rybtchinski, *J. Phys. Chem. B* **2008**, *112*, 8855; e) V. V. Roznyatovskiy, D. M. Gardner, S. W. Eaton, M. R. Wasielewski, *Org. Lett.* **2014**, *16*, 696.
- [206] a) J. Baram, E. Shirman, N. Ben-Shitrit, A. Ustinov, H. Weissman, I. Pinkas, S. G. Wolf, B. Rybtchinski, *J. Am. Chem. Soc.* **2008**, *130*, 14966; b) G. S. Vadehra, R. P. Maloney, M. A. Garcia-Garibay, B. Dunn, *Chem. Mater.* **2014**.
- [207] D. Schmidt, D. Bialas, F. Würthner, *Angew. Chem. Int. Ed.* **2015**, *54*, 3611.
- [208] M. Gsänger, J. H. Oh, M. Könemann, H. W. Höffken, A. M. Krause, Z. N. Bao, F. Würthner, *Angew. Chem. Int. Ed.* **2010**, *49*, 740.
- [209] G. Battagliarin, Y. Zhao, C. Li, K. Müllen, *Org. Lett.* **2011**, *13*, 3399.
- [210] J. Gao, C. Xiao, W. Jiang, Z. Wang, *Org. Lett.* **2014**, *16*, 394.
- [211] A. Ramanathan, L. S. Jimenez, *Synthesis* **2010**, *2010*, 217.
- [212] a) Z. Chen, M. G. Debije, T. Debaerdemaeker, P. Osswald, F. Würthner, *ChemPhysChem* **2004**, *5*, 137; b) F. Würthner, P. Osswald, R. Schmidt, T. E. Kaiser, H. Mansikkamäki, M. Könemann, *Org. Lett.* **2006**, *8*, 3765.
- [213] S. Hünig, H. Balli, H. Conrad, A. Schott, *Liebigs Ann.* **1964**, *676*, 52.
- [214] a) L. Michaelis, *Chem. Rev.* **1935**, *16*, 243; b) L. Michaelis, M. P. Schubert, *Chem. Rev.* **1938**, *22*, 437.
- [215] a) H. Zollinger, *Color Chemistry: Syntheses, Properties, and Applications of Organic Dyes and Pigments*, 3rd ed., Wiley-VCH, Weinheim, **2003**; b) H. Moustroph, *Dyes, General Survey in Ullmann's Encyclopedia of Industrial Chemistry*, 7th ed., Wiley-VCH, Weinheim, **2014**.
- [216] H. Marom, Y. Popowski, S. Antonov, M. Gozin, *Org. Lett.* **2011**, *13*, 5532.
- [217] W. Gottardi, *Monatsh. Chem.* **1967**, *98*, 507.
- [218] G. Seybold, G. Wagenblast, *Dyes Pigm.* **1989**, *11*, 303.
- [219] Gaussian 09, Revision D.01, G. W. T. M. J. Frisch, H. B. Schlegel, G. E. Scuseria, M. A. Robb, J. R. Cheeseman, G. Scalmani, V. Barone, B. Mennucci, G. A. Petersson, H. Nakatsuji, M. Caricato, X. Li, H. P. Hratchian, A. F. Izmaylov, J. Bloino, G. Zheng, J. L. Sonnenberg, M. Hada, M. Ehara, K. Toyota, R. Fukuda, J. Hasegawa, M. Ishida, T. Nakajima, Y. Honda, O. Kitao, H. Nakai, T. Vreven, J. A. Montgomery, Jr., J. E. Peralta, F. Ogliaro, M. Bearpark, J. J. Heyd, E. Brothers, K. N. Kudin, V. N. Staroverov, R. Kobayashi, J. Normand, K. Raghavachari, A. Rendell, J. C. Burant, S. S. Iyengar, J. Tomasi, M. Cossi, N. Rega, J. M. Millam, M. Klene, J. E. Knox, J. B. Cross, V. Bakken, C. Adamo, J. Jaramillo, R. Gomperts, R. E. Stratmann, O. Yazyev,

- A. J. Austin, R. Cammi, C. Pomelli, J. W. Ochterski, R. L. Martin, K. Morokuma, V. G. Zakrzewski, G. A. Voth, P. Salvador, J. J. Dannenberg, S. Dapprich, A. D. Daniels, Ö. Farkas, J. B. Foresman, J. V. Ortiz, J. Cioslowski, D. J. Fox, Gaussian, Inc., Wallingford, CT, **2009**.
- [220] a) A. D. Becke, *Phys. Rev. A* **1988**, *38*, 3098; b) A. D. Becke, *J. Chem. Phys.* **1993**, *98*, 5648; c) C. Lee, W. Yang, R. G. Parr, *Phys. Rev. B* **1988**, *37*, 785.
- [221] F. Weigend, R. Ahlrichs, *Phys. Chem. Chem. Phys.* **2005**, *7*, 3297.
- [222] E. A. Cobar, R. Z. Khaliullin, R. G. Bergman, M. Head-Gordon, *PNAS* **2007**, *104*, 6963.
- [223] GaussView, Version 5, R. Dennington, T. Keith, J. Millam, Semichem. Inc., Shawnee Mission, KS, **2009**.
- [224] G. M. Sheldrick, *Acta Crystallogr., Sect. A* **2008**, *64*.
- [225] H. G. Nam, D. W. Lim, J. Y. Kim, S. M. Park, S. H. Jang, S. Y. Lee, J. S. Ham, K. O. Cho, H. D. Kim, **2013**, WO2013180376A1.
- [226] X. Wang, L. Feng, L. Zhang, *Dyes Pigm.* **2013**, *97*, 318.
- [227] R. S. Sprick, J.-X. Jiang, B. Bonillo, S. Ren, T. Ratvijitvech, P. Guiglion, M. A. Zwijnenburg, D. J. Adams, A. I. Cooper, *J. Am. Chem. Soc.* **2015**, *137*, 3265.
- [228] L. Wang, J. Li, X. Cui, Y. Wu, Z. Zhu, Y. Wu, *Adv. Synth. Catal.* **2010**, *352*, 2002.
- [229] W. Yao, H. Fang, S. Peng, H. Wen, L. Zhang, A. Hu, Z. Huang, *Organometallics* **2016**, *35*, 1559.
- [230] A. Spek, *Acta Crystallogr., Sect. A* **1990**, *46*, c34.

Danksagung

An dieser Stelle möchte ich mich bei allen Personen bedanken, die mich während meiner Doktorarbeit in den letzten Jahren unterstützt haben.

Mein besonderer Dank gilt Herrn Prof. Dr. Frank Würthner für die Möglichkeit, ein sehr interessantes Forschungsthema zu bearbeiten und seine Unterstützung sowie das entgegengebrachte Vertrauen während der letzten Jahre. Außerdem bedanke ich mich bei ihm für wertvolle Diskussionen und die erstklassige bereitgestellte Ausstattung, die es mir ermöglichten, mich fachlich weiterzuentwickeln.

Prof. Dr. Christoph Lambert und Herrn Michael Moos danke ich für die die Möglichkeit der Durchführung der Spektroelektrochemie und die dafür bereitgestellten Geräte.

Des Weiteren möchte ich mich bei allen Mitarbeitern der Institute für Organische und Anorganische Chemie für die Bereitstellung und Durchführung analytischer Methoden bedanken. Für die Durchführung der Elementaranalysen danke ich Frau Timmroth und Frau Michels. Für die Messung von NMR-Spektren danke ich Herrn Dr. Matthias Grüne, Frau Juliane Adelman sowie Frau Patricia Altenberger. Weiterhin danke ich Herrn Dr. Michael Büchner, Herrn Fritz Dadrich, Frau Antje Heckmann und Frau Juliane Adelman für die Aufnahme der Massenspektren.

Einen besonderen Dank für die Unterstützung möchte ich auch einigen Mitarbeitern des Arbeitskreises aussprechen. Für die Messung und Lösung der Einkristallstrukturen danke ich Dr. David Schmidt und Ana-Maria Krause. Danke auch an Herrn Dr. David Bialas, Herrn Dr. Vincenzo Grande und Herrn Dr. Kazutaka Shoyama für die Durchführung und Diskussion von DFT-Rechnungen. Für die Unterstützung bei der Erstellung von Manuskripten und ausgiebige fachliche Diskussionen gilt mein besonderer Dank Herrn Dr. Chantu Saha-Möller und Herrn Dr. David Schmidt. Für die Unterstützung bei synthetischen Arbeiten möchte ich mich bei Joachim Bialas, Johannes Thein, Christian Simon, Petra Seufert-Baumbach und Anja Hofmann bedanken. Außerdem bedanke ich mich bei meinem Auszubildenden Yannik Reuß, meinen Praktikanten Raphael Wirthensohn, David Mims und meinen Bachelorstudenten Christian Gentsch und Markus Ebert. Bei Christiana Toussaint, Joachim Bialas, Johannes Thein, Christian Simon und Jennifer Begall möchte ich mich für organisatorische Angelegenheiten bedanken. Ihr habt dazu beigetragen, dass unser Arbeitsalltag immer reibungslos weiterlaufen konnte.

Weiterhin Danke ich Dr. Chantu Saha-Möller, Dr. David Schmidt, Christoph Kerpen, Eva Kirchner, Dr. Matthias Stolte und Christine Seifert für das Korrekturlesen der Arbeit.

Außerdem möchte ich mich bei dem gesamten Arbeitskreis für das gute Arbeitsklima und die stets gegenwärtige Hilfsbereitschaft bedanken. Ein besonderer Dank geht an Eva Kircher, Annike Weissenstein, Valentin Kunz, Andreas Liess, Stefanie Herbst, Ayan Dhara, Marcus Schulze und Jana Gershberg für ihre Unterstützung bei fachlichen Fragen aber auch für unterhaltsame Stammtischabende und andere Aktivitäten.

Von Herzen danke ich meiner Familie und Christoph. Ihr habt mir während der gesamten Zeit Unterstützung und Rückhalt gegeben.

List of Publications

Base-Selective Five- versus Six-Membered Ring Annulation in Palladium-Catalyzed C–C Coupling Cascade Reactions: New Access to Electron-Poor Polycyclic Aromatic Dicarboximides

S. Seifert, D. Schmidt, K. Shoyama, F. Würthner, *Angew. Chem. Int. Ed.* **2017**, *56*, 7595.

A cross-coupling-annulation cascade from peri-dibromonaphthalimide to pseudo-rylene bisimides

S. Seifert, D. Schmidt, F. Würthner, *Org. Chem. Front.* **2016**, *3*, 1435.

An Electron-Poor C₆₄ Nanographene by Palladium-Catalyzed Cascade C–C Bond Formation: One-Pot Synthesis and Single-Crystal Structure Analysis

S. Seifert, K. Shoyama, D. Schmidt, F. Würthner, *Angew. Chem. Int. Ed.* **2016**, *55*, 6390.

An ambient stable core-substituted perylene bisimide dianion: isolation and single crystal structure analysis

S. Seifert, D. Schmidt, F. Würthner, *Chem. Sci.* **2015**, *6*, 1663.

Modulation of the charge transfer and photophysical properties in non-fused tetrathiafulvalene-benzothiadiazole derivatives

F. Pop, S. Seifert, J. Hankache, J. Ding, A. Hauser, N. Avarvari, *Org. Biomol. Chem.* **2015**, *13*, 1040.

Tetrathiafulvalene-1,3,5-triazines as (Multi)Donor–Acceptor Systems with Tunable Charge Transfer: Structural, Photophysical, and Theoretical Investigations

F. Pop, F. Riobé, S. Seifert, T. Cauchy, J. Ding, N. Dupont, A. Hauser, M. Koch, N. Avarvari, *Inorg. Chem.* **2013**, *52*, 5023.

Overview of Synthesized Compounds

